
THE UNIVERSITY
*of* EDINBURGH

# Self-assembling Block Copolymers in the Nucleation of Hydroxyapatite


Yasmeen Renée Jhons

Doctor of Philosophy

The University of Edinburgh

2020

# Declaration

I declare the research detailed within this thesis has been collected by myself in the duration a PhD studentship under the supervision of Dr Fabio Nudelman, School of Chemistry, University of Edinburgh.

The work, data, and interpretation presented here is that of myself, except when analysing prior work or where a significant collaborative contribution made, in which case it has been clearly specified.

This work has not been submitted for any other degrees or professional qualifications.

Signed:

Yasmeen Renée Jhons

10th January 2019

# Abstract

Dental erosion is a pandemic affecting 3.6 billion people in the world. Over 95 % of enamel is composed of calcium hydroxyapatite (HAP). Enamel is acellular, and as a result of our lifestyle and daily wear and tear this HAP is irreparably damaged. Currently the main treatment for this damage is a metal or porcelain filling which loses adhesion over time creating larger dental carries. To develop a method that can regenerate natural enamel would provide an evasive alternative to the current dental methods and help stop the dental erosion pandemic.

In nature, the growth and nucleation of HAP during enamel formation is regulated by a protein called amelogenin. The protein has hydrophilic-hydrophobic polarity which allows the protein to assemble and has a phosphinic acid group on serine-16 that is crucial in growth and regulation of HAP. Taking inspiration from this protein, self-assembling block copolymers could be used as a synthetic alternative. The benefit of using synthetic polymers in enamel restoration and erosion prevention is that the promotion of CaP can be tuned by changing the functional groups and size of the polymer easily by using controlled radical polymerisation (CRP). They also provide an inexpensive alternative to using protein induced mineralisation methods.

Block copolymers can be formed by CRP. They have been useful in many applications such as drug delivery due their ability to form self-assembled structures such as micelle and cylinders. In previous research on dental erosion the focus has been on the ability of polymers to prevent enamel erosion however their ability to promote HAP growth has not been yet investigated.

Here phosphonic and carboxylic acids containing block copolymers have been synthesised through ring opening polymerisation (ROP) and reversible addition fragmentation chain-transfer (RAFT) polymerisation in order to form self-assembled structures that promote HAP growth and prevent erosion. PEG-poly(heptenolactone) and PEG-polycaprolatone-poly(heptenolactone) containing carboxylic acids and phosphonate moieties were synthesised using PEG and PEG-polycaprolatone as initiators.

In the RAFT polymerisation , phosphonate monomer di(methacryloyloxy)methyl phosphonate (MAPC1), tert-butyl methacrylate (TBuMA), hydroxyethylmethacrylate (HEMA) and 2-(dimethylamino)ethyl methacrylate (DMAE) were polymerised with methyl methacrylate (MMA). The resulting polymers were coupled with PEG through esterification and then further polymerised with a second monomer to give a triblock copolymer. Many of the triblock copolymers had critical micelle concentrations and dispersities which were determined through fluorescence spectroscopy and gel permeation chromatography respectively.

The morphology of nine polymers were explored further though transmission electron microscopy (TEM). It was found that PMMA-*b*-PMAPC1acid-*b*-PEG, PMAPC1acid-*b*-PMMA-*b*-PEG, PDMAE-*b*-PMMA-*b*-PEG all formed spheres between 25 to 50 nm. PHEMA-*b*-PMMA-*b*-PEG formed a mixture of short cylinders (worms) and spheres (20 nm and 35 nm respectively) and PMAPC1-b-PEG, PMAPC1acid-*b*-PEG and PMAA-*b*-PMMA-*b*-PEG did not self-assemble. The ability of block copolymers to promote CaP growth was analysed by dynamic light scattering (DLS) as a preliminary test. Of these polymers, PMMA-*b*-PMAPC1 acid-b-PEG, PMAPC1acid-*b*-PMMA-*b*-PEG, PHEMA-*b*-PMMA-*b*-PEG and PMAPC1acid-*b*-PEG promoted the precipitation CaP. PMAPC1acid-*b*-PMMA-*b*-PEG, on the other hand, did not. PMMA-*b*-PMAPC1 acid-b-PEG was taken forward and the morphology of the CaP was view under scanning electron microscopy (SEM) and transmission electron microscopy (TEM). The SEM micrographs showed a ball-like matrix of CaP which was confirmed electron dispersive x-ray spectroscopy (EDS). The TEM micrographs also show the ball-like matrix and electron diffraction was also utilized and showed that these structures are amorphous.

The PMAPC1acid-*b*-PMMA-*b*-PEG, PHEMA-*b*-PMMA-*b*-PEG and PMAPC1acid-*b*-PEG polymers were taken to investigate their ability to protect enamel against acid erosion. Profilometry was used to measure the loss of enamel and SEM was used to observe changes in the enamel surface. PHEMA-*b*-PMMA-*b*-PEG and PMAPC1acid-*b*-PEG provided an acid resistant covering over the enamel resulting in a reduction in enamel loss, however PMAPC1acid-*b*-PMMA-*b*-PEG showed minimal reduction.

This work has displayed the potential for block copolymers to be a prospective candidate in enamel restoration. However how the polymer controls CaP precipitation needs to be explored further. In particular, how many phosphonic and hydroxyl groups are needed to promote CaP growth. It would also be essential to determine the stability of the amorphous CaP form with PMMA-b-PMAPC1acid-b-PEG to see if at longer periods, the CaP crystallizes.

# Lay Summary

Dental erosion is a pandemic affecting 3.6 billion people globally and specifically acid erosion is caused by dietary intake. Acid erosion occurs when the environment inside the mouth becomes acidic for a prolonged period of time and as a result the mineral, hydroxyapatite, in the enamel is dissolved. Initially the damage is not easily detected by eye and by the time it is visible the damage is done. The layer below the enamel, dentine, is exposed and causes tooth sensitivity. Enamel formation is regulated by a protein, amelogenin, however once the enamel is matured this protein is degraded. Mature enamel contains no living cells thus damage caused by acid erosion is irreversible. Commercially available toothpastes and mouthwashes contain fluoride to prevent acid erosion. A disadvantage to these products is they contain a limited amount of fluoride as too much fluoride can lead to fluorosis in the most severe cases. Once the dentine layer is exposed, dentist fill the eroded area with a composite filling which is an invasive, painful treatment, that usually has to be repeated after a number of years. Acid erosion is also a major issue in young children. In 2018, children in the UK consumed the equivalent of 4800 sugar cubes a year and one of the main causes of child hospitalisation is tooth extraction.

In dentistry there has been an increased interest in the restoration of enamel. There has been evidence that proteins found in saliva can be used in growing new hydroxyapatite, however this would be too expensive to mass produce. Others have used amorphous calcium phosphate, the precursor to hydroxyapatite, to influence the growth of the mineral. This has been proven successful however the size and shape is difficult to control. Another approach was to take inspiration from the structure of amelogenin and produce polymers, with similar characteristics. Amelogenin has a self-assembled structure and contains an acidic phosphorous group which stabilises the calcium phosphate and controls the growth of hydroxyapatite. It was found that copolymers containing an acidic phosphorous group protected enamel from acid erosion. However, the structure and the ability of the polymer to growth calcium phosphate was not examined.

This thesis aims to make a library of different copolymers that can promote the growth of HAP to restore a lesion and protect the enamel from acid erosion. The copolymers produce contains hydrophobic (water-hating), hydrophilic (water-loving) and charged polymer blocks that are chemically bonded together. When these copolymers are placed in water they self-assemble to form a variety of structures such as spheres and worms. The structure of the copolymers can be seen using scanning and transmission electron microscopy techniques. It was found that a copolymer with the structure of hydrophilic-acidic phosphorous group-hydrophobic block formed spheres and promoted the growth of amorphous calcium phosphate. However, it did not mineralise hydroxyapatite nor protect the enamel from acid attack. An acidic phosphorous copolymer that did not self-assemble and an alcohol based copolymer that self-assembled into worms promoted the growth of calcium phosphate and protected enamel from acid attack. Future work could consist of testing the ability of the copolymer to mineralise hydroxyapatite while it is a film covering enamel from acid erosion. The copolymer could provide an inexpensive alternative method in the protection and restoration of enamel.

# Acknowledgements

First and foremost, I would like to thank Fabio Nudelman for taking over as my primary supervisor in the final year of my PhD. Despite polymers not being his expertise, his enthusiasm and encouragement has been infallible, and the majority of this work has been completed under his care. He has helped me regain confidence in my scientific ability and pushed me to go for opportunities that I would have never thought possible. To my GSK supervisor Christabel Fowler, who it has been a pleasure to work with and has always been optimistic about the progress of the project. Thank you to GSK who have sponsored my PhD, and given me the opportunity to pursue a doctorate while providing me with an insight into what life in industry is like.

To the 2016 GML group, Ben, Emily, Fern, Stefan, Dan, Jake, Mo, Gerry, Meng, Murph, Vishal and Eszter for making my first year such a great experience. I will always remember the trip to Glasgow, the Xmas flat crawl and Chinese take aways in the office. To Emily and Fern for helping me get my project started, Meng the Merciless for being the personification of hard work and determination and Vishal for being one of the most helpful and reliable people I know. To my fumehood neighbour Dan for showing me the ropes, always being there for a chat, keeping the boredom at bay and for always having a soup on hand. To Stefan and Alisia for always looking out for me even after they had finished in Edinburgh and for driving the entire garden route while I slept. To the partnership of Ben and Gerry - it was definitely an experience sitting between you two, having the constant fear of being a casualty from your table tennis games and finding all the post-it notes you scattered in my belongings which I am still finding to this day. Thank you to Gerry for intimidating me on my first day, but then being a person to talk to about gaming, animated tv shows and keeping me on the right path. To the Garden and Love group for their encouragement. To the Nudelman group past and present for taking the time to teach me microscopy and for their support. Thank you Dahlia for being a great housemate, keeping me calm while writing this thesis and having an obsession of Friends, and to Ed for helping me with diffraction. A massive thank you to Eszter, Stefan, Vishal, Gerry, Dahlia and Nicola for proofreading my thesis.

In addition, I would like to thank Karina for her help with the profimetry - there's no other person I would like to spend multiple hours in a clean room with. Thank you to Lorna Murray and Juraj Bella from NMR spectroscopy, Nicola Cayzer from SEM and Maarten Tuijeen from the TEM facilities whose expertise has made my journey smoother. To the Bradley group, especially Shao and Nestor, for letting me monopolise their GPC and DLS in the later stages of my PhD. To the chemistry stores team of Tim, Mark and Simon for always putting a smile on my face after a visit.

Furthermore, thank you to the friends I made along the way. Thank you to Jamie and Hannah, the people I started my journey with, and the times we went to Mary's Milk Bar or when we dress in Steam Punk attire. To EUSWPC for giving me an outlet from work in the form of water polo and letting me play outside of the goals.

Outside of research I have had the unwavering support of my family. Thank you to my mum, dad, brother, grandmother, grandfather and Chris. They have given me emotional support in the darker times and lifted my spirits, not to mention relocated me the whole of the UK multiple times. Thank you to Charly for the support, cuddles with Angus the cat and being a great friend from home. Thank you to James for making my final year my most memorable, believing in me and for providing with a mountain of conspiracy theories to read about.

Finally, I would like to thank the people who have shaped my future goals. Thank you to Fabio for believing in me and for making a career in academia a possibility for me again, to Ben "B-Money" Lake for showing me what a good post doc is like and to Melanie, Nicola and Sarah for

being fantastic students, progressing the project and helping me become a better educator. Thank you to Elaine and Bob who allowed me to demonstrate 1st year labs for the past 3 years - it has been a hoot.

# Contents

# Abbreviations

| | |
|---|---|
| AIBN | 2,2'-Azobis(2-methylpropionitrile) |
| ATRP | atom transfer radical polymerisation |
| BAPOS | phenylbis(2,4,6-trimethylbenzoyl)phosphine oxide |
| BSE | back scattered electrons |
| CaP | calcium phosphate |
| cmc | critical micelle concentration |
| CPAD | 4-cyano-4-(phenylcarbonothioylthio)pentanoic acid |
| CPID | 2-cyano-2-propyl benzodithioate |
| CRP | controlled radical polymerisation |
| Đ | $M_w/M_n$ |
| DCM | dichloromethane |
| DMAc | N,N-dimethylacetamide |
| DMAE | 2-(dimethylamino)ethyl methacrylate |
| DMAP | 4-(Dimethylamino)pyridine |
| DPP | dentin phosphophoryn |
| EDC | N-(3-Dimethylaminopropyl)-N'-ethylcarbodiimide hydrochloride |
| EDX | energy dispersive x-ray spectroscopy |
| *Et al*. | *et alia* (and others) |
| $E_{t3}N$ | triethyl amine |
| ε-CL | ε-caprolactone |
| FAP | fluorohydroxyapaptite |
| FRP | free radical polymerisation |
| GPC | gel permeation chromatography |
| HAP | hydroxyapatite |
| HCl | hydrochloric acid |
| HEMA | hydroxyethyl methacrylate |
| IPA | propan-2-ol |
| MAA | methacrylic acid |
| MAPC1 | di(methacryloyloxy)methyl methacrylate |
| MAPC1acid | di(methacryloyloxy)methyl phosphonic acid |
| MCiPA | 1-Mercapto-2-propionic acid |
| MCPA | 3-Mercaptopropionic acid |
| MMA | methyl methacrylate |
| $M_n$ | number average molecular weight |
| $Mn(OAc)_2$ | manganese Acetate |
| MOEP | methacryloyloxyethylphosphate |
| $M_w$ | weight average molecular weight |
| PAA | poly(acrylic acid) |
| PCL | poly(caprolactone) |
| PDMAE | poly(2-(dimethylamino)ethyl methacrylate) |
| PEG | poly(ethylene glycol) |
| PEG-OH | poly(ethylene glycol) methyl ester |
| PHA | poly(hydroxyalkanoate) |
| PHEL | poly(β-6-heptenolactone) |
| PHEL(P) | poly(β-heptenelactone-1-diphosphonate) |
| PHEL(S) | poly(β-6-heptenolactone-(3-mercaptopropionic acid) |
| PHEL($S_{iso}$) | poly(β-heptenolactone-1-(2-mercaptopropionic acid) |
| PHEMA | poly(hydroxyethyl methacrylate) |
| PMAA | poly(methacrylic acid) |
| PMAPC1 | poly(2-(dimethylamino)ethyl methacrylate) |
| PMAPC1acid | poly(di(methacryloyloxy)methyl phosphonic acid) |
| PMMA | poly(methyl methacrylate) |

| | |
|---|---|
| PMOEP | poly(methacryloyloxyethylphosphate) |
| PTBuMA | poly(tert-butyl methacrylate) |
| RAFT | reversible addition fragmentation chain-transfer |
| ROP | ring Opening Polymerisation |
| SEM | scanning electron microscopy |
| TBuMA | tert-butyl methyacrylate |
| TEM | transmission electron microscopy |
| THF | tetrahydrofuran |
| TMSBr | trimethylsiylbromide |
| w/v | weight by volume |
| βBL | β-butyrolactone |
| βHEL | β-6-Heptenolactone |
| βHPL | β-heptanolactone |
| βTDL | β-tridecalactone |
| βVL | β-valerolactone |

# Compounds Abbreviations

In this thesis the following compounds are given abbreviations due to their high appearance throughout a chapter.

**Chapter 2 compounds and abbreviations:**

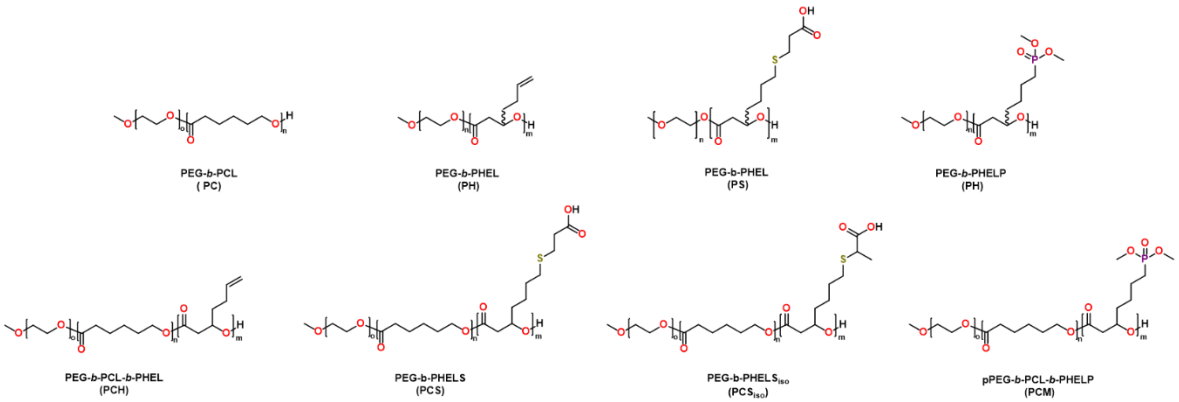

**Chapter 3 compounds and abbreviations:**

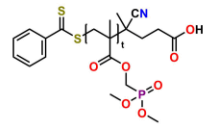

PMAPC1
(D)

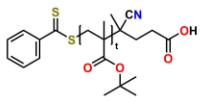

PMMA
(N)

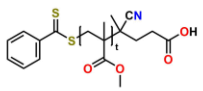

PTBuMA
(T)

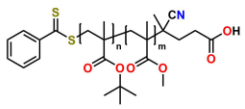

PMMA-*b*-PTBuMA
(NT)

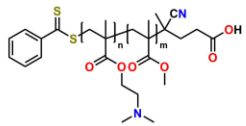

PMMA-*b*-PDMAE
(NA)

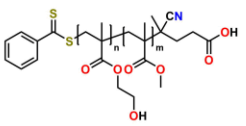

PMMA-*b*-PHEMA
(NE)

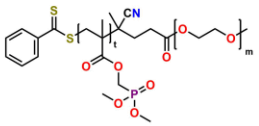

PEG-*b*-PMAPC1
(PD)

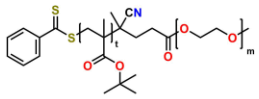

PEG-*b*-PTBuMA
(PT)

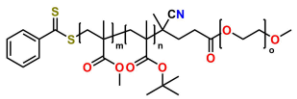

PEG-*b*-PTBuMA-*b*-PMMA
(PTN)

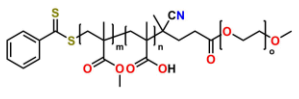

PEG-*b*-PMAA-*b*-PMMA
(PQN)

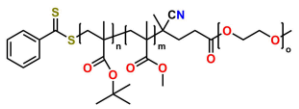

PEG-*b*-PMMA-*b*-PTBuMA
(PNT)

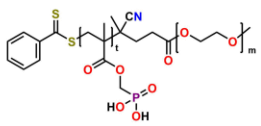

PEG-*b*-PMAPC1acid
(PF)

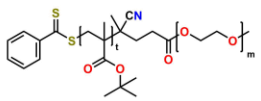

PEG-*b*-PTBuMA
(PT)

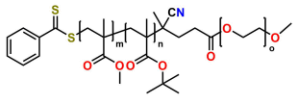

PEG-*b*-PTBuMA-*b*-PMMA
(PTN)

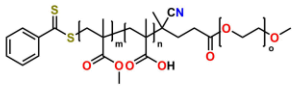

PEG-*b*-PMAA-*b*-PMMA
(PQN)

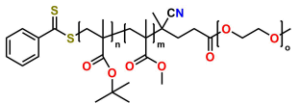

PEG-*b*-PMMA-*b*-PTBuMA
(PNT)

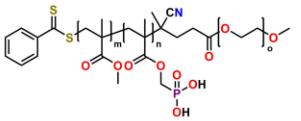

PEG-*b*-PMAPC1acid-*b*-PMMA
(PFN)

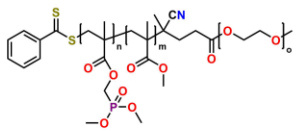

PEG-b-PMMA-b-PMAPC1
(PND)

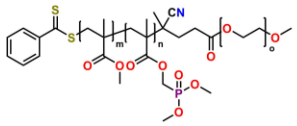

PEG-*b*-PMAPC1-*b*-PMMA
(PDN)

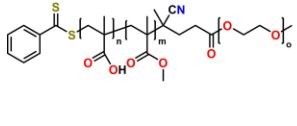

PEG-*b*-PMMA-*b*-PMAA
(PNQ)

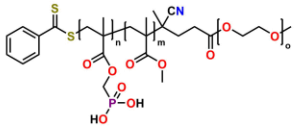

PEG-b-PMMA-b-PMAPC1acid
(PNF)

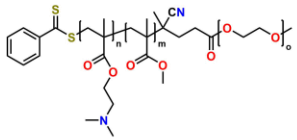

PEG-b-PMMA-b-PDMAE
(PNA)

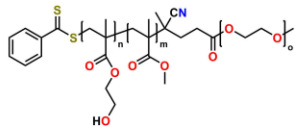

PEG-b-PMMA-b-PHEMA
(PNE)

# Chapter 1 Introduction

## 1.1. Structure of enamel

Enamel is the outmost layer of the tooth and is the hardest mineralized tissue.[1,2] Enamel protects the crown of the tooth and the softer dentine layer and is strong enough to withstand mastication without damaging the tooth (Figure 1.1).[3–7]

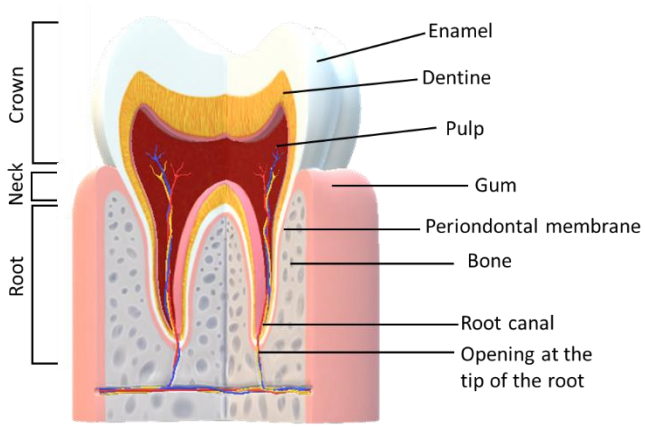


*Figure 1.1 An annotated structure of the tooth.*

Enamel is comprised of 95 % by weight of hydroxyapatite (HAP) which is a mineralised form of calcium phosphate (CaP). HAP in enamel exists as a non-stoichiometric carbonated crystal form, $(Ca_{10-x}(PO_4)_{6-x}(CO_3)_x(OH)_{2-x}$, where x is between 0 and 2. [8–10] The $Ca^{2+}$ ions can be substituted $Na^+$ and $Mg^{2+}$ ions and the $OH^-$ ions replaced with fluoride ions.[9,11] This dynamic exchange of ions causes the physical properties of enamel to be constantly changing. For instances when the fluoride is substituted for the hydroxyl groups, the HAP become more crystalline and less soluble.[12,13] The thickness of enamel is 1-2 mm and is made up of elongated rods that are 25 – 100 nm in diameter however can be up to 100 nm -100 µm in length.[7,14,15] The HAP crystals are arranged in highly structured hexagonal prisms which are 300 – 400 nm in length (Figure 1.2).[1] These prisms give enamel good mechanical properties, which allows large forces to be exerted when mastication occur. The mechanical properties are shown in the it's young's modulus and hardness parallel to the HAP rods of 87.5 GPa and 3.8 GPa respectively.[3,16]

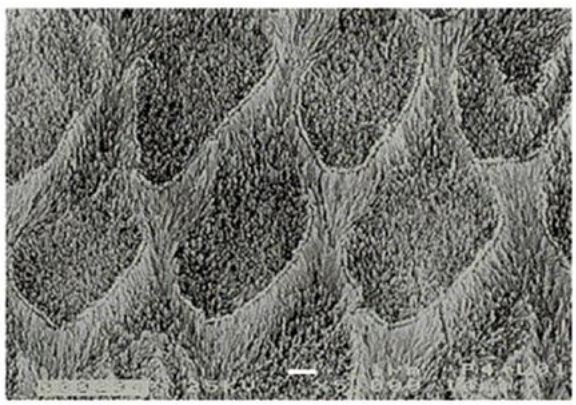

*Figure 1.2 SEM image of HAP enamel prism. Picture taken from Kniep et al.[7]*

## 1.2. Proposed mechanism for the formation of hydroxyapatite (HAP)

The formation of the complex structure of enamel is regulated by proteins and is a complicated process. Many have investigated the mechanism of the nucleation of enamel HAP but still more insight is needed to determine the process. However there has been extensive studies on the crystallisation of synthetic HAP which has aided the formation of theories on of the nucleation of HAP in enamel. There are multiple routes to crystallisation but the classical and non-classical theories will be discussed here. In the classical theory, crystals are formed by monomer by monomer addition of simple chemical species to a stable nucleus.[17] The formation of the nuclei is a result of overcoming the free energy barrier to nucleation, this barrier is lower in supersaturated solutions. Ostwald described the growth that the nuclei goes through as a thermodynamic process where the kinetically favoured nuclei are formed first and then are dissoluted and added to the more thermodynamically stable nuclei (Ostwald ripening).[18] The non-classical theory of crystallisation is one that exhibits a multi-stage process in which ion clusters interact to form more stable structures.[19]

Habraken *et al.* investigated the mechanisms behind the nucleation of synthetic HAP through a variety of *in situ* techniques. The authors describe the nucleation of HAP in terms of both classical and the non-classical theories of crystal nucleation. It was found that clusters of calcium triphosphate ions associate and aggregate to form branched polymeric structures (Figure 1.3A). The polymeric structures then take up calcium in order to form amorphous calcium phosphate (ACP) where these structures form 1.2 nm clusters (Figure 1.3B). The continued calcium intake transforms the ACP into octacalcium phosphate (Figure 1.3C).[19]

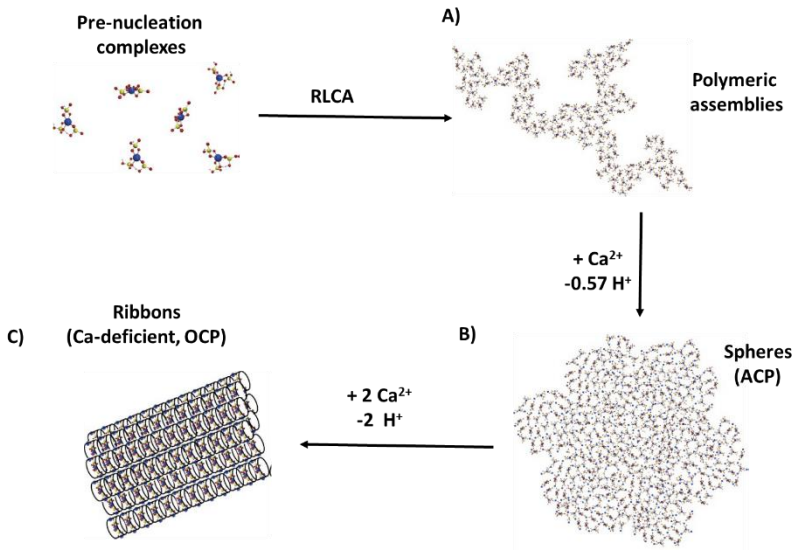


*Figure 1.3 The mechanism of aggregation. Pre-nucleation complexes in solution from branched polymeric assembles through reaction limiting aggregation (A). Nucleation of ACP occurs through the binding of additional calcium ions and increased aggregation results in ACP spheres (c). Further uptake of calcium results in ribbons of calcium deficient octacalcium phosphate (OCP) and then apatite (AP). Modified from Habraken et al.[19]*

Habraken *et al.* could not explain the formation of ACP by the classical nucleation theory directly. However, it was shown that with the presence of pre-nucleation complexes lower the thermodynamic barrier to nucleation.[19] Habraken and coworkers described the mechanism as an "extended nucleation theory".[19] Regardless of the work carried out by Habraken *et al.* being significant in the mineralisation field, there is much to learn about the biomineralisation of HAP such as proteins that are incorporated in the process. It is unknown is if the crystallisation of biological systems follow a similar route to make such complexes.

## 1.3. Proteins in the biomineralisation of enamel

Proteins are macromolecules which are composed of a primary sequence of amino acids. Proteins can self- assemble and form more complex structures such as α – helices and β-pleated sheets. Proteins are involved in many biological processes such as biomineralisation. Biomineralisation is the process in which living organisms produce minerals. The processes in which enamel HAP is biomineralisation is called amelogenesis. Amelogenesis comprises of four stages; the presecretory, secretory, transition and maturation which are defined by the life cycle of the ameloblasts.[20,21] The process of biomineralisation of enamel starts at the dentine-enamel junction, where the ameloblasts differentiate and develop a secretory specialisation. In the secretory stage a extracellular protein matrix is secreted and HAP crystals grow in a controlled manor and the enamel starts to thicken.[4] Once the enamel layer is established, the transition and maturation stages start. In these stages the enamel grows in width and thickens. As the enamel grows the protein matrix begins to degrade and the maturing enamel fills extracellular space the protein matrix occurpied.[4] After the enamel has fully matured there is no protein matrix left and the enamel becomes abiotic.

The extracellular protein matrix that was secreted by the ameloblasts in the secretory stage mainly consists the protein amelogenin. It has been reported that amelogenin is key in the organisation of the enamel prism, control of crystal size, the regulation of elongated crystal growth and enamel thickness.[4,22] It should be noted that due to amelogenin being a labile protein, a crystal structure is yet to be determined. However, Diekwisch *et al.* have performed solid-state $^{1}H$ NMR spectroscopic studies to determine the structure of the N and C termini of the protein (Figure 1.4).[23]

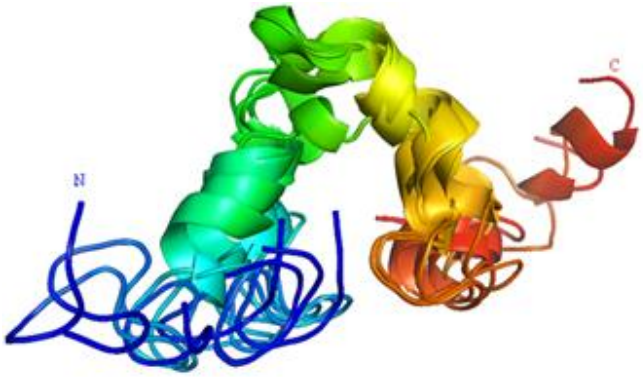


*Figure 1.4 Computer generated structure from 6 lowest conformers of amelogenin based on solid state NMR reproduced from Diewisch et al.[23]*

The structure of amelogenin is important to the biomineralisation of HAP. The primary structure of the protein has hydrophobic-hydrophilic polarity which enables the protein to self-assemble into different structures.[4] It has been reported that removing the hydrophilic C terminus of the protein decreases its affinity for HAP crystals.[24,25] While the C terminus is hydrophilic, the N terminus is hydrophobic and contains a single phosphate group. This is thought to be involved with the protein - calcium phosphate interactions and contributes to amelogenin's ability to stabilize the calcium HAP precursor, amorphous CaP.[4] This theory was reinforced by Shaw *et al.* when they investigated leucine-rich amelogenin polypeptides. Even though the amelogenin was still able to bind to the calcium HAP without phosphorylated serine, the binding of the N-terminus was stronger when the serine was phosphorylated.[26,27]

There are two proposed mechanisms for amelogenin regulated calcium HAP mineralization. In the classical approach, the protein has an affinity to bind to octacalcium phosphate at the (010) face rather than the (100), inhibiting growth on the (010) face and promoting growth of

elongated rods.[7] In the non-classical mechanism, amelogenin binds to amorphous calcium phosphate and assembles into intermediate pre-nucleation clusters before going on to form the organised HAP crystals.[4]

Dentin phosphoryn (DPP) is also present during tooth formation. It is an aspartic acid-serine rich protein which is important in the formation of HAP in dentine.[4,28,29] The aspartyl and seryl residues comprise 75 % of the amino acid residues in the protein and 85 % of the seryl residues are phosphorylated.[28] Similarly like amelogenin the structure of the protein cannot be fully characterised.[4,28] DPP is a labile protein however it has been assumed that upon binding with $Ca^{2+}$ ions, the protein forms β-sheet structures which could be used as templates for oriented crystal growth.[28] Furthermore, the DPP proteins have two mineral-binding sites as a result the protein can bind to $Ca^{2+}$ ions through the phosphorylated serine and aspartic acid. As well as binding to the $PO_4^{3-}$ through the hydroxyl groups on the seryl residues.[28,29]

## 1.4. Demineralisation – remineralisation of enamel

The increased consumption of soft drinks has made dental erosion a more apparent problem, with 3.6 billion people worldwide suffering from tooth decay with 486 million children with erosive lesions on their permanent teeth.[30,31] Enamel erosion is caused by acidic beverages and fruit that are consumed in one's daily diet. This introduces an acidic oral environment, where the enamel is demineralised. Demineralisation is the process in which mineral ions are removed from HAP. The extent of this process depends on many factors such as the acid which is attacking the enamel and the concentration of calcium in the saliva. The acids which are consumed in one's diet are usually weak acids such as citric and phosphoric acids. The acid dissociates in the water and forms $H^+$ ions, these then bind with the carbonate or phosphate ion located at the surface of the enamel and removes them. This would be the only pathway to demineralisation for a strong acid such as HCl. However with weak acids such as citric acid which contains carboxylates, they can directly bind to the $Ca^+$ ions of HAP. The carboxylate and phosphonate groups have multiple binding sites, which allows for stronger binding to the calcium ions (Figure 1.5). The ability for the anion to bind to the calcium in HAP is dependent on their $pK_a$, for example, acetic acid binds less effectively than citric acid as its $pK_a$ is higher and only has one hydrogen dissociation. Whereas there is potential for three hydrogens to dissociate from citric acid meaning three binding sites. Phosphoric acid also has 3 hydrogen dissociation constants and like citric acid can cause damage at higher pHs. Acids which contain a hydroxyl group can experience greater binding to calcium than expected and can cause demineralisation at pH 6.[13]

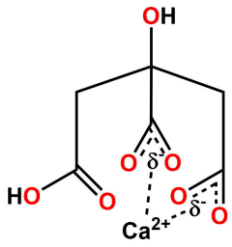


*Figure 1.5 Scheme of a citrate ion binding to a calcium ion when two hydrogens have dissociated.*

Demineralisation itself is a reversible process and to minimise the extent of mineral loss, enamel needs to exist in an environment which favours remineralisation. Saliva is an extracellular fluid excreted by glands in the mouth that has the ability to remineralise enamel. At physiological pH, saliva is supersaturated with calcium species which includes phosphates, bicarbonates and apatites. Salvia has two main roles when remineralising enamel, it provides calcium and phosphate ions to the mineral-deficient legions and also acts as a buffer to increase the pH back to physiological conditions. However the saliva mineralisation is a slow process and is limited to

the surface of the enamel.[5,32] Saliva also contains salivary phosphoproteins which help regulate the diffusion of the ions into the mineral-deficient legions and prevents demineralisation on the healthy areas of enamel. In addition the proteins create a covering on the enamel surface which contains an excess of calcium and phosphate ions. When the pH decreases it provides not only a protected layer but also readily available source of calcium and phosphate ions for remineralisation. [29]

Saliva also contains fluoride ions which can help decrease the effects of demineralisation. This knowledge has lead to fluoride-containing toothpastes and mouthwashes being used in order to prevent enamel erosion. The fluoride ions can be substituted for the hydroxyl groups in the mineral to form fluorohydroxyapaptite (FAP). By incorporating the fluoride ions, the enamel becomes less soluble, resulting in the mineral becoming more resistant to acid attack. However for fluoride to be incorporated into the mineral the levels of calcium and phosphate ions need to be sufficient so that FAP can grow. In commercial products, one way to ensure this is to include casein phosphopeptide and amorphous calcium phosphate in the products.[12,33] This provides a supersaturation of calcium and phosphate with respect to the enamel which enhances remineralisation. However incorporating fluoride does not help serve demineralisation legions and overcompensating with fluoride can lead to dental fluorosis. When demineralisation occurs composite fillings are used to fill the lesion which is an invasive and temporary treatment. Non-fluoride based alternatives to enamel erosion have been explored such as using polymers films.[34,35]

## 1.5. Method of enamel remineralisations

The area of enamel remineralisation has been researched extensively. However the natural remineralisation of enamel is challenging because enamel is abiotic and therefore it cannot repair itself like bone.[29] The techniques in enamel remineralisation need to be able to crystallise HAP that has similar mechanical properties to that as natural enamel, this would mean that precipitating calcium phosphate would not be sufficient. To ensure that the synthetic HAP has similar mechanical properties to natural HAP, the remineralisation methods have to regrow the apatite rods in enamel or promote epitaxial nucleation on top of existing enamel. Self-assembling poly peptides have been explored as a method to remineralise enamel. Proteins are crucial in the regulation of the formation of enamel. Kirkham *et al.* design a self-assembling peptide which contained three glutamic acids in the peptide sequence. The peptide formed a β-sheets when solvated. The peptide was mixed with gelatine to form a peptide scaffold that was painted onto an enamel disc.[36] This disc was place in acid solution followed by a crystallisation mixture of $CaCl_2$ and $KH_2PO_4$. The results showed that the peptide was able to remineralise enamel. Leucine-rich amelogenin peptides have promoted directional crystal growth of HAP along the c-axis, which also occurs in amelogenesis.[37,38] The structure of the leucine-rich peptide comprises of the C- and N- termini of amelogenin which are responsible for binding to and directing the growth of the mineral. The disadvantage to amelogenin peptides mediated remineralisation is that it takes a long period of time to occur, making it an unsuitable alternative.[29] However, another method is using ACP which is the precursor to HAP. ACP has been used with casein phosphopeptide (as briefly mentioned above) which works by the protein being able to stabilize the calcium and phosphate in solution.[11] More recently Shao and co-workers have synthesised calcium phosphate ion clusters by the evaporation of triethylamine. These clusters were 1.5 nm in diameter and were placed on a demineralised lesion on a tooth. The calcium phosphate ion clusters spontaneously transformed into ACP.[39] The tooth was placed in a simulated oral fluid and the results show epitaxial growth of new HAP which was identical to the native enamel.[39] However this growth was limited to 2.8 µm which is dependent on the stability of ACP.

A potential method in remineralising enamel is the use of block copolymers. Block copolymers have the ability to self-assemble to higher ordered structures like proteins and functional groups can be easily incorporated. This would give a method of remineralisation that can be easily fine-tuned to promote the growth of epitaxial HAP. This could be done by using a block copolymer which has self-assembled into cylinders, this morphology could then be used to promote direction growth by confining the nucleation inside the cylinder.[40] Block copolymers have not yet been targeted the remineralisation of enamel however they have proven useful in offering enamel protection from acid attack.[34]

## 1.6. Block copolymers

Block copolymers are Janus materials, they consist of two or more chemically different homopolymers that are covalently bonded together.[41] These copolymers are being broadly researched in many areas such as drug delivery, sensors and films.[42–44] When the block copolymer is solvated it self-assembles into different structures that contain distinct domains of each homopolymer.[41] The self-assembly of block copolymers is a thermodynamic process and is driven by the entropy gain that the solvent obtains as a result of solvophobic segment withdrawing from the solvent, this causes a decreases in interfacial free energy between the solvent and solvophobic block.[45] The self-assembling nature of the block copolymers gives rise to interesting morphologies such as micelles. By changing the molar ratio of the homopolymers and the solvent, it is possible to access other morphologies such as the lamellae phase (Figure 1.6). Furthermore, the self-assembled structure can be predicted by using the Flory-Huggins parameter for polymer mixing.[41,46]

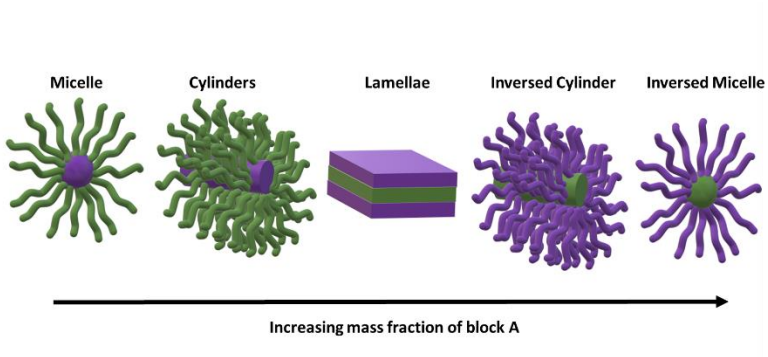


*Figure 1.6 Morphologies accessed through diblock copolymer self-assembly, block A is purple segment and block B is the green segment.*

Micelles are used in a plethora of applications, and especially in drug delivery systems, partly because they can be used in the encapsulation of drugs.[47] Amphiphilic block copolymers do not form micelles until the critical micelle concentration (cmc) is reached. The cmc is both solvent and temperature dependant. The formation of micelles is directed by two opposing forces; the repulsive forces of the insoluble blocks and the attractive forces between soluble blocks. Micelle formation is favourable above the cmc because it minimises unfavourable solvent interactions. The shape of the micelle is dependent on the length of both the A and B parts of the diblock and can be described by the packing parameter, $p$ (Equation 1.1).[48,49] When there is high curvature and a large molar ratio of A then a spherical micelle will form ($p < \frac{1}{3}$), for medium curvature and similar molar ratios, cylindrical micelles ($\frac{1}{3} < p > \frac{1}{2}$) will form and lastly for a small molar ratio of A and low curvature a polymersome (polymer vesicle, $\frac{1}{2} < p > 1$) will form.[49] While solvated, micelle stability is dependent on the solvophobic part of the copolymer, the longer it is, the lower the cmc and the more stable the micelle is.[50]

$$p = \frac{v}{a_o l_c}$$

*Equation 1.1* The packing parameter equation of micellar morphology, v = volume of the core block, $a_0$ = interfacial area, $l_c$ =length of core block

Block copolymers can be synthesised by a multitude of ways including atom transfer polymerisation (ATRP), however ring opening polymerisation (ROP) and reversible-addition fragmentation chain-transfer (RAFT) polymerisations are the focus.[51–54] In ROP, a macroinitiator is formed first, then another monomer is added to the solution and the polymerisation occurs. Whereas in RAFT polymerisation, the more reactive monomer is added to the RAFT agent and the polymerisation begins, then sometime after, the second monomer is added.

Many have accessed the different micellar morphologies by increasing the $M_n$ of the homopolymers within the block copolymer.[55–57] In literature, RAFT dispersion polymerisation is the method of choice for polymer induced self-assembly, as the soluble polymer's $M_n$ increases, the chain becomes increasingly insoluble which in turns drive self-assembly.[58,59] Armes *et al.* uses aqueous RAFT dispersion polymerisation to synthesis poly(methacryloxymethylphosphonate-*co*-benzyl methacrylate)(($PMP_x$-$PBzMA_y$) with differing $M_n$ of the homopolymers to determine the morphology change of the block copolymer in solution. The results showed that the micellar morphology changes from small spheres to cylinders (worms) to vesicles, with $PMP_{42}$-$PBzMA_{300}$ forming large spheres.[60] From these results a phase diagram was constructed and showed the most prevalent morphologies of the block copolymers are spheres and vesicles.[60]

Charge polymers can influence the crystal growth of minerals, in this literature the effect of two block copolymers were investigated in relation to its occlusion into calcite, a polymorph of calcium carbonate. It was found that the vesicles and worm assemblies of $PMPA_x$-$BzMA_y$(Poly(methacryloxymethyl-phosphonic acid-*co*-benzyl methacrylate) had greater effect on occlusion into calcite than its non-ionic counterpart. Moreover, the effect of occlusion into calcite was greater with higher block copolymer concentrations (Figure 1.7)[60]

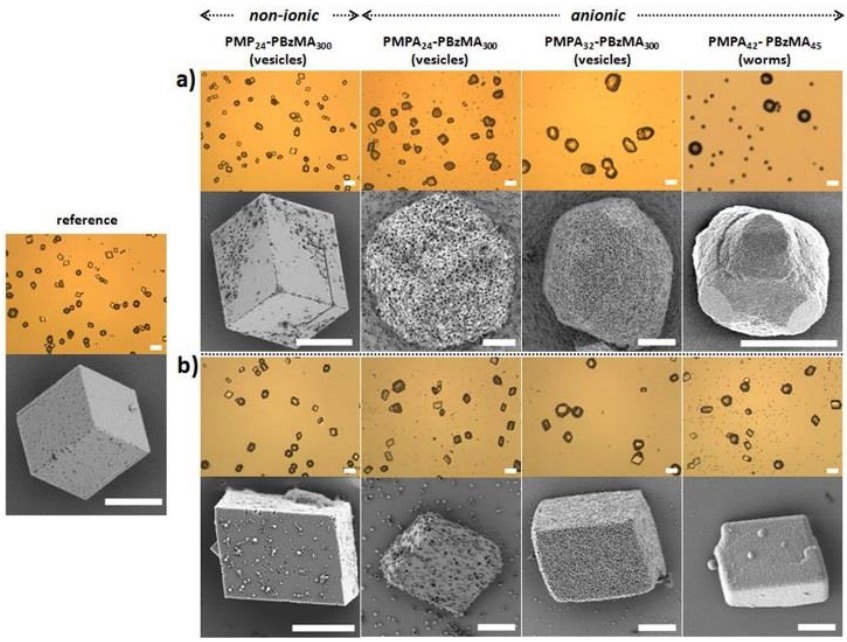


*Figure 1.7 Optical micrograph and corresponding SEM images for a series of $CaCo_3$ crystals with either (a) 0.010 % w/w or (b) 0.005 % w/w PMPA-PBzMA or PMP-PBzMA diblock copolymer. The reference image are from calcite crystals precipitates in the abscence of diblock copolymers. Images taken from Armes et al.[60]*

The nucleation of calcium HAP by block copolymers has also been reported in literature particularly as bone scaffolds, however none has explored the morphology of the block copolymers and how it effects calcium HAP nucleation in enamel.[35,61–64] There is still a need to produce a reminersalisation technique that is able to grow synthetic HAP similar to of that found in native enamel. The growth of HAP still needs to be perfected and be clinically and commercially viable. Self- assembling block copolymers provide an inexpesive remineralisation method that can be easily fine tune to give the best HAP nucleation conditions. Their ability to self-assemble into different structures could regulate the growth of HAP similar to proteins such as amelogenin.

## 1.7. Aims

The overall aim of this thesis was to synthesise a library of self assembling block copolymers that were able to nucleate hydroxyapatite for the remineralisation of enamel. It was planned to investigate the incorporation of hydroxy, acids and amine groups into block copolymers synthesised by ROP and RAFT polymerisation and characterised them by gel permeation chromatography (GPC) and nuclear magnetic resonance (NMR). The block copolymer morphology would be investigated to determine if self-assembly affects nucleation. The material precipitated by the polymer would be examined through scanning electron microscopy (SEM), energy dispersive Xray spectroscopy (EDS), transmission electron microscopy (TEM) and electron diffraction to confirm the chemical composition and crystallinity of the material. Lastly, the secondary aim was to investigate the ability of the block copolymers to protect the enamel from acid attack and to see if self-assembly helps with acid resistance.

In Chapter 2 it was planned to synthesise a series of polyesters block copolymers by ROP. The polymerisation of ε-caprolactone (ECL) by a PEG-*b*-poly(heptenolactone) (PEG-*b*-PHEL) macrointiator would be investigated and the resultant polymer would be functionalised through hydrophosphorylation with $Mn(OAc)_2$ and thiol-ene click chemistry. In Chapter 3 a series of diblock and triblock copolymers containing carboxylic acid, amine and hydroxyl groups would be prepared by RAFT polymerisation. Furthermore, a collection of novel block copolymers containing di(methacryloyloxy)methyl methacrylate (PMAPC1) would be synthesised by a two-step polymerisation and PEGylation. The critical micelle concentration of both the ROP and RAFT polymerisation synthesised copolymers would be determined through dynamic light scattering (DLS) and TEM to observe the polymer morphology. In chapter 4 the ability of the copolymers synthesised in chapter 3 would be studied to see if their self-assembled structures influenced the nucleation of HAP. This would be determined through preliminary experiments with DLS. SEM, TEM and EDX would then be used to confirm the morphology of precipitated material and finally electron diffraction to determine its crystallinity. Lastly the copolymer's ability to protect enamel from acid attack would be explored with the use of surface profilometry and SEM.

# Chapter 2 Ring opening polymerisation (ROP)

## 2.1. Introduction

### 2.1.1. Polymerisation mechanisms

Traditionally, polymerisations are separated into two groups depending on their growth mechanisms, they are chain- and step-growth polymerisations. The latter is used to produce polyesters and polyamide based polymers by the elimination of a small molecule, such as water. In step-growth polymerisations, bifunctional monomers such as dicarboxylic acids and diols react iteratively to form a polymer chain (Figure 2.1).[65]

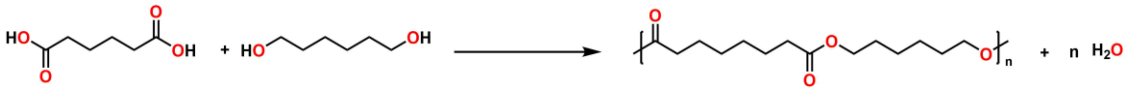

*Figure 2.1 A schematic of a step-growth polymerisation.*

The disadvantage of using step-growth polymerisation is that high $M_n$ polymers are difficult to obtain. The degree of polymerisation (DP) can be described by *Equation 2.1*, where the DP is proportional to the monomer conversion, *p*.[66] It was found that the removal of water was crucial to achieve higher DP values.[67] In step-growth polymerisations a broad dispersity is usually observed, this is attributed to the random nature of polycondensation.

$$DP = \frac{1}{1-p}$$

*Equation 2.1 The degree of polymerisation equation for a step-growth polymerisation. p = the fractional monomer conversion*

In chain-growth polymerisations, polymers with low dispersities can be produced. Unlike step-growth polymerisations, in chain-growth polymerisations proceed through the formation of an active centre.[66] The polymerisation occurs as monomers are iteratively added to the chain at the active centre and the $M_n$ grows in a linear fashion with respect to monomer consumption.[65] The general reaction mechanism for most chain growth polymerisations is the formation of the active species by an initiator, then the propagation of the polymer chain through reacting with additional monomers and finally the active polymer is quenched in the termination step. Free radical polymerisation is a type of chain growth polymerisation and it is used widely in industry, as it has a high tolerance for protic solvents, monomers and insensitivity to oxygen.[68] A disadvantage to this polymerisation is that the molecular weight distribution of the resultant polymers are not well controlled resulting in large dispersities.

Ring opening polymerisation (ROP) is a type of chain growth polymerisation, in which, the driving force of the polymerisation is the ring strain of the monomer. Some common examples of cyclic esters and cyclic amide monomers used in ROP are shown below in Figure 2. 2.

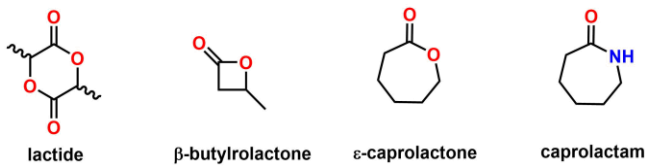


*Figure 2. 2 Examples of cyclic esters and a cyclic amide.*

Like polycondensation, polyesters can be synthesised using ROP. Polyesters can be degraded chemically or enzymatically and this has led to increased use of ROP in research to produce biodegradable polymers. In ROP, the $M_n$ of the polymer can be controlled by the monomer to

initiator ratio, a larger ratio would afford a higher $M_n$ polymer, as there would be fewer active chains. There are many ways ROP can be undertaken, in this thesis cationic, anionic and coordination insertion ROP are explored.

### 2.1.2. Cationic and anionic ring opening polymerisation (ROP)

Cationic ROP is initiated by an electrophile and a positively charged intermediate is formed. Common initiators for cationic ROP are strong brönsted acids, alkyl esters and lewis acids. There are two mechanistic pathways that the polymerisation can progress by and this is dependent on neighbouring group participation.[69] If the intermediate cation is sufficiently stabilised an $S_N1$ mechanism will be more prevalent, however, if not sufficiently stabilised an $S_N2$ mechanism is favoured (Figure 2.3).[70,71]

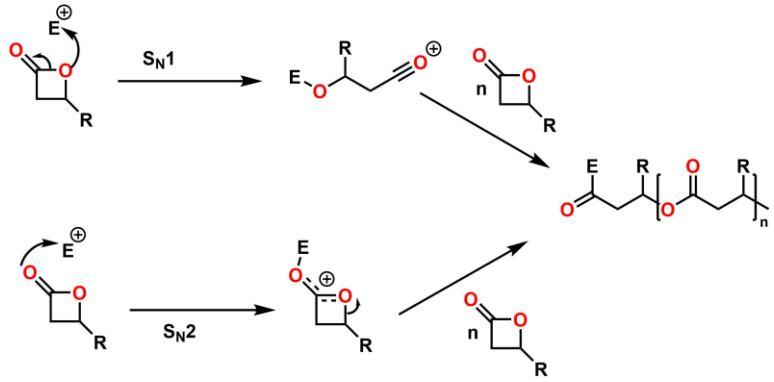


*Figure 2.3 The two possible pathways for a cationic ROP.*

An anionic ROP is initiated by a nucleophile which attacks the carbonyl site of the monomer (Figure 2.4). In the case of asymmetric heterocycles, the nucleophile would attack at the least substituted carbon atom.[69] A wide range of Lewis bases have been used in anionic ROP, however, due to their basicity, the active site can abstract protons from monomers and initiate new chains.

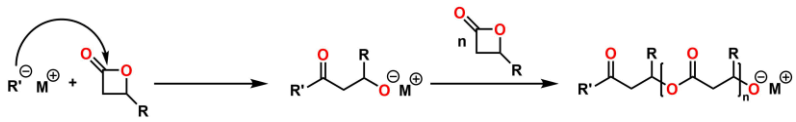


*Figure 2.4 The mechanism of anionic ROP.*

Transesterification is a side reaction which may occur during the ROP of cyclic esters. It is common undesired side reaction as it can lead polyesters with lower than expected $M_n$ values and broadened dispersities. The process occurs when the active site reacts with the carbonyl group in the chain itself (intramolecular) or another chain (intermolecular). Intramolecular transesterification produces cyclic polymers and oligomers. If intermolecular transesterification occurs, then chains of differing lengths are formed causing a broadening in dispersity of the polymer (Figure 2.5). Furthermore, the presence of transesterification reactions can be detrimental to the formation of block copolymers when both blocks are polyesters, as it would lead to a more random sequence. Transesterification can often be minimised by decreasing the reaction time and the temperature of the polymerisation.[72]

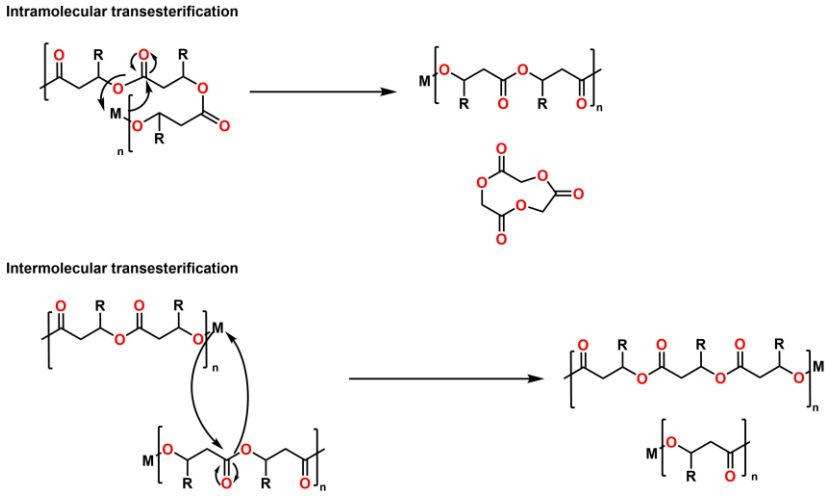


*Figure 2.5 The mechanisms for intramolecular and intermolecular transesterification.*

### 2.1.3. Coordination insertion ring opening polymerisation (ROP)

Both cationic and anionic ROP have their disadvantages when they are used to produce polyesters, the former resulting in oligomers and poor reactivity and the later producing side reactions (transesterification). To improve the control of the ROP, the use of metallo-organic species as catalysts was investigated. The portion of the metallo-organic compound that participates in the polymerisation process are primarily alkoxides. However, metal-alkoxides are not stable as monomers, as they form multimeric oxo-bridged compounds over time.[73] As a result, these species are usually made *in situ* either by the addition of an alcoholic initiator or a suitable metal precursor.[73] The mechanism for coordination insertion is as follows: first the nucleophilic attack of the carbonyl of the monomer by the alkoxide. Then ring is opened by the cleavage of the acyl-oxygen (Figure 2.6). The polymerisation can be terminated by the addition of HCl or methanol to cleave the metal centre off.[74,75]

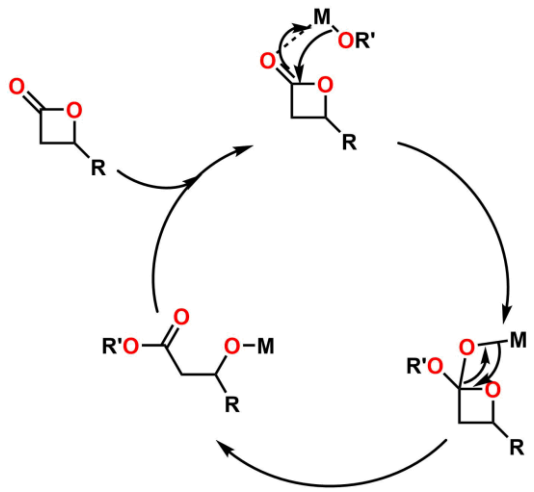

*Figure 2.6 Coordination – insertion mechanism using a metal alkoxide.*

Tin (II) 2-ethylhexanoate (tin octanoate), is the most commonly used catalyst in the industry for its versatility and ease of handling.[76] Tin octanoate is highly soluble in the majority of organic solvents and can polymerisation lactide to high molecular weights. However, with the depletion of monomer, transesterification of poly(lactide) occurs and the molecular weight plateaus while the dispersity of the polymer broadens.[77–79] Furthermore, the removal of tin octanoate is difficult and as a result, different catalysts have been explored.[79,80] Aluminium tri-isoproxide has also been researched in the ROP of lactide. Aliminium tri-isoproxide is toxic, however, unlike tin

octanoate the compound forms aggregates at low temperature as a result an induction period is observed. It was found that the solvent polarity, nature of substituents and the presence of coordinating ligands affects the size and type of aggregates.[77,81,82]

There was a large interest in aluminium based catalysts due to the ease of synthesising them and the wide variety of complexes that can be formed. In particular, tetradentate salicaldimine(salen)aluminium complexes showed promise as changing the sterics and electronic nature of the ligand could enable high catalyst activity and in the case of lactide, control of stereochemistry of the resultant polymer.[83] Spassky and coworkers demonstrated the selectivity of a binaphtyl derived chiral (salen)aluminium complex in the ROP of *rac*-lactide. The polymerisation showed 19 % conversion after 5 hours with a dispersity of 1.10. The polymer showed 88 % selectivity for D-lactide, however the conversions were not as high as other aluminium alkoxide predecessors.[84,85] In more recent years, Jacobsen ligands could be used to give excellent control over molecular weight, dispersity (1.05 after 4 days polymerising) and isotactic selectivity (0.92 in toluene). Feijen *et al.* showed that Jacobsen ligands base aluminium salen complexes can also selectively polymerise lactide like binaphtyl derived chiral (salen)aluminium complex. however, to obtain over 90 % conversion of monomer, the mixture needed to left to polymerise over 4 days.[86] Gibson and coworkers investigated the substitution of different phenoxide rings substituents and the chain length of the diamine linker on the effect of Al[salen] complexes (Figure 2. 7).[87,88]

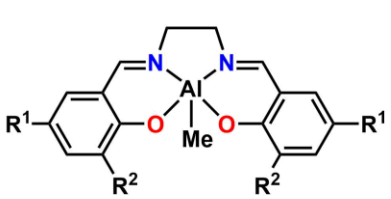


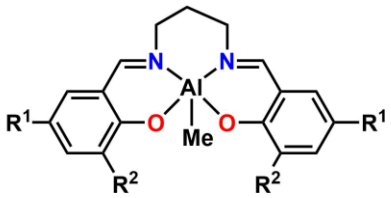


| | $R^1 = R^2$ | $k_{apps}$ / $s^{-1}$ | $M_n$ | $M_w/M_n$ |
|---|---|---|---|---|
| 1A | H | 59 x $10^{-6}$ | 4390 | 1.76 |
| 1B | Cl | 181 x $10^{-6}$ | 4290 | 1.58 |
| 1C | tBu | 1 x $10^{-6}$ | 5900 | 1.27 |

| | $R^1 = R^2$ | $k_{apps}$ / $s^{-1}$ | $M_n$ | $M_w/M_n$ |
|---|---|---|---|---|
| 2A | H | 661 x $10^{-6}$ | 6560 | 1.40 |
| 2B | Cl | 1009 x $10^{-6}$ | 9700 | 1.08 |
| 2C | tBu | 133 x $10^{-6}$ | 9590 | 1.07 |

*Figure 2. 7 The structure of two Al[Salen] complexes that were investigated by Gibson and coworkers, with the rate of polymerisation, molecular weight and dispersity ($M_w/M_n$) of the resultant poly(lactide) shown.*

It was found that increasing the size of the phenoxide substituents gave a more controlled polymerisation however lowered the rate of polymerisation. This was attributed to the bulky *tert*-butyl groups obstructing the activity Al centre from the lactide monomer. Furthermore by having electron withdrawing groups on the phenoxides increased polymerisation activity increasing the activity of the metal centre. Gibson *et al.* also found that incorporating a $C_3$ linker rather than a $C_2$ diamine linker increased polymerisation with each phenoxide substituent significantly. This was hypothesised to be due to the $C_3$ providing more flexibility to the salen complex, and increasing the bite angle from 76°– 78° to 83° – 88° which accommodates the intermediate more effectively.[88] This was also seen in the work of Nomura and coworkers.[89] Shaver *et al.* expanded on the monomer scope of the Al[Salen] complexes by using it in a homopolymerisation of β-butyrolactone (βBL). In previous work from Spassky and coworkers, the polymerisation of βBL with catalysts based on a (N,N'-bis(salicylidene)-1,2-ethanediimine) ligand afforded oligomers of poly(3-hydroxybutyrate).[90] In research by Shaver *et al.* the *tert*-butyl substituted phenoxide Al[Salen] ligand was used as the catalyst and within 18 hrs, 92 %

conversion was achieved and the resulting polymer had a dispersity of 1.14.[91] This work has led to more research in the homopolymerisation and copolymerisation of poly(hydroxyalkanoates).

### 2.1.4. Poly(hydroxyalkanoates) (PHAs)

Poly(hydroxyalkanoates) (PHAs) are a class of aliphatic polyesters that are synthesised in nature by microorganisms as an energy store.[92] These bio-polymers have had increased interest due to their renewability, biocompatibility and biodegradability as single use plastics and in biomedical applications.[93] Poly((R)3-hydroxybutyrate) is the most explored PHA, it is a hydrophobic, high crystalline, thermoplastic which like all PHA is found in its R isomer due to enzymatic synthesis (Figure 2.8). Poly(3-hydroxybutyrate) can be formed through the ROP of butyrolactone however the synthesis of this monomer has been challenging due to the inherent ring strain present in four-membered rings. A method that has been used to produce such rings is the carbonylation of epoxides.

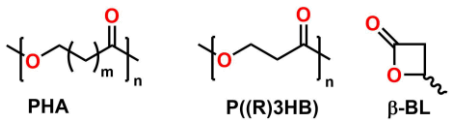


*Figure 2.8 Poly(hydroxyalkanoate (PHA, left), poly((R)3-hydroxybutyrate) (P((R)3HB), middle), β-butyrolactone (β-BL, right).*

### 2.1.5. Carbonylations of epoxides to β-lactones

Aider *et al.* were first to report the cabonylation propylene oxide into β-lactones by using a Lewis acid and $PPNCo(CO)_4$ which gave moderate yields (50 % - 80 %).[94] However it is known that carbonylations can give rise to competing side reactions such as regioselective isomers, ketones and polyesters.[95,96] Coates and coworkers provided a synthetic route in which lewis acid – base pairs could catalyse the carbonylation (Figure 2.9).[96] The mechanism shows that the metal coordinates to the epoxide to allow the $[Co(CO)_4]^-$ to nucleophilically attack the less hindered carbon. Next, the epoxide ring opens, and the carbon monoxide inserts into the C-Co bond. Finally, the ring closes and the β-lactone is expelled, and the catalyst is regenerated.

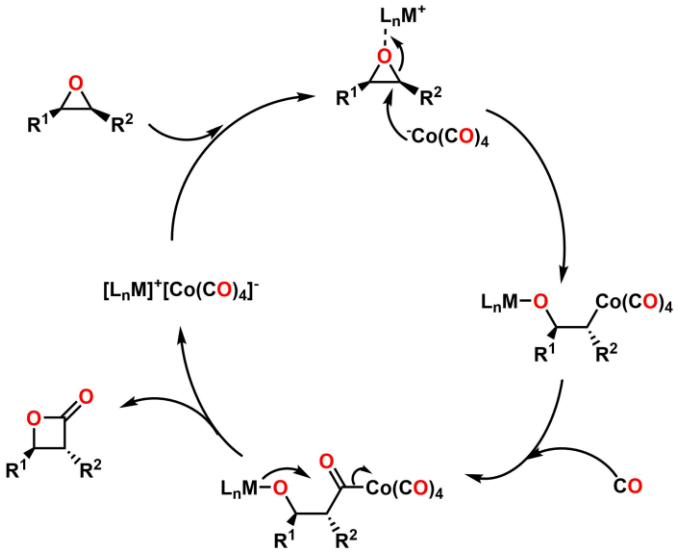


*Figure 2.9 The catalytic cycle for carbonylation of epoxides.*

Coates and *et al.* synthesised two catalysts a chromium porphyrin and an aluminium salen complex (Figure 2.10). The carbonylation of epoxides using catalyst **4** gave conversions above 99 % for most epoxides using 62 bar of CO. While catalyst **3** gave poor conversions (50 %) and showed evidence of side reactions such as isomerization to ketones.[96] Attempts were made to use these catalysts to carbonylate bicyclic epoxides, however, neither yielded much β-lactone.

The chromium porphyrin complex was modified (catalyst **5**) which caused the rate of carbonylation to increase. This was attributed to the complex being more soluble than catalyst **4**. Catalyst **5** was able to carbonylate bicyclic epoxides and epoxides containing amines and silyl ethers.[97] As well as this the pressure of CO could be reduced to 14 bar without the rate of carbonylation decreasing.[97] Coates and coworkers further built on this work by introducing a catalyst which can carbonylate epoxides at 1.01 bar (catalyst **6**), which makes the formation of β-lactones more accessible. The chromium[salph] complex was able to carbonylate various epoxides to 99% conversion without the ketone side product at 7 bar of CO. At 1.01 bar, the epoxide conversion was high (greater than 98 %), however, there was up to 15 % ketone in the isolated product.[74] Coates *et al.* have expanded the range of β –lactones available from the carbonylation of epoxides, which in turn has allowed for a library of PHAs to be synthesised.

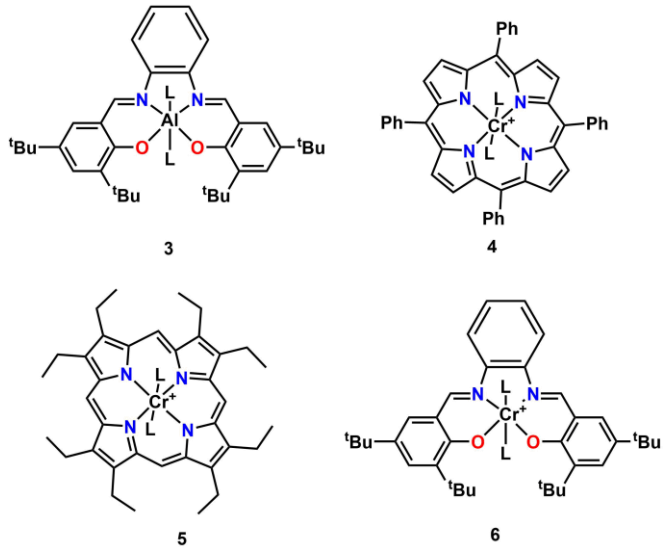


*Figure 2.10 Lewis acid carboxylation catalysts. **3** aluminium(salph), **4** and **5** chromium porphyrins, **6** chromium(salph).*

### 2.1.6. Ring opening polymerisation and modification of β-lactones

The ring opening polymerisation of β-lactones has increased in interest due to the need to form more biodegradable plastics. Shaver *et al.* have demonstrated the homopolymerisation of β-butyrolactone using catalyst **2C**.[91] The group investigated this further by homopolymerising a series of lactones, β-butyrolactone (R = Me, βBL), β-valerolactone (R = Et, βVL), β-heptanolactone (R = $^{n}$Bu, βHPL), and β-tridecalactone (R= $C_{10}H_{21}$, βTDL). It was found that increasing the alkyl chain from 2 (βVL) to 10 (βTDL) increased the reaction time, from 16 hours to 40 hours at 85 $^{o}$C, to achieve high monomer conversions. However, low conversion (less than 20 %) was seen when tin octoate was used at 120 $^{O}$C. βBL, βVL, βHPL were also used in the copolymerisation of lactide, to form a ABA triblock copolymer (Figure 2. 11). Homopolymers of poly(lactide) usually are brittle and have poor mechanical properties, however, by copolymerising lactide these properties can be improved and make the polymers more viable for commercial use. Shaver and coworkers saw that the elastomeric properties of PLA was greatly improved when the β-lactones were incorporated.[98]

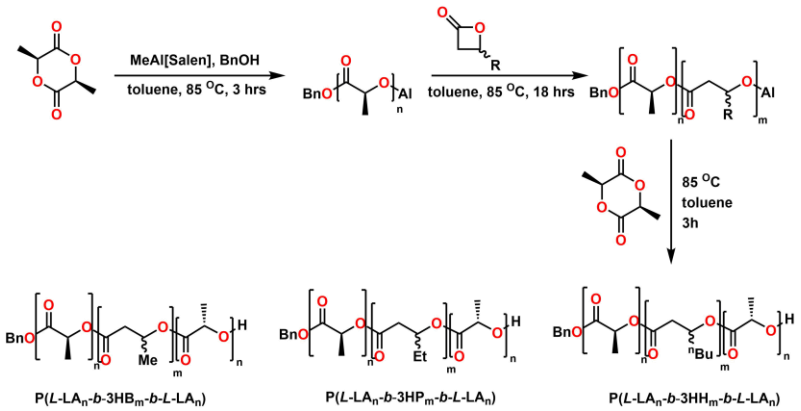


*Figure 2. 11 The action scheme for the formation of ABA poly(lactide-β lactone-lactide) triblock copolymers.*

Shaver *et al.* expanded the scope of β-lactones by using them in copolymerisations. However, the hydrophobic nature of PHAs limits their use in the biomedical field. Poly(benzyl β-malolactonate) (PMLABe) was thought to be able to provide a pathway to produce water soluble PHAs. The benzyl group can be hydrogenated to form poly(malic acid) (PMLA). However only carboxylic acids can be incorporated when using MLABe as a monomer.

Through Coates and coworkers research the carbonylation of olefin containing epoxides have been successfully synthesised (Figure 2.12).[97] β-heptenolactone (βHL) can be synthesised *via* the carbonylation of 1,2-epoxy-5-hexene. The olefin moiety offers a plethora of pre- and post-polymerisation functionalisations that would make the use of β-lactones viable in many applications.

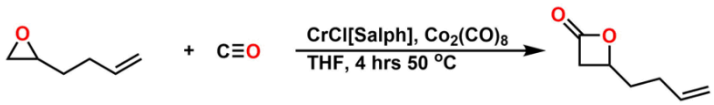


*Figure 2.12 A schematic for the carbonylation of βHL.*

Guillaume *et al.* investigated the hydroboration of βHL pre- and post- ROP (Figure 2.13). It was found that the hydroboration of βHL was successful, however, the polymerisation did not proceed. It was assumed that the polar boronate group inhibited the Rh ROP catalyst.[99] However, the hydroboration was successful after polymerisation using the same Rh catalyst used in the pre-polymerisation functionalisation.

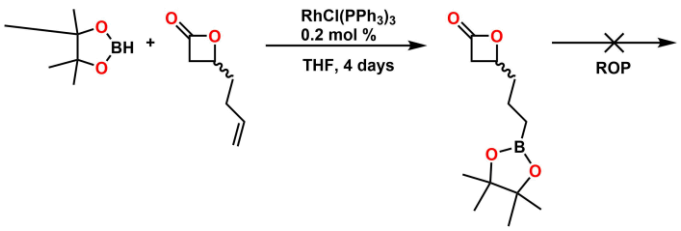


*Figure 2.13 The hydroboration of βHL.*

Sinclair *et al.* have demonstrated that post polymerisation cross metathesis is also possible when type 1, type 2 and type 3 olefin are used.[100] This has led to the incorporation of epoxides, hydroxyl and β-lactones as pendant groups in PHAs homo and block copolymers. Raycraft *et al.* has used click chemistry in the post polymerisation functionalisation of PEG-*b*-PHEL which was used to incorporate a carboxylic acid moiety. In this work the hydrophilic mass fractions were calculated for PEG-*b*-PHEL in order to predict the morphology of the copolymers when self-assembled (Equation 2. 2).[101]

$$f = \frac{M_r\ PEG}{M_r\ copolymer}$$

*Equation 2. 2* Hydrophilic mass fraction, f, the equation for a PEGylated block copolymer.

It was found that $PEG_{45}$-*b*-$PHEL_{45}$ formed micelles and this polymer was used in the thiol-ene click reactions (Figure 2.1). The partial incorporation of three thiols was successful, and the changed in self-assembled morphology was investigated.

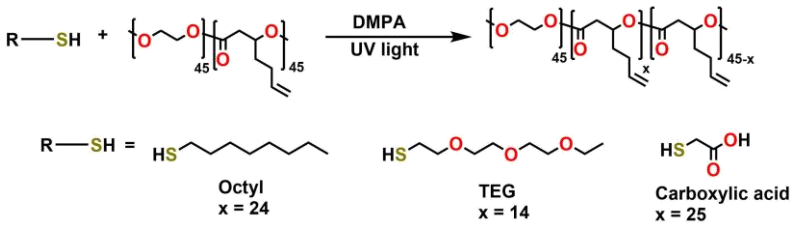


*Figure 2.14 The thiol-ene click reaction of three thiols with $PEG_{45}$-b-$PHEL_{45}$. Reproduced from Raycraft et al.*[101]

It was seen that the inclusion of the octyl thiol decreased the hydrophilic mass fraction from 0.28 – 0.19, as a result, the morphology changed from micelles to worms.[101] The carboxylic acid functionalised $PEG_{45}$-*b*-$PHEL_{45}$ was esterified with anticancer drug paclitaxel (PTX, Figure 2.15). The motivation behind this was to increase retention of hydrophobic drugs within the body, however, due to the bulkiness of PTX complete incorporation was not possible. Furthermore, the hydrophobic nature meant the hydrophilic mass fraction was extremely low resulting in aggregation of the block copolymer rather than self-assembly.

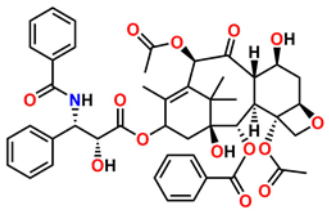

*Figure 2.15 The structure of paclitaxel.*

In this chapter, **PH**, (PEG-*b*-PHEL) was synthesised by ROP (Figure 2.16) and then functionalised with thiol-ene click reactions to incorporate carboxylic acid moieties into the polymer. The copolymer also underwent hydrophosphorylation using $Mn(OAc)_2$ as a catalyst. The PEG portion of the block copolymer was selected for its biocompatibility with the body and its alcohol end-group. B-6-heptenolactone (βHEL) was chosen because it could be easily functionalised with the methods described above and ε-caprolactone (ε-CL) was chosen as it has been previously used in biomedical applications and it produces a hydrophobic polymer.[102] A PEG-*b*-PCL macrointitator was synthesised to be used in the polymerisation of βHL. Phosphinic and carboxylic acid moieties were targeted because it was found bother bind to HAP, thus polymers containing these were synthesised in order to explore their ability to nucleate HAP which is the main component in enamel.[34,61]

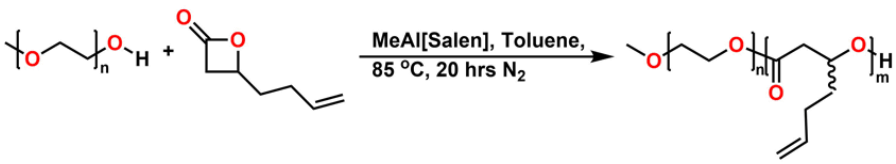


*Figure 2.16 A schematic of the synthesis of **PH** (PEG-b-PHEL).*

## 2.2. Synthesis of PEG-*b*-PHEL

The synthesis of PEG-*b*-PHEL is analogous to the polymerisation method reported in the work by Raycraft *et al* (Figure 2.16).[101] However, in this thesis the DP of PEG monomethyl ether was varied (Table 2. 1).

*Table 2. 1 ROP of βHL using a PEG-OH macroinitiator at 85 °C. Here the targert $M_{n(Theo)}$, $M_{n(NMR)}$ and $M_{n(GPC)}$ are shown.*

| Entry | PEG units | βHL units | Time / hrs | [a]βHL conversion / % | PEG: βHL Ratio | Target $M_{n(Theo)}$ / g $mol^{-1}$ | [a]$M_{n(NMR)}$ / g $mol^{-1}$ | [b]$M_{n(GPC)}$ / g $mol^{-1}$ | [b]Đ |
|---|---|---|---|---|---|---|---|---|---|
| **PH1** | 141 | 20 | 20 | 95 | 141: 25 | 7500 | 9300 | 29700 | 1.30 |
| **PH2** | 141 | 13 | 24 | 93 | 141:9 | 6600 | 7300 | 22400 | 1.34 |
| **PH3** | 143 | 75 | 24 | 98 | 143: 50 | 14500 | 12500 | 31600 | 1.38 |
| **PH4** | 47 | 21 | 22 | 98 | 47: 15 | 4600 | 4000 | 14900 | 1.21 |
| **PH5** | 46 | 10 | 22 | 97 | 46: 9 | 3200 | 3200 | 12500 | 1.18 |
| **PH6** | 147 | 15 | 24 | 96 | 147: 14 | 6900 | 8300 | 26800 | 1.26 |
| **PH7** | 142 | 25 | 24 | 97 | 142: 25 | 8200 | 9400 | 26400 | 1.27 |

Conditions: Toluene was used as a solvent. [M]:[I]:[Al]:[Tol] = y:1:1:357,[a]conversion and $M_{n(NMR)}$ were determined by $^1$H NMR, [b]determined by DMF GPC relative to PMMA standards through conventional calibration

The results show that increasing the DP of PEG from 48 to 140 has little effect on the Đ or βHL conversion. The GPC $M_n$ increases in the same manner as the $M_n$ obtained from $^1$H NMR and the $M_{n(NMR)}$ is between 30 – 40 % of the $M_n$ obtained from the GPC. The $Mn_{(GPC)}$ is much larger than the $M_n$ obtained from the NMR, this is due to the polymer having a different hydrodynamic volume to the polymer standards. In order to determine the 'true' $M_n$ of the synthesise polymers a correction factor would need to be use, however these are hard to calculate for block copolymers. Furthermore in the GPC trace the peak goes into a negative refractive index value, which would suggest that polymer could have formed some aggregates (Figure 2.18). To ensure that two homopolymers have not been formed $^1$H DOSY NMR was employed. It can be seen with **PH7** that there is only one signal present in the spectrum indicating that only one species is in the sample (Figure 2.17). This is emphasised by the GPC trace, as only one peak is present (Figure 2.18).

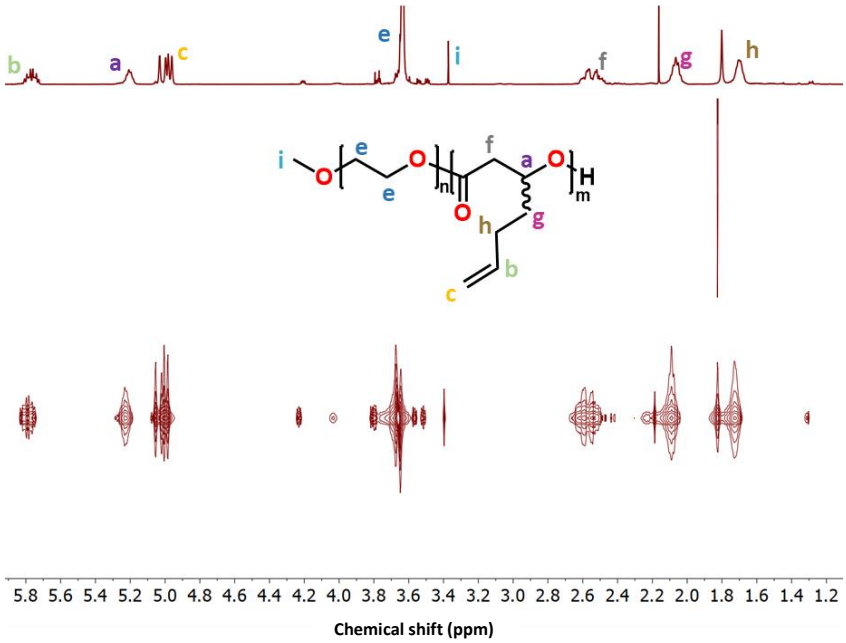


*Figure 2.17 $^{1}$H DOSY NMR of **PH7** which proton environments highlighted.*

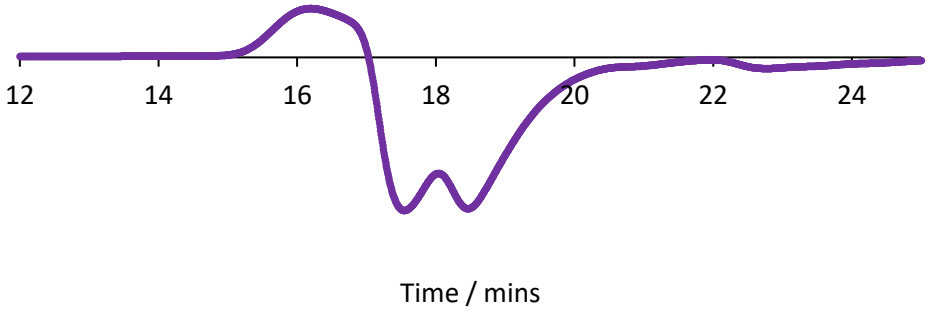


*Figure 2.18 GPC trace of **PH7**.*

The hydrophilic fractions were calculated for each diblock, which showed that the majority of the polymers would form micelles as the hydrophilic mass fraction is larger than 0.5 (Table 2.2).

*Table 2.2* The hydrophilic mass fraction, f, for each polymer.

| Entry | Hydrophilic mass fraction, $f_x$ | Cmc / mg cm$^{-3}$ |
|---|---|---|
| **PH1** | 0.66 | - |
| **PH2** | 0.68 | - |
| **PH3** | 0.50 | - |
| **PH4** | 0.51 | - |
| **PH5** | 0.63 | - |
| **PH6** | 0.78 | - |
| **PH7** | 0.66 | 0.00133 |

The formation of latexes was attempted for each polymer by the solvent co-evaporation method in which the copolymers were dissolved in DCM and mixed with water then the DCM was evaporated. This is a different preparation method to Raycraft *et al.* and it is known that the different methods result in different particle sizes and dispersities.[50] The cmcs were calculated by using the fluorescence probe method in which pyrene was used as the probe. Pyrene is doped

into the latex and above the cmc it migrates into the hydrophobic core of the micelle. This is shown by the evolution of a peak at 383 nm in the emission spectrum (Figure 2.19). Above the cmc the ratio between $I_{383}/I_{373}$, ($I_{373}$ is when the pyrene is in a hydrophilic environment) increases with increased micellation. This can be plotted against Ln[conc], and if two distinct data sets can be observed, then a cmc can be determined as the point at which these data sets intersect.

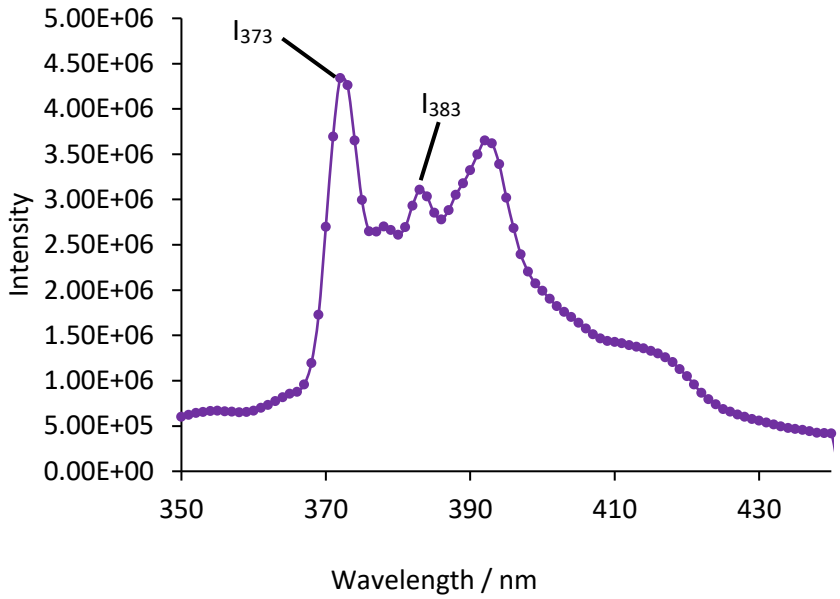


*Figure 2.19 The pyrene emission spectrum when doped into 7.22 x10$^{-2}$ mg cm$^{-3}$ of **PH7**.*

The cmc value could only be determined for **PH7** (Figure 2.20A). It was found that many of the copolymers underwent aggregation and precipitated out upon the evaporation of the DCM. However, in the case of **PH6** the block copolymer had a high hydrophilic fraction. Yet, self-assembly did not occur which is evident from the cmc graph in which there was no order in the data set (Figure 2.20B). In the case of **PH6** where the hydrophilic fraction was large and the cause of lack of assembly from the copolymer.

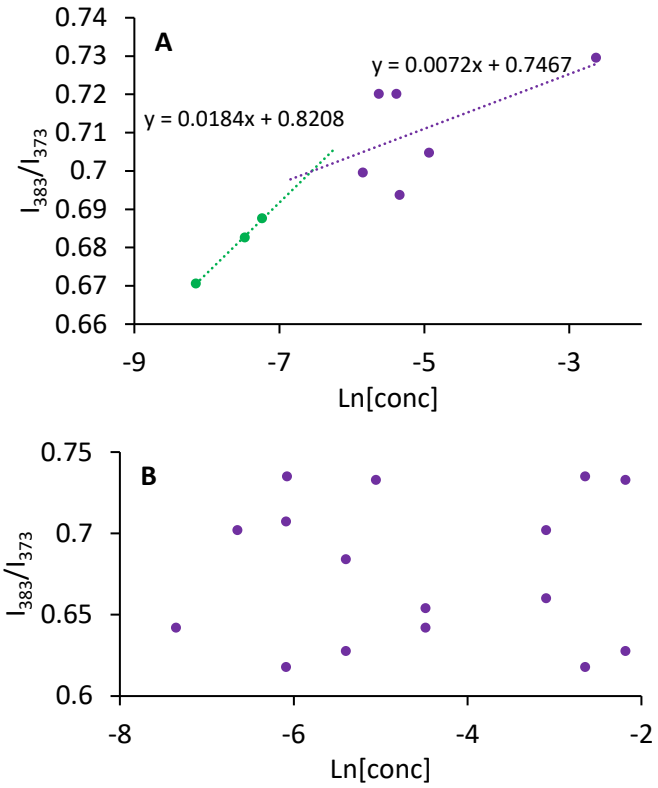


*Figure 2.20 The cmc graphs for **PH7** (A) and **PH6** (B).*

## 2.3. Synthesis of PEG-*b*-PCL

A triblock copolymer was synthesised using PCL as the hydrophobic segment. Polymerisation between PEG-OH and ε-CL acted as a macroinitiator for the polymerisation of βHL (Figure 2.21).

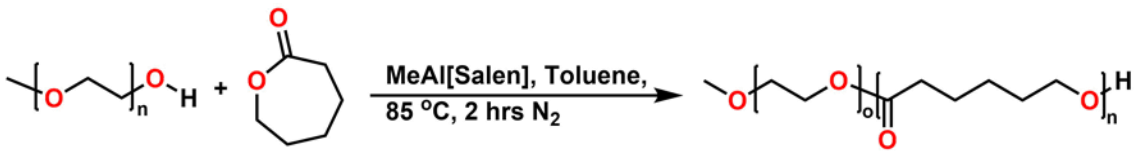


*Figure 2.21 A schematic for the ring opening polymerisation of CL using a PEG macroinitiator.*

ε-CL was chosen as the monomer as it has biocompatibility and has a similar number of carbons to that of βHL. So when the PHEL is fully functionalised there will still be a hydrophobic segment in the resulting triblock copolymer. For the polymerisations between PEG-OH and ε-CL the reaction time was reduced to three hours to avoid transesterification of the resultant block copolymers (Table 2 3).

*Table 2 3 R*OP of εCL using a PEG-OH macroinitiator at 85 °C for three hours.

| Entry | PEG units | εCL units | [a]εCL conversion / % | PEG: PCL | Target $M_{n(Theo)}$ / g mol$^{-1}$ | [a]$M_{n(NMR)}$ / g mol$^{-1}$ | [b]$M_{n(GPC)}$ / g mol$^{-1}$ | [b]Đ |
|---|---|---|---|---|---|---|---|---|
| **PC1** | 242 | 90 | 98 | 242.3: 102 | 20300 | 22300 | 6308 | 1.40 |
| **PC2** | 143 | 80 | 97 | 143.2: 98 | 14000 | 17500 | 30300 | 1.73 |
| **PC3** | 133 | 40 | 96 | 133: 44 | 9600 | 10900 | 33000 | 1.50 |
| **PC4** | 52 | 25 | 94 | 52: 27 | 4800 | 5400 | [c]12900 | [c]1.63 |

Conditions: Toluene was used as a solvent and polymerisation were carried out for 3 hrs [M]:[I]:[Al]:[Tol] = y:1:1:357,[a]conversion and $M_{n(NMR)}$ were determined by $^1$H NMR, [b]determined by DMF GPC relative to PMMA standards through conventional calibration, [c]determine by $CHCl_3$ GPC

The polymerisation showed that the theoretical ratio matched the experimental results indicating a successful polymerisation. In the **PC** polymers there is no pattern between the $M_{n(NMR)}$ and the $M_{n(GPC)}$, as there was for the PEG-*b*-PHEL block copolymers. The hydrophilic mass fraction was calculated for this set of polymers and was found to be slightly lower than the PEG-*b*-PHEL block copolymers (Table 2.4).

Table 2.4 *The hydrophilic mass fraction, f, for each PEG-b-PCL.*

| Entry | $f_x$ value |
|---|---|
| **PC1** | 0.48 |
| **PC2** | 0.36 |
| **PC3** | 0.53 |
| **PC4** | 0.42 |

Savic *et al.* calculated of the hydrophilic mass fractions for various PEG-*b*-PCL diblock copolymers, between 20 % < *f* > 40 % vesicles would be obtained between 40 % < *f* > 50 % gave worms and above 50 % micelles were obtained (Figure 2.22).[103] According to Savic and co worker's research, **PC1** and **PC4** would have a worm morphology while **PC2** and **PC3** would form vesicles and micelles respectively. Unfortunately, with the solvent coevaporation method, precipitation of the copolymers was observed and the cmc of each polymer could not be determined.

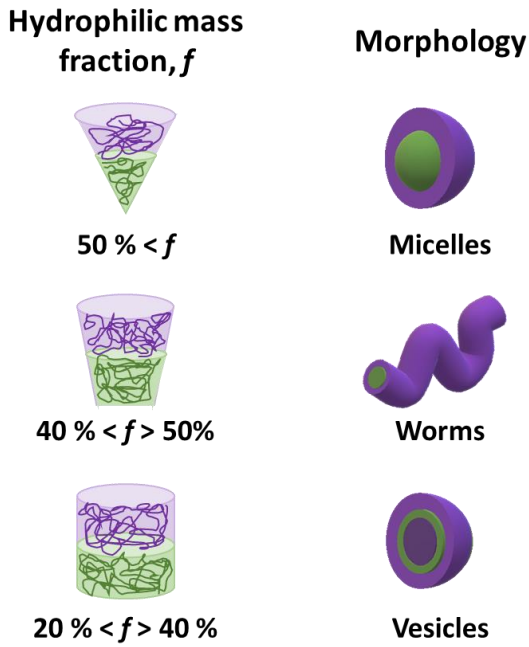


*Figure 2.22 The hydrophilic fraction morphologies as describe by Savic et al.[103]*

## 2.4. Synthesis of PEG-*b*-PCL-*b*-PHEL

The triblock copolymers were synthesised by using the diblocks synthesised from section 2.3 as a macroinitiator for the polymerisation of βHL (Figure 2.23).

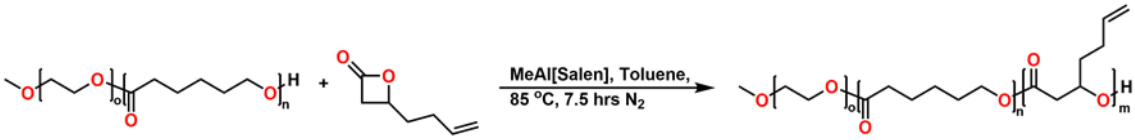


*Figure 2.23 A schematic for the ring opening polymerisation of βHL using a PEG-b-PCL macroinitiator.*

The polymerisations were carried out for 24 hours and the conversion of βHL was above 80 % for all polymerisations (Table 2.5).

Table 2.5 *ROP of βHL using a PEG-b-PCL macroinitiator at 85 °C for 24 hours.*

| Entry | Precursor | βHL units | [a]βHL conversion / % | PEG: PCL:PHEL | Target $M_{n(Theo)}$ / g mol$^{-1}$ | [a]$M_{n(NMR)}$ / g mol$^{-1}$ | [b]$M_{n(GPC)}$ / g mol$^{-1}$ | [b]Đ |
|---|---|---|---|---|---|---|---|---|
| [c]**PCH1** | **PC2** | 54 | 91 | 144 : 99 : 30 | 24300 | 21400 | 800<br>33100 | 1.26<br>1.61 |
| **PCH2** | **PC1** | 81 | 84 | 241 : 100 : 50 | 32500 | 28300 | 190400 | 1.42 |
| **PCH3** | **PC3** | 47 | 98 | 140 : 43 : 48 | 17200 | 17100 | 121400 | 1.40 |
| **PCH4** | **PC4** | 17 | - | 49 : 23 : 20 | 7200 | 7300 | 80900 | 1.31 |

Conditions: Toluene was used as a solvent and polymerisation were carried out for 22 hrs [M]:[I]:[Al]:[Tol] = y:1:1:357,[a]conversion and $M_{n(NMR)}$ were determined by $^1$H NMR, [b]determined by DMF GPC relative to PMMA standards through conventional calibration [c]Bimodal distribution

Here the theoretical ratio agrees with the experimental results and the conversion for βHL was above 80 % which suggests that the polymerisation was successful. However the conversion for **PCH4** could not be determined due to a solvent peak covering the $CH_2$ group of the lactone ring. The DP of PCL was unchanged from their precursors PEG-*b*-PCL which is a strong indication that transesterification did not occur. In addition, the dispersities remained close to that of the diblock copolymers indicating minimal transesterification.[104] However it is difficult to determine

if the triblock is undergoing transesterification as the common method to determine this is by using MALDI-TOF mass spectrometry. However due to the nature of the triblock, locating three different repeat units in the chromatogram would prove near on impossible. One method to determine if transesterification had occurred is using $^{13}C$ NMR. If there are multiple small peaks in the carbonyl region it would suggest that there are many different polymer block environments. Transesterification is known to be more prevalent at higher temperatures and in more concentrated reaction mixtures.[104] To explore this further a reaction condition scope would be useful in determining the best conditions for the triblock preparation.

The hydrophilic mass fraction was calculated for these polymers however like before many of the polymers macroprecipitated out with the exception of **PCH2** which has a PEG unit of 10600 g mol$^{-1}$, suggesting that a longer PEG chain helps with solvation (Table 2. 6).

*Table 2. 6 Hydrophilic mass fraction, $f_x$ of PEG-b-PCL-b-PHEL triblock polymers*

| Entry | Hydrophilic mass fraction, $f_x$ |
|---|---|
| **PCH1** | 0.26 |
| **PCH2** | 0.37 |
| **PCH3** | 0.36 |
| **PCH4** | 0.30 |

Fluorescence spectroscopy was used to determine the cmc of **PCH2**. The graph shows a linear line between 0.003 mg cm$^{-3}$ to 0.179 mg cm$^{-3}$ indicating that the polymer could undergo self-assembly (Figure 2.24). However, there is microprecipitation of the triblock copolymer at high concentrations and the polymer concentration is too low for the nucleating HAP. From the gradient of the line, it would indicate the cmc is below 0.003 mg cm$^{-3}$.

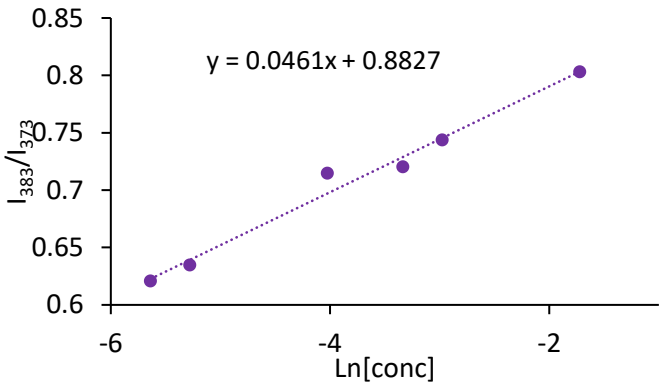


*Figure 2.24 The cmc graph for **PCH2.***

## 2.5. Functionalisation of PEG-b-PHEL and PEG-*b*-*PCL*

### 2.5.1. Thiol-ene click reactions

Functionalisation of PHEL has been researched extensively with hydroboration, thiol-ene click chemistry and using cross metathesis.[99,100] Here 3-Mercaptopropionic acid (MCPA) was used for the functionalisation of **PH2** (Figure 2.25).

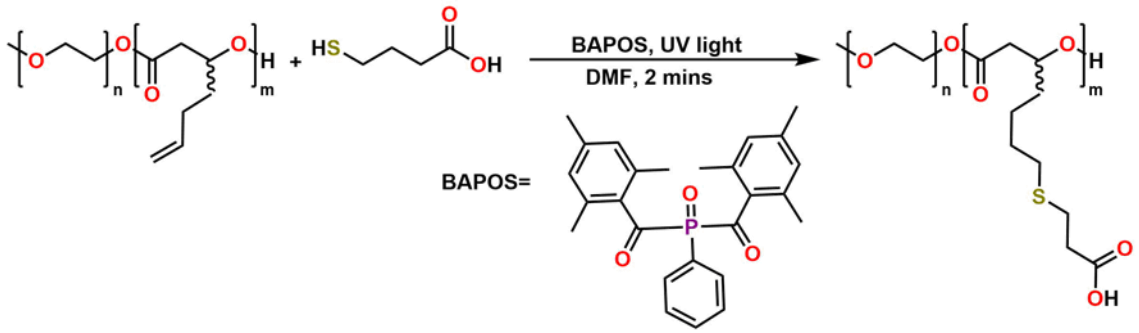


*Figure 2.25 A schematic showing the thiol-click reaction of PEG-b-PHEL.*

The sample was irradiated with UV light for 2 minutes, which was sufficient time to observe the disappearance of the alkene peaks in the $^{1}$H NMR spectrum (Figure 2.26). When comparing the IR spectrum of **PH2** and **PS1** there was a reduction in the peaks at 1738 cm$^{-1}$ and 1641 cm$^{-1}$ which represent the alkene peaks in PHEL (Figure 2.27).

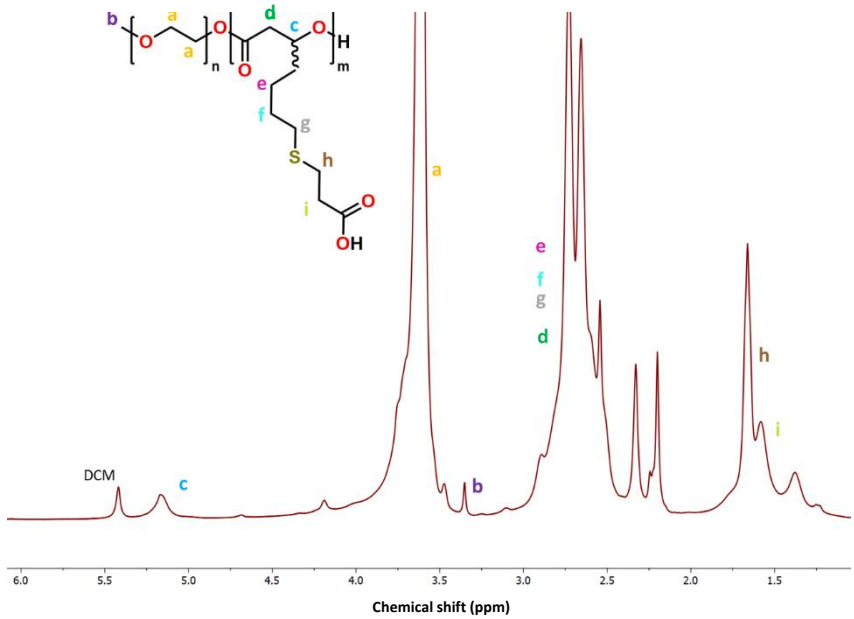


*Figure 2.26 An annotated NMR spectrum of **PS1.***

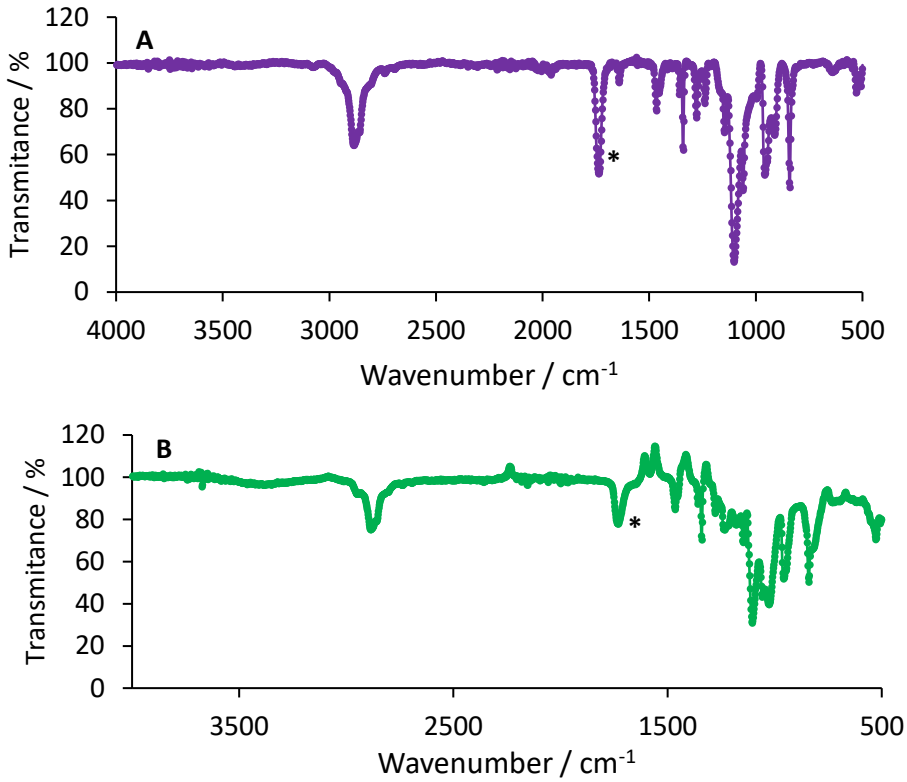


*Figure 2.27 IR spectra of **PH2** (A) and **PS1** (B). The asterisk represents the peak associated with the alkene moiety in PEG-b-PHEL.*

In Table 2.7, it can be seen that the dispersities has slightly increased upon functionalisation; this can be attributed to the carboxylic acid moieties interacting with the columns, this is also a phenomenon that Raycraft *et al.* encountered.[105] The hydrophilic mass fraction could not be calculated for this polymer due to the ionic nature of the carboxylic acid, as the group would also contribute to the hydrophilicity of the polymer.

*Table 2.7 A comparison between PH2 and PS1 after thiol-ene click functionalisation.*

| Exp | $^{a}M_{n(NMR)}$ / g mol$^{-1}$ | $^{b}M_{n(GPC)}$ / g mol$^{-1}$ | $^{b}Đ$ |
|---|---|---|---|
| **PH2** | 7300 | 22400 | 1.34 |
| **PS1** | 8300 | 16500 | 1.52 |

$^{a}M_{n(NMR)}$ were determined by $^{1}$H NMR, $^{b}$determined by DMF GPC relative to PMMA standards through conventional calibration

The cmc was determined for **PS1** and was not reached before 2 mg cm$^{-3}$, which is indicated by the shallow line (Figure 2.28). The **PS** series would be expected to have high cmc value due to the lack of a hydrophobic core. It is well known that a hydrophobic group helps stability the of the self-assemble structure but is also the driving force for the assembly.

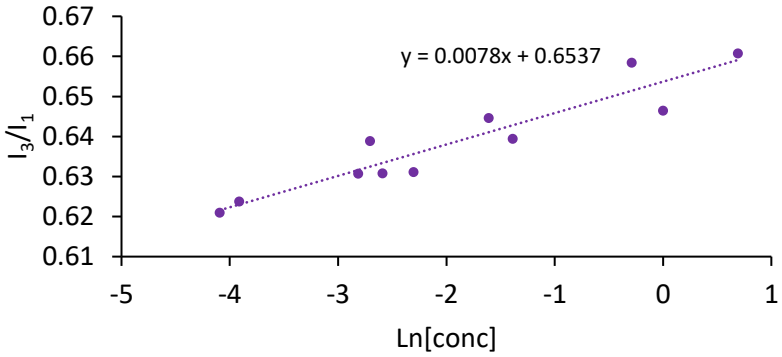


*Figure 2.28 The cmc graph for **PS1.***

When working with the thioglycolic acid, Raycraft *et al.* did not functionalise all the PHEL fully, which left a random hydrophobic segment that would have helped self-assembly of the polymer. In this thesis complete functionalisation was desired to ensure there were no reactive groups in the polymer that could cause complications within the body.

The PEG-*b*-PCL-*b*-PHEL triblock polymers were also functionalised with thiol-ene click chemistry. The PCL block in the centre of the copolymer should help drive the formation of the assembled structures. The polymers were successfully functionalised is supported by the reduction of the alkene peaks in the $^{1}$H NMR (Figure 2.29).

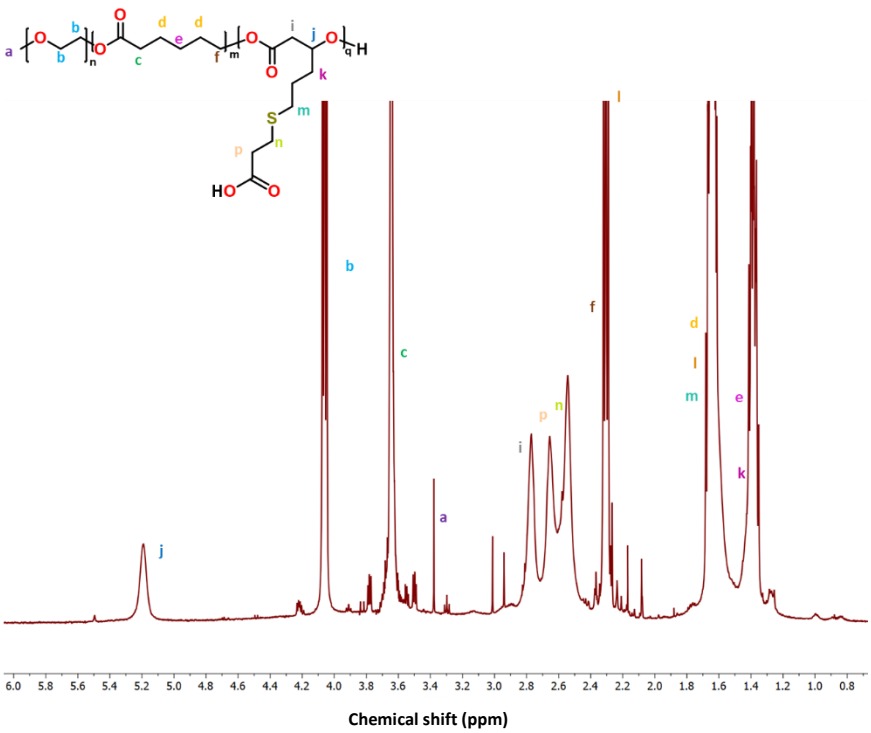


*Figure 2.29 The annotated NMR spectrum of **PCS2.***

The general trend from the GPC data is that the $M_{n(NMR)}$ and $M_{n(GPC)}$ has increased with the addition of the thiol and in the dispersities have either decreased or not changed (Table 2.8). However, in the case of **PCS1** the triblock GPC trace became bimodal, this could indicate a of self-assembly inside the column. There is no significant trend when the $M_{n(NMR)}$ and $M_{n(GPC)}$ like in the previous diblock copolymers. However, it should be noted that the larger dispersity values tend to be paired with the polymers that have a larger acidic thiol segment.

*Table 2.8 The $M_n$ and D of the PEG-b-PCL-PHEL(S) polymers compared with their predecessors.*

| Entry | [a]$M_{n(NMR)}$ / g mol$^{-1}$ | [b]$M_{n(GPC)}$ / g mol$^{-1}$ | [b]Đ |
|---|---|---|---|
| **PCH1** | 21400 | 33100 | 1.61 |
| **PCS1** | 24500 | 150000 | 1.25 |
| | | 20900 | 1.38 |
| **PCH2** | 28300 | 190400 | 1.42 |
| **PCS2** | 33700 | 1057600 | 1.19 |
| **PCS$_{ISO}$** | 33800 | 891400 | 1.22 |
| **PCH3** | 17100 | 121400 | 1.40 |
| **PCS3** | 21000 | 127300 | 1.42 |

[a]$M_{n(NMR)}$ were determined by $^1$H NMR, [b]determined by DMF GPC relative to PMMA standards through conventional calibration

Triblock **PCS$_{ISO}$** was functionalised with MCiPA rather than MCPA to investigate if a change in isomer would give a substantial change in cmc. The $^1$H NMR spectrum of **PCS$_{ISO}$** is similar to that of the other PEG-*b*-PCL-PHEL(S), except a multiplet appears at 3.40 ppm (Figure 2.30).

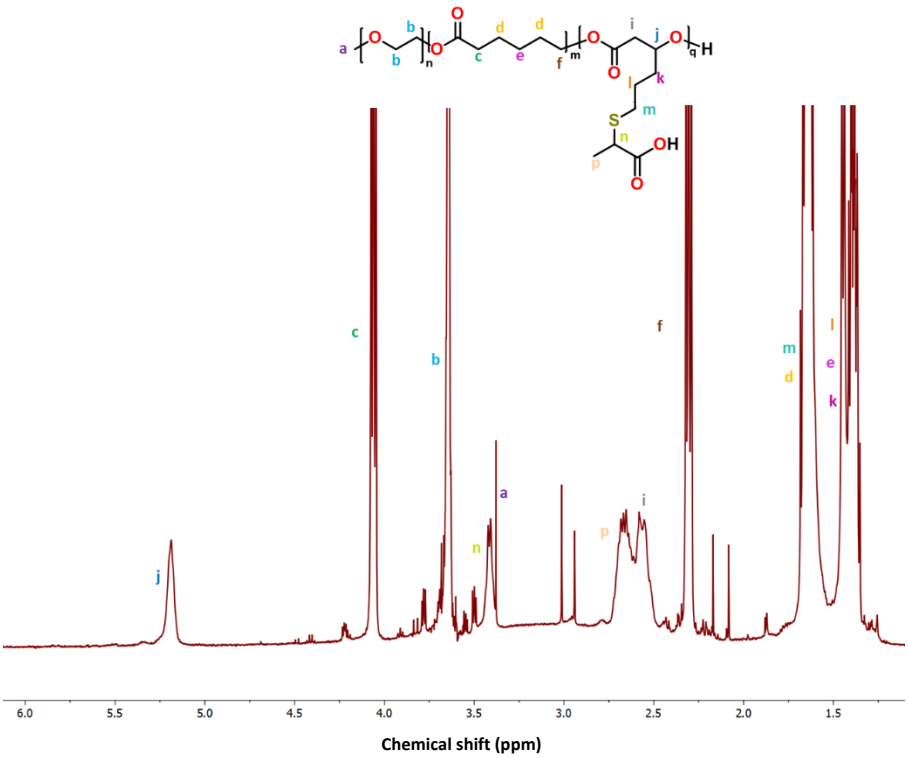


*Figure 2.30 An annotated $^1$H spectrum of **PCS$_{ISO}$**.*

The cmc determination was attempted for **PCS1, PCS2** and **PCS$_{ISO}$**. For **PCS1** the cmc could not be determined as the randomness of the data set suggest that this polymer cannot self-assemble (Figure 2.31A). However for **PCS$_{ISO}$** a linear relationship can be observed between the $I_{383}/I_{373}$ and Ln[conc]. The gradient of the graph would suggest that the triblock is self-assembled at these concentrations (Figure 2.31B). This could be confirmed with electron microscopy to observe the polymer morphology. Unfortunately, **PCS2** underwent macroprecipitation and as a result fluorescence spectroscopy could not be used to determine the cmc.

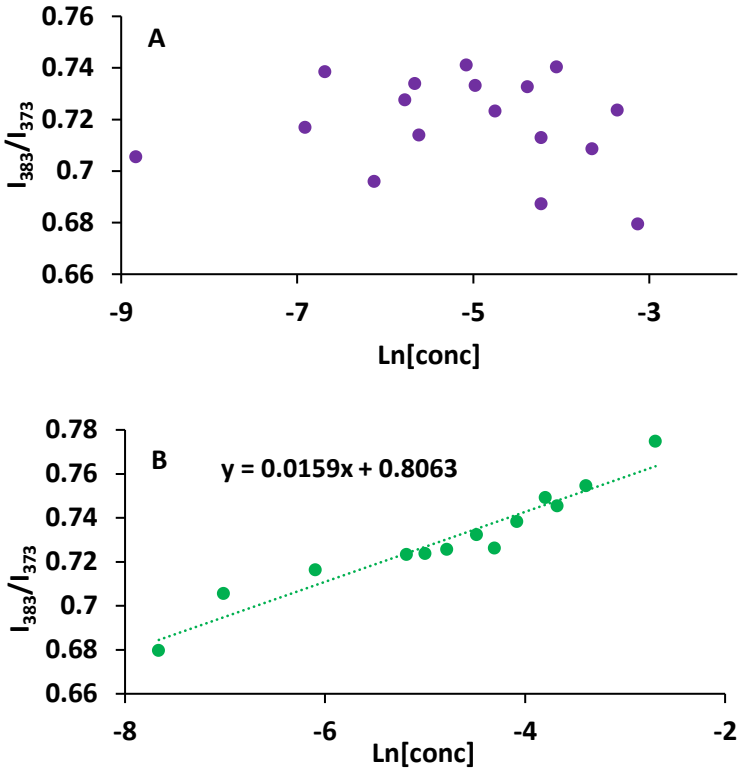


*Figure 2.31 The cmc graphs for **PCS1** (A) and **PCS$_{ISO}$** (B)*

### 2.5.2. Hydrophosphorylation

The other functionalisation that was explored in this chapter was incorporating a phosphinic acid into the polymer. It has been discovered that polymers containing phosphinic groups have a higher affinity to binding to HAP.[34] The conventional way of incorporating phosphorus unit into a compound is the Michaelis–Arbuzov reaction in which a trialkyl phosphite is reacted with an alkyl halide at high temperatures (Figure 2.32).[106] The disadvantages with this reaction is the use of toxic alkyl halides and this reaction does not allow for addition across a double bond.

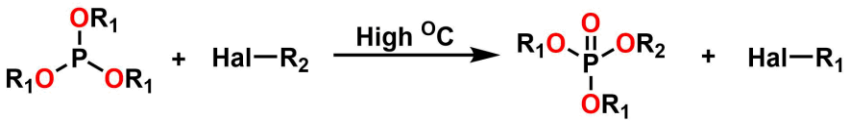


*Figure 2.32 The schematic of an example Michaelis-Arbuzov reaction.*

Phosphorylation across an alkene has been largely investigated using a phosphonate and thermal initiators such as AIBN or peroxides at high temperatures.[107,108] These conditions could potentially cause an issue as the PHEL as the units could undergo cross linking between the chains. In small molecule synthesis triethyl borane has been used at room temperature and has had yields as high as 95 %.[109] In this chapter, Mn(II)$(OAc)_2$ was chosen as a catalyst for hydrophosphorylation. Tayama *et al.* investigated the generation of phosphorous radicals through the one-electron oxidation of Mn(II)$(OAc)_2$ with diethyl phosphonate.[110] The results showed reasonable yields and the phosphonate tended to be added to the least substituted carbon of the alkene.[110] Mn(II)$(OAc)_2$ was added to a neat solution of dimethyl phosphonate and the polymer and then stirred for 1.5 hours at 90 °C (Figure 2.33).

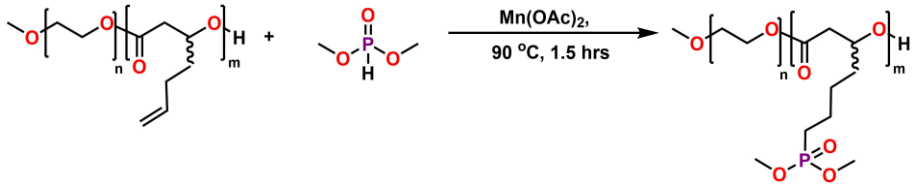


*Figure 2.33 Schematic for the hydrophosphorylation of PEG-b-PHEL.*

It was expected that the elevated temperature would not cause crosslinking between the PHEL blocks in the reaction with $Mn(OAc)_2$ as it lacked a thermal initiator. **PH6** and **PH7** were used in the hydrophosphorylation and it can be seen by $^{1}H$ NMR spectra that the vinyl signals have reduced, moreover in the $^{31}P$ NMR spectra a signal at 34 ppm can be observed which is indicative of the addition of the phosphonate (Figure 2.34).

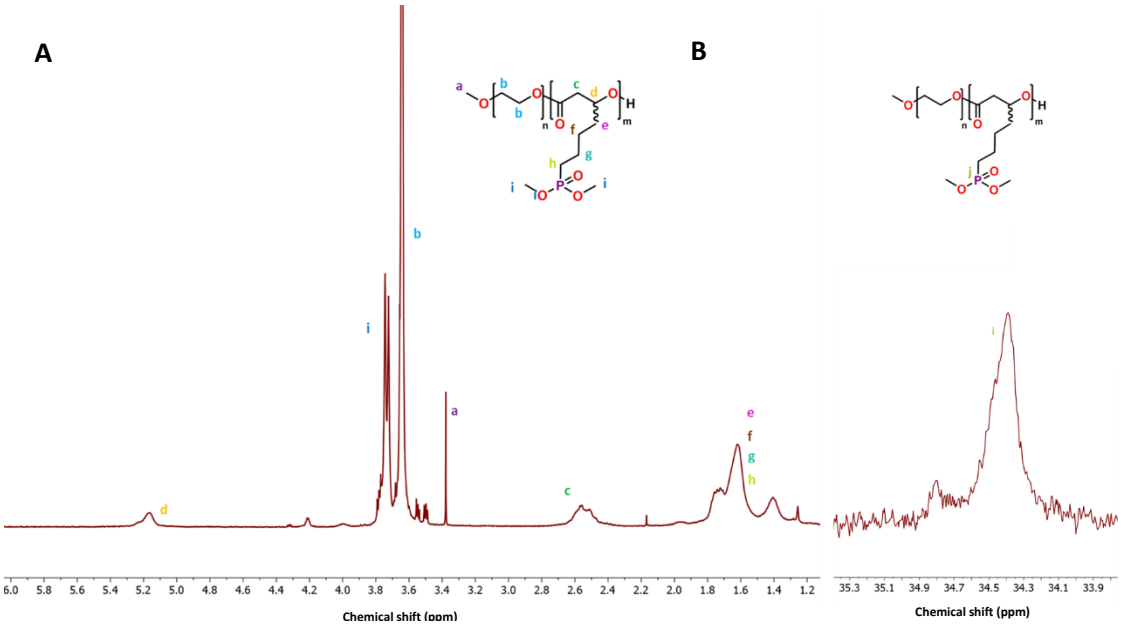


*Figure 2.34 The $^{1}H$ (A) and $^{31}P$ (B) NMR spectra of **PM1.***

The IR spectrum of **PM1** shows that there is an appearance of another peak around 1681 $cm^{-1}$ which is indicative of the P=O bond (Figure 2.35).

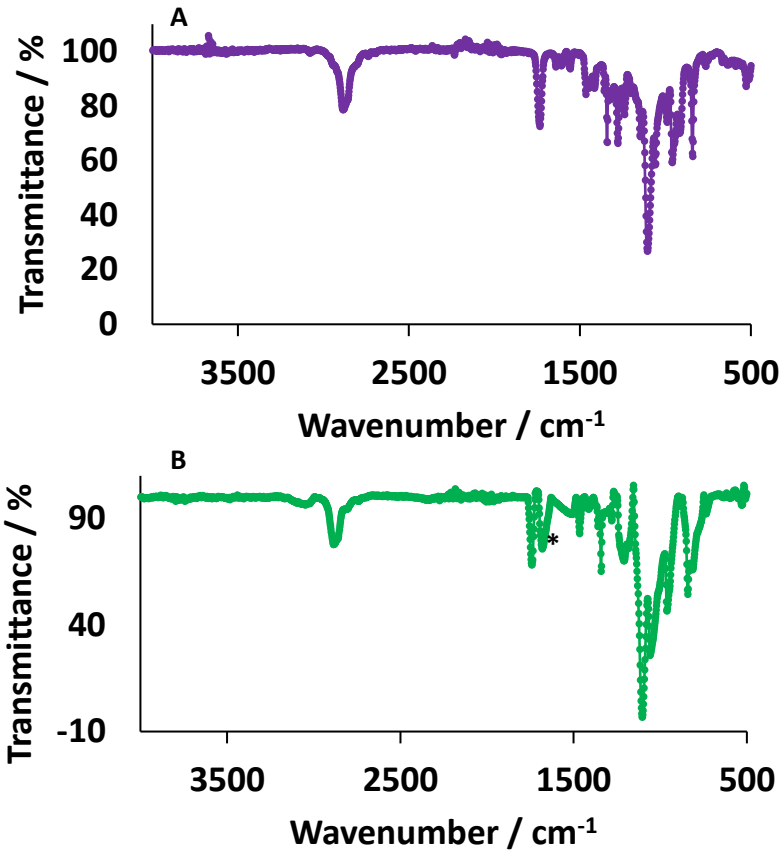


*Figure 2.35 IR spectrum of **PH6** (A) and **PM1** (B), the asterisk indicates the P=O signal.*

The $M_{n(NMR)}$ has increased upon the addition of the dimethyl phosphate which is to be expected. However, the $M_{n(GPC)}$ has decreased upon addition. It is known that phosphates interact with the GPC in DMF, the same phenomena can be expected for these polymers (Table 2.9).[111]

*Table 2.9* Shows the comparison of data of *PEG-b-PHEL*(P) polymers and their predecessors.

| Entry | $^{a}M_{n(NMR)}$ / g mol$^{-1}$ | $^{b}M_{n(GPC)}$ / g mol$^{-1}$ | $^{b}Đ$ |
|---|---|---|---|
| **PH6** | 8300 | 26800 | 1.26 |
| **PM1** | 9800 | 23100 | 1.46 |
| **PH7** | 9400 | 26400 | 1.26 |
| **PM2** | 12000 | 26400 | 1.68 |

,$^{a}M_{n(NMR)}$ were determined by $^{1}$H NMR, $^{b}$Determined by DMF GPC relative to PMMA standards through conventional calibration

The dispersity has increased with functionalisation, the main difference between **PM1** and **PM2** is that the latter polymer has 10 more PHEL units. This increase in dispersity attributed to an increase in steric bulk around the polymer, this was also seen in Raycraft *et al.'s* work when the PEG-PHEL was functionalised with a hydrophobic drug.[101]

Unlike the polymers mentioned in section 2.5.1 the hydrophilic mass fraction can be calculated, and it was 0.66 for **PM1** and 0.54 for **PM2**. Fluorescence spectroscopy was used to determine the cmc for **PM1** however similar to the case of **PS1** the data shows complete randomness indicating the polymer does not self-assemble. This is due to there not being a sufficient hydrophobic core in the block copolymer (Figure 2.36). As a result, it was decided not to deprotect the phosphonate.

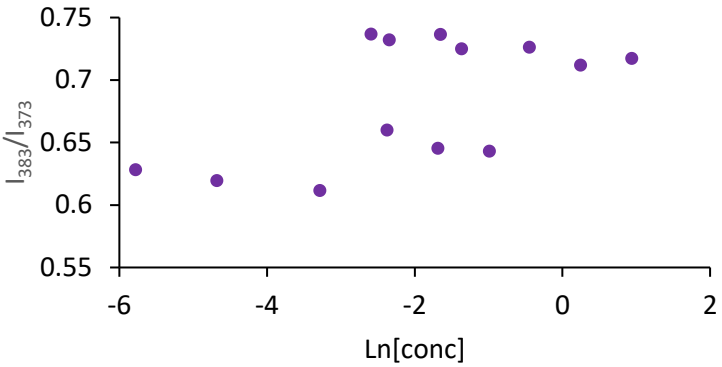


*Figure 2.36 The cmc graph of **PM1.***

The same hydrophosphorylation conditions were used for PEG-*b*-PCL-*b*-PHEL (**PCH2**), the $^{1}$H NMR spectrum confirms complete functionalisation with the reduction of the vinyl signals and the appearance of the doublet at 3.73 ppm due to C**H$_3$**-O-P from the phosphonate (Figure 2.37).

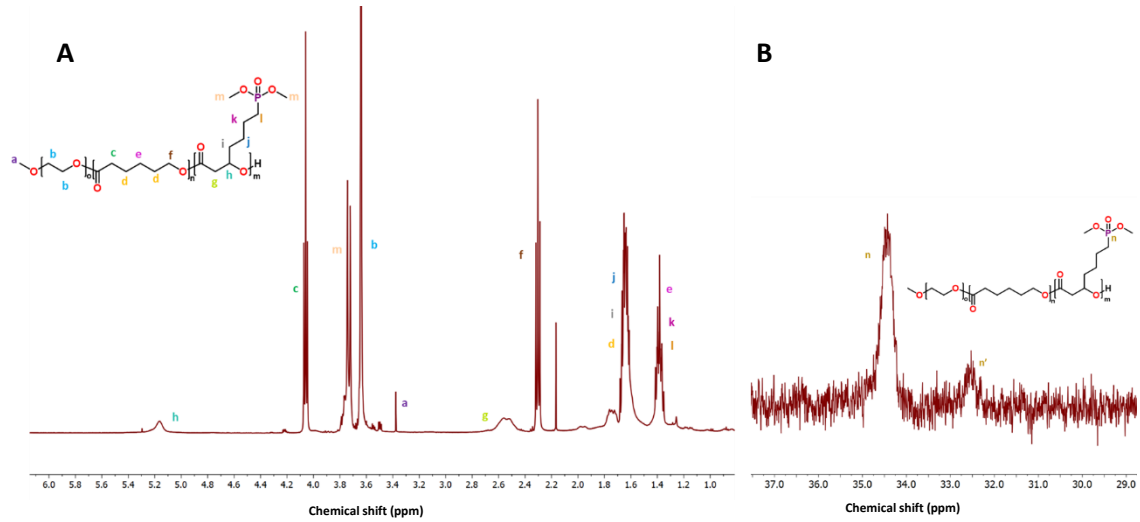


*Figure 2.37 The $^{1}$H (A) and $^{31}$P (B) NMR spectra of **PCM1.***

The $^{31}$P NMR also shows a peak **n'** which is most likely an isomer of the phosphorous moiety. The results from the GPC shows that the dispersity has remained similar, however the $M_{n(GPC)}$ has decreased. This could be due to the polymer forming aggregates in the GPC column (Table 2.10).

*Table 2.10* A comparison between PCH2 and PCM1 after thiol-ene click functionalisation.

| Entry | [a]$M_{n(NMR)}$ / g mol$^{-1}$ | [b]$M_{n(GPC)}$ / g mol$^{-1}$ | [b]Đ |
|---|---|---|---|
| **PCH2** | 28300 | 190400 | 1.42 |
| **PCM1** | 32400 | 54700 | 1.40 |

[a]$M_{n(NMR)}$ were determined by $^{1}$H NMR, [b]determined by DMF GPC relative to PMMA standards through conventional calibration

The hydrophilic mass fraction was determined to be 0.34 for **PCM1**, this was made into a latex and the cmc was found to be 0.012 mg cm$^{-3}$ (Figure 2.38).

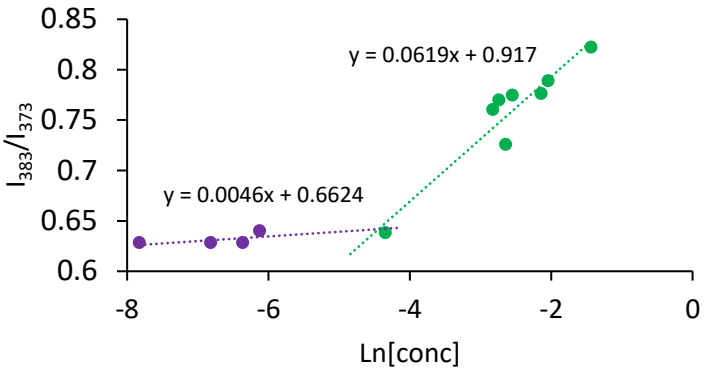


*Figure 2.38 The cmc graph for **PCM1.***

The equations show that when the concentrations are above the cmc, the gradient of the line is a magnitude larger than that of concentrations below the cmc. This has been observed in Figure 2.28 and Figure 2.31. **PCM1** was deprotected using TSMBr and methanol then freeze-dried. It could be seen that the polymer's solubility had changed, however it was very insoluble in many conventional NMR solvents and as a result the cmc and an NMR could not be obtained.

## 2.6. Conclusion and future work

In this chapter seven polymer families were successfully synthesised, PEG-*b*-PHEL synthesis had similar aspects to that synthesis by Raycraft *et al.* however the PEG-*b*-PHEL was fully functionalised. PEG-*b*-PCL-*b*-PHEL and PEG-*b*-PHEL have been hydrophosphorylated. The resulting diblocks **PS** and **PM** could not self-assemble at low concentrations, this was due to the lack of a hydrophobic core to drive the process. The synthesis of PEG-*b*-PCL-*b*-PHEL was successful however it is unknown if transesterification occurred due to the complicity of MALDI spectrum that would be acquired. In future polymerisations lower reaction temperatures and concentrations should be investigated to prove that transesterification does not occur. The method used to make the latexes, the solvent coevaporation method, gave mixed results as many of the polymers macroprecipitated upon the evaporation of DCM. In order to explore different morphologies, the solvent exchange method of producing self-assembled structures should be conducted. **PCM1** had a cmc of 0.012 mg $cm^{-3}$ and was deprotected, however the resultant polymer was insoluble in water and most solvents so it could not be characterised. The next steps for the **PCH** polymers would be to change the ratio of the blocks and specifically reduce the PCL block so that the polymer can become more soluble and able to self-assemble in water rather than macroprecipitate out at concentrations of 0.1 mg $cm^{-3}$. From there the polymers could be fully characterised with TEM to observe the morphology and size of the self-assembled objects but to also see if these polymers can nucleate the growth of HAPs. The triblock sequence of **PCH** has been explored in this work, however the arrangement of **PHC** should also be synthesised. After functionalisation, the PHEL could be extended into the corona of the structure which could provide a different morphology and in turn different physical properties.

# Chapter 3 RAFT polymerisation of triblock copolymers

## 3.1. Introduction

### 3.1.1. Controlled radical polymerisation

Free radical polymerisation has been used in industry for decades, however the demand for monodispersed polymers has increased. This had led to the development of controlled radical polymerisation (CRP) techniques. In CRP, the molecular weight of the resulting polymer is easily controlled with low dispersity. CRP also allows access to different polymer morphologies that FRP cannot, such as star and graft copolymers.

CRP is a type of chain growth polymerisation where the radical can be transferred to another growing polymer chain once the monomer feedstock is depleted. The CRP mechanism contains an equilibrium step which keeps the active radical concentration low. This results in fewer propagating polymers chains, keeping the number of propagating radicals to a minimum. The most broadly applied CRP methods are atom transfer radical polymerisation (ATRP), nitroxide-mediated polymerisation (NMP) and reversible addition chain-transfer (RAFT) polymerisation. ATRP is the most used CRP technique however it is air and moisture sensitive like ROP. Furthermore, like ROP an acidic monomer cannot be polymerised directly, as a result protected monomers such as *tert*-butyl methacrylate are polymerised and then hydrolysed in a post-polymerisation deprotection step. There are many hypotheses for the inactivity of the acidic monomers in ATRP such as the displacement of the halide on the Cu(II) complex and competitive coordination from the carboxylate groups to the copper.[112,113] However Matyjaszewski *et al.* have managed to synthesis poly(methacrylic acid) by eATRP, where the Cu(I) complex is generated electrochemically. The group synthesised the polymer with reasonable dispersity ($< 1.5$) and achieved high conversions (96 %).[114] The termination of the polymerisation was primarily due to intramolecular cyclisation of the poly(methacrylic acid) chains. Whilst the polymerisation of acidic monomers has proven a challenge in ATRP, with RAFT polymerisation it is a facile process.

### 3.1.2. RAFT polymerisation mechanism

RAFT polymerisation differs from ATRP since the propagating radical is in equilibrium with the inactive species (Figure 3.1). As a degenerative chain transfer mechanism,[115] the process requires an external source of radicals to continue the polymerisation. RAFT agents are usually species that contain a thiocarbonylthio group, which are designed to introduce functionality into the polymers.

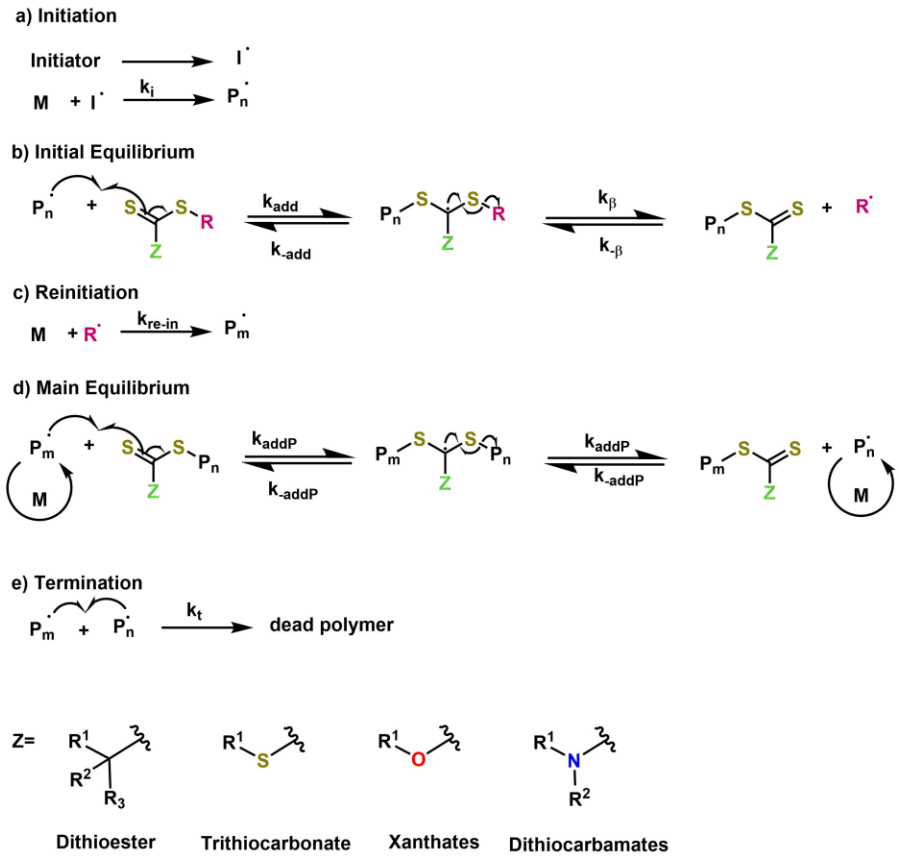


*Figure 3.1 Mechanism of RAFT polymerisation*

There are 5 steps in the RAFT polymerisation shown in Figure 3.1, first the initiation step, **a)**. The radicals formed, $P_n^{\cdot}$, attacks the RAFT reagent and the S=C bond is broken then reformed resulting in another radical, $R^{\cdot}$, **b)**. The $R^{\cdot}$ attacks monomer resulting in $P_m^{\cdot}$, **c)**. The reinitiation step ends when there is no more RAFT agent to consume and the polymerisation carries on to the main equilibrium stage, **d)**, then terminates, **e)**.

The ratio of RAFT agent to monomer can be used to predict the molecular weight of the resulting polymer. The monomer to initiator ratio influences the rate of reaction. However, too low a ratio can cause uncontrolled polymerisation.[116–118] A well-controlled polymerisation is where the number of polymer chains initiated from the initiator can be defined in Equation 3.1.

$$M_n(calc.) \approx \left(\frac{([M]_0 - [M]_t)}{[RAFT]_0} \times M_M\right) + M_{RAFT}$$

*Equation 3.1: The equation for the molecular weight of a polymers from a well-controlled RAFT polymerisation. $M_n(calc.)$ = Molecular weight of polymers, $[M]_0$ = Initial monomer concentration, $[M]_t$ = Monomer concentration at time t, $[RAFT]_0$ = Initial RAFT agent concentration, $M_M$ = molar mass of the monomer, $M_{RAFT}$ = molar mass of the RAFT agent*

Two factors that can affect the RAFT polymerisation are the concentration of RAFT agent and the Z group functionality. The concentration of the RAFT agent is crucial, since it determines the number of polymer chains produced and the functionality of the polymer chain end if the RAFT agent is not cleaved after polymerisation. When choosing a RAFT reagent, it is important to have one that complements the radical stability of the monomer. The Z group functionality can increase or decrease the activity of the RAFT agent. More "activated" monomers have conjugated groups adjacent to their vinyl groups, these includes styrenes, methacrylates and nitriles groups. "Less activated" monomers have nitrogens, halogen, sulphur lone pairs and saturated carbons next to the vinyl groups. Xanthates and dithiocarbamates are used to decrease the activity of the radical whereas dithioesters and trithiocarbonates are used to increase radical reactivity.[115] For example, trithiocarbonates are used in styrene polymerisations as styrene radicals are stabilized by resonance and inductive effects.[115] The thiocarbonyl thio groups are particularly vulnerable to side reactions where the group is cleaved from the rest of the RAFT agents, this leads to uncontrolled polymerisations.[119] However this cleavage can be minimised by tuning the reaction conditions. Yildirim *et al.* synthesised a series of polyaminde based block copolymers using CPAD (Figure 3.2). Amino based polymerisations tend to undergo aminolysis of the dithiobenzoate moiety.[120] To prevent this unfavourable reaction the 2-aminoethyl methacrylate hydrochloride salt was used and led to a well control polymers (resultant polymer dispersity was 1.15).[121]

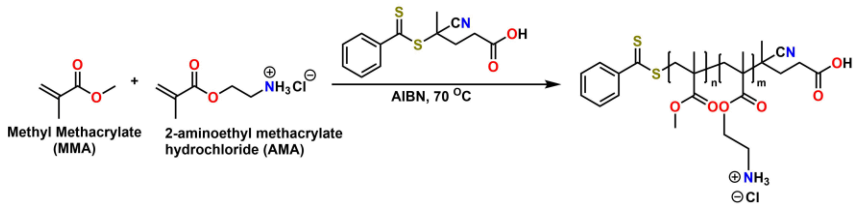


*Figure 3.2 The schematic of the copolymerisation of methyl methacrylate and 2-aminoethyl methacrylate hydrochloride*

A RAFT polymerisation emerged from Thang *et al.*, where they performed polymerisations on a number of monomers with different functionalities including acids and alcohols in different solvents and with various RAFT agents. Each experiment showed excellent control over the $M_n$ and Đ of the resultant polymers.[116]

Acrylic acid was used in the polymerisations and yielded low dispersities (Đ =1.33) however it's conversion was only 18 %.[116] Poly(acrylic acid) has been a challenging monomer, since ATRP cannot be used and side reactions with solvents limit the synthesis of high $M_n$ polymers.[122] Ladaviere *et al.* screened various solvents and RAFT agents, and were able to achieve high conversions (98 %) and low dispersites (Đ = 1.2) though there was a large difference between the experimental and theoretical $M_n$.[123] More recently, Bangal *et al.* synthesised poly(acrylic acid) in water by neutralizing the carboxylic acid groups.[124] The group synthesised a water soluble RAFT agent (Figure 3.3) and the polymerisation took place at 65 °C.

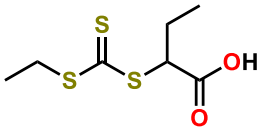


*Figure 3.3 RAFT agent used by Bengal et al.*[124]

The results showed good control and reasonable conversions. Again the theoretical and experimental data for $M_n$ are very different for the higher molecular weight poly(acrylic acid). This is due to chain transfer reactions with the solvent.[124]

Here it has been shown that RAFT polymerisation has a few advantages over ATRP and ROP, for example moisture insensitivity and the direct polymerisation of acidic monomers. However it also has its disadvantages. There are many RAFT agents that have been synthesised and each one has a limited monomer scope where a controlled polymerisation can occur. It can also be difficult to produce a high molecular weight polymer due to the addition of an external initiator.[125] Furthermore, the RAFT agent can give the resultant polymer a yellow colour and an unpleasant odour, as a result further purification is often needed.

Recently there has been an increase in using sustainable monomers in RAFT polymerisations such as extracting the monomers from plant oils and terpenes.[126–128] Stearic acid which is a long chain fatty acid naturally found in cocoa butter was modified in the work by Jena and co-workers (Figure 3.4)[129]. The modified stearic acid moiety provided the hydrophobic segment in the copolymerisation. The homopolymerisation showed the same amount of control as its block copolymerisation with Boc-L-phenylalanine methacryloyloxyethyl ester (BOC-PhE-HEMA) both having a dispersity of 1.08.[129] The recent advances in renewable and sustainably chemistry has lead to a library of sustainable RAFT monomers. However there has yet to be any phosphorous based monomers that have come from renewable sources.

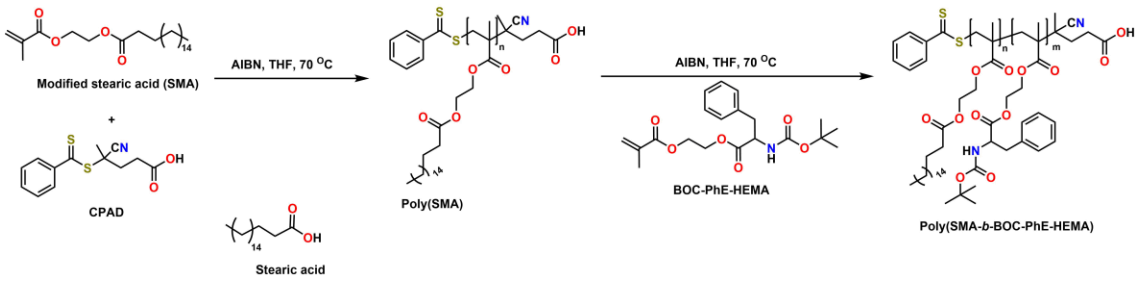


*Figure 3.4 The schematic of the copolymerisation of modified stearic acid and Boc-L-phenylalanine methacryloyloxyethyl ester and the structure of stearic acid reproduced from Jena et al.*[128]

### 3.1.3. RAFT polymerisation of phosphorous based polymers

Phosphorous containing polymers have had a notable increase in interest over the past decade. It has been discovered that phosphorous is useful in many applications such as flame-resistant, anti-fouling and biomaterials.[130–133] However until recently the incorporation of the phosphorous moieties has been mainly through free radical polymerisation with a comonomer or post-polymerisation as seen in Chapter 2.[110] Many monomers such as monoacryloxyethyl phosphate and 2-(methacryloyloxy)ethyl phosphate have been successfully polymerised through RAFT polymerisation however they are usually in low concentration when compared to the its comonomer.[134]

There has been attempted to polymerise di(methacryloyloxy)methyl methacrylate (MAPC1) through RAFT polymerisation and ATRP. David *et al.* first attempted to incorporate MAPC1 into a diblock copolymer with MMA, by first synthesising a PMMA macroinitiator.[134] It was found that the homopolymerisation of MAPC1 was unsuccessful as the conversions were only 22 %

after 20 hours.[134] The phosphorous unit can complex with the copper catalyst used in ATRP which results in the early termination of the polymerisation. David *et al.* then chose to deprotect the PMMA-*b*-TBuMA polymer then couple the resultant PMMA-*b*-PMAA moieties with hydroxymethyl dimethylphosphonate to add the phosphorous functionality. The phosphous diblock copolymer had a very low dispersity of 1.08.[134] Later Mukumoto *et al.* revisited the homopolymerisation of MAPC1 using ATRP, however in their ATRP system they added Cu(II)$Br_2$ into the reaction mixture which is peculiar for conventional ATRP conditions.[135] The Cu(II)$Br_2$ was added to the reaction mixture to decrease the radical concentration at the start of the polymerisation. It was discovered that at high concentrations of Cu(II)$Br_2$ and using bipyridiene as the ATRP ligand 80 % conversion of MAPC1 could be achieved after 4 hours at 60 °C with a polymer dispersity of 1.35. The dispersity decreased further when the polymerisation was carried out at 40 °C.[135] However when Mukumoto *et al.* attempted initiator for continuous activator regeneration ATRP (ICAR) the results were less fruitful. At high conversions, the $M_n$ deviated from linearity indicating chain breaking reactions.[135] However, the group successfully used PMAPC1 as a macroinitiator for the polymerisation of styrene. Standard ATRP conditions were used, meaning that Cu(II)$Br_2$ was not included in the reaction mixture. It was found that after 24 hours styrene conversion was only 20 % with an intermediate dispersity of 1.58.[135] Mukumoto *et al.* and other research groups have not researched further into copolymerisation of MAPC1.

However RAFT polymerisation has been more successful in the polymerisation of MAPC1. MAPC1 has a lower reactivity than MMA even though they have similar chemical structures. It was found that MAPC1 has a $k_p/(k_t)^{1/2}$ one magnitude lower than MMA, this also means that the side reactions caused by traces of oxygen have a greater effect when polymerising MAPC1 compared to other alkyl monomers.[119] Canniccioni *et al.* explored various polar solvents in the homopolymerisation of MAPC1, as solvents can enhanced the rate of polymerisation.[111] DMF, DMAc, 1,4-dioxane, DMSO and water were used as solvents and in all solvents the polymerisation reached over 50 % conversion and had dispersities lower than 1.4.[111,136] Due to the polar nature of MAPC1 polarity of the solvent has a large effect on the rate of polymerisation. However, if MMA is used then there is little observable effect on the molecular weight and weight distribution.[111] It was found that when less polar solvents such as dioxane were used in the polymerisation, then only 50 % conversion was reached this is due to the rate of polymerisation being lower. However with highly polar solvents (water and DMSO) the polymerisation reached over 75 % conversion however transfer reactions took place leading to a deviation in $M_n$.[111] Canniccioni *et al.* investigated two chain transfer agents, cyanoisopropyl dithiobenzoate (CPID) and 4-cyanopentanoic acid dithiobenzoate (CAPD), which are similar in structure however CPAD has a carboxylic acid moiety on the R end of the chain (Figure 3.5).

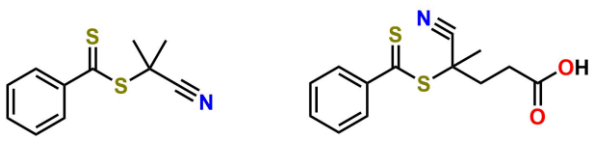


*Figure 3.5 The structures of RAFT agents used by Canniccioni et al.[110]*

The group found that there was no significant difference between the polymer synthesised using CPAD and CPID, with $M_n$ and Đ of $M_n$ = 7500 g $mol^{-1}$, Đ = 1.28 and $M_n$ = 7600 g $mol^{-1}$, Đ = 1.23 respectively.[111] Finally Canniccioni *et al.* probed the possibility of PMAPC1 being used as a macrochain transfer agent for the polymerisation of MAPC1. The polymerisation was carried out at 70 °C for 4 hours and the conversion reached 56 %. The resulting copolymer has a dispersity of 1.30 which suggests that polymerisation was controlled.

With the work that has been demonstrated by Cannicciono *et al.*, MAPC1 has become a more accessible monomer to work with and has now been used in PISA by Hanisch *et al.* to be occluded into calcite crystals.[60] Here we use PMAPC1, PMMA and PTuBMA as a macrochain transfer agents for the polymerisation of MMA, MAPC1, HEMA, DMAE and TBuMA to produce a library triblock copolymers for the nucleation of HAP. MMA was chosen for the hydrophobic block in the RAFT polymerisation as it will help drive self-assembly of the triblock copolymers. TBuMA is used as an alternative to directly polymerising methacrylic acid. This monomer allows the number of monomer units incorporated into the polymer to be easily calculated. In nature carboxylic acid, amines and alcohols all play a role in the nucleation and regulation of hydroxyapatite, using this as inspiration TBuMA, HEMA and DMAE were polymerised (Figure 3.6).

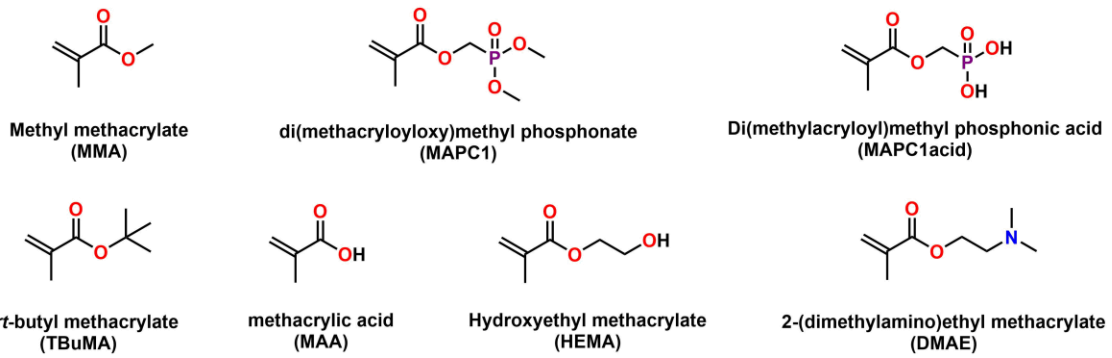


*Figure 3.6 The structures of the methacrylate based monomers used to synthesise the polymers in Chapter 3*

## 3.2. Synthesis of macrochain transfer agents

### 3.2.1. PMAPC1 homopolymers

Following a similar procedure to that work done by Canniccioni *et al.* polar solvents such as DMF, DMAc and DMSO were used in the polymerisation of MAPC1 due to its low reactivity.[119] Here CPAD was chosen as the RAFT agent due to its carboxylic acid moitety. After the polymerisations the polymers were PEGylated through an EDC coupling with CPAD. From the polymerisation of MAPC1 it can be seen that there is not significant differences in the dispersities of the polymers when using a 3:1 and 5:1 CTA:AIBN ratios in any solvent. However from Canniccioni *et al.* it is know that MAPC1 undergoes transfer reactions in DMSO regardless of its low dispersities (Table 3.1).[111,136]

*Table 3.1* The reaction conditions and results of the polymerisation of MAPC1 at 70 °C for 7 hours. The $M_{n(NMR)}$, $M_{n(TOPO)}$, $M_{n(GPC)}$ and Đ of the resultant diblock polymers are shown. The target $M_{n(Theo)}$ was calculated.

| Entry | MAPC1 units | Sol | CTA: AIBN | [a]MAPC1 conversion / % | Target $M_{n(Theo)}$ / g mol$^{-1}$ | [a]$M_{n(NMR)}$ / g mol$^{-1}$ | [a]$M_{n(TOPO)}$ / g mol$^{-1}$ | [b]$M_{n(GPC)}$ / g mol$^{-1}$ | [b]Đ |
|---|---|---|---|---|---|---|---|---|---|
| **D1** | 137.1 | DMF | 2.9: 1 | 89 | 9800 | 13400 | 1700 | [c]67200 | [c]1.37 |
| **D2** | 137.1 | DMAc | 1.0: 1 | 80 | 28500 | 1900 | 1800 | 276000 | 2.01 |
| **D3** | 137.1 | DMAc | 5.0: 1 | 84 | 5700 | 11000 | 10500 | 111200 | 1.29 |
| **D4** | 137.1 | DMSO | 3.0: 1 | 94 | 9500 | 8300 | 3400 | 113200 | 1.29 |
| **D5** | 137.1 | DMAc | 3.0: 1 | 88 | 9500 | 11300 | 6700 | 61700 | 1.31 |

[a]conversion and $M_{n(NMR)}$ were determined by $^1$H NMR, [b]Determined by DMF GPC relative to PMMA standards through conventional calibration, [c]Determined by $CHCl_3$ GPC

There are two methods that can be used to determine the $M_{n(NMR)}$ which are comparing the intergrals phenyl hydrogens from the CPAD and the methylene group at 8.0 – 7.2 ppm and 4.5 – 4.2 ppm respectively. The other method is to use an external standard, trioctylphosphine and

comparing the area of the two phosphorous signals which can be used int the two equations (Equation 3.2 and Equation 3.3).[34]

$$Mols\ of\ MAPC1 = \frac{A_1}{A_2} \times \frac{vol \times C_2}{M_{n_{TOPO}}}$$

*Equation 3.2: The equation for finding the number of mole of MAPC1 from using a TOPO external standard. $A_1$ = area of the sample, $A_2$ = area of the internal standard, TOPO and $C_2$ = concentration of MAPC1*

$$Mn\ of\ block\ copolymer = vol \times C_1 \div \left(\frac{(vol \times C_1) - (Mn_{MAPC1} \times mol_{MAPC1})}{M_{n_{PRAFT}}}\right)$$

*Equation 3.3: The equation in determining the $M_n$ of the block copolymer by using the moles of MAPC1. $C_1$ = concentration of TOPO, $C_2$ = concentration of MOEP, $M_n$ = molecular number average*

At higher $M_n$ the TOPO method seems to deviate, as a result using the phenyl protons to calculate the $M_{n(NMR)}$ is used in this chapter. The $M_{n(NMR)}$ and disperisties for **D1** and **D5** are similar, this could be attributed to the polymerisations taking place in DMF and DMAc respectively. The structure of these two solvents are very similar and they have similar polarities as a result the polymers would have similar properties. Furthermore when comparing the polymers that were polymerised in DMAc but with different CTA : AIBN ratios a trend was observed. It shows that at higher CTA:AIBN ratios the polymerstions were more controlled and the resultant polymers had lower dispersities. With smaller CTA : intiator ratios a larger amount of radicals are active within the reaction mixture, this means that there are more termination reactions occurring. This would in turn lead to a higher dispersity and uncontrolled polymerisation; this is what is observed in **D2**.[115] The discrepancy between $M_{n(NMR)}$ and $M_{n(GPC)}$ is similar to what was seen in Chapter 3 with the ROP polymers, however in these polymers the $M_{n(NMR)}$ is approximately 10 – 20 % of that of $M_{n(GPC)}$ this is due to a different polymers being used as the standards instead of PMAPC1. These polymers are used a macroinitator for MMA in which the chosen solvent is DMAc because of its good compatibility with MAPC1. In the $^{31}P$ NMR spectrum of **D5** the peak is split into two, this is due to the phosphorous being next to two different environments that methoxy and the methylene group (Figure 3.7). This splitting pattern is present in each of the PMAPC1 polymers.

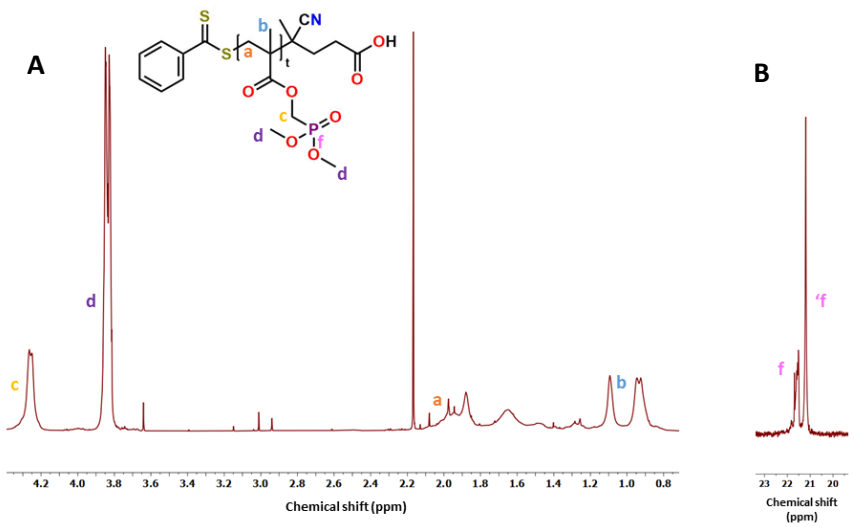


*Figure 3.7 $^1H$ NMR spectrum for **D5** (A) and its $^{31}P$ decoupled NMR spectrum (B)*

### 3.2.2. PMMA and PTBuMA homopolymers

MMA was also used as a macroinitiator to provide a pathway of synthesising a block copolymer with an alternate structure. This way the PMAPC1 block would be separated by the PMMA block from the PEG segment, rather than the PMMA block being in the core and the PMAPC1 block extending into the corona of the assembled structure. The polymerisations were carried out in various solvents and CTA: AIBN ratios (Table 3.2). It can been seen that **N1** has the best dispersity of the group however like the other MMA polymerisations the $M_{n(GPC)}$ is a larger than the $M_{n(NMR)}$ even though the GPC was calibrated with PMMA standards which is peculiar. Also **N3** and **N4** still have low disperisties values although the CTA:AIBN ratio is 1.5 : 1. However, in with **D2** the dispersity dramatically increased at low CTA : AIBN ratio, this could be attributed to the low reactivity of MAPC1 so there is more active radicals than dormant chains. Whereas in the case of MMA it is a more reactive monomer thus this affect is not observed.

*Table 3.2* The reaction conditions and results of the polymerisation of MMA and TBuMA at 70 °C for 7 hours. The $M_{n(NMR)}$, $M_{n(TOPO)}$, $M_{n(GPC)}$ and Đ of the resultant diblock polymers are shown. The target $M_{n(Theo)}$ was calculated.

| Entry | Monomer | Units | Solvent | CTA: AIBN | [a]Monomer conversion / % | Target $M_{n(Theo)}$ / g $mol^{-1}$ | [a]$M_{n(NMR)}$ / g $mol^{-1}$ | [b]$M_{n(GPC)}$ / g $mol^{-1}$ | [b]Đ |
|---|---|---|---|---|---|---|---|---|---|
| **N1** | MMA | 112 | DMAc | 3.0: 1 | 54 | 3700 | 2300 | 43260 | 1.06 |
| **N2** | MMA | 112 | DMAC | 3.0: 1 | 51 | 3700 | 2400 | 10300 | 1,25 |
| **N3** | MMA | 80 | Dioxane | 1.5: 1 | 96 | 5300 | 7100 | 14200 | 1.25 |
| **N4** | MMA | 60 | Dioxane | 1.5: 1 | 77 | 4000 | 3600 | 9700 | 1.18 |
| **T1** | TBuMA | 360 | DMAc | 3.0: 1 | 82 | 17000 | 21000 | 14000 | 1.24 |

[a]conversion and $M_{n(NMR)}$ were determined by $^1$H NMR, [b]Determined by DMF GPC relative to PMMA standards through conventional calibration

**N1** and **N3** cannot be directly compared due to the difference in CTA:AIBN ratio however, it could be suggested that the change in solvent does not have as drastic effect in molecular weight and dispersity as it does with MAPC1 (as mentioned by Canniccioni) again this could be due to the reactivity of monomer. The polarity of the monomer itself could attribute as well, as MAPC1 is more polar than MMA when in the intermediate form. The solvents would provide more stabilisation or destabilisation in the case of water and 1,4-dioxane. However, with MMA the stabilisation remains relatively similar in the two differing polar solvents. Although it does seem that MMA polymerisation is slower in DMAc then in that of dioxane however, the polymerisation itself seem more controlled. In future work changing the CTA: AIBN ratios and longer polymerisation should be investigated in order to optimise the polymerisation of MMA in DMAc.

TBuMA was chosen as a macroinitiator to give a different functional group in the triblock, a carboxylic acid moiety. MAA could have been used and provide a shorter synthesis route however it is more difficult to determine the conversion and $M_{n(NMR)}$ because of the lack of functional group peaks in the spectrum. As a result an external standard would have to be used to determine these. The benefit of using TBuMA is that the *tert*-butyl peaks that appear at 1.45 – 1.39 ppm in the $^1$H NMR spectrum which can be used to calculate the molecular weight (Figure 3.8).

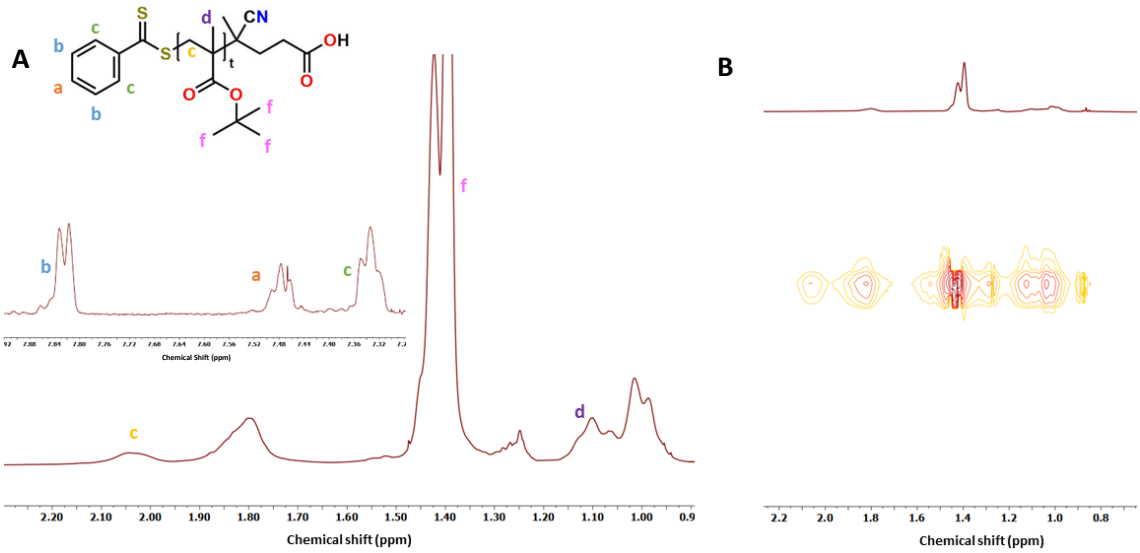


*Figure 3.8 $^{1}$H NMR spectrum of **T1** (A) and its $^{1}$H DOSY NMR spectrum (B)*

**T1** and **D5** have similar monomer conversions after 7 hours, which could indicate that they have similar reactivities in DMAc. TBuMA is a less active monomer than MMA because of the +I effect the *tert*-butyl group has on the monomer which in turns stabilises the radical formed in the RAFT process. Furthermore, **T1** has a lower dispersity than **D5**, which could be indicative of the monomer not being as susceptible to traces of oxygen in the reaction mixture as MAPC1.

## 3.3. PEGylations of homopolymer

PEGylations have been used extensively throughout many fields and are key in the drug delivery industry as mild conditions are needed to bind PEG to different proteins.[137,138] PEGylations of CTAs has allowed for a simple route to synthese diblock copolymers. It has been shown that by incorporating PEG chains into a latex can help stabilise the particle through steric stabilisation, however the effectiveness depends on the anchoring of the PEG on to the surface of the latex.[139] CPAD is a good choice in CTA for this reaction due to its compatibility with many monomers and its carboxylic acid functional group. In RAFT polymerisation the addition of a PEG chain is commonly prepared by an esterification between CPAD and a PEG-OH however groups have coupled the PEG unit with an amide bond.[140,141] In all these experiments dicyclohexylcarbodiimide (DCC) is used as the coupling agent along with DMAP. In this method the by product, dicyclohexylurea, is formed and the product has to be filtered.[141] In this chapter EDC is used as a substitute due to it being easier to handle but more importantly the urea by product is water soluble so it is easy to remove via dialysis or solvent extraction. The PEGylation is carried out at two different points in the polymer synthesis, in some polymers it was carried out after the first polymerisation and in the other polymers it was carried out after the second set of polymerisations. It was chosen not to use a CPAD-PEG RAFT agent because it was difficult to separate the PEG-OH and the CPAD-PEG from each other after esterification when high $M_n$ PEG-OH was used. A benefit to choosing to perform PEGylation after the polymerisations is that the reactivity of the CPAD will be larger because the R group would have a similar structure to the monomer and it would be smaller, so the radicals can move more freely in solution and less likely to become tangled (Figure 3.9). It should be noted that PEGylations carried out post polymerisation is not abundant in the literature.

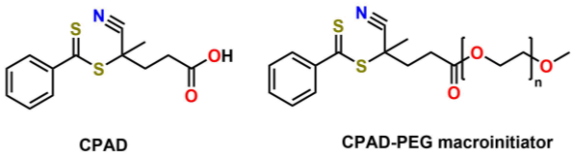


*Figure 3.9 The structure of CPAD (left) and the PEGylated CPAD macroinitiator (right)*

The homopolymers of PMAPC1 and PTBuMA were PEGylated after the first polymerisation and the esterification was carried out for 48 hours. It can be seen from the PMAPC1-PEG polymers that the dispersity values slightly increase, this would be attributed to the dispersity of the PEG unit being attached (Table 3.3).

*Table 3.3* PEGylations of PMAPC1 and PTBuMA homopolymers. The $M_{n(NMR)}$, $M_{n(TOPO)}$, $M_{n(GPC)}$ and Đ of the resultant diblock polymers are shown. The target $M_{n(Theo)}$ was calculated.

| Entry | Precursor | PEG units | Blocks in polymer | PEG: Block | Target $M_{n(Theo)}$ / g mol$^{-1}$ | [a]$M_{n(NMR)}$ / g mol$^{-1}$ | [b]$M_{n(GPC)}$ / g mol$^{-1}$ | [b]Đ |
|---|---|---|---|---|---|---|---|---|
| **PD1** | **D3** | 132 | PMAPC1 | 146: 12 | 14700 | 8900 | 93200 | 1.36 |
| [c]**PD2** | **D4** | 126 | PMAPC1 | 126: 40 | 12800 | 14000 | 97400 | 1.21 |
| **PD3** | **D1** | 49 | PMAPC1 | 49: 7 | 15600 | 3600 | 67200 | [d]1.37 |
| **PD4** | **D5** | 38 | PMAPC1 | 47: 6 | 13400 | 3300 | 61700 | 1.31 |
| **PT1** | **T1** | 47 | PTBuMA | 47: 21 | 23100 | 5100 | 3100 | 1.05 |

[a]conversion and $M_{n(NMR)}$ were determined by $^1$H NMR, [b]Determined by DMF GPC relative to PMMA standards through conventional calibration, [c]Aqueous GPC used, [d]bimodal distribution

Once the homopolyers have been PEGylated, the $M_{n(NMR)}$ is calculated by using integral of the methoxy group of the PEG as it is a strong singlet at 3.38 ppm whereas the aromatic protons can be very weak and masked by the NMR baseline (Figure 3.10). Overall $M_{n(NMR)}$ is far less than expected for all copolymers which suggests that calculating the $M_{n(NMR)}$ from the phenyl ring from the CPAD is an overestimation. In the $^1$H DOSY NMR spectrum of **PT1** homopolymers two species are present. However, in the GPC trace only one peak is present (Figure 3.11). In $^1$H DOSY NMR both traces contain both the PEG and PTBuMA signals, this could potentially suggest that both species have similar molecular weights and the GPC could not separate them or that the $^1$H DOSY NMR has unreal solvent line which is known to happen.

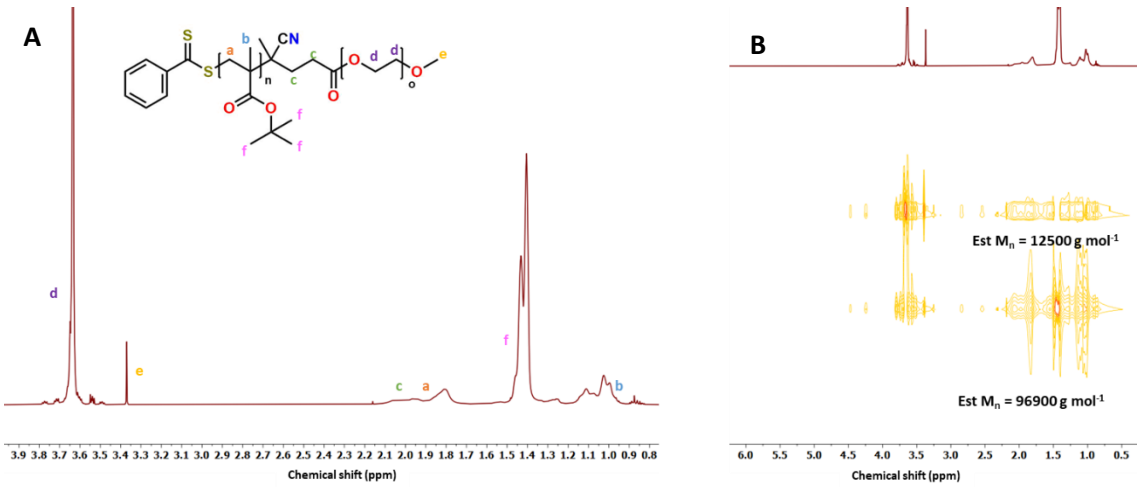


*Figure 3.10 $^1$H NMR spectrum of **PT1** (A) and its $^1$H DOSY NMR spectrum (B).*

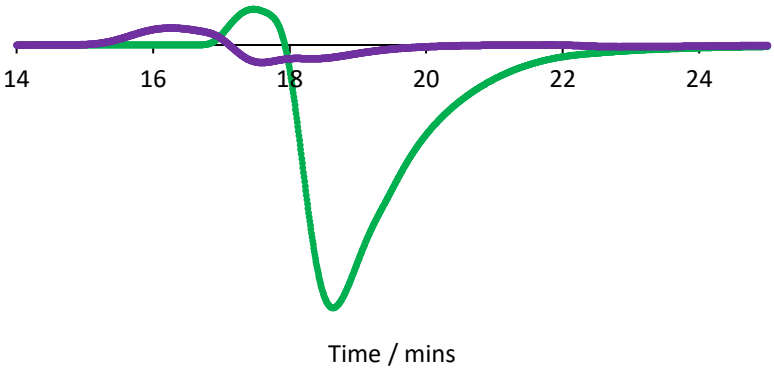


*Figure 3.11 The GPC traces of **T1** (green) and **PT1** (purple).*

Furthermore $^{1}$H DOSY NMR also measure the hydrodynamic volume like in GPC as shown in Figure 3.10, the estimated $M_{n(NMR)}$ of these species are 12500 g mol$^{-1}$ and 96900 g mol$^{-1}$ respectively. If these $M_{n(NMR)}$ are true then these would show as a bimodal peak in the GPC, this would suggest the latter scenario is more likely. In the case of **PD3** only one signal is present in the $^{1}$H DOSY NMR which would indicate one species in the sample (Figure 3.12). However there is a bimodal distribution in the GPC trace which indicates two different $M_n$ polymers (Figure 3.13). **D1** the predecessor to **PD3** also showed a bimodal distribution which could have meant that there was traces of oxygen in the reaction mixture which lead to early termination of the polymerisation. It was decided to use the GPC trace to give an indication if two homopolymers were formed rather than $^{1}$H DOSY NMR. In the future the NMR sample of **PD3** could be doped with PEG-OH and its predecessor, **D1** and a $^{1}$H DOSY NMR ran. If any of the diffusion co-efficient match any of the signals, then the PEGlaytion did not go to completion.

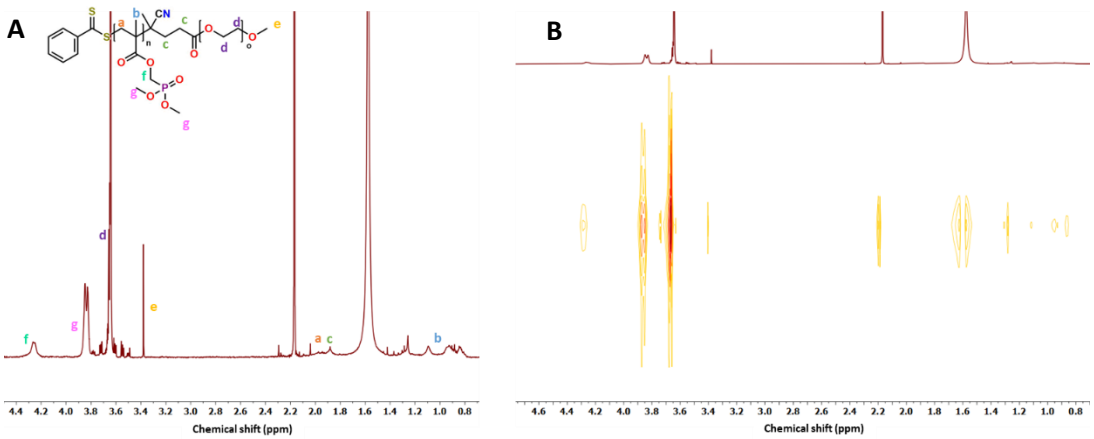


*Figure 3.12 $^{1}$H NMR spectrum of **PD3** (A) and its $^{1}$H DOSY NMR spectrum (B)*

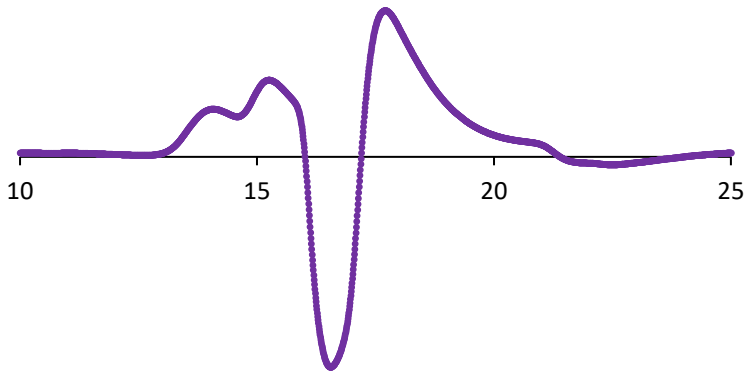


*Figure 3.13 GPC trace of **PD3***

## 3.4. Second polymerisation of PEGylated diblock copolymers

PMAPC1-PEG and PTBuMA-PEG were used macroCTAs in the polymerisation of MMA, the polymerisations were carried out for 24 hours because macroCTAs tends to be less reactive as they have a larger molecular weight. Unfortunately the PEG peak at 3.60 ppm overlaps with the PMMA peak at 3.64 ppm, as a result the DP of PMMA was calculated by integrating that section then subtracting the value of the PEG group (Table 3.4).

*Table 3.4 The RAFT polymerisation of MMA using PMAPC1-PEG and PTBuMA-PEG macroCTAs at 70 °C for 24 hrs. The $M_{n(NMR)}$, $M_{n(TOPO)}$, $M_{n(GPC)}$ and Đ of the resultant diblock polymers are shown. The target $M_{n(Theo)}$ was calculated.*

| Entry | Precursor | Blocks in polymer | CTA: AIBN | Monomer Conversion / % | PEG: Block: MMA | Target $M_{n(Theo)}$ / g mol$^{-1}$ | [a]$M_{n(NMR)}$ / g mol$^{-1}$ | [b]$M_{n(GPC)}$ / g mol$^{-1}$ | [b]Đ |
|---|---|---|---|---|---|---|---|---|---|
| **PDN1** | **PD3** | PMAPC1-PEG | 3: 1 | 69 | 49: 7: 22 | 7300 | 5800 | 83900 | 1.59 |
| **PDN2** | **PD1** | PMAPC1-PEG | 5: 1 | 34 | 146: 12: 15 | 12600 | 9400 | 98700 | 1.37 |
| **PDN3** | **PD2** | PMAPC1-PEG | 3: 1 | 61 | 126: 23: 50 | 18400 | 15300 | 86000 | 1.29 |
| **PTN1** | **PT1** | PTBuMA-PEG | 3: 1 | 61 | 47: 21: 16 | 6600 | 6700 | 17500 | 1.48 |

[a]$M_{n(NMR)}$ were determined by $^1$H NMR, [b]Determined by DMF GPC relative to PMMA standards through conventional calibration

It can be seen that changing the CTA:AIBN ratio has an effect on the monomer conversion, as the conversion of **PDN3** is double that of **PDN2.** In the PMMA-PMAPC1-PEG series the triblock polymers' dispersity do not increase significantly indicating that the original rise was due to the PEGylation mentioned in section 3.3. However, **PTN1** the dispersity increases significantly with addition MMA, this could be caused by the length of the macroCTA. The $^{1}$H DOSY NMR shows that **PDN1** still has a bimodal distribution after the addition of PMMA (Figure 3.14), this is also shown in the GPC trace (Figure 3.15). The retention time of **PDN1** has decreased which signifies the increase in $M_{n(GPC)}$ of the triblock copolymer.

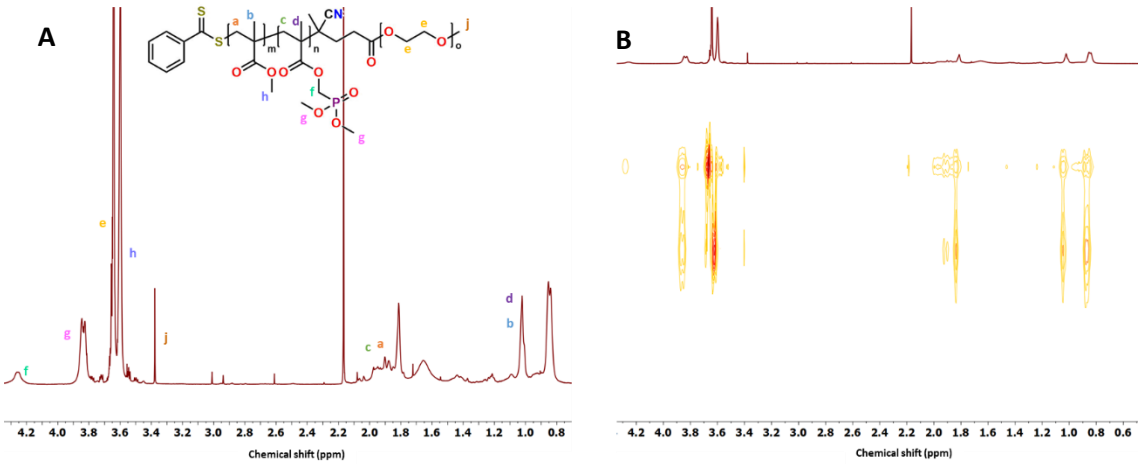


*Figure 3.14 $^{1}$H NMR spectrum of **PDN1** (A) and its $^{1}$H DOSY NMR spectrum (B)*

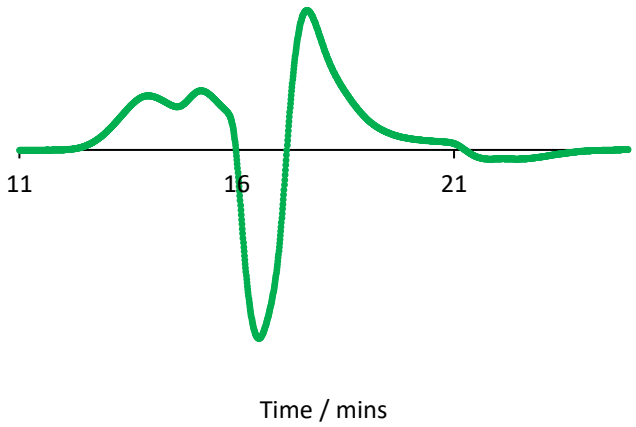


*Figure 3.15 The GPC trace of **PDN1** showing its bimodal distribution*

## 3.5. Second polymerisation of homopolymers

The PMMA based homopolymers were used as macrochain transfer agents in the next step rather than being PEGylated first. The CTA: AIBN ratios were 5, 3 and 1.5 respectively, and the polymerisations were carried out for 24 hours. The dispersity of each polymer has increased significantly, this would suggest that the polymerisations were not as well controlled as the previous set (Table 3.5). This could be attributed to the length of the macrochain transfer agent, as the chains become longer they become more entangled in solution and the radicals are less accessible, as a result the rate of polymerisation decreases. The $M_{n(NMR)}$ was calculated using the

$CH_3$-O- of the PMMA block which appear at 3.60 ppm rather than the aromatic peaks of the CTA as these aromatic peaks have diminished into the baseline of the NMR.

*Table 3.5* The RAFT polymerisations of various monomers using a PMMA macroCTA for 24 hrs at 70 $^{O}$C. The $M_{n(NMR)}$, $M_{n(TOPO)}$, $M_{n(GPC)}$ and Đ of the resultant diblock polymers are shown. The target $M_{n(Theo)}$ was calculated.

| Entry | Precur-sor | Mono-mer | CTA: AIBN | Monomer Conversion / % | Monomer: MMA | Target $M_{n(Theo)}$ / g mol$^{-1}$ | [a]$M_{n(NMR)}$ / g mol$^{-1}$ | [b]$M_{n(GPC)}$ / g mol$^{-1}$ | [b]Đ |
|---|---|---|---|---|---|---|---|---|---|
| **ND1** | **N1** | MAPC1 | 5: 1 | 96 | 50: 23 | 5300 | 12700 | 102100 | 1.45 |
| **ND2** | **N2** | MAPC1 | 5: 1 | 90 | 75: 23 | 5400 | 17900 | 53500 | 1.61 |
| **NA1** | **N3** | DMAE | 1.5: 1 | 70 | 99: 71 | 12300 | 22600 | 21100 | 1.52 |
| **NE1** | **N3** | HEMA | 1.5: 1 | 56 | 116: 71 | 13000 | 22200 | 80000 | 1.70 |
| **NT1** | **N3** | TBuMA | 1.5: 1 | 64 | 43: 71 | 12300 | 222000 | 18000 | 1.37 |
| **NT2** | **N4** | TBuMA | 3: 1 | 75 | 29: 36 | 10700 | 7700 | 13100 | 1.27 |

[a]$M_{n(NMR)}$ were determined by $^1$H NMR, [b]Determined by DMF GPC relative to PMMA standards through conventional calibration, [c]Bimodal distribution

When comparing **NT1** and **NT2** the dispersity is lower with the larger CTA: AIBN ratio however PMMA segment is also half the size **NT1** which could also contribute to the different in dispersity. The block copolymers which had **N3** as their macroCTA have relatively high dispersities. For a reasonably controlled block copolymer the dispersity is usually between 1.2 – 1.5. **NE1** shows the highest disparity value at 1.78 upon looking at the $^1$H DOSY NMR spectrum there is two species in the sample, however in the GPC trace there is only one peak albeit broad (Figure 3.16).

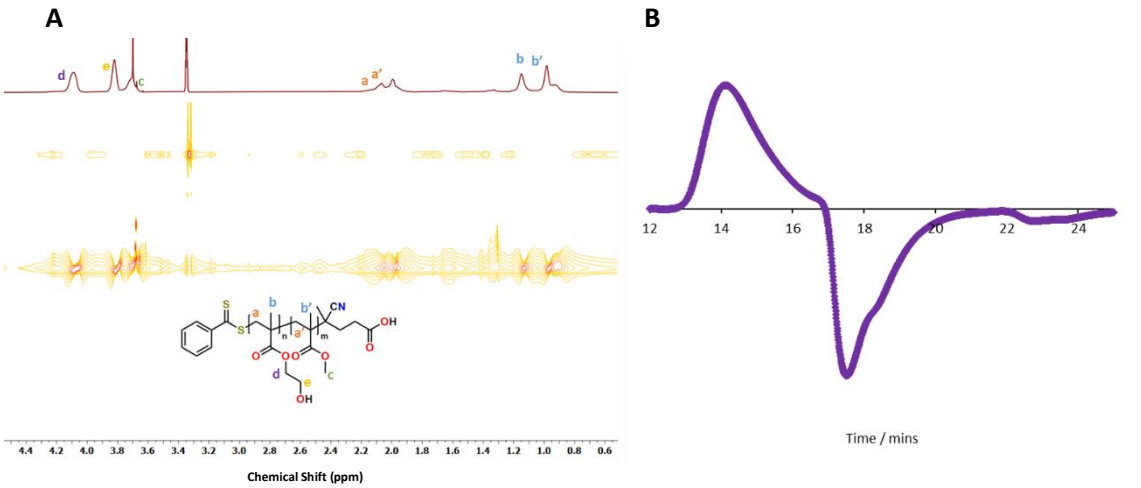


*Figure 3.16 The annotated $^1$H DOSY NMR spectrum of **NE1** (A) and its GPC trace (B).*

From the polymers that have used **N3** as their macroCTA, it could be suggested that HEMA is the least reactive monomer in DMAc due to it having the lowest conversion. This could be due to the polar hydroxyl group interacting with DMAc. RAFT polymerisations of HEMA are usually carried out in polar aqueous solvents such as a methanol/water mixture. During the polymerisation of **NA1** a colour change from red to orange was observed when DMAE was added to the reaction mixture. Usually with this RAFT agent a colour change during the polymerisation to orange would suggest the decomposition of thiobenzoate.[119] If PDMAE was used as a chain transfer agent it would be assumed that the chain fidelity would have been lost and the resulting polymer would be polydispersed. Therefore, PDMAE was not used as a macroCTA for MMA polymerisations.

The PMAC1-PMMA polymers show a large increase in dispersity even when a higher CTA:AIBN ratio was used. This could be a result of the long reaction times as more chains can terminate in that duration. In future work, different polymerisation times should be investigated to minimise the chance of dead chains and oligomers forming.[119]

## 3.6. PEGylations of PMMA diblock copolymers

The PEGylations were carried out on the diblock copolymers from section 3.4 in the same procedure as in section 3.3. The $M_{n(NMR)}$ are all much lower than expected due to the overestimation of the molecule weight when using the aromatic protons on the CTA to calculate the $M_{n(NMR)}$ (Table 3.6). Although the dispersity of the triblock copolymers have not increased significantly and in some cases like **PNT2** the dispersity decreased.

*Table 3.6* PEGylations of the PMMA based diblock copolymers from section 3.5. The $M_{n(NMR)}$, $M_{n(TOPO)}$, $M_{n(GPC)}$ and Đ of the resultant diblock polymers are shown. The target $M_{n(Theo)}$ was calculated.

| Entry | Precursor | PEG units | Blocks in polymer | PEG: PMMA: Block | Target $M_{n(Theo)}$ / g mol$^{-1}$ | [a]$M_{n(NMR)}$ / g mol$^{-1}$ | [b]$M_{n(GPC)}$ / g mol$^{-1}$ | | | [b]Đ |
|---|---|---|---|---|---|---|---|---|---|---|
| **PND1** | **ND1** | 114 | PMAPC1-PMMA | 140: 19: 10 | 11500 | 7200 | 20600 | | | 1.50 |
| **PND2** | **ND2** | | 122 | PMAPC1-PMMA | | 122: 11: 3 | 10800 | 7100 | 21500 | 1.57 |
| **PNE1** | **NE1** | | 43 | PHEMA-PMMA | | 43: 7: 10 | 14900 | 3900 | 80000 | [c]1.78 |
| **PNA1** | **NA1** | | 47 | PDMAE-PMMA | | 47: 12: 7 | 14400 | 4400 | 14800 | 1.43 |
| **PNT1** | **NT2** | | 47 | PTBuMA-PMMA | | 47: 11: 9 | 12800 | 4500 | 12300 | 1.22 |
| **PNT2** | **NT1** | | 45 | PTBuMA-PMMA | | 45: 10: 5 | 14300 | 3700 | 15400 | 1.49 |

[a]$M_{n(NMR)}$ were determined by $^1$H NMR, [b]Determined by DMF GPC relative to PMMA standards through conventional calibration, [c]Bimodal distribution

The dispersity of **PNE1** has increased to 1.78 and the $^1$H DOSY NMR shows 2 lines indicating two species in the sample. The GPC trace shows a bimodal distribution, this could be cause by some of the PEG-OH not coupling to **NE1** (Figure 3.17). The two signals in the $^1$H DOSY NMR both contain the PHEMA and PEG signals.

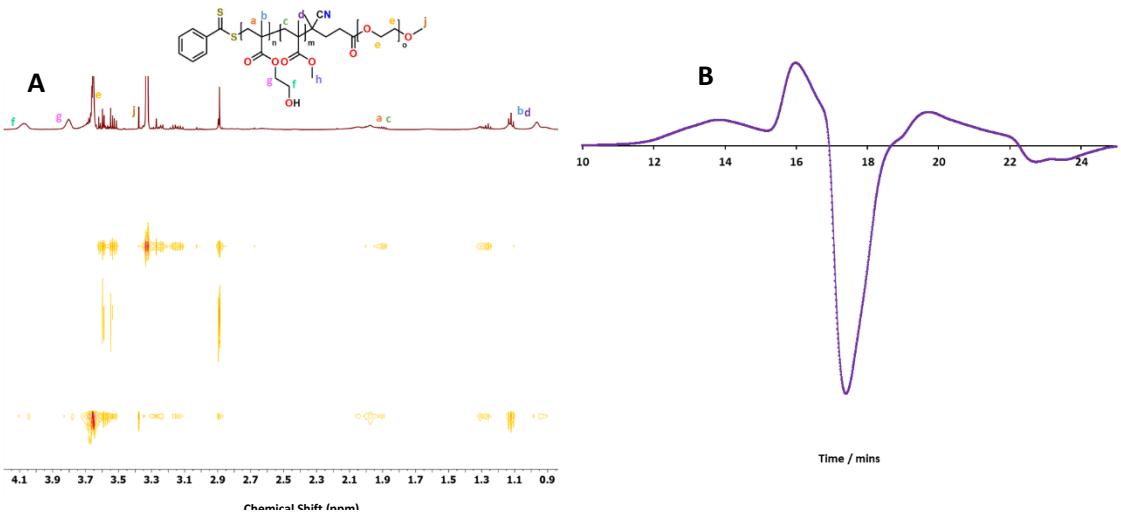


*Figure 3.17 The annotated $^{1}$H DOSY NMR spectrum of PNE1 (A) and its GPC trace (B).*

Furthermore, in the $^{1}$H NMR of **PNE1** the methoxy peak from the PMMA is absent at 3.60 ppm. This could be due to the triblock polymer self-assembling in the solution.[142] When the micelles are formed the mobility of the PMMA group would be reduced which results in the corresponding NMR signal to decrease. However, the DP of PMMA can still be calculated due to the multiplet at 1.4 – 0.8 ppm, since the integration is larger than expected for the $-CH_2$-C-C**H$_3$**- of the PHEMA, it can be assumed that the rest of the integral is the –C-$CH_3$- group of the PMMA.

Other than the case of **PNE1** the PEGylation has given a similar result to which is mentioned in section 3.3 indicating that there is not a significant difference in performing the PEGylation before or after the second RAFT polymerisation. All triblock copolymers including **PNE1** were successfully synthesised.

## 3.7. Deprotection of triblock copolymers

The PMAPC1 and PTBuMA containing triblock copolymer were deprotected using TMSiBr and TFA respectively. When using the TMSiBr method the intermediate fully dissolved when methanol was added. This was an indication that the deprotection was successful because the protected version was not soluble in methanol. Neither the $M_{n(GPC)}$ nor dispersity could be calculated for the deprotected block copolymers, this is due to the triblock copolymers having limited solubility in DMF and water and it can be assumed that they self-assemble in these solvents (Table 3.7).

*Table 3.7* Result table for the deprotected block copolymers, show the polymer sequence and $M_{n(NMR)}$.

| Entry | Precusor | Block sequence | $^{a}M_{n(NMR)}$ / g mol$^{-1}$ |
|---|---|---|---|
| PNF1 | PND1 | PEG-PMMA-PMAPC1 | 9800 |
| PNF2 | PND2 | PEG-PMMA-PMAPC1 | 7800 |
| PFN1 | PDN1 | PEG-PMAPC1-PMMA | 5600 |
| PFN2 | PDN2 | PEG-PMAPC1-PMMA | 10300 |
| PF1 | PD4 | PEG-PMAPC1 | 3100 |
| PNQ1 | PNT2 | PEG-PMMA-PMAA | 3800 |
| PNQ2 | PNT1 | PEG-PMMA-PMAA | 4300 |
| PQN1 | PTN1 | PEG-PMAA-PMMA | - |

$^{a}M_{n(NMR)}$ were determined by $^{1}$H NMR

Like in the case of **PNE1** the PMMA peak at 3.60 ppm could not be seen, this is due to the polymers self-assembling and the hydrophobic block, PMMA, being in the core of the assembled

structure. In the $^{1}$H NMR spectrum of **PNF1** there is no appearance of the peaks at 4.10 and 3.70 ppm which corresponded to the methoxy groups and the methylene group in PMAPC1 which suggests the polymer was deprotected. Also there is the appearance of a broad singlet at 4.20 ppm which corresponds to the phosphonic acid OHs. In the $^{31}$P{H} NMR the peak has shifted from 31 ppm to 16 ppm which also indicates that a new phosphorous environment (Figure 3.18).

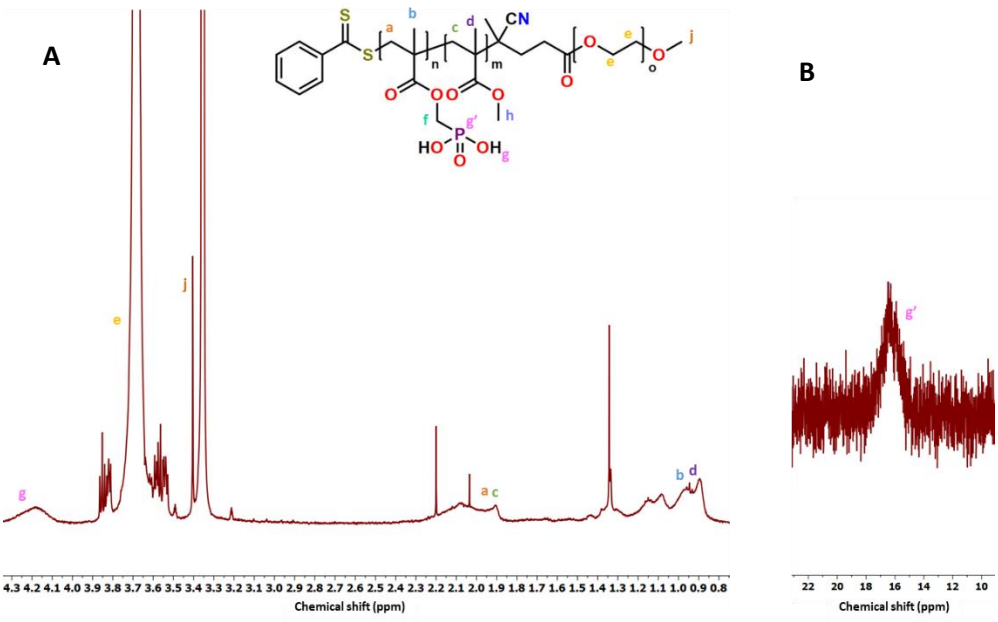


*Figure 3.18 Annotated $^{1}$H NMR (A) and $^{31}$P{H} NMR (B) spectra of **PNF1.***

The TBuMA deprotections were also successful. There was a complete reduction in the peak at 1.40 ppm which corresponded to the *tert*-butyl peak of the PTBuMA (Figure 3.19). However, $^{1}$H DOSY NMR could not be used to determine one species was present. $^{1}$H DOSY NMR is an ineffective way to confirm that only one species was present in these sample because the deprotected sample is not completely soluble in many common deuterated solvents.

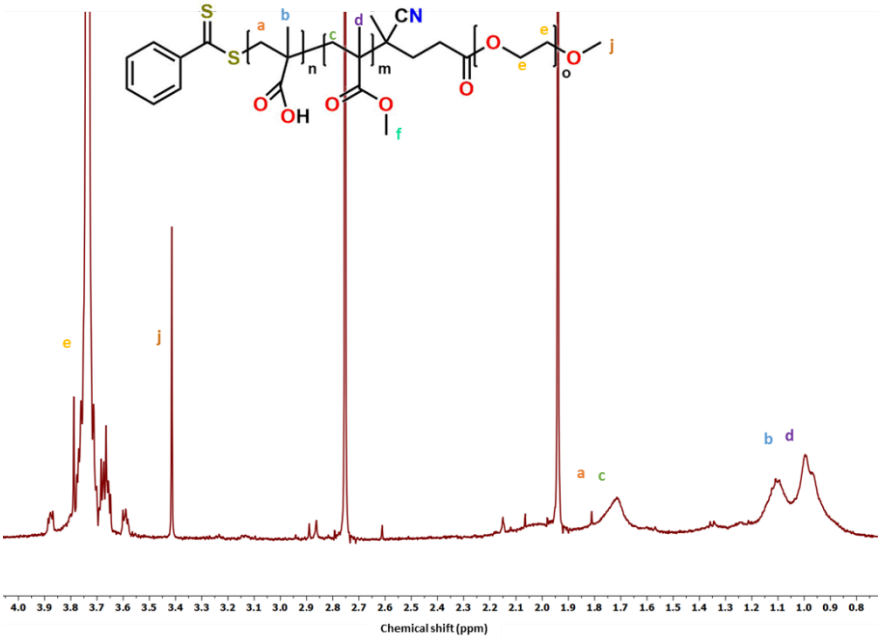


*Figure 3.19 Annotated $^{1}$H NMR spectrum of **PNQ2.***

The deprotection of **PQN1** could not be determined as a success through NMR spectroscopy due to its insolubility in the majority of common solvents, a clear NMR was impossible to obtain. In order to give an indication of the polymer structure IR spectroscopy was employed. There was a broad signal at 3350 $cm^{-1}$ that corresponds to a OH group of carboxylic acid which would suggests that **PQN1** has been deprotected (Figure 3.20).

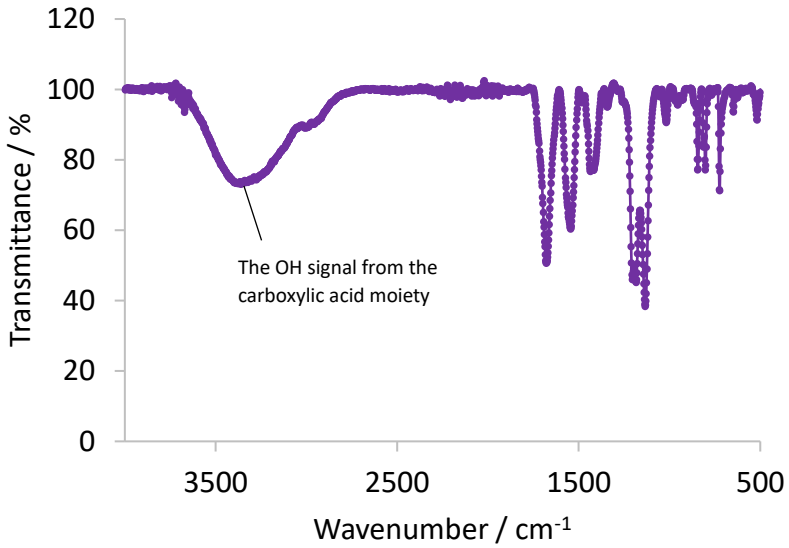


*Figure 3.20 IR spectrum of **PQN1.***

## 3.8. Conclusions and future work

A library of triblock polymers have been synthesised by RAFT polymerisation and deprotected. It was shown that the reaction conditions in which DMAc and CPAD were used could be further optimised for MMA RAFT polymerisation. Additionally when PMMA was incorporated into the block copolymer it gave rise to the largest increase in disperisity in all polymers indicating that the polymerisation of MMA is not well controlled under these conditions. Regardless of if MMA was the first or second block polymerised, the MMA conversion only reached 50 %. MAPC1 was successfully polymerised and incorporated into a block copolymer with MMA. Polymer **PD1** showed a bimodal distribution in the GPC trace indicating that the polymerisation could have contained by oxygen, resulting in early termination. The PEGylations of the diblock and homopolymers were successful and there is minimal difference in dispersities suggesting that the PEGylation can be performed at any stage of the synthesis. Increasing the CTA: AIBN ratio showed that the polymerisation proceeded at a slower rate, this is due to there being less radicals formed in the reaction. In the homopolymerisation of MAPC1 it was shown that lowering the CTA: AIBN ratio to 1: 1 resulted in an uncontrolled polymerisation due to there being a large excess of radicals in the polymerisation. Three other monomers were polymerised using a PMMA macroCTA: HEMA, DMAE and TBuMA. All three monomers were polymerised successfully, however, there dispersity of the copolymers increased significantly from 1.25 to 1.52, which suggests that the current conditions need further optimisations. The polymerisation of DMAE showed colour change from red to orange which suggests that the monomer has interacted with CPAD. The resulting polymer was also orange which gives a strong indication that the fidelity of the CTA has been compromised and would not be useful as a macroCTA. After the deprotection of the triblock copolymers in both the PMAPC1 and PTBuMA copolymers there was a disappearance of the PMMA signal at 3.60 ppm which indicates that the triblock copolymers had self-assemble. In the case of **PQN1** where the triblock was insoluble in the

common deuterated NMR solvents, IR spectroscopy was used to confirm that the *tert*-butyl deprotection has taken place.

In the future the polymerisation of HEMA, DMAE, TBUMA and MMA would need to be optimised to ensure that the polymerisations are controlled. It would be beneficial to synthesise triblock copolymers which had the block sequence of PEG-*b*-PDMAE-*b*-PMMA and PEG-*b*-PHEMA-*b*-PMMA. These polymers would be analogous to PEG-*b*-PMAPC1-*b*-PMMA since the polymer sequence can drastically change the solubility and nucleation properties. It would be advantageous to investigate the ratio of PMMA incorporated into the triblock copolymers, because the hydrophobic block is the driving force behind self-assembly of block copolymers and would change the cmc. In this thesis, the PMMA block is a large proportion of the polymer structure, potentially providing a smaller PMMA segment would increase the solubility of the copolymer in water while maintaining its ability to self-assemble.

# Chapter 4 Polymer induced nucleation of hydroxyapatite

## 4.1 Introduction

Biomineralisation of HAP is a complex cell controlled process which is initiated when the cells secrete an extracellular matrix which determine the morphology of the HAP.[28] Proteins are a major component in the extracellular matrix, and the interactions of these with the structural framework of the tooth and their ability to attract ions is how crystallisation is initiated. The growth and regulation of the resulting crystallites are also regulated by proteins. There is a supersaturated solution of calcium and phosphate ions in the extracellular matrix and without the regulation of the proteins, HAP would spontaneously precipitate out.[28]

Amelogenin and DPP are two labile proteins that are important for the formation of the tooth. These proteins can self-assemble into many different structures such as ribbons or spheres. However the self-assemble is sensitive to many factors such as pH, temperature and presence of ions.[4,28] In the presence of calcium ions amelogenin can self-assemble into 14 nm spheres and can assemble into higher ordered structures such as chains.[3,38] In the case of DPP, when calcium ions bind to the protein the flexibility of the structure decreases and it assembles into β-sheets.[28] Both proteins contain a large number of charged amino acids, which directs the growth of the HAP crystals by preferentially binding to the (100) face rather than (001) face. This promotes growth along the c-axis of the crystal.[4,7,143] In amelogenin, the C-termus contains many charged groups which bind to the HAP crystal, however when the terminus is removed the affinity for the protein to bind to HAP decreases.[24,25] DPP is a highly charged protein where the majority of amino acids are aspartic acids and phosphorylated serines. The highly charged nature of the proteins means it can act as a sink for calcium ions. The protein also contains two binding sites, so it can bind to both calcium and phosphate ions as well as HAP.[29] The binding ability of DPP was hindered when the protein was dephosphorylated, this indicates the importance of the phosphorylated serine groups in mineralisation.[29,143,144]

In amelogenisis, it is indicative that the self-assembly and the charged groups of the proteins are important for the growth and regulation of HAP. With this knowledge a series of block copolymers were synthesised by RAFT polymerisation. In this chapter the triblock copolymers synthesised in Chapter 3 are investigated in their ability to nucleate HAP and to act as a protective film against enamel erosion by acids. The block copolymers were formed of a PEG block, PMMA block and a block which contained a functional group; hydroxyl, carboxylic acid, phosphonic acid and amine groups. The PMMA block was used for its hydrophobic properties and this will drive self-assembly of the triblock copolymer. Furthermore PMMA can act as a hydrophobic barrier against acid attack in the protection of enamel.[34] The PEG group was chosen because it is biocompatibility and is used to provide another hydrophilic block in the copolymer in order to make the block copolymer more soluble. This will decrease the possibility of precipitation and favour the self-assemble of the triblock. A novel triblock polymer containing phosphonic acid moieties, PEG-*b*-PMAPC1acid-*b*-PMMA, and one containing PMAA were investigated as both functional groups bind strongly to tooth enamel in previous research.[34,61] Moreover, these groups are present in DPP and in the C-terminus of amelogenin which are responsible to directing the growth of HAP in biomineralisation.[4,28,61,143,145] HEMA and DMAE were chosen as the hydroxyl and amine blocks respectively. The hydroxyl group has been shown to nucleate HAP when used as a self-assembled monolayer and is suspected to bind to the calcium ions first.[146] An amine self-assembled monomer layer has been found to precipitate calcium phosphate, although they are usually used in the nucleation of HAP when partnered with another functional group such as carboxylic acids.[147] Amines have also been shown to affect the growth of silica and calcite.[60,148] The use of three chemically different monomers in the

polymers means that these triblock copolymers are also classed are terpolymers. The benefits of using terpolymers is that many more morphologies can been accessed such as micelles with a ring morphology, this gives more option for fine-tuning the polymers for the nucleation of HAP.[149–151]

## 4.2 Morphology of RAFT synthesised polymers

The self-assembling ability of the block copolymers from Chapter 3 were explored (Figure 4.1) and their hydrophilic mass fractions were calculated. The mass fractions were not calculated for the PMAA and PMAPC1acid containing copolymers because it is uncertain how much the ionic strength from the acids contribute to the hydrophilic mass fractions.

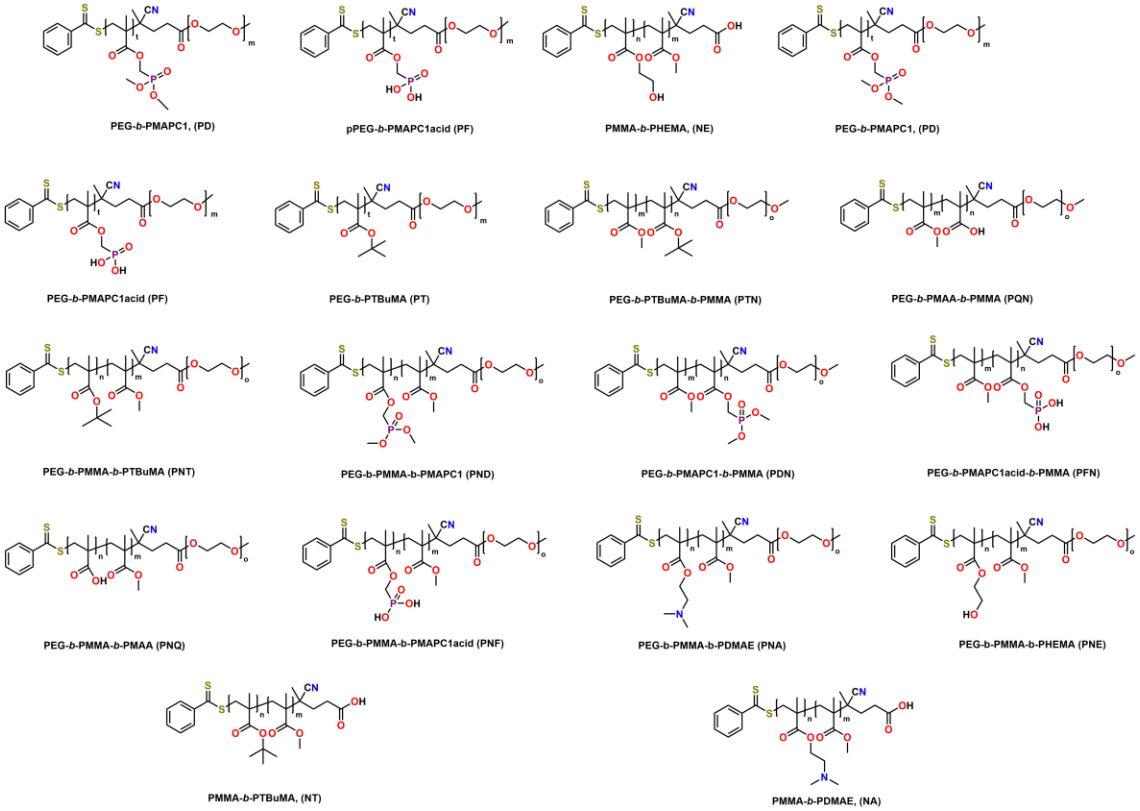


*Figure 4.1 The structures of the copolymers synthesised by RAFT polymerisation Chapter 4*

In the cases of PHEMA and PDMAE containing copolymers the equation mentioned in Chapter 2 was slightly altered so that the mass of PHEMA and PDMAE were included in the hydrophilic segment as they are both classed as hydrophilic blocks (Table 4.1). The polymers such as PMMA-*b*-PMAPC1 a hydrophilic mass fraction could not be calculated since there is no hydrophilic segment in the copolymer. The majority of block copolymers have a hydrophilic mass fraction above 0.5. When PMMA is added the mass fraction is lowered and the reverse occurs when PEG is coupled to the polymer. The majority of polymers should exhibit a micellular self-assembly according to the research carried out by Savic *et al.*[103]

*Table 4.1 A table showing the hydrophillic mass fractions, f and cmc, of the RAFT synthesised block copolymers where applicable, Mn = Mn(NMR), asterisk indicates a linear regression line however no two distinct data sets*

| Entry | Block Sequence | Block $M_n$ / g $mol^{-1}$ | PEG $M_n$ / g $mol^{-1}$ | PMMA $M_n$ / g $mol^{-1}$ | Hydrophilic fraction, *f* | Cmc / mg $cm^{-3}$ |
|---|---|---|---|---|---|---|
| **PQN1** | PEG-*b*-PMAA-*b*-PMMA | 1800 | 2100 | 1600 | - | - |
| **NA1** | PMMA-*b*-PDMAE | 15500 | - | 7100 | 0.69 | $2.91 \times 10^{-3}$ |
| **ND1** | PMMA-*b*-PMAPC1 | 10400 | - | 2300 | - | $2.54 \times 10^{-2}$ |
| **ND2** | PMMA-*b*-PMAPC1 | 15400 | - | 2300 | - | - |
| **NT1** | PMMA-*b*-TBuMA | 6100 | - | 7100 | - | - |
| **NT2** | PMMA-*b*-PTBuMA | 4100 | - | 3600 | - | - |
| **NE1** | PMMA-PHEMA | 15100 | - | 7100 | 0.68 | - |
| **PD1** | PEG-*b*-PMAPC1 | 2500 | 6400 | - | 0.72 | 1.04 |
| **PD2** | PEG-*b*-PMAPC1 | 8300 | 5500 | - | 0.40 | * |
| **PD3** | PEG-*b*-PMAPC1 | 1500 | 2200 | - | 0.61 | 1.16 |
| **PD4** | PEG-*b*-PMAPC1 | 1250 | 2100 | - | 0.64 | * |
| **PF1** | PEG- *b*-PMAPC1acid | 1000 | 1700 | - | - | 0.447 |
| **PDN1** | PEG-*b*-PMAPC1-*b*-PMMA | 1500 | 2200 | 2200 | 0.38 | $4.28 \times 10^{-3}$ |
| **PDN2** | PEG-*b*-PMAPC1-*b*-PMMA | 2500 | 6400 | 1500 | 0.68 | $9.46 \times 10^{-4}$ |
| **PDN3** | PEG-*b*-PMAPC1-*b*-PMMA | 8300 | 5500 | 5000 | 0.36 | * |
| **PFN1** | PEG-PMAPC1acid-PMMA | 1200 | 2200 | 2200 | - | $7.47 \times 10^{-3}$ |
| **PFN2** | PEG-*b*-PMAPC1acid-*b*-PMMA | 2100 | 6400 | 1500 | - | $6.55 \times 10^{-3}$ |
| **PNA1** | PEG-*b*-PMMA-*b*-PDMAE | 1100 | 1900 | 700 | 0.68 | $1.12 \times 10^{-2}$ |
| **PND1** | PEG-*b*-PMMA-*b*-PMAPC1 | 2100 | 6200 | 1900 | 0.86 | $9.38 \times 10^{-2}$ |
| **PND2** | PEG-*b*-PMMA-*b*-PMAPC1acid | 600 | 6200 | 1100 | 0.76 | 0.179 |
| **PNE1** | PEG-*b*-PMMA-*b*-PHEMA | 1300 | 2100 | 1200 | 0.87 | $1.21 \times 10^{-2}$ |
| **PNF1** | PEG-*b*-PMMA-*b*-PMAPC1acid | 1800 | 6200 | 1900 | - | 0.235 |
| **PNF2** | PEG-*b*-PMMA-*b*-PMAPC1acid | 500 | 6200 | 1100 | - | $1.98 \times 10^{-2}$ |
| **PNQ1** | PEG-*b*-PMMA-*b*-PMAA | 500 | 2100 | 1200 | - | 0.156 |
| **PNQ2** | PEG-*b*-PMMA-*b*-PMAA | 900 | 2200 | 1200 | - | $2.83 \times 10^{-2}$ |
| **PNT1** | PEG-*b*-PMMA-*b*-PTBuMA | 1300 | 2200 | 1200 | 0.47 | - |
| **PNT2** | PEG-*b*-PMMA-*b*-TBuMA | 710 | 2100 | 1200 | 0.54 | - |
| **PT1** | PEG-*b*-PTBuMA | 3000 | 2100 | - | 0.41 | - |
| **PTN1** | PEG-*b*-PTBuMA-*b*-PMMA | 3000 | 2100 | 1600 | 0.31 | - |

With the hydrophilic mass fractions in mind the cmcs were determined through fluorescence spectroscopy and DLS. These two techniques give comparable results, as demonstrated by Bakkour et al.[152] For the fluorescence spectroscopy, pyrene was doped into the polymer solution, the same as in Chapter 2. In DLS, the mean count rate is used to determine the cmc of the polymers. The RAFT polymers, **PNT2**, **PNT1**, **PT1**, **NT2**, **PTN1** and **NT1** did not have their cmcs calculated, as two blocks of the copolymers are highly hydrophobic, as a result it was assumed that precipitation would occur rather than micro segregation of the blocks. The addition of PMMA to the PEGylated diblock showed a decrease in the cmc, this was evident in **PD3** which cmc was 1.16 mg $cm^{-3}$ (Figure 4.3). Then when the PMMA block was incorporated the cmc decreased to 4.28 x $10^{-3}$ mg $cm^{-3}$ (Figure 4.21) in **PDN1**. The addition of the PMMA block increases the interfacial free energy between the polymer and water, as a result lower concentrations are needed for micelle formation to decrease that interfacial free energy. In the case of PEG-*b*-PMAPC1 polymers some of the copolymers **PD2** and **PD4** did not reach a cmc however showed linearity in the data set which would indicate that self-assemble could occur at higher concentrations than that what was investigated (Figure 4.12 and Figure 4.14 respectively). **PD4** has a larger PMAPC1 segment than it does PEG which could also contribute to the lack of self-assembly. The PEG chain can form hydrogen bonds and have dipole-dipole interactions with the water. If there is an insufficient PEG coverage around the micelle, the hydrophobic core would be exposed to the water and destabilises the micelle.[50]

In both **PDN2** and **PDN1** deprotecting the PMAPC1 block causes a slight increase in their cmcs (Figure 4.19 and Figure 4.21 respectively). This indicates the stabilisation that the self-assemble structure gains from the PMMA is sufficient to maintain the assembly even with the introduction of a charged block. However cmc of **PDN2** increases in almost a magnitude upon deprotection (9.45 x $10^{-4}$ mg $cm^{-3}$ to 6.55 x $10^{-3}$ mg $cm^{-3}$) whereas in the deprotection of **PDN1** the cmc increases by 0.40 x $10^{-3}$ mg $cm^{-3}$. The reason for this could be due to the ratio of hydrophobic block to hydrophilic. In **PDN2** the ratio of hydrophobic-hydrophilic is 38 : 62 but when deprotected it becomes 15 : 85. This means overall there is a small hydrophobic segment which leads to a lower interfacial free energy , as a result a higher concentration of polymer is needed to force micellation. In the polymers where PEG was added to the PMMA diblock copolymer there was an increase in cmc for all the copolymers. **PFN2** and **PNF1** have similar block molecular weights however **PNF1** has a much higher cmc (0.235 mg $cm^{-3}$) than **PFN2** (6.55 x $10^{-3}$ mg $cm^{-3}$) (Figure 4.10 and Figure 4.7 respectively). The difference in behaviour could be due to the difference in the structure, **PFN2** has PMAPC1 extended into the corona of the micelle along with the PEG chain, whereas **PNF1** has the PMMA block separating them. By having the PMMA between the two hydrophilic blocks would disrupt the interactions between the water molecules less than having the PMMA on the end of the triblock, which means that it has a lower interfacial free energy, leading to a higher cmc for **PNF1**. **PNF1** has a much higher cmc than **PNF2** (Figure 4.6) because **PNF1** has a much larger PMAPC1 block contributing to the hydrophilic part of the triblock, which increases the cmc of the polymer. Triblock **NA1** (Figure 4.9) cmc increases from 2.91 x $10^{-3}$ mg $cm^{-3}$ to 1.12 x $10^{-2}$ mg $cm^{-3}$ when PEGylated (**PNA1,** Figure 4.5), this is due to the PEG chain providing interactions with the water which hydrates the micelle increasing the cmc.[153] The PEG-*b*-PMMA-*b*-PMAA copolymers have similar structures except in **PNQ1**'s PMAA unit is 400 g $mol^{-1}$ shorter than that of **PNQ2**, however there cmcs are very different 0.156 mg $cm^{-3}$ and 2.83 x $10^{-2}$ mg $cm^{-3}$ respectively (Figure 4.13 and Figure 4.17). This could be attributed to the PMAA block in **PNQ1** not covering all the surface of the PMMA core resulting in the destabilisation of the micelle and increasing the cmc of the copolymer. **PNE1** showed a cmc of 1.21 x $10^{-2}$ mg $cm^{-3}$ (Figure 4.4) however with its predecessor the cmc could not be determine even when water (20 % ethanol v / v) was used to help dissolve the polymer like in **PNE1**. This would indicate that the PMMA block of **NE1** is too long for micellation instead causing

macroprecipitation to occur. The cmc for **PQN1** could not be determined because the polymer was insoluble in water even when 20 % ethanol was used.

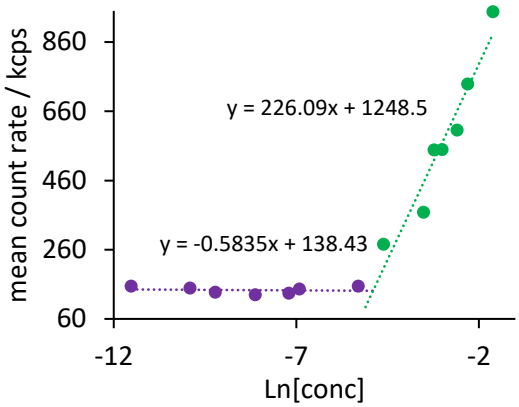


*Figure 4.2 The cmc graph of **PFN1** by DLS*

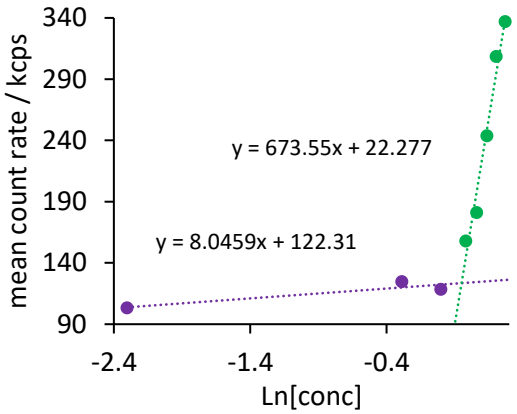


*Figure 4.3 The cmc graph of **PD3** by DLS*

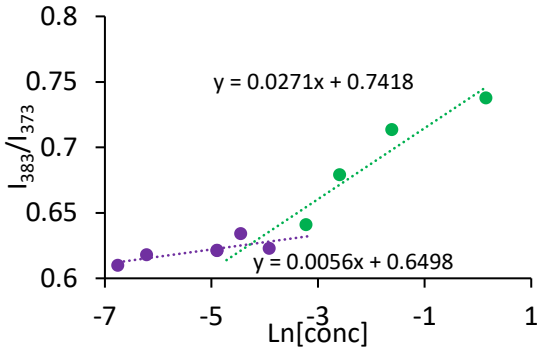


*Figure 4.4 The CMC graph for **PNE1** by fluorescence spectroscopy*

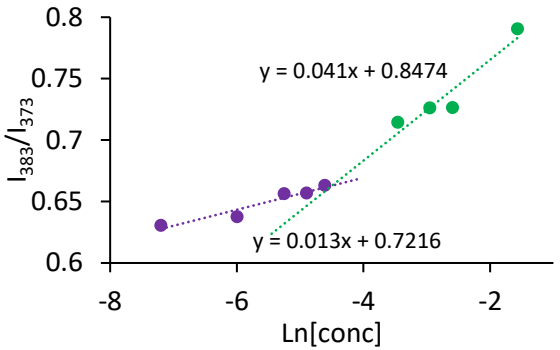


*Figure 4.5 The cmc graph of **PNA1** by fluorescence spectroscopy*

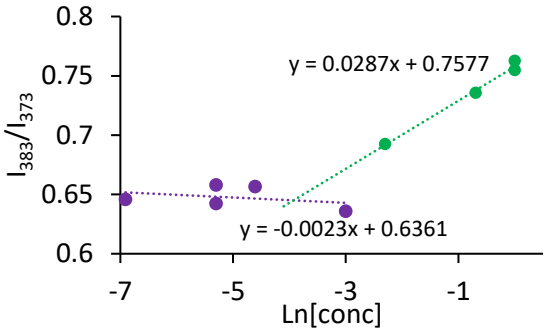


*Figure 4.6 The cmc graph for **PNF2** by fluorescence spectroscopy*

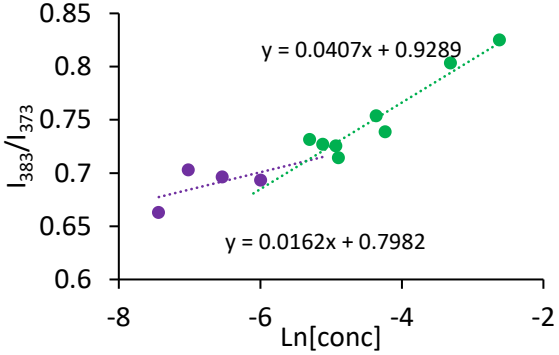


*Figure 4.9 The cmc graph **NA1** by fluorescence spectroscopy*

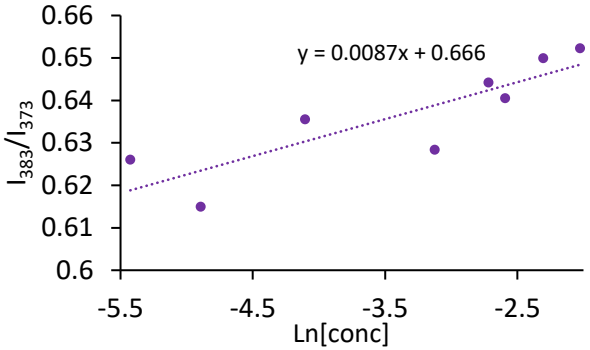


*Figure 4.8 The cmc graph of **PFN2** by fluorescence spectroscopy*

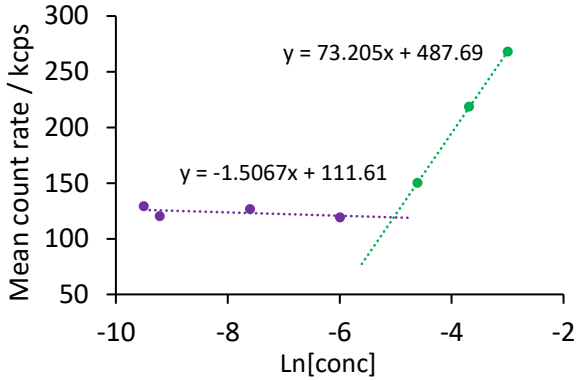


*Figure 4.7 The cmc graph of **PFN2** by DLS*

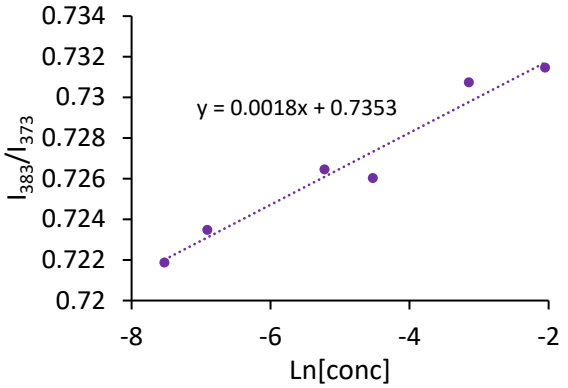


*Figure 4.12 The cmc graph of **PD3** by fluorescence spectroscopy*

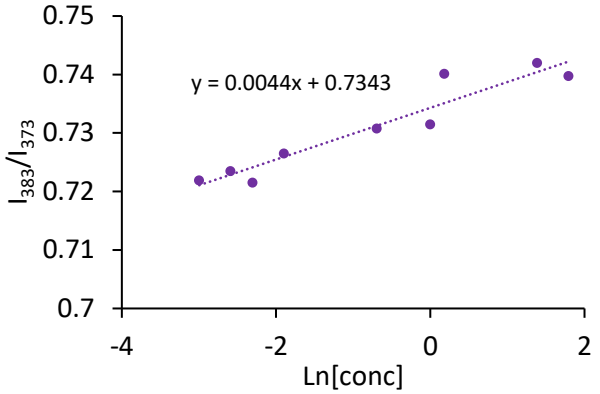


*Figure 4.11 The cmc graph of **PD2** by fluorescence spectroscopy*

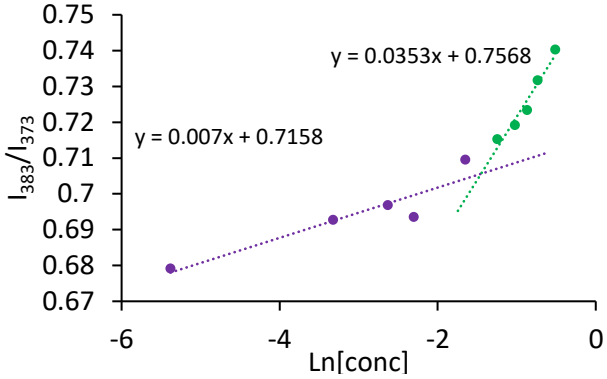


*Figure 4.10 The cmc graph of **PNF1** by fluorescence spectroscopy*

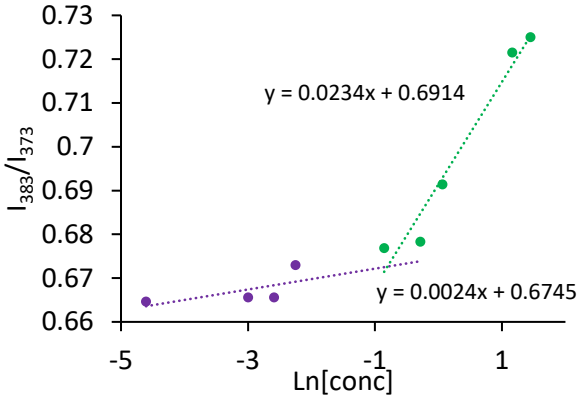


*Figure 4.15 The cmc graph of **PF1** by fluorescence spectroscopy*

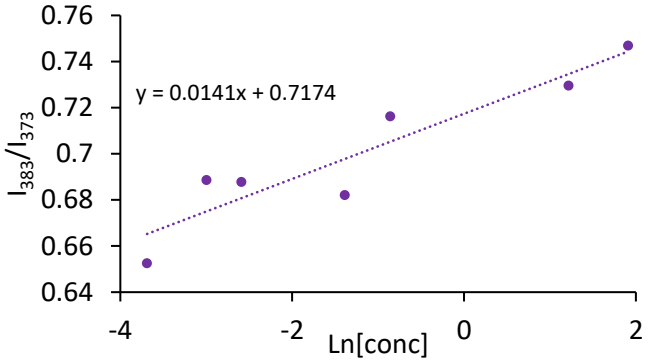


*Figure 4.14 The cmc graph for **PD4** by fluorescence spectroscopy*

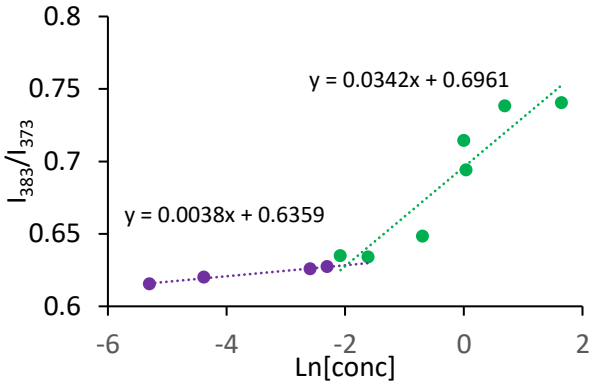


*Figure 4.13 The cmc graph of **PNQ1** by fluorescence spectroscopy*

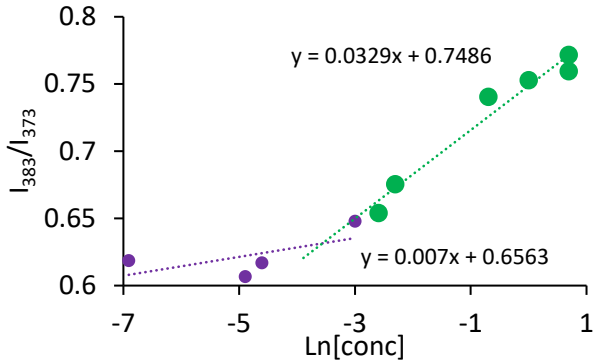


*Figure 4.17 The cmc graph of **PNQ2** by fluorescence spectroscopy*

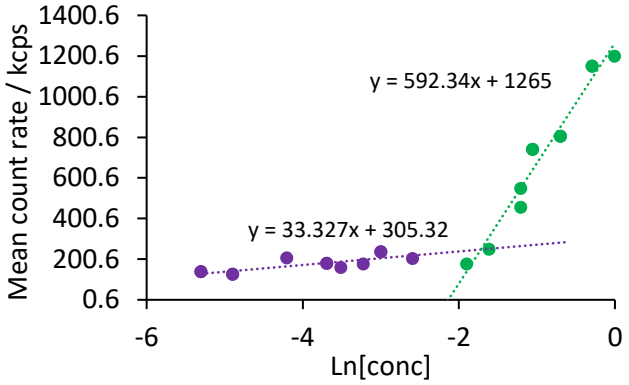


*Figure 4.16 The cmc graph of **PND2** by DLS*

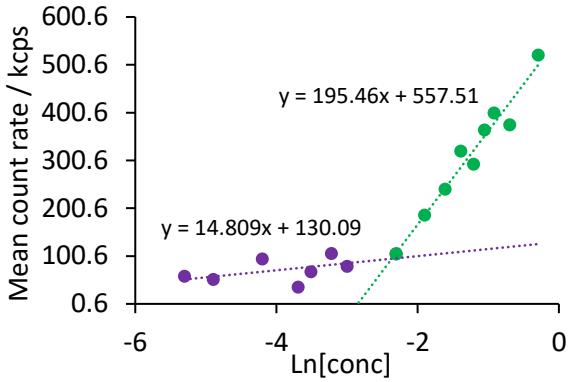


*Figure 4.18 The cmc graph of **PND1** by DLS*

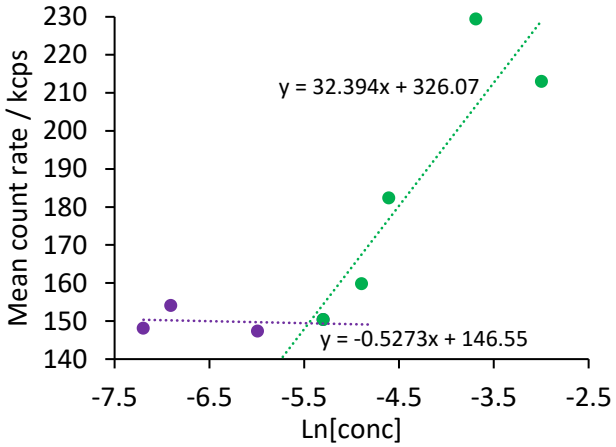


*Figure 4.21 The cmc graph of **PDN1** by DLS*

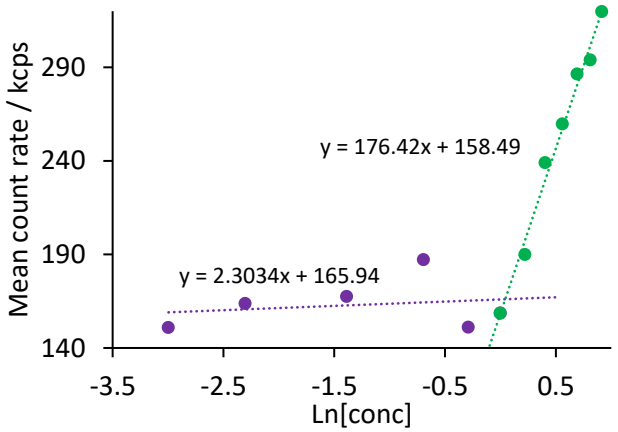


*Figure 4.20 The cmc graph of **PD1** by DLS*

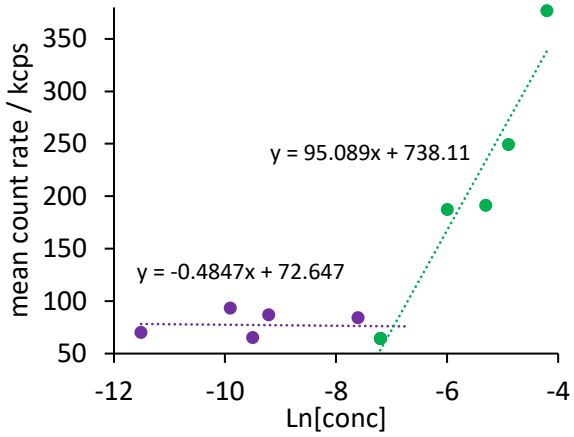


*Figure 4.19 The cmc graph of **PDN2** by DLS*

Subsequently, the self-assembling morphology above the cmc was analysed for the following polymers: **PD2**, **PDN3**, **PFN1**, **PFN2**, **PF1**, **PNA1**, **PNE1**, **PQN1**, **PNQ1** and **PNF2**. These polymers were taken to give a representation of each polymer class synthesised by RAFT polymerisation. The imaging was conducted using TEM with uranyl acetate used as a negative staining agent to give clear images of the copolymers (Figure 4.22).

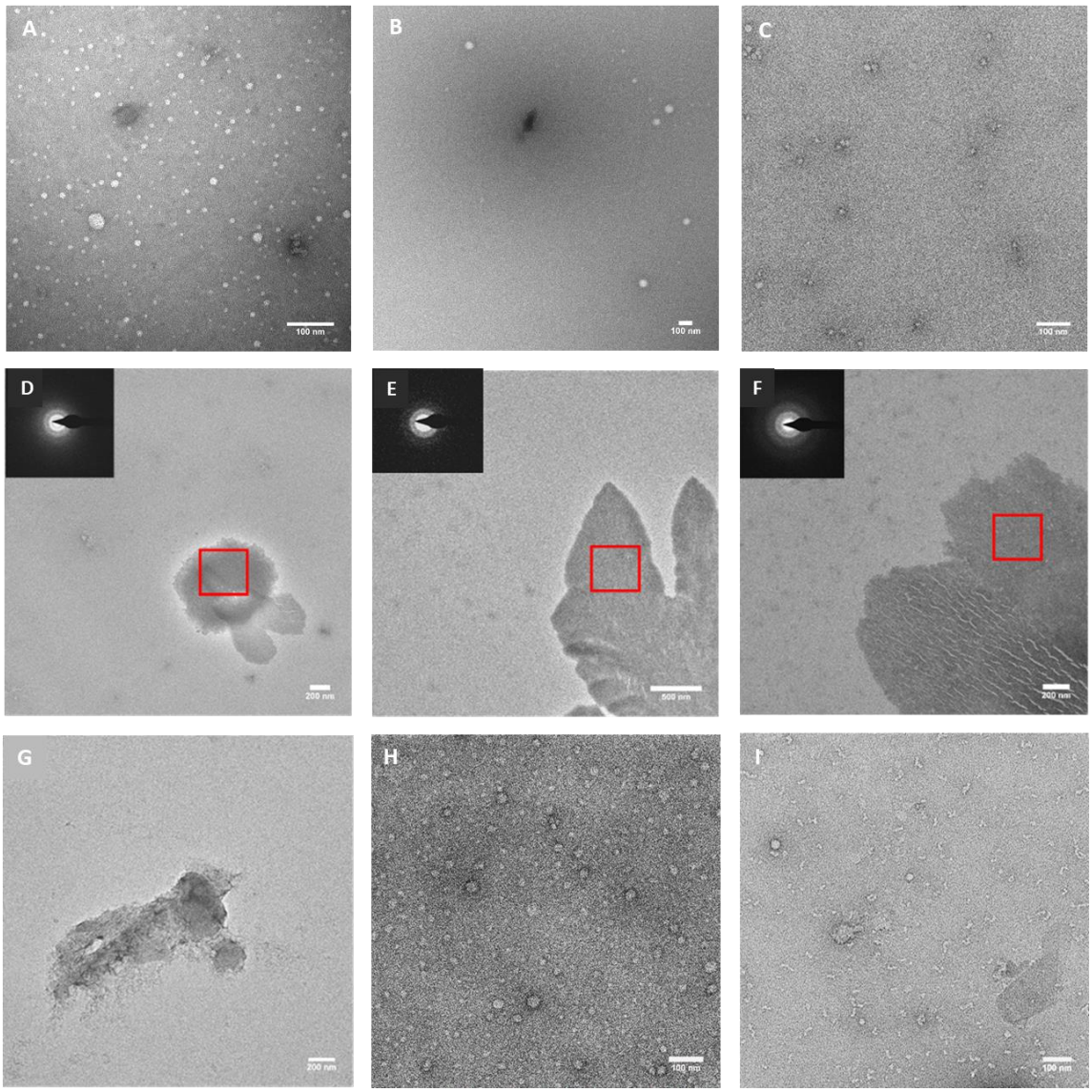


*Figure 4.22 A series of negatively stained TEM micrographs and electron diffraction patterns of **PFN1** at 0.1 mg cm$^{-3}$ (A), **PDN3** at 0.1 mg cm$^{-3}$ (B), **PNF2** at 1 mg cm$^{-3}$ (C), **PD2** at 0.1 mg cm$^{-3}$ (D) **PNQ1** at 0.1 mg cm$^{-3}$ (E), **PF1** at 0.1 mg cm$^{-3}$ (F), **PQN1** at 0.11 mg cm$^{-3}$ (G), **PNA1** at 0.1 mg cm$^{-3}$ (H) and **PNE1** at 0.1 mg cm$^{-3}$ (I). The red square indicates were the diffraction pattern was taken from*

At 0.1 mg cm$^{-3}$ **PFN1** forms two sets of self-assembled species, larger micelles at around 40 nm and smaller micelles at approximately 13 nm (Figure 4.22A). The range in micelle size would be attributed to the bimodal dispersity of the block copolymers, as **PDN1** had a Đ = 1.59. **PDN3** has also been imaged at 0.1 mg cm$^{-3}$ and also shows micelles of 70 nm in size. (Figure 4.22B). The size difference between **PDN3** and **PFN1** could be attributed to the lack of electrostatic stabilisation. **PNF2** forms spheres approximately 20 nm in diameter (Figure 4.22C). **PD2**, **PNQ1**, **PF1** and **PQN1** were polymers PEG-*b*-PMAPC1, PEG-PMMA-*b*-PMAA, PEG-*b*-PMACP1acid and PEG-*b*-MAA-*b*-PMAA respectively. Each of these polymers were shown not to self-assemble below 2 mg cm$^{-3}$. In the TEM images for each polymer, a film can be observed which indicates that the uranyl acetate has interacted with the polymer (Figure 4.22D-G). With these images

there are two scenarios for the polymers' self-assembling properties. First the polymers have formed films due to them being dehydrated. Secondly the polymers have a lamellae self-assembly and this assembly would not be able to be tracked through DLS. These films could be observed through polarised light microscopy to observe the polymers in their native environments and prove which scenario is correct. If the films are smaller than the resolution provided by the polarised light microscope then cryo-TEM could be utilized. Furthermore electron diffraction confirms that structures in Figure 4.22D-F are not uranyl acetate crystals or other salts since the structure do not show signs of crystallinity.

**PNA1 (**PEG-*b*-PMMA-*b*-PDMAE**)** was tested because PAH contains an amino moiety which has been shown to influence calcite nucleation and an amine containing compound can be used to nucleate silica crystals.[148,154,155] PHEMA was chosen to see if a non-ionic functional group could also influence the growth of CaP. **PNA1** has a similar morphology to the phosphonic triblock copolymers that self-assembled, it as well showed spheres (Figure 4.22H). The spheres are 22 nm in diameter which is similar to that of **PNF2** and **PFN1**. However in the case of **PNE1 (**PEG-*b*-PMMA-*b*-PHEMA**)** two morphologies are observed, worms and spheres (Figure 4.22I). The spheres were 30 nm in diameter and the worms were 40 nm in length respectively. The main difference between **PNE1** and the PMAPC1acid, PMAA and PMDAE polymers is that **PNE1** is classed as a non-ionic polymer whereas the others are classed as ionic polymers. It has been reported that the electrostatic repulsion caused by the ionic moieties prevents micelles from fusing to form worms or vesicles.[50,156] This suggests that **PFN1**, **PNF2** and **PNA1** are kinetically trapped spheres. This could be investigated further by synthesising triblock copolymers where PMAPC1acid, PMAA and PMDAE blocks are different lengths and see if the morphology changes from spheres, if not then it would be a strong indication of a kinetically trap morphology.

For the polymers which had self-assembled, their structure stability in water were also looked at over 45 mins by DLS. From the DLS measurements the hydrodynamic diameter can be determined, which gives an idea of the micelle size in solution (Table 4.2).

*Table 4.2* Diameter of the self-assembled polymers by DLS and TEM

| Sample | Polymer concentration / g $mol^{-1}$ | Hydrodynamic diameter / nm | TEM Diameter / nm |
|---|---|---|---|
| **PFN1** | 0.1 mg $cm^{-3}$ | 59.1 ± 11 | 13 |
| **PFN2** | 1.0 mg $cm^{-3}$ | 181.6 ± 19 | - |
| **PNF2** | 1.0 mg $cm^{-3}$ | 6.0 ± 14 | 20 |
| **PNA1** | 0.1 mg $cm^{-3}$ | 138.0 ± 20 | 22 |
| **PNE1** | 0.1 mg $cm^{-3}$ | 186.8 ± 50 | 30 – 40 |

When comparing the sizes obtained from the TEM and the DLS, the hydrodynamic radius is much larger for the majority of the polymers **PFN2**, **PNA1** and **PNE1**. DLS is a bulk technique so having dust particles which are around 1 µm in diameter can increase the mean particle size significantly, which could have happened here. Furthermore, during preparation the TEM samples have to dried in preparation for TEM, which could have caused shrinkage or aggregation of the self-assembled structures. To confirm the size of the structures in water cryo-TEM could be used to observe the polymer morphology. Additionally the size given by DLS is not accurate with structures that are anisotropic because these structures are seen as multiple entities, as a result a change in the length of the worm particles would drastically affect the size given by the DLS. This would suggest the size given for **PNE1** is not the true size. DLS can also provide other useful information such as the charge of the particles which should be studied in the future to

see how much electrostatic repulsion occurs in these polymeric micelles and give more information of the latex's stability.

## 4.3 The nucleation of hydroxyapatite

The polymers; **PD2**, **PDN3**, **PFN1**, **PFN2**, **PF1**, **PNA1**, **PNE1**, **PQN1**, **PNQ1** and **PNF2** were mixed with $CaCl_2$ and $KH_2PO_4$ to give final concentrations of $Ca^{2+}$ and $PO_4^{3-}$ 2.25 mM and 1.05 mM respectively. The growth of CaP was monitored by DLS, which calculates particle size based on the Brownian motion of particles. Particles experience Brownian motion, so smaller particles move faster in solution and have higher kinetic energy, while bigger particles move slower and tend to sediment faster as they possess less kinetic energy. The relation between the speed of the particles and particle size is given by the Stokes-Einstein equation (Equation 4.1).

$$D = \frac{k_B T}{6\pi\eta R_H}$$

*Equation 4.1 The Stokes-Einstein equation. D = translational diffusion coefficient, $k_B$ = Boltzman constant, T = temperature, $\eta$ = viscosity, $R_H$ = hydrodynamic radius*

The growth of the crystals would be observed in DLS as an increase in size, once these crystals begin to sediment this would be seen as a size decrease. Many researchers have used DLS as a probe to determine if precipitation has occurred. Nudelman *et al.* used DLS to determine the effect polyaspartic acid had on CaP precipitation, showing that the polymer inhibited mineral precipitation (Figure 4.23B).[157]

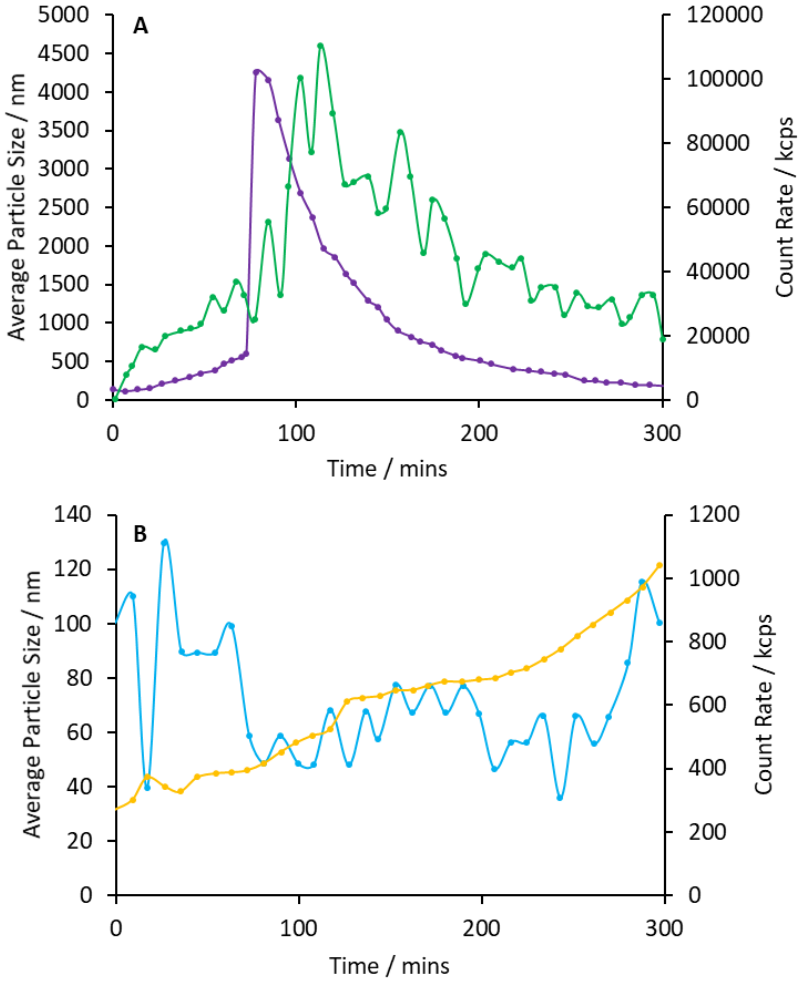


*Figure 4.23 Dynamic light scattering measurements of calcium phosphate precipitation in absence (**A**) or presence (**B**) of pAsp (10 µg/ml), depicting average particle size (purple (**A**) and blue (**B**) lines) and count rate (green (**A**) and yellow (**B**) lines) reproduced from Nudelman et al.[157]*

The disadvantage of DLS is that it can only be used to measure particle size or determine if precipitation is occurring. It does not provide further characterisation of the material, such as crystallinity or composition. Futhermore DLS assumes that particles are hard spheres as a result the hydrodynamic radius calculated for anisotropic materials may not be 100 % accurate. Therefore, DLS must be verified with other techniques such as TEM to determine the size, morphology and crystallinity of the material. Here DLS, SEM and TEM were used to determine the precipitation of CaP, elemental composition and morphology of the CaP precipitate by the polymers.

### 4.3.1 PNQ1 and PQN1

**PNQ1** and **PQN1** were first to be probed for altering the precipitation of calcium phosphate (Figure 4.24). For this the number average data was used to track the growth of CaP as the number mean observes smaller particles whereas the volume and intensity mean measures the larger particles, hence is more affected by dust particles. The control (Figure 4.24, green line) contains no additives and does not show any increase in particle size over 600 minutes which means no material is precipitating. **PNQ1** and **PQN1** both contain a methacrylic acid block, with varying block orders of PEG-*b*-MMA-*b*-MAA and PEG-*b*-MAA-*b*-MMA respectively. Methacrylic acid has been demonstrated by Lei *et al.* to have the ability to bind to HAP.[34,61] With this knowledge these polymers have the potential to be able to promote CaP precipitation.

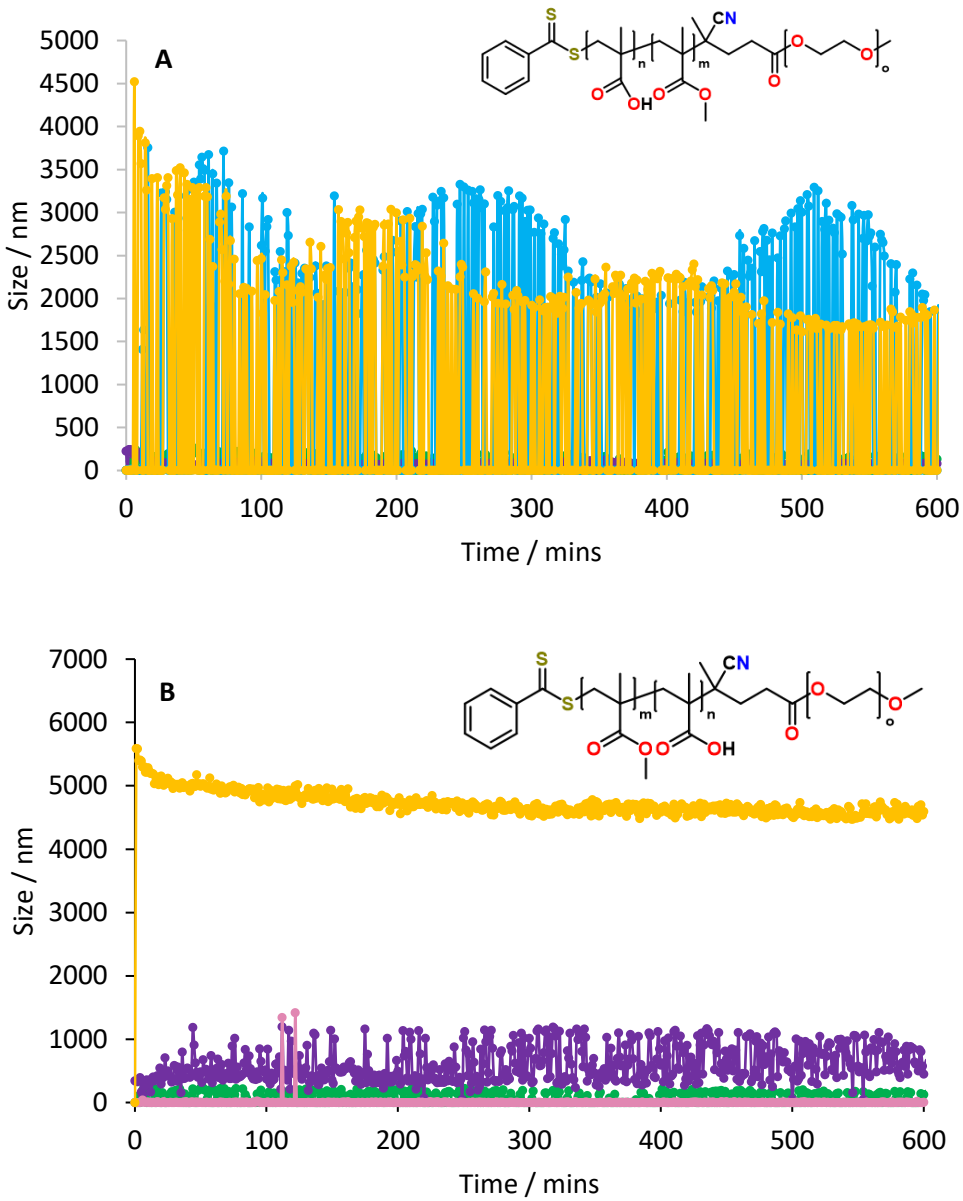


*Figure 4.24 Particle size over time for **PNQ1** (A) and **PQN1** (B) at different polymer concentrations 0.1 mg cm$^{-3}$ (purple), 0.02 mg cm$^{-3}$ (blue), 0.011 mg cm$^{-3}$(pink), 0.0075 mg cm$^{-3}$ (yellow) against the control (green) carried out at 37 $^{O}$C . The polymer structure of each is also shown*

The **PNQ1** DLS graph is very noisy and it can be suggested that there is no particle growth occurring due to the levelness of the 0.0075 mg cm$^{-3}$ (Figure 4.24A, yellow line) and the 0.02 mg cm$^{-3}$ Figure 4.24A, blue line) data series however it is not conclusive. It should be noted that the 0.11 mg cm$^{-3}$ (Figure 4.24A, pink line) sample of **PNQ1 is** masked by the other two concentrations however the data is at the baseline of the graph, indicating no particle growth. This could be attributed to polymer's cmc occurring at 0.156 mg cm$^{-3}$, in future work the DLS measurements should be taken at concentrations higher than 0.156 mg cm$^{-3}$ to determine if a self-assembled carboxylic acid promotes precipitation. The **PQN1** DLS data shows that there is no particle growth in any of the polymer concentrations (Figure 4.24B). However at 0.1 mg cm$^{-3}$ the particle size is maintained at 5000 nm, which indicates that this large particle size is due to the polymer. **PQN1** is only partially soluble in water, as a result polymer aggregates could be present in the sample, SEM is needed to confirm this.

### 4.3.2 PNA1

**PNA1** is an amide based triblock copolymer with the structure of PEG-*b*-PMMA-*b*-PDMAE. In the remineralisation of enamel by saliva there are proline rich proteins which selectively adsorb onto the enamel surface and regulate ions exchange.[5] Furthermore amide groups aid in the maturation of HAP.[4] This was the inspiration to investigate an amide copolymer in the precipitation of CaP. The DLS data shows that at 0.1 mg $cm^{-3}$(Figure 4.25, purple line) and at 0.0075 mg $cm^{-3}$ (Figure 4.25, yellow line) no increase in particle size, indicating that **PNA1** does not precipitate CaP at these concentrations. However at 0.02 mg $cm^{-3}$ the sample shows an increase in particle size even though the trace is noisy (Figure 4.25, blue line). The polymer itself is sparingly soluble in water at high concentration, as a result the 0.1 mg $cm^{-3}$ may have not precipitated CaP because it had macroprecipitated out of solution. An SEM micrograph is needed to confirm that the 0.02 mg $cm^{-3}$ sample has precipitated CaP. In the future the nucleation experiments with **PNA1** should be carried out again however with the amine moiety protonated. This could change enable the polymer to precipitate CaP. Furthermore the polymer could be tested for the nucleation of calcite and silica, since poly(allylamine hydrochloride) has been shown to influence the growth of calcite.[157]

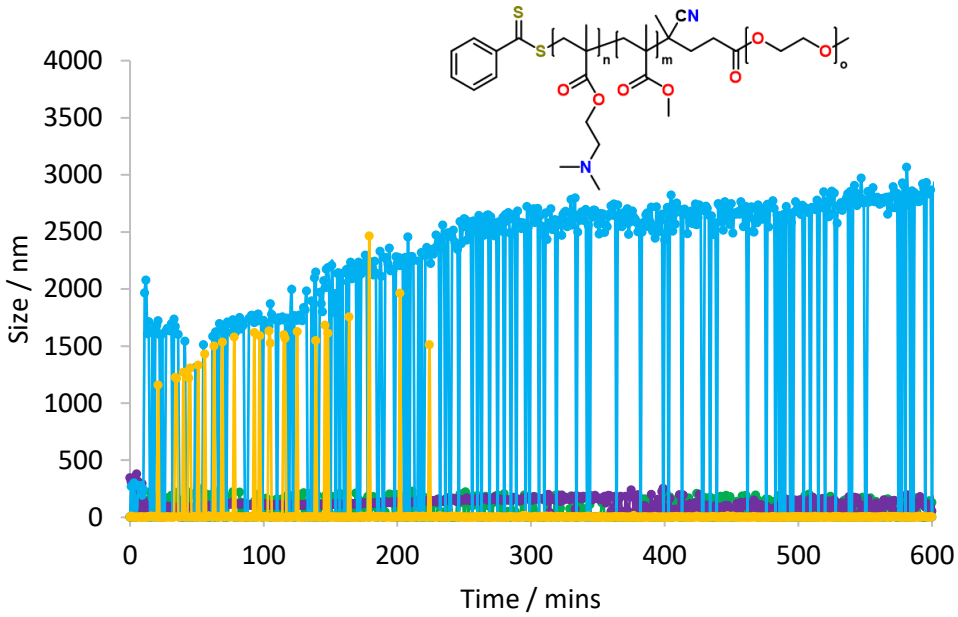


*Figure 4.25 Number average mean of **PNA1** at 0.0075 mg $cm^{-3}$ (yellow), 0.02 mg $cm^{-3}$ (blue) and 0.1 mg $cm^{-3}$ (purple) against the control (green). The $CaCl_2$ and $KH_2PO_4$ concentrations are 2.25 mM and 1.05 mM respectively. The structure of **PNA1** is also shown.*

### 4.3.3 PNE1

**PNE1** is a hydroxyl containing polymer with a block sequence of PEG-*b*-PMMA-*b*-PHEMA. Hydroxy groups were chosen be investigated because in the demineralisation of enamel by acids the hydroxyl group in lactic acid is able to bind to the enamel and cause acid etching at a high pH. This shows that hydroxyl groups can bind to HAP. Furthermore self-assembling monolayers have been developed with hydroxyl groups that can promote growth of HAP.[146] From the DLS it is clear that all three concentrations of **PNE1** show an increase in particle size indicating that they promote particle precipitation. As expected 0.1 mg $cm^{-3}$ (Figure 4.26, purple line) promotes particle growth faster than the other two concentrations as the peak particle growth occurs within 12 minutes. In the case of 0.0075 mg $cm^{-3}$ (Figure 4.26, yellow line) has an incubation time of 10 minutes before the particle size increases rapidly. The 0.02 mg $cm^{-3}$ (Figure 4.26, blue line) sample shows the particle size peaks at 1400 nm and is then maintained. The next step for

**PNE1** is to conduct SEM and TEM experiments to determine the precipitated material's morphology and crystallinity.

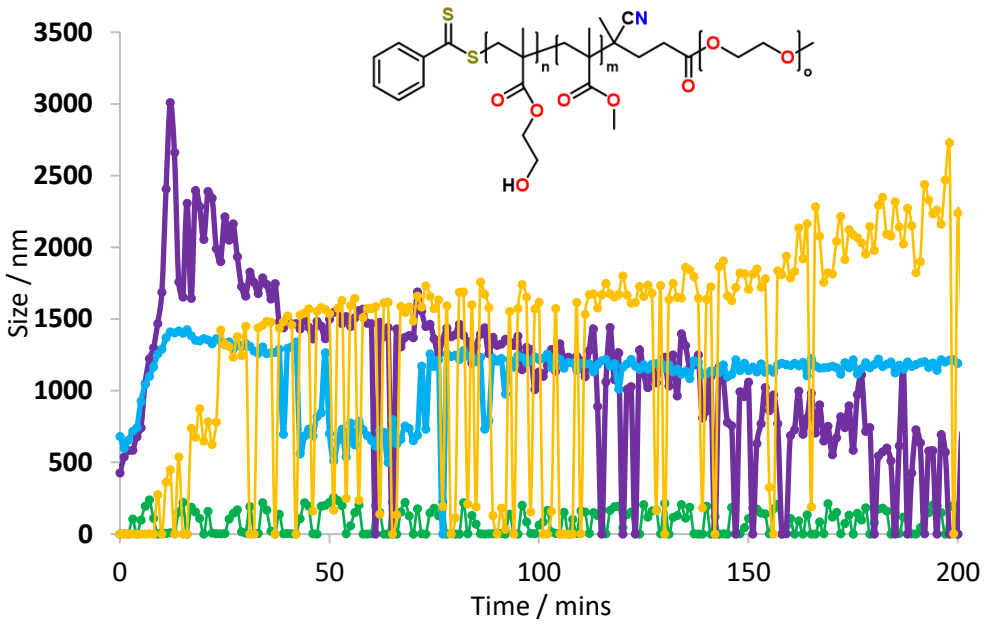


*Figure 4.26 Number average mean of **PNE1** at 0.0075 mg cm$^{-3}$ (yellow), 0.02 mg cm$^{-3}$ (blue) and 0.1 mg cm$^{-3}$ (purple) against the control (green). The $CaCl_2$ and $KH_2PO_4$ concentrations are 2.25 mM and 1.05 mM respectively. The structure of **PNE1** is also shown*

### 4.3.4 PFN1

**PFN1** was chosen to determine if phosphonic acids have the ability to precipitate CaP. Phosphonic acid containing copolymers have shown to produce acid resistant films for enamel and influence the nucleation of Calcite.[34,60] From the DLS data all three **PFN1** concentrations exhibit an increase in particle size. The trend shows that the precipitation of CaP could be polymer concentration dependant because the 0.1 mg cm$^{-3}$ sample (Figure 4.27, purple line) shows the highest rate of precipitation and the 0.0075 mg cm$^{-3}$ sample (Figure 4.27, yellow line) shows the slowest rate. A reasonable assumption is at higher concentrations there is a larger proportion of phosphonic acid moieties in the solution. These groups could complex with the calcium forming a heterogeneous nucleation site allowing for faster precipitation. In the 0.2 mg cm$^{-3}$ sample the starting particle size is higher than the other two (Figure 4.27, blue line), this could be due to dust in the sample. In the 0.1 mg cm$^{-3}$ and the 0.0075 cm$^{-3}$ samples there is an incubation period before the particle size increases (7 and 15 minutes respectively), this is also seen in the work produced by Nudelman and coworkers (Figure 4.23A).[157] The 0.1 mg cm$^{-3}$ and 0.02 mg cm$^{-3}$ samples shows a decline in particle size after 30 minutes, this is indicative of the CaP is sedimenting due to Brownian motion.

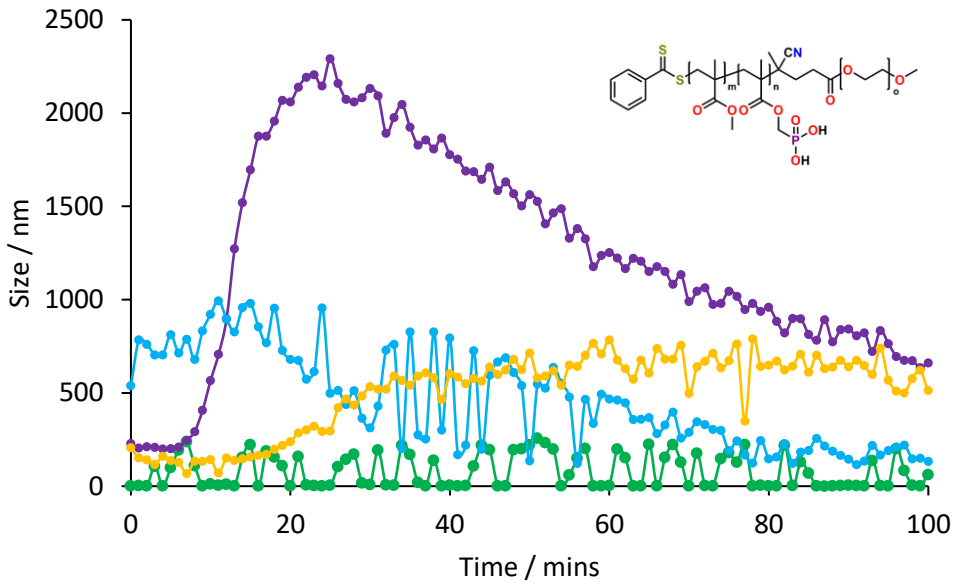


*Figure 4.27 Number average mean of **PFN1** at 0.0075 mg cm$^{-3}$ (yellow), 0.02 mg cm$^{-3}$ (blue) and 0.1 mg cm$^{-3}$ (purple) against the control (green). The $CaCl_2$ and $KH_2PO_4$ concentrations are 2.25 mM and 1.05 mM respectively. The structure of **PFN1** is also shown*

From the DLS experiment, 30 minutes, 240 minutes and 24 hours were targeted for SEM experiments in which energy-dispersive x-ray spectroscopy (EDX) was used to determine the chemical composition of the precipitate. After 30 minutes incubation at 37 $^{O}$C in all of the **PFN1** samples the particle size is still increasing, therefore it would be expected to observed material in all the SEM samples. It can be seen that in the 0.1 mg cm$^{-3}$ and the 0.02 mg cm$^{-3}$ samples there is material that has precipitated out (Figure 4.28H and Figure 4.28E). The EDX spectra confirms that the material precipitated is calcium phosphate (Figure 4.28G and Figure 4.28J). However in the SEM image of the 0.0075 mg cm$^{-3}$ sample does not show any calcium phosphate according to the EDX data (Figure 4.28C and Figure 4.28D). The material that is present in the SEM image of 0.0075 mg cm$^{-3}$ could be silica particles from breaking the silica wafer. The SEM image of the control shows no material on the wafer which is in agreement with the DLS data (Figure 4.28A). Back scatter electron micrographs have been taken for the 0.1 mg cm$^{-3}$ and 0.02 mg cm$^{-3}$ sample which show that the precipitated material as bright which indicates the material has a higher atomic mass than carbon (Figure 4.28I and Figure 4.28F respectively. This would reinforce the precipitation of calcium phosphate from the samples. Furthermore, large round spheres can be seen the 0.1 mg cm$^{-3}$ and the 0.02 cm$^{-3}$ samples, these are polymer spheres. In the back-scatter electron images of these show as darker than the precipitated material which indicates they have a lower atomic mass and suggests they are comprised of organic material.

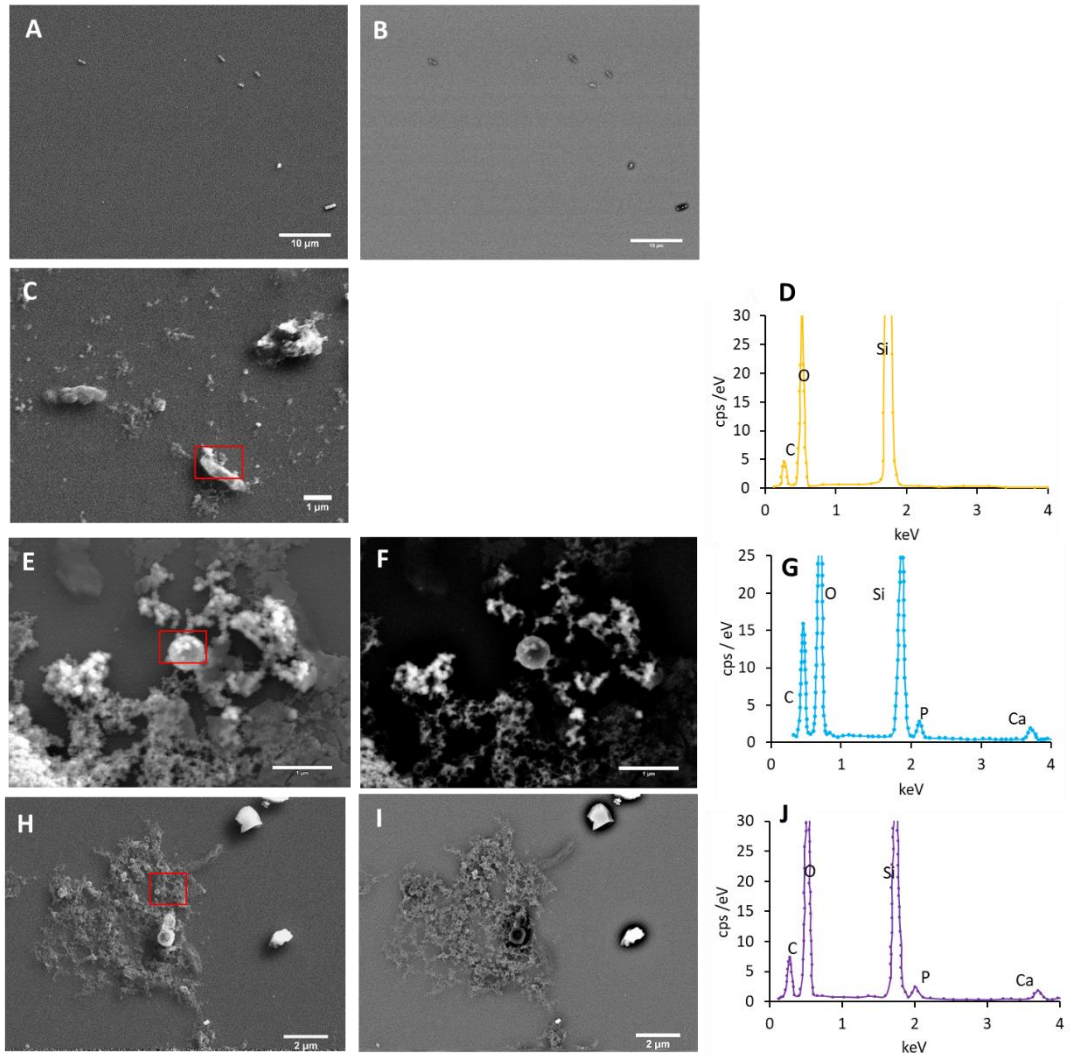


*Figure 4.28 SEM secondary electron micrographs (left), SEM back scatter electron micrographs (middle) and the EDX spectra (right) of the control (A - B) and **PFN1** at 0.0075 mg cm$^{-3}$ (C - D) and 0.02 mg cm$^{-3}$ (E - G) and 0.1 mg cm$^{-3}$ (H - J) after 30 minutes incubation at 37$^{o}$C. The red box indicates the area where the EDX was taken.*

After 240 minutes the majority of the precipitation of CaP would have occurred. This is seen as a decrease in particle size for 0.1 mg $cm^{-3}$ sample of **PFN1** (Figure 4.27, purple line) which is indicative of material sedimentation. In the SEM sample there is more CaP material in the 0.1 mg $cm^{-3}$ and the 0.02 mg $cm^{-3}$ **PFN1** samples (Figure 4. 29I and Figure 4. 29F respectively) at 240 minutes than at 30 minutes. In the 0.0075 mg $cm^{-3}$ sample there is now material present in the sample (Figure 4. 29C) which is confirmed to be CaP by the EDX spectrum (Figure 4. 29E), however it appear to have a slightly different morphology to the other two concentrations. In the control there is still no precipitation of phosphate (Figure 4. 29A), and the artifacts in the control appear bright in the BSE micrograph indicating silicon from the breaking of the wafers (Figure 4. 29B). In samples 0.1 mg $cm^{-3}$ and 0.02 mg $cm^{-3}$ large particles can be observed, these are larger polymer spheres and in the BSE micrographs these are darker than the precipitated material indicating that they are organic material rather than CaP (Figure 4. 29J and Figure 4. 29G respectively).

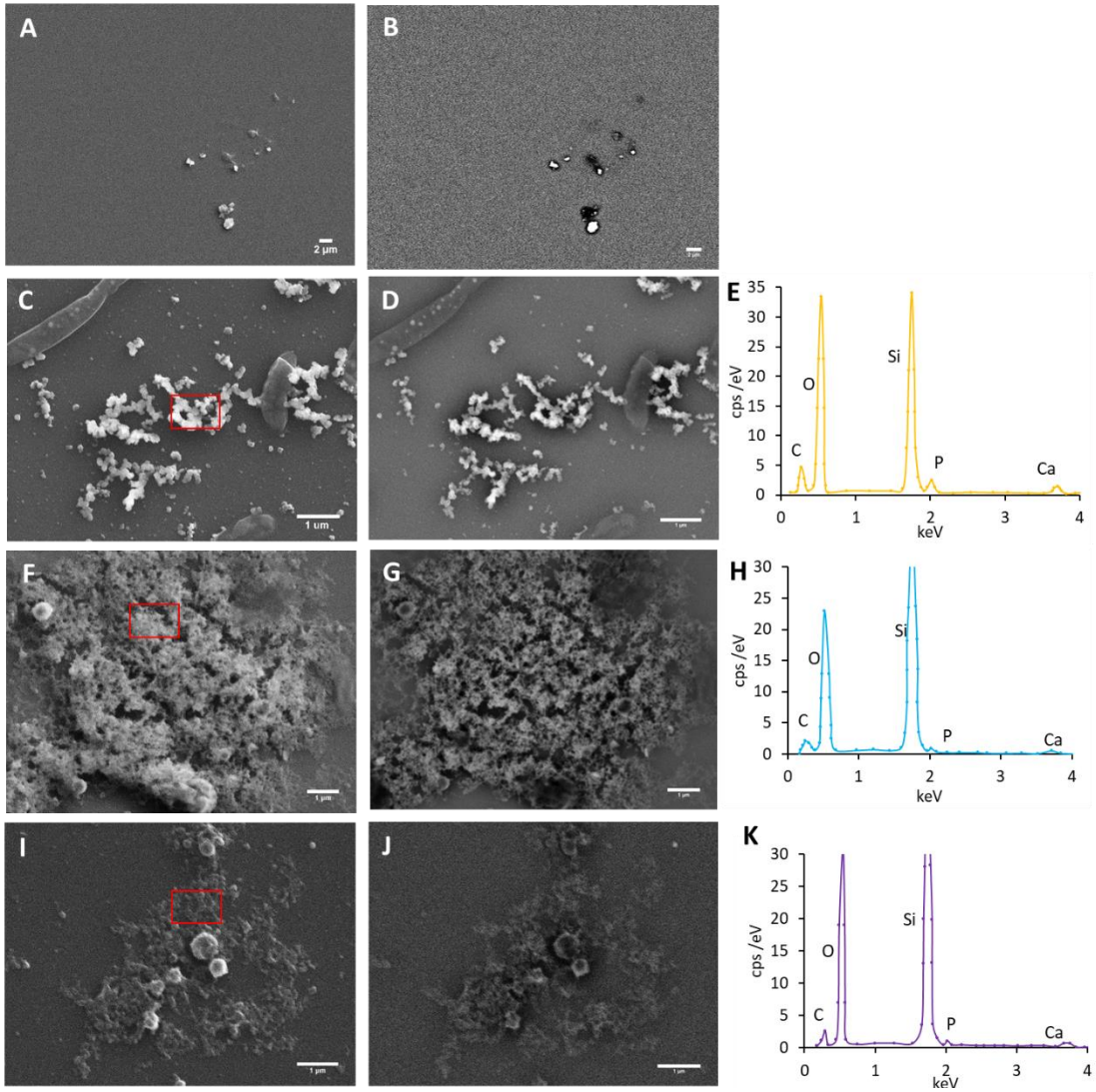


*Figure 4. 29 SEM secondary electron micrographs (left), SEM back scatter electron micrographs (middle) and the EDX spectra (right) of the control (A - B) and **PFN1** at 0.0075 mg cm$^{-3}$ (C - E) and 0.02 mg cm$^{-3}$ (F - H) and 0.1 mg cm$^{-3}$ (I - K) after 240 minutes incubation at 37$^{o}$C. The red box indicates the area where the EDX was taken.*

After 24 hours all samples even the control shows precipitation of calcium phosphate indicated by the presence of Calcium and phosphate in the EDX spectrum (Figure 4.30).

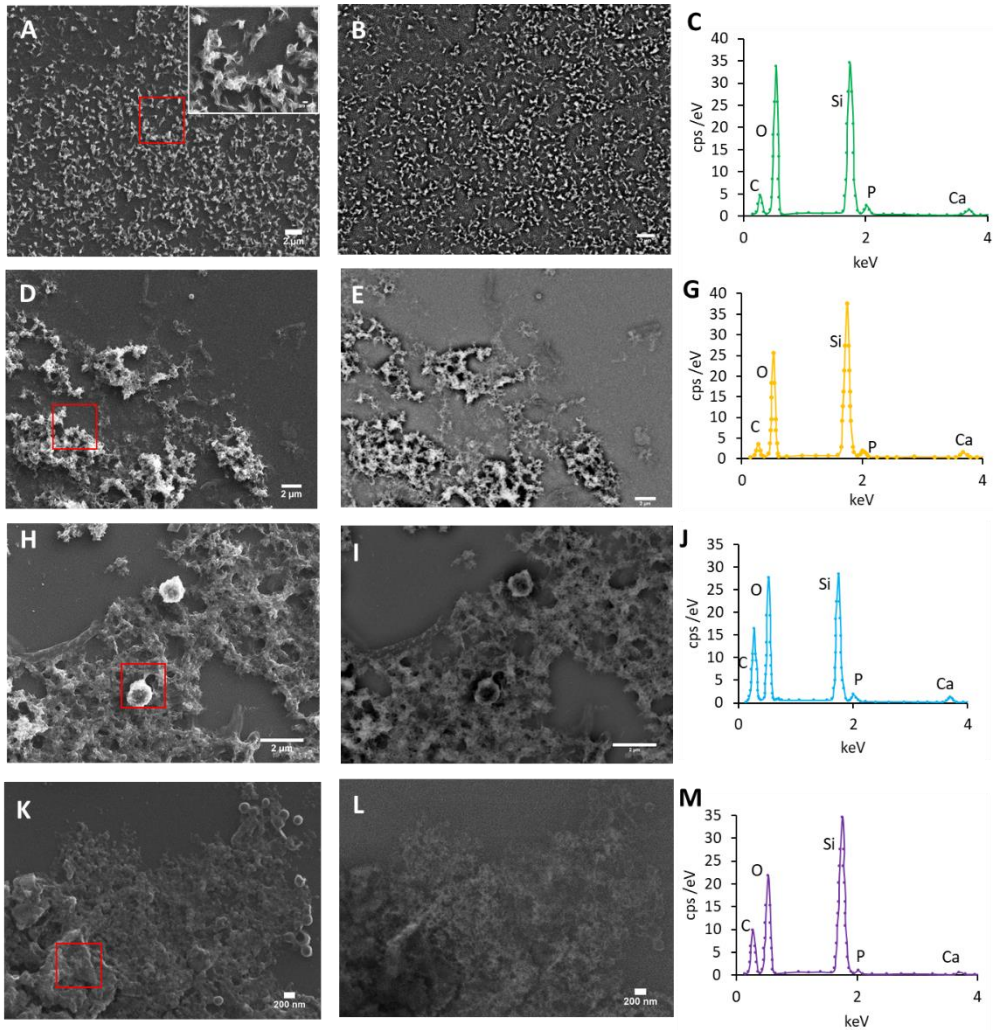


*Figure 4.30 SEM secondary electron micrographs (left), SEM back scatter electron micrographs (middle) and the EDX spectra (right) of the control (A - C) and **PFN1** at 0.0075 mg cm$^{-3}$ (D - G) and 0.02 mg cm$^{-3}$ (H - J) and 0.1 mg cm$^{-3}$ (K - M) after 24 hours incubation at 37°C. The red box indicates the area where the EDX was taken.*

In Figure 4.30, there is a difference in morphology the control (Figure 4.30A) and **PFN1** at 0.1 mg $cm^{-3}$ (Figure 4.30K), in the control characteristic rods of HAP can be seen. However in **PFN1** at high concentrations the material matrix is more ball like (Figure 4.31A). The BSE of **PFN1** at 0.1 mg $cm^{-3}$ after 24 hours indicates that the ball like matrix is CaP (Figure 4.31B) and the polymer sphere shown in Figure 4.31A is covered in CaP. In all the polymer samples after 24 hours there seems to be a large amount of material deposited, this could be attributed to the 13 nm spheres of **PFN1** that are also present in the sample (Figure 4.22A).

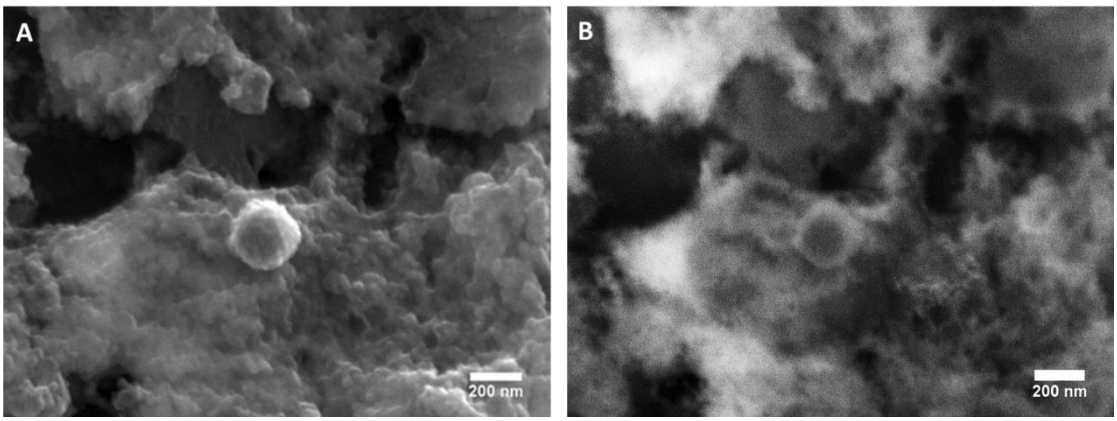


*Figure 4.31 A SEM secondary electron micrograph (A) and the back scattered electron micrograph of **PFN1** at 0.1 mg $cm^{-3}$ after 24 hours at 37 $^{o}C$*

The CaP precipitated by **PFN1** at 0.1 mg $cm^{-3}$ was viewed in TEM in order to be able to perform electron diffraction on the precipitate to determine its crystallinity. Samples were taken after 24 hrs and 6 days of incubation to give an indication of the stability of the material. After 24 hours in the TEM micrographs areas of ball like material can be seen (Figure 4.32A). However the electron diffraction shows that the materials are amorphous which indicates that **PFN1** promotes the growth of amophorous CaP. The radial distribution of the diffraction pattern confirms the absences of reflections, showing only two broad humps with similar d-spacing to that reported by Habraken *et al.* for amorphous calcium phosphate.[19] After 6 days of incubation, the amorphous ball-like network of material is still present in the **PFN1** sample at 0.1 mg $cm^{-3}$, which would indicate that the material is stable for 6 days (Figure 4.32B). The ball like material is similar to that seen in the SEM images (Figure 4.30K). Furthermore, the amophorous ball material is larger in size than the **PFN1** spheres confirming that this is precipitated material rather than the polymer spheres aggregating together.

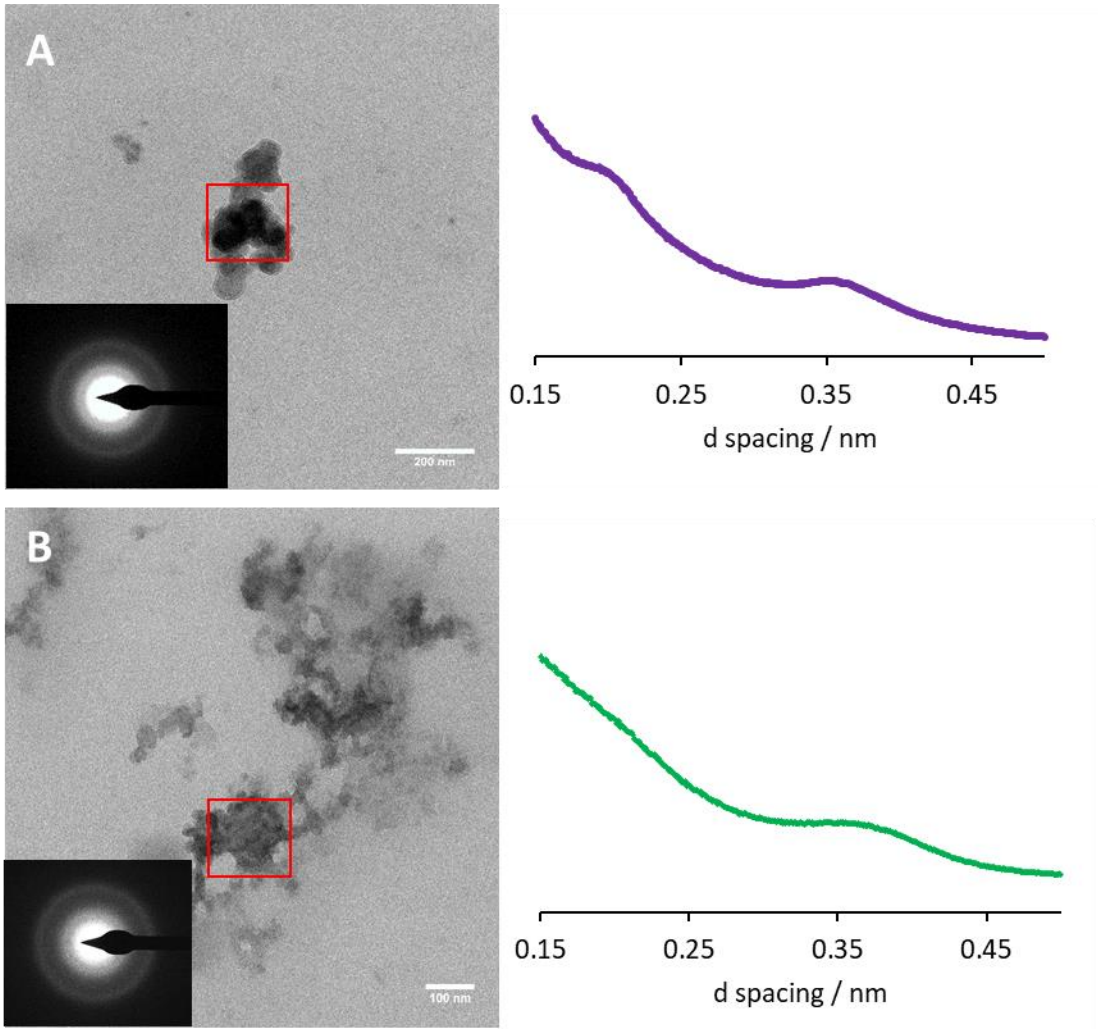


*Figure 4.32 TEM micrographs and electron diffraction patterns (left) of **PNF1** at 0.1 mg cm$^{-3}$ after 24 hours (A) and 6 days (B) of incubation at 37 $^{O}$C with their corresponding radially averaged electron fraction data (right).*

The control was also observed with TEM to see if crystalline calcium phosphate is formed after 24 hours and 6 days. After 24 hrs in the control not much can be observed (Figure 4.33A), however after 6 days incubation there a network of amorphous material (Figure 4.33B). Furthermore, there are large spherical objects in the sample which has been seen in **PFN1** after 24 hours (Figure 4.32B), these could be CaP. However time points between 24 hrs and 6 days would need to be investigated to see if these circles are observed before the amorphous material forms.

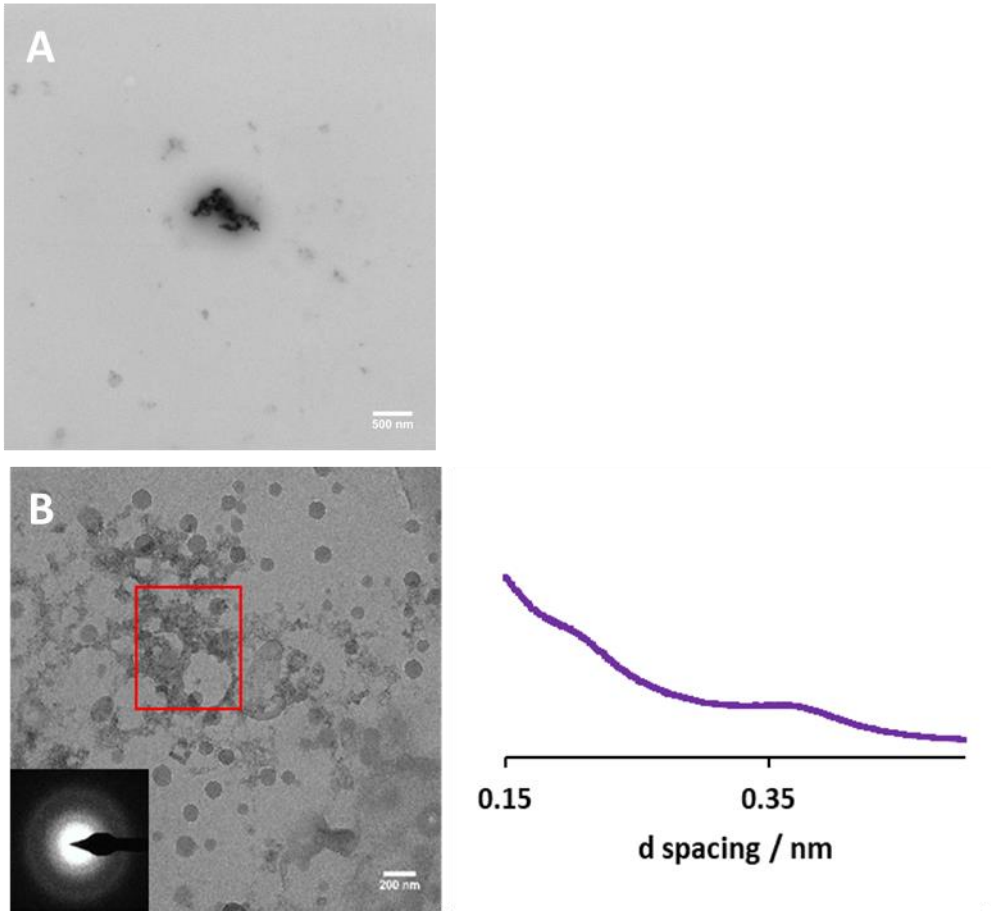


*Figure 4.33 TEM micrographs and electron diffraction pattern (left) of control after 24 hours (A) and 6 days (B) incubation at 37 $^{O}$C with their radically averaged diffraction distribution data (right). The red square indicates what area was used in the electron diffraction.*

### 4.3.5 PFN2

**PFN2** has the same structure as **PFN1** (PEG-PMAPC1acid-PMMA) but has a larger PMAPC1acid and PEG segment (2100 g mol$^{-1}$ and 6400 g mol$^{-1}$ respectively). From the DLS results of **PFN1** it would be suspected that **PFN2** follows a similar trend and can promote particle growth. The 0.02 mg cm$^{-3}$ (Figure 4.34, blue line) and the 0.0075 mg cm$^{-3}$ (Figure 4.34, yellow line) samples show no particle size growth and is not as noisy as the control data (Figure 4.34, green line). However the 0.1 mg cm$^{-3}$ sample shows a particle size increase to 2000 nm indicating growth (Figure 4.34, purple line). The polymer self assembles at 6.55 x 10$^{-3}$ mg cm$^{-3}$ so therefore each concentration should promote CaP precipitation. The main difference between **PFN2** and **PFN1** is the length of the PEG segment. It could be possible that the PEG segment is affecting the PMAPC1acid block's ability to bind to $Ca^{2+}$, by obstructing the phosphorous sites. In order to confirm the initial DLS results, SEM images of 0.02 mg cm$^{-3}$ and 0.0075 mg cm$^{-3}$ samples are needed to see if samples these samples do in fact precipitate CaP. Futhermore another block copolymer could be synthesised with a larger PEG chain than **PFN2** and a shorter PEG chain than **PFN1** to determine if those polymers will nucleate CaP or not. If the longer chain has a similar trend to **PFN2** then it could be possible the PEG chain is hindering precipitation.

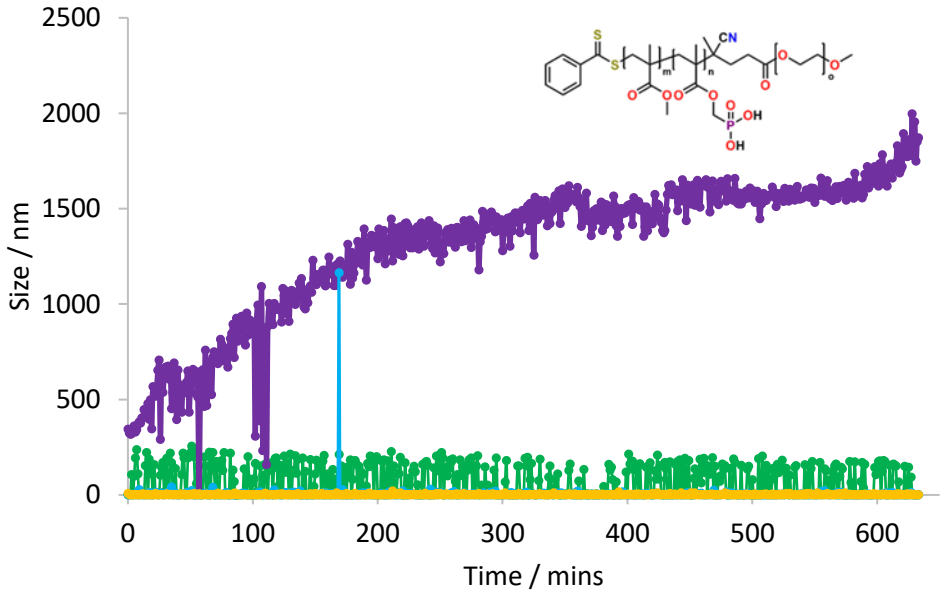


*Figure 4.34 Number average mean of **PFN2** at 0.0075 mg cm$^{-3}$ (yellow), 0.02 mg cm$^{-3}$ (blue) and 0.1 mg cm$^{-3}$ (purple) against the control (green). The $CaCl_2$ and $KH_2PO_4$ concentrations are 2.25 mM and 1.05 mM respectively. The structure of **PFN2** is also shown.*

### 4.3.6 PNF2

**PNF2** has an alternative structure to **PFN1**, in this arrangement the PMMA is in the centre of the molecule separating the two hydrophilic blocks (PEG-*b*-PMMA-*b*-PMAPC1acid). **PNF2** has a high cmc (1.98 x 10$^{-2}$ mg cm$^{-3}$) compared to **PFN1**, and as such it required different concentrations to ensure that micelles were present. From the DLS data it shows concentrations 1 mg cm$^{-3}$ and 0.2 mg cm$^{-3}$ do not promote particle growth (Figure 4.35, red line and pink line respectively).

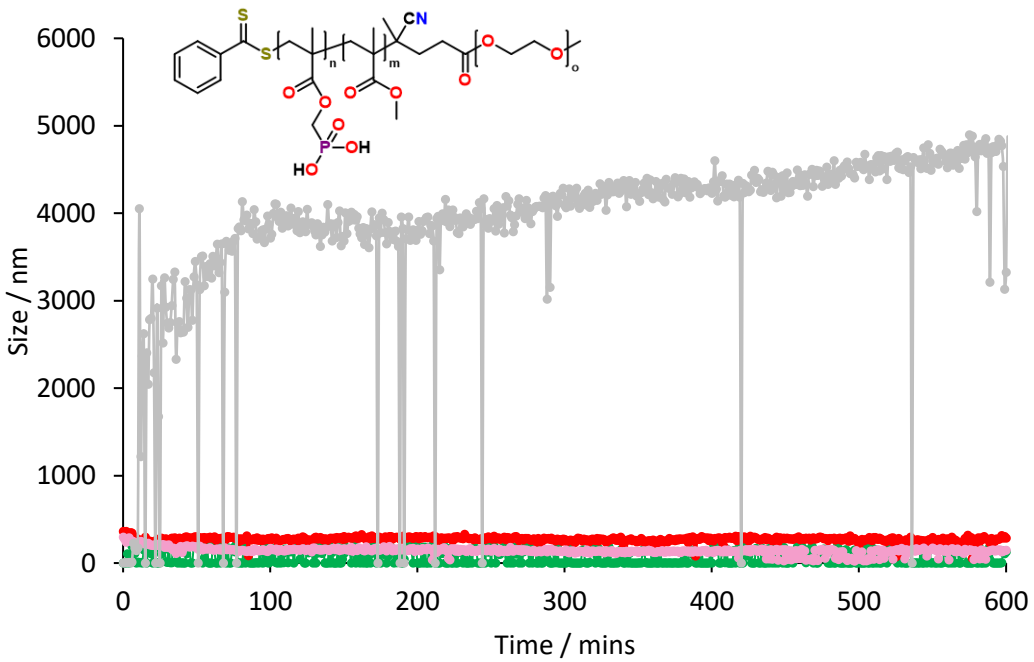


*Figure 4.35 Number average mean of **PNF2** (B) at 0.005 mg cm$^{-3}$ (grey), 0.2 mg cm$^{-3}$ (pink) and 1 mg cm$^{-3}$ (red) against the control (green). The $CaCl_2$ and $KH_2PO_4$ concentrations are 2.25 mM and 1.05 mM respectively. The structure of **PNF2** is shown*

However, at 0.005 mg $cm^{-3}$ there is significant increase in the size (Figure 4.35, grey line). A reason for this could be that the PMAPC1acid segment is exposed to the water as this concentration is below the cmc, which means that the calcium and phosphate ions have a place to nucleate from. The TEM images show that **PNF2** forms micelles of the same shape and size as **PFN1** however there could be a difference in the structure of the micelle. In **PFN1** the PMAPC1acid block is extended into the corona of the micelle. This would be classed as a mixed corona micelle. In the case of **PNF2** the PMAPC1acid would be within the core of the micelle and as PMMA is a hydrophobic block it would try to minimise the interfacial energy by forming a core around PMAPC1acid block. This would be classed as a core-shell-corona micelle, or compartmentalised core micelle (Figure 4.36).[151] This is the presumed case and as such a PMMA forms a shell around the PMAPC1acid block making the phosphonic acid groups inaccessible to the $Ca^{2+}$ ions thus promoting particle growth is not possible. In the future it would be advantages to perform zeta-potential measurement to investigate if having the charged block in the centre of the micelle reduces the charge in the polymer solution. If this is the case then **PNF2** should have different charge profile to **PFN1** as **PFN1** has a mixed corona morphology.

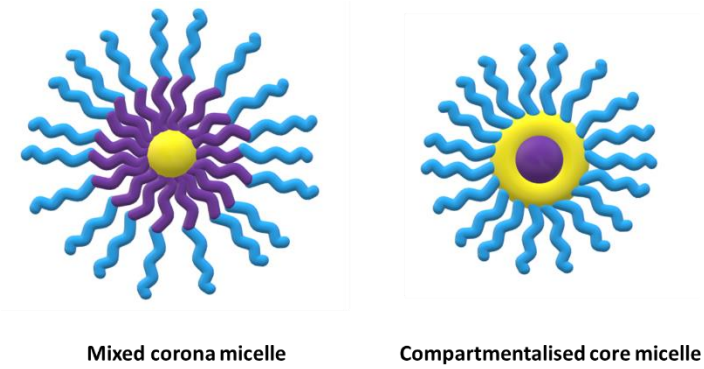


*Figure 4.36 A schematic showing two different micelle arrangements. Blue is PEG block, purple PMAPC1acid and yellow represents PMMA*

### 4.3.7 PF1

**PF1** is a deprotected phosphonic acid diblock (PEG-*b*-PMAPC1acid). This polymer was tested due to the results of **PNF2** where particle precipitation occurred below the cmc. This suggested that precipitation of CaP can occur and is more dependent on the concentration of PMAPC1acid present in the samples not whether the polymer has self-assembled. The DLS data of **PF1** showed that all three concentrations had an increase in particle size indicating the precipitation of material (Figure 4.37). The 0.1 mg $cm^{-3}$ (Figure 4.37, purple line) showed a high rate of particle growth and the material sedimented in 400 minutes. All concentrations showed no particle growth after 200 minutes which means that there is a much longer incubation time than observed in the self-assembled polymers that showed precipitation such as **PFN1** and **PNE1**. This would suggest that when the polymer self-assembles it provides a surface for the CaP to growth off, this would be a heterogeneous nucleation site. Samples 0.02 mg $cm^{-3}$ and 0.075 mg $cm^{-3}$ (Figure 4.37 blue and yellow lines respectively) shows particle growth, however sedimentation does not occur in 800 minutes indicating that the particles are still growing. Next **PF1** needs to undergo SEM imaging to confirm the precipitate is CaP.

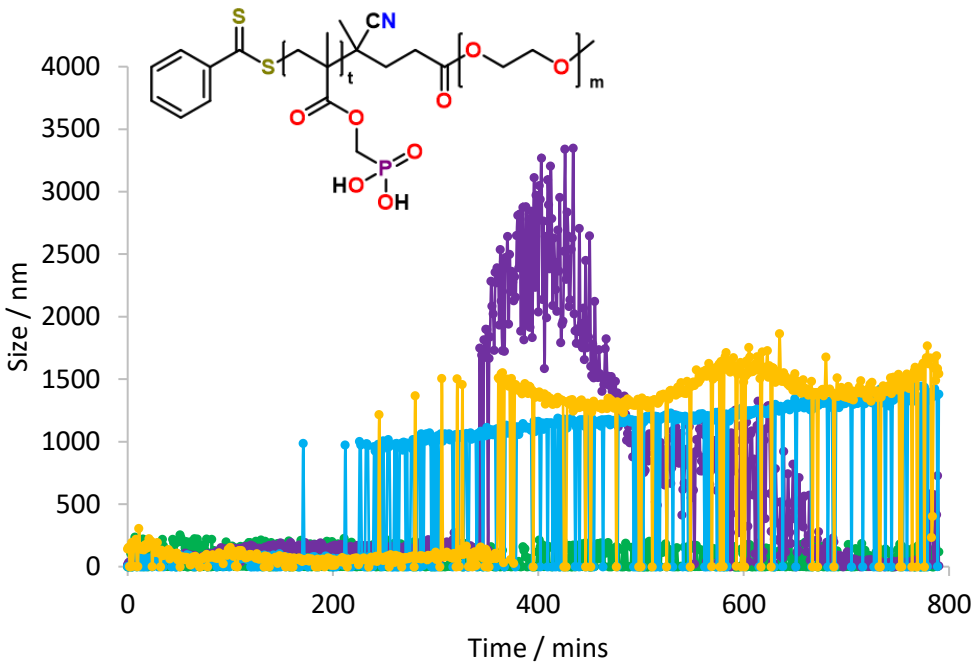


*Figure 4.37 Number average mean of **PF1** at 0.0075 mg cm$^{-3}$ (yellow), 0.02 mg cm$^{-3}$ (blue) and 0.1 mg cm$^{-3}$ (purple) against the control (green). The $CaCl_2$ and $KH_2PO_4$ concentrations are 2.25 mM and 1.05 mM respectively. The structure of **PF1** is also shown.*

### 4.3.8 PD2 and PDN3

**PD2** which is a protected diblock (PEG-*b*-PMAPC1) and **PDN3** which is a protected triblock with the same block sequence as **PFN1** (PEG-*b*-PMAPC1-*b*-PMMA) were investigated with DLS to determine if a phosphonic acid is needed to promote the growth of CaP. **PD2** and **PDN3** show that at each concentration there is not a noticeable change in size (Figure 4.38A and Figure 4.38B). However all signals apart from the control show very large particle sizes (3000 nm to 5000 nm). This would be attributed to the polymer in solution however to confirm these results the polymers were imaged by SEM.

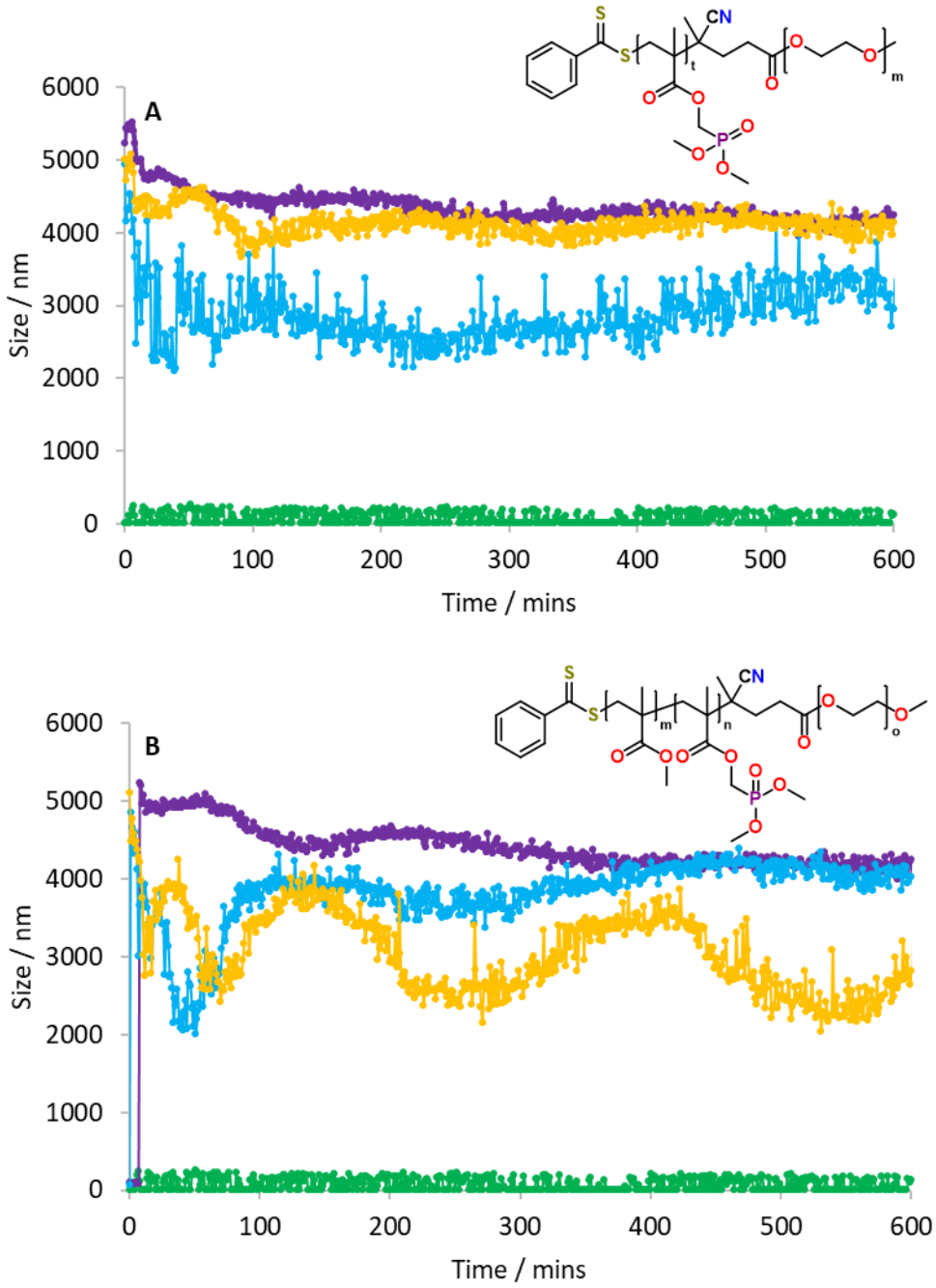


*Figure 4.38 Number average mean of **PD2** (A) and **PDN3** (B) at 0.0075 mg cm$^{-3}$ (yellow), 0.02 mg cm$^{-3}$ (blue) and 0.1 mg cm$^{-3}$ (purple) against the control (green). The $CaCl_2$ and $KH_2PO_4$ concentrations are 2.25 mM and 1.05 mM respectively. The structures of both copolymers is shown.*

Both polymers did not show an increase in particle size from the DLS data, as a result the 24 hrs time point was looked at to confirm if any material had precipitated. After 24 hours incubation of **PD2** in the 0.1 mg cm$^{-3}$ and 0.02 mg cm$^{-3}$ there is no precipitation of CaP (Figure 4.39). The artefacts that can be seen in the micrographs do not contain any calcium or phosphorous this suggests that material is silica from the wafer.

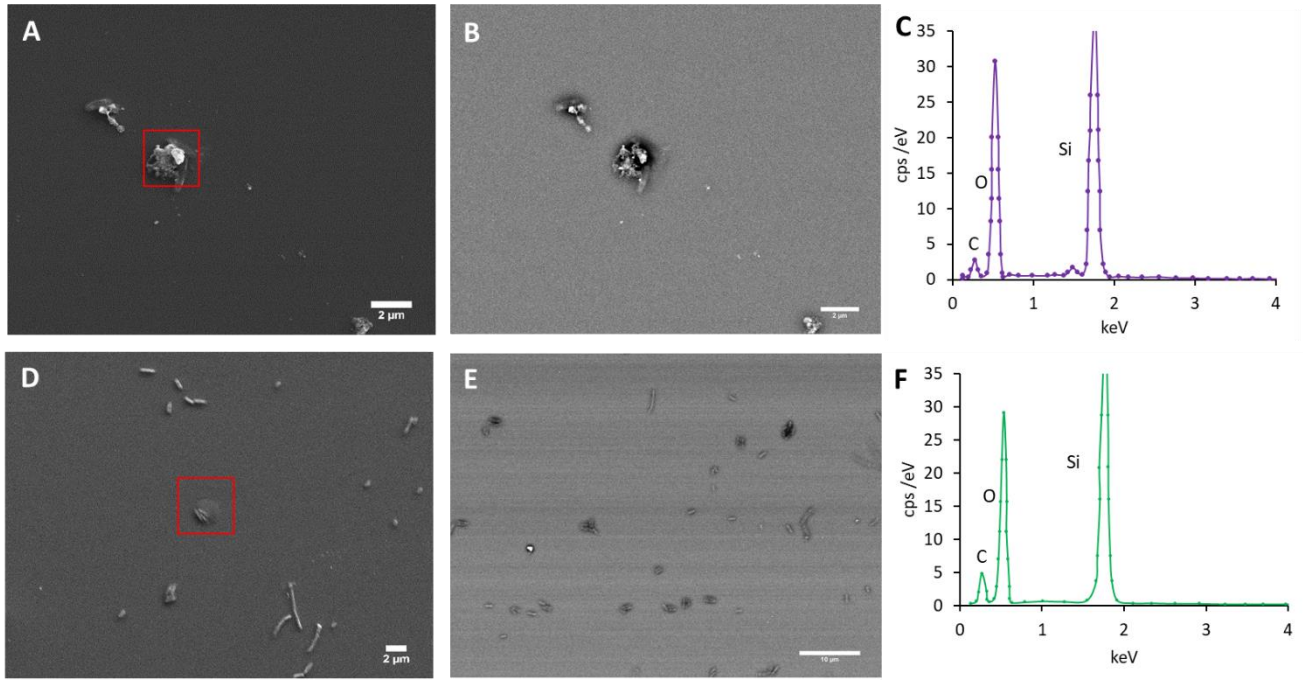


*Figure 4.39 SEM secondary electron micrographs (left), SEM back scatter electron micrographs (middle) and the EDX spectra (right) of **PD2** at 0.1 mg cm$^{-3}$ (A - C) and 0.02 mg cm$^{-3}$ (D - F) after 24 hours incubation at 37$^{o}$C. The red box indicates the area where the EDX was taken.*

Similar SEM images were obtained for **PDN3**, again there was no CaP present in the samples. However in the 0.1 mg cm$^{-3}$ there are small areas of material, although these show no evidence of CaP so they can be deemed as polymer aggregates (Figure 4.40). The SEM and EDX spectrums of **PD2** and **PDN3** have strongly indicate that by having the PMAPC1 block protected the growth of CaP is not promoted. The lack of CaP precipitation is due to there not being a binding site, phosphonic acid in this case, for the calcium ion to complex to. These triblock copolymers were not viewed under TEM.

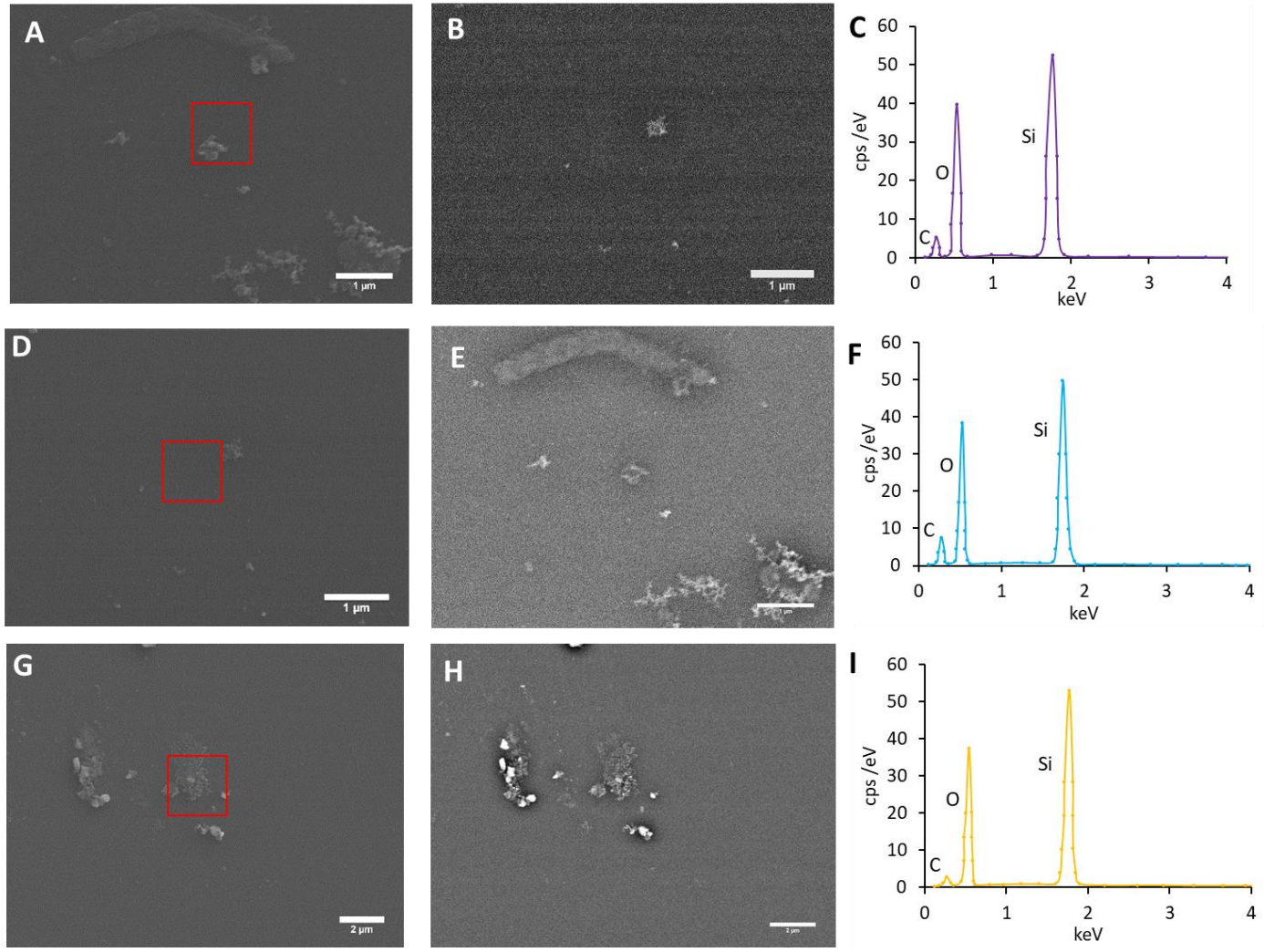


*Figure 4.40 SEM secondary electron micrographs (left), SEM back scatter electron micrographs (middle) and the EDX spectra (right) of **PDN3** at 0.1 mg cm$^{-3}$ (A - C), 0.02 mg cm$^{-3}$ (D - F) and 0.0075 mg cm$^{-3}$ (G – I) after 24 hours incubation at 37$^{o}$C. The red box indicates the area where the EDX was taken.*

## 4.4 Acid etching of enamel

The polymers have been investigated for their ability to promote CaP growth and it showed that copolymers **PF1**, **PNE1** and **PFN1** were the most successful. In research by Lei *et al.* only the ability to protect the enamel from acid attack was examined. Here the three copolymers mentioned above were also assessed for this ability. Acid erosion can be measured with various methods such as nanoindentation, confocal laser scanning electron microscopy, atom force microscopy and iodine permeability tests.[158] In this section, SEM was used to observe the effect of acid erosion on the surface of the enamel and contact profilometry was used to quantify the enamel loss caused by acid erosion.

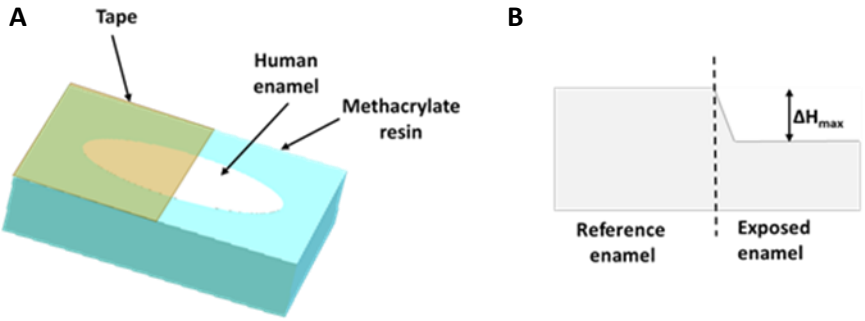


*Figure 4.41 A schematic of enamel covered by chemical resistant tape (a). A schematic of what happens after the enamel is exposed to citric acid, $\Delta H_{max}$ is the difference between the reference and exposed enamel.*

Surface profilometry measures the surface roughness of a sample, as a result it can give an idea of the topology of a material. The stylus tip of the profilometer traverses the material at a constant force and speed, it is the displacement of the tip (caused by the material) from its trajectory that is measured. The data that is collected is displayed as a line profile which can be used to determine the surface roughness. The enamel samples was prepared by taping half the enamel disc with acid resistant tape (Figure 4.41A), this covered surface acted as the reference enamel. Then the disc was submerged in a polymer solution for 2 minutes and then submerged in citric acid (1 % w/v at pH 3.8) for 5 minutes. Citric acid at pH 3.8 was used as a mimic for orange juice, as it is able to dissolve enamel at higher concentrations of calcium and phosphate ions, leading to enamel loss of up to several micrometers in depth.[159] The difference between the reference (taped) enamel and the exposed enamel after the acid etching would be the amount of enamel lost during the acid etching process (Figure 4.41B). Below is a line profile from one of the control discs, which an enamel disc that was not treated with polymer (Figure 4.42). In the line profile there are two large troughs at the beginning and end of the profile. These are when the stylus tip moved onto and off the enamel sample from the methacrylate resin. The start of the reference enamel is indicated by “step 1” and the edge of the etched enamel is indicated by “step 2”. The difference in these values is the amount of enamel lost in the sample. The SEM image of one of the control enamel discs showed that the enamel has been etched, whereas the reference has not been affected (Figure 4.43).

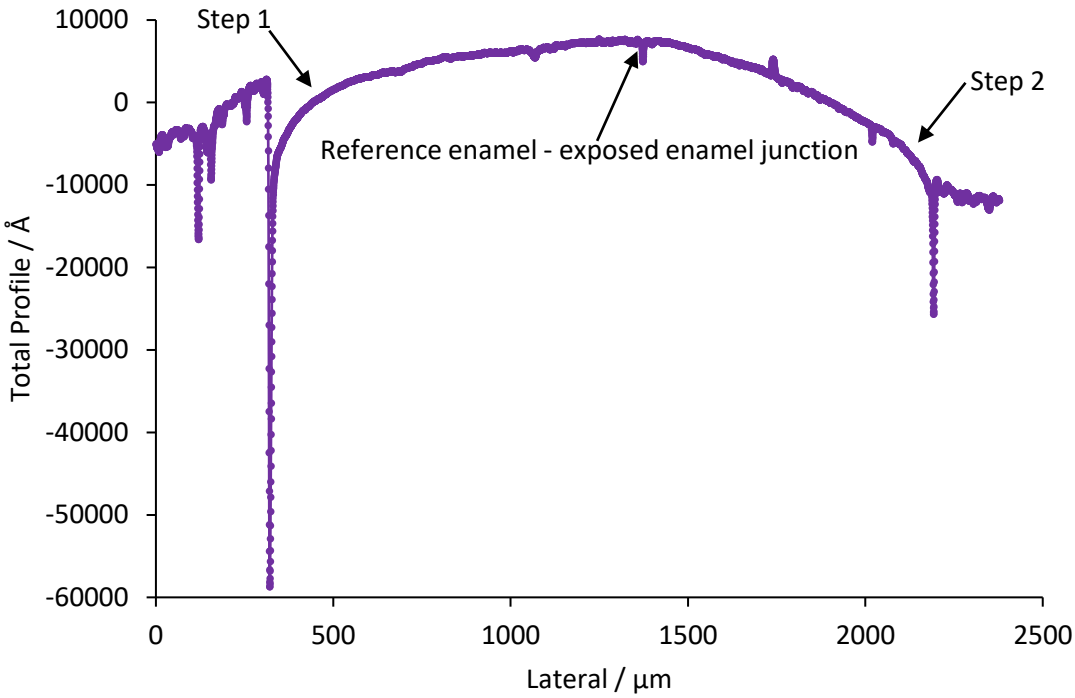


*Figure 4.42 A line profile of an enamel control sample showing the reference enamel-expose enamel junction.*

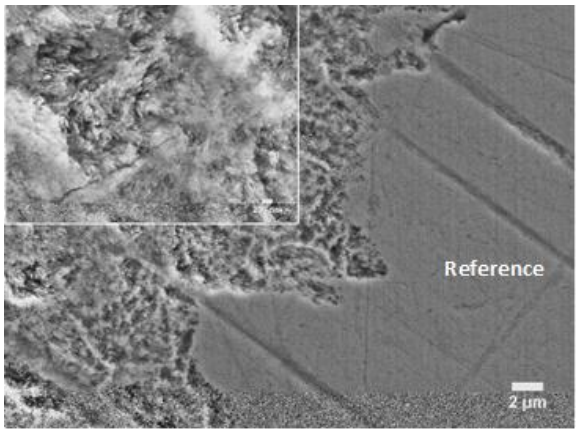


*Figure 4.43 The SEM image of a controlled enamel disc after acid etching*

The three copolymer films covered enamel were tested by profilometry, it was decided to investigate 1 mg $cm^{-3}$ rather than 0.0075 mg $cm^{-3}$ to see if increasing the polymer concentration further protects from acid erosion. The line profiles indicated that **PFN1** does not protect from acid attack as it has a very similar enamel loss as experienced in the control (Figure 4.44).

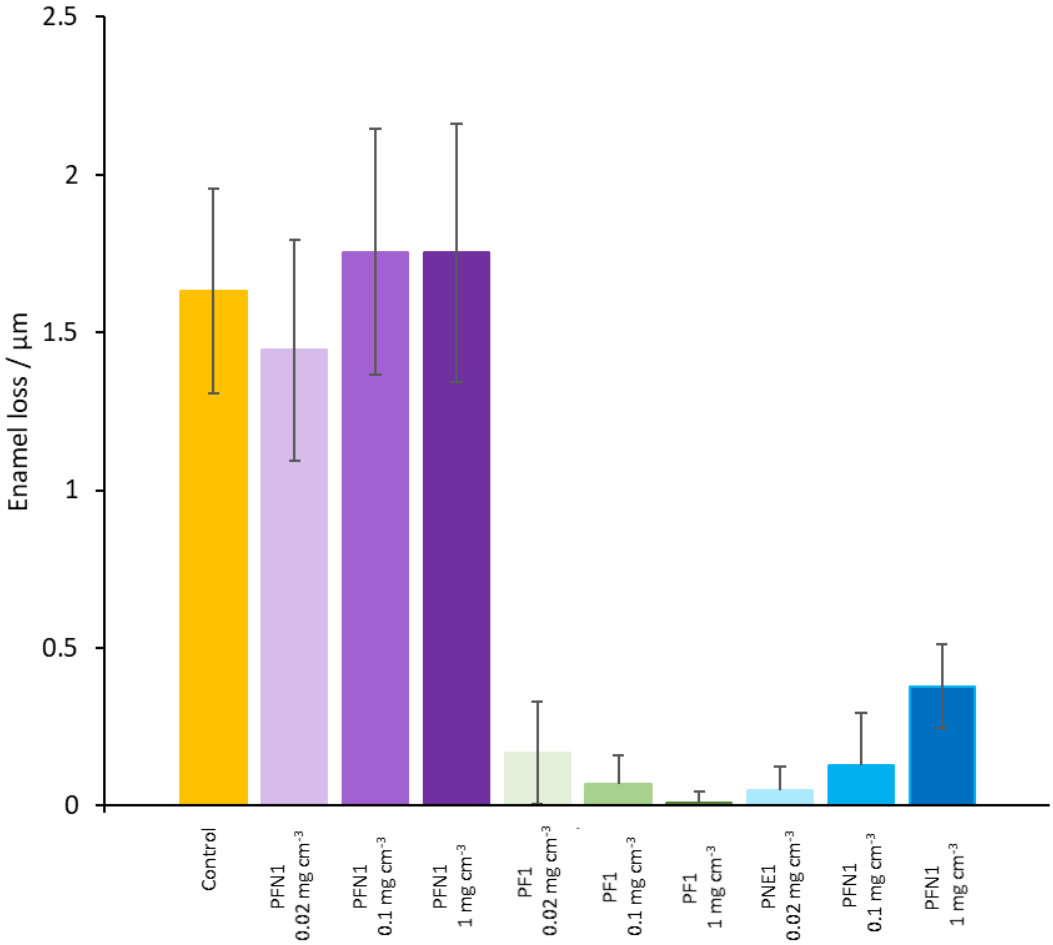


*Figure 4.44 A graph to show the enamel loss from the enamel disc of the control (yellow) and polymer covered enamel discs of **PFN1** (purple), **PF1** (green) and **PNE1** (blue) at three concentrations.*

However, **PF1** reduces the enamel loss of the exposed enamel significantly. A hypothesis behind the difference between **PFN1** and **PF1** is that the polymer spheres of **PFN1** provides less coverage for the enamel. The polymer has self-assembled into spheres, and when compared to the film made by **PF1** there is less coverage of the enamel. Furthermore, as **PFN1** forms spheres it means that there are less phosphate groups that are accessible to bind to the enamel surface. Also when the spheres pack and form a covering over the enamel there would be gaps in between the sphere. This would allow the acid to interact with the surface of the enamel and cause acid erosion. In the case of **PF1** the polymer forms a film therefore the phosphate groups can freely bind to the enamel and can provide more surface coverage to the enamel. **PFN1** shows that at higher concentration enamel loss increases which would indicate more polymer spheres are present. This could be caused by the copolymer oversaturating the enamel surface, so not all the polymer binds to the enamel. When the enamel discs of **PFN1** at 0.1 mg $cm^{-3}$ and 1 mg $cm^{-3}$ were placed in the acid solution a white precipitate was observed, indicating some of the polymer has not bounded as strongly to the enamel. At concentrations below 1 mg $cm^{-3}$ **PNE1** provides good protection from acid attack, similar to that of **PF1** which would indicate that the worm morphology of **PNE1** can be more efficiently packed than **PFN1**. However, at

1 mg $cm^{-3}$ the enamel loss increases, which would suggest, like in **PFN1**, the polymer is oversaturating the enamel surface, as a result some worms are not as tightly bound to the enamel surface. In the future, the degree of which the polymer binds to the enamel should be investigated, this could be carried out using UV-vis spectroscopy and using the RAFT agent benzothioate group to determine how much is bound by to mixing it with HAP powder in solution.

These samples were viewed with SEM to observe the topography of the enamel surface after acid etching. The SEM micrographs of the samples are in good agreement with the profilometry data (Figure 4.45). Out of the three polymers **PFN1** samples showed the most damage, with 1 mg $cm^{-3}$ sustaining the most (Figure 4.45C). **PF1** samples displayed the least amount of damage from acid attack. In the 0.1 mg $cm^{-3}$ and the 0.02 mg $cm^{-3}$ samples of **PF1** the etched enamel looks similar (Figure 4.45E and Figure 4.45D respectively). In the **PNE1** images the 0.02 mg $cm^{-3}$ (Figure 4.45G) and the 0.1 mg $cm^{-3}$ (Figure 4.45H) have very similar surfaces after etching indicating that the enamel damage by the acid is similar. However in the 1 mg $cm^{-3}$ sample of **PNE1** (Figure 4.45I) the enamel damage is more serve, which agrees with the profilometry data. In all the SEM images there are deep lines present on the exposed enamel side which could be due to the preparation of the enamel discs. Howevwer it has proven that the diamond tip of the profilometer is enough to mark the soften enamel. Heurich *et al.* investigated this effect of contact profilometry on softened enamel and showed that confocal laser scanning microscopy is a good alternative for measure enamel loss. [159]

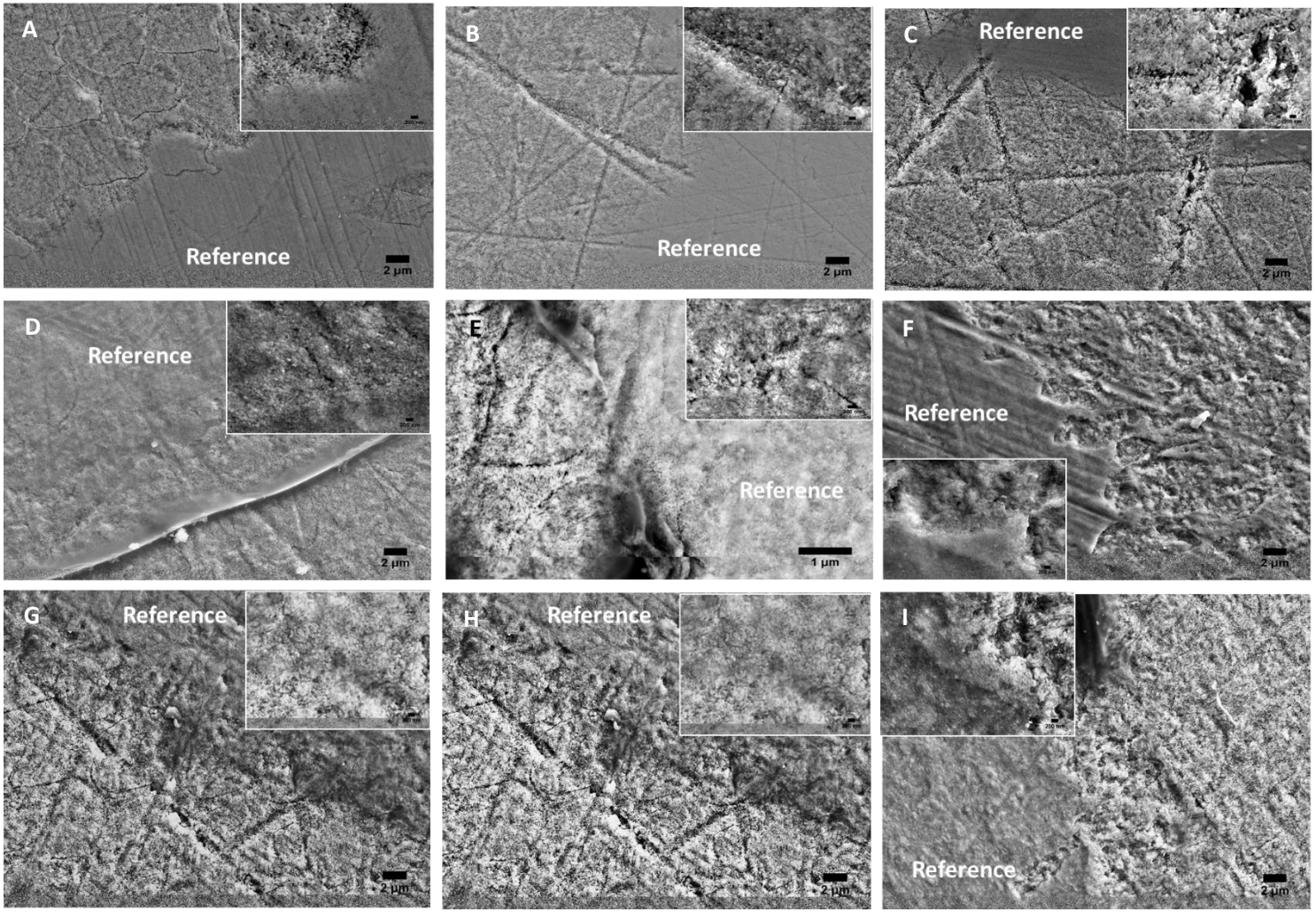


*Figure 4.45 SEM micrographs of the polymer treated enamel at different concentrations, left to right 0.02 mg cm$^{-3}$, 0.1 mg cm$^{-3}$ and 1 mg cm$^{-3}$. **PFN1** (A - C), **PF1** (D - F), **PNE1** (G - I)*

## 4.5 Conclusion

In this chapter the copolymers synthesised in chapter 3 were investigated primarily for their ability to promote CaP growth and to determine their self-assembled morphologies. It was found that having a longer PEG chain increases the cmc in the majority of the polymers and increasing the PMMA block has the reverse effect. **PDN1** which has the structure of PEG-*b*-PMAPC1-*b*-PMMA's cmc increases upon deprotection (**PFN1**). This is due to the increase in the hydrophilic segment of the block, which in turn slightly destabilises the micelle. **PNF2** and **PFN1** both showed micelles of 20nm and 13 nm respectively, which it is thought to be as a result of a kinetically frozen morphology which is caused by the electrostatic repulsion of the PMAC1acid block. **PNA1** and **PNE1** formed micelles and worms/micelles respectively. The worm morphology observed in the **PNE1** sample could be due all blocks similar volume fractions, which would decrease the curvature of the self-assembled complex. The packing parameter would need to be calculated to confirm this. **PNQ1**, **PD2**, **PQN1** and **PF1** formed films below 0.1 mg $cm^{-3}$ which were observed in the TEM micrographs (Figure 4.22D-G).

**PD2** and **PDN3** have the structures of PEG-*b*-PMAPC1 and PEG-*b*-PMAPC1-*b*-PMMA respectively. They were compared with **PFN1** which had the structure of PEG-*b*-PMAPC1acid-*b*-PMMA which showed precipitation of CaP in the initial DLS experiments however **PD2** and **PDN3** did not. This indicated that nucleation cannot occur with a phosphonate and that a phosphonic acid is needed. **PFN1** precipitated CaP that was a ball-like network, which was confirmed to be amorphous CaP through electron diffraction. The amorphous material precipitated by **PFN1** was stable up to 6 days. **PFN2** has a similar structure to that of **PFN1** except with a longer PEG chain. In **PFN2** only the 0.1 mg $cm^{-3}$ sample showed particles growth (Figure 4.34) even though it has a cmc of 6.55 x $10^{-3}$ mg $cm^{-3}$. This could be attributed to the longer PEG chain interfering with the phosphoric acid moieties ability to bind to $Ca^{2+}$. **PNF2** which has a PMMA block separating the PEG and PMAPC1acid blocks showed an increase in particle size in the DLS data at 0.0075 mg $cm^{-3}$ which is below the polymer's cmc (Figure 4.35). This suggests that the morphology of the micelle is a core-shell-corona morphology (Figure 4.36) in which the PMMA block protects the PMAPC1acid, as a result the phosphonic acid cannot interact with the calcium ions to promote precipitation. **PF1** is a diblock copolymer (PEG-*b*-PMAPC1acid) which formed a film, promoted the growth of CaP (Figure 4.37). It was shown that at higher concentrations the particle growth rate was quicker. However compared to **PFN1** there is a long incubation time before the particle growth starts. From this it can be assumed that phosphonic acids increases the precipitation of CaP. However by forming a micelle in which the phosphonic acid moieties are able to interact with the water phase, t accelerates the rate of precipitation of CaP further. This is due to the micelle providing a surface for the calcium ions to bind as a result the calcium ions are in closer proximities and will help promote heterogeneous nucleation. **PNQ1** and **PQN1** which contain carboxylic acid moieties did not show evidence of CaP precipitation in the initial DLS experiments (Figure 4.38A and Figure 4.38B respectively) indicating that carboxylic acid moieties may inhibit the growth of calcium phosphate. A hypothesis for this is that the double the amount of carboxylic acids would be needed to be present promote the growth of CaP than phosphonic acids as they only have 1 binding site whereas phosphonic acids have 2 binding sites. This would mean that a there would be a lower local supersaturation of $Ca^{2+}$ ions if the same concentration of carboxylic acid and phosphonic acids are present, resulting in no CaP growth. **PNA1** showed some particle growth in the 0.02 mg $cm^{-3}$ sample however the other concentrations did not despite being above the polymer's cmc. A worm morphology was observed for **PNE1** which contains hydroxyl groups as the functional group, particle growth was seen in all concentrations tested. It is suspected that the hydroxyl group like the phosphonic acids in **PFN1** provides a heterogeneous nucleation site for the $Ca^{2+}$ ions to bind to. There has been

research intro hydroxyl self-assembling monolayers which can nucleate the growth of HAP by the absorption of the $Ca^{2+}$ on to the monolayer which acted as a calcium sink and concentrated the $PO_4^{3-}$ ions.[146,147] The worm morphology observed with **PNE1** could be due to the combination of less electrostatic repulsions between chains and structures.

In future experiments, the number of PMAPC1acid and PHEMA units need to precipitate CaP would need to be investigated because the ability of the copolymers to precipitate CaP could be linked to the number of functional groups present in the solution as there would be a critical concentration of them needed to influence CaP precipitation. This could be done by testing copolymers that have difference MAPC1acid and PHEMA blocks and investigating how the CaP precipitation changes with polymer concentration. The amount of CaP precipitated could be tracked by thermogravimetric analysis which in would also give information about the form of the CaP precipitated, as in whether is amorphous of crystsline. Or the number of polymer chains in a micelle could be determine by the calculating the specific volume of the polymer (Equation 4.2 and Equation 4.3). This would give an idea of how many phosphonic acids and hydroxy groups are in the assembled structures.

$$N_{ag} = \frac{4\pi N_A R^3}{3v^2}$$

*Equation 4.2 The equation to determine the aggregation number of a micelle, $N_A$ = avogadro's constant, R = radium of the micelle, v = specific volume of the polymer*

$$N_{agg} = \frac{M}{M_0}$$

*Equation 4.3* A simplified aggregation number equation. M = molecular weight of one micelle, $M_0$ = molecular weight of polymer backbone

The stability of the CaP produced from the polymer could be investigated further, especially in the case of **PFN1** where a longer period of time than the 6 days could lead to crystalline CaP. **PNE1** and **PF1** would need to be investigated by SEM, EDX and TEM to determine if the material precipitated during the DLS experiments is CaP and if it is crystalline. X-ray diffraction would give extra information about the bulk crystallisation of the samples which would also give a faster determination of crystallinity than electron diffraction. **PNE1** showed surprising results in the precipitation of CaP, which could also mean other groups such as sulfates or a combination of functional groups may have interesting effects. It would also be interesting to use the block copolymers which have been synthesised here in the nucleation of other crystal systems like in calcite and silica to see if they can influence the crystal growth of these compounds.

The secondary objective was to examine if the copolymers could protect enamel from acid attack. **PF1, PNE1** and **PFN1** were investigated for their anti-erosion properties. It was found that **PFN1** only provided minimal protected against acid attack if any, suggesting that spheres give a poor surface coverage over the enamel. Furthermore **PNE1** gives effective protection at concentrations below 1 mg $cm^{-3}$ above this the enamel surface became oversaturated with polymer and the excess were only weakly bound. The effective protection by **PNE1** at low concentrations suggests that the worm morphology packs more efficiently than the **PFN1's** sphere morphology. **PF1** gives the best protection of enamel against acid attack and increases with polymer concentration, reinforcing that non-assembling polymers are more beneficial for this application. However with these three block copolymers the poly-coated enamel needs to be examined under SEM before the acid erosion testing to confirm that the sphere, worms and

film morphologies occur on the surface of the enamel like it does in block solutions of the polymers.

In future experiments, the adsorption of the copolymers to enamel should be examined as it would give an indication of which functional group has a higher affinity for HAP, this could be done through IR spectroscopy and UV vis spectroscopy. **PNF2**, **PNA1** and the carboxylic containing polymers (which were not effective in promoting particle growth) would need to be tested for acid erosion properties. Especially the carboxylic acid based polymers because they have shown promise in the literature.[34,61]

# Chapter 5 Conclusions and Future work

The primary focus of restorative research on enamel has been remineralising enamel by using proteins found in saliva or using amorphous CaP. However, the former would be too expensive to produce commercially and in the latter case the morphology has not yet been controlled. Polymers provide an inexpensive alternative to the use of proteins if they could nucleate the HAP and regulate the morphology. Films of polymers have been shown to provide an acid resistant layer for enamel and reduce erosion damage significantly. The polymers that showed the greatest protection contained a charged moiety such as a carboxylic or phosphonic acids.[34] However the ability of polymers to nucleate HAP has been overlooked. There has been research in which self-assembled monolayers of various compounds have been shown to nucleate HAP growth but is limited to external applications.

The research presented in this thesis has built upon the research surrounding enamel restoration. The main focus of this thesis was to synthesis block copolymers that had the ability to nucleate hydroxyapatite and how the self-assembly of these polymers influenced nucleation. The secondary aim was to investigate if the block copolymers synthesised could provide an acid resistance coating for enamel. Here a library of block copolymers were synthesised through two different polymerisation methods ROP and RAFT polymerisation. In Chapter 2, triblock copolymers were synthesised by ROP and then functionalised by thiol-ene click chemistry and hydrophosphorylation to incorporation carboxylic and phosphonic acid moieties. This the first known report of using hydrophosphorylation with $Mn(OAc_2)$ in the functionalisation of a polymer. The triblocks with the structure of PEG-*b*-PCL-*b*-PHEL did not undergo transesterification upon the second polymerisation. It was also found that without incorporating a hydrophobic block such as PCL self-assembly could not occur, this was also the case in Chapter 3 with **PF1**. However incorporating too long a hydrophobic segment caused polymer precipitation rather than self-assembly which was seen in the majority of the copolymers synthesised through ROP and in the RAFT polymers where PEG had yet to be coupled (**ND1**). For this reason the copolymers synthesised by ROP were not investigated for their ability to nucleate HAP.

In order to make the polymerise synthesised in ROP viable for biomaterial applications, ROP synthesis needs to be optimised. The length of the PCL block needs to shorter to avoid macroprecipitation of the polymer. This would enable the polymer to be for the nucleation of HAP. [Al](Salen) is not an FDA approved catalyst, as a result other catalysts such as tin(II) octanoate should be explored such to ensure the polymer is viable in future applications. The ROP polymers are polyesters meaning that the ester bonds can be degraded enzymatically. In literature poly(lactic acids) and poly(caprolactones) are used as micelles in drug release due to their ability to enzymatically and chemically degrade.[160–162] This means that the polymers synthesised by ROP would need to undergo enzymatic degradation experiments to determine its stability against degradation by the enzyme in saliva. In the copolymers synthesised by RAFT polymerisation, the order of the blocks has different effects of its ability to precipitate CaP. This would mean that the block arrangements in the copolymers synthesised by ROP also needs to be investigated, to do this a PEG-*b*-PHEL macroinitiator would need to be used to polymerise εCL. In literature there has been limited research on triblock copolymers which incorporate PHEL, this could be due to PEG-*b*-PHEL not being a practical macroinitiator due to its reactivity. It has been known that when monomers which are more reactive are polymerised with a macroinitiator which has a lower reactivity, transesterification occurs.

In the RAFT polymerisations four functional groups were investigated, carboxylic acids, phosphonic acids, amines and alcohols. It was shown that the PEGylation could be performed before or after the second polymerisation and have similar results. In literature the PEGylation of the RAFT agent is more common than PEGylation of the resultant polymer. When MMA was polymerised in DMAc, the polymers had a larger dispersity which indicated that these polymerisations were less controlled. This was attributed to the reaction conditions not being optimal for MMA polymerisation. The majority of polymers that could self-assemble were ionic copolymers. These polymers formed micelle which were a kinetically frozen morphology. This was due to the electrostatic repulsion between the charged groups.

In previous research polyphosphonic acids have been shown to provide an acid resistant film though were not tested for their nucleation ability. Here it was found that self-assembled phosphorous copolymer (**PFN1**) could promote the growth of CaP, which was confirmed by EDX. Importantly, the phosphonic block has to be extended into the corona of the micelle rather than in the core to promote CaP growth. The assembled PEG-*b*-PMAPC1-*b*-PMMA showed a ball-like amorphous CaP which was stable up to 6 days of incubation. The alternative phosphorous triblock arrangement PEG-*b*-PMMA-*b*-PMAPC1acid could precipitate CaP when not assembled but could not when self-assemble (**PNF2**) which was indicated by DLS. This is due to the PMMA providing a shell around the PMAPC1acid which inhibits the PMAPC1acid's ability to interact with the calcium ions.[151] The non-assembling phosphorous diblock copolymer could also precipitate calcium phosphate. This indicates that a phosphonic acid needs to be present to promote the precipitate of calcium phosphate. However when the self-assemble phosphorus triblock copolymers are used rather than the diblock copolymers the precipitate of CaP occurs sooner. The PEG-*b*-PMMA-*b*-PHEMA had a morphology of worms and micelles and showed promotion of CaP through DLS. The polymers which contained carboxylic acid moieties did not precipitate CaP even though these carboxylic acid copolymers have been shown to bind with HAP by Lei *et al.*[61] This means that precipitation of CaP is not just about having a charged moiety on the copolymer It appears that a charged group is needed to precipitate CaP as the protected polymers, PEG-*b*-PMAPC1-b-PMMA and PEG-*b*-PMAPC1 (**PDN3** and **PD3** respectively) did not precipitate any material. The amine based polymer also didn't precipitate CaP which could imply a negatively charged moiety is needed for nucleation.

This research has given an insight into polymers being able to promote the precipitation of CaP. However the number of phosphonic acids and hydroxyl moieties needed to precipitate CaP could be investigated through changing the degree of polymerisation of the polymer blocks and by increasing the concentration of the latex. It would be expected that a certain concentration of functional groups would be needed to promote the growth of CaP. The number of polymer chains in the micelle ($N_{agg}$) would be beneficial to investigate the nucleation conditions because it would give an idea of how many sites are available to bind to $Ca^{2+}$ ions. This can be determined by the specific volume of the polymer and through DLS measurements. The amorphous CaP formed in the presence of **PFN1** would need to be monitored and measured at longer durations to determine if the material will crystallize. A method which would provide an alternative and faster determination of bulk crystallisation would be x-ray diffraction which could be utilise in the future. Polymers which had precipitated CaP indicated by the DLS experiments should be also viewed with SEM in order to determine the chemical composition by EDS. Then the polymers should be viewed under the TEM to confirm if HAP has been crystallized. Once these are investigated the biocompatibility of the polymer would need to be investigated, PEG is known to be biocompatible however it is unknown if PMAPC1 is. As a result, cytotoxicity tested would need to be completed.

The next steps would be to incorporate multiple functional groups in the copolymer, the two groups that would be in particular interest would be a combination of phosphinic acids and hydroxyl groups. In RAFT polymerisation this could be conducted, by polymerising HEMA and MAPC1 in a gradient copolymer then polymerising further with MMA. An alternative method would be to synthesis a monomer which contains both a hydroxyl and phosphonate group (Figure 5.1).

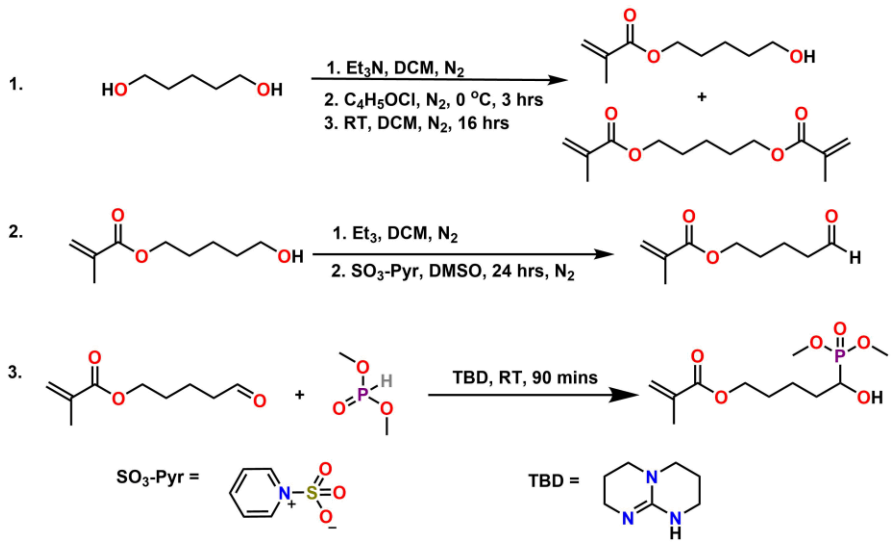


*Figure 5.1 A schematic of reaction to synthesis a methylacrylate monomer containing both a hydroxyl and phosphonate on the same carbon.*

Following on from the research on polymer films, PEG-*b*-PMAPC1acid-b-PMMA (**PFN1**), PEG-*b*-PMAPC1acid (**PF1**) and PEG-*b*-PMMA-*b*-PHEMA (**PNE1**) were used to make protective films. It was revealed that a copolymer which formed a film was better suited for making an acid resistant film than copolymers which assembled spheres in solution. At higher concentrations the ability of PEG-*b*-PMAPC1acid-b-PMMA and PEG-*b*-PMMA-*b*-PHEMA to protect decreases as the polymers oversaturate the enamel and become detached. The hypothesis for the lack of protection from **PFN1** was that a sphere morphology does not pack efficiently on the enamel as a result is leaves spaces in which acid can penetrate the exposed enamel and erosion can occur. Furthermore the one polymer sphere covers a smaller area of enamel compared to the same number of polymers chains arranged as a film. The worm morphology as seen in the PEG-*b*-PMMA-*b*-PHEMA reduced enamel loss as well because in this morphology the polymer can pack efficiently compared to the polymers spheres and thereby covering a larger surface area on the enamel. However SEM images prior to the acid etching are needed to confirm the morphologies of these polymers and support the hypotheses made here. To progress this research further the polymers with film and sphere morphologies which have different functional groups (**PQN1, PNQ1 and PNA1**) should be investigated for their acid-resistant properties.

In the future, it would be beneficial to have a material that could both protect existing enamel from acid erosion and help to nucleate new enamel. This could potentially be done by adding just $CaCl_2$, $KH_2PO_4$ and the material or with the addition of amorphous CaP as demonstrated by Shao *et al.*[39] This research has shown block copolymers could be a potential candidate for this application.

# Chapter 6 Experimental

## 6.1. Materials

All commercial reagents were purchased from Sigma Aldrich, Alfa Aesar and Fisher unless stated otherwise. MAPC1 was purchased from Specific Polymers Ltd. $Et_3N$, was dried over Calcium hydride and distilled under vacuum. PEG-OH, dimethyl phosphite, TMSBr, Calcium Chloride dihydrate, postassium dibasic, pyrene, DMAc, DMF, acetone, 1,4-dioxane, EDC, MnOAc, MCAA, MCPA, methanol, 2,4-ditert-butylsalicylaldehyde, BAPOS, HEMA, MMA, DMAE, TBuMA, MCiPA and IPA were used as received. AIBN and DMAP was recrystallized from hot methanol and toluene respectively. The DCM, toluene and THF was dried using the innovate technologies SPS-4007-7 solvent system

## 6.2. General Considerations

All air-sensitive manipulations were performed in a Vigor glovebox equipped with a -35 °C freezer, [$O_2$] and [$H_2O$] analysers or on a dual manifold Schlenk line using standard Schlenk techniques.

All $^{1}H$, $^{13}C\{^{1}H\}$ and $^{31}P\{^{1}H\}$ NMR spectra were obtained on a Bruker Avance III 400, and 500 MHz spectrometers or on a Bruker Avance I 600 MHz spectrometer. All spectra were obtained at ambient temperature unless otherwise stated. The chemical shifts (δ) and coupling constants (J) were recorded in parts per million (ppm) and Hertz (Hz) respectively. $^{1}H$, $^{13}C\{^{1}H\}$, $^{31}P\{^{1}H\}$ multiplicities and coupling constants are reported where applicable. The residual solvent peak of the deuterated solvent was used as a reference and spectra are reported relative to it.

Samples dialysed against ultrapure water with a spectrum lab dialysis machine using regenerated cellulose dialysis membranes (MWCO 3.5 kDa and 6-8 kDa). The samples were freeze dried on a Lablyo mini freeze dryer.

GPC was carried out using two PLgel Mixed-C columns (200 - 2,000,000 g $mol^{-1}$, 5 µm) using DMF with 0.1 % w/v LiBr at 60 °C at 1 $cm^3$ $min^{-1}$ as eluent on an Agilent 1100 GPC. The GPC data for **PC4** and **D1** were measured with a Viscotek GPC Max1000 system equipped with a refractive index detector and two KF-805L Shodex columns (300-2,000,000 g $mol^{-1}$, 10 µm) at a flow of 1 $cm^3$ $min^{-1}$ using chloroform as an eluent.

DLS analyses were carried out using a Malvern, Nano-Zs with a plastic cuvette at a scattering angle of 1730, wavelength of 633 nm and laser of 4 mW.

A FEI F20 Tecnai electron microscope with 200 keV field emission gun, equipped with a Gatan room temperature holder was used for imaging. Images were recorded on an 8k x 8k CMOS TVIPS F816 camera.

SEM imaging was carried out using a ZEISS Sigma HD microscope operating at 5 keV, which was also equipped with backscattering detectors. EDX analysis was conducted using a working distance (WD) detector and elemental spectras were obtained using Aztec Software (Oxford Instruments).

A Bruker DektakXT stylus profiler was used in the acid erosion experiment to measure surface roughness with a diamond stylus tip. The force used on the sample was 10 mg.

### 6.2.1. Determination of the critical micelle concentration (cmc)

Fluorescence excitation spectra were obtained on a the Spex FluoroMax fluorimeter, the excitation occurred at 334 nm, integration time 0.5 s and scan length from 350 nm to 440 nm. The $\lambda_{max}$ of pyrene was measured on a Hitachi U-2001 UV-vis spectrometer determined to 334 nm.

The preparation of the samples for the fluorescence studies is as follows; Pyrene was dissolved in a 100 $cm^{-3}$ of acetone (2.0 x $10^{-5}$ M). Then an aliquot of the pyrene solution was added to a clean vial and the acetone was allowed to evaporate. The desired volume of water doped with polymer was added and allowed to stir for 24 hours and the resultant concentration of pyrene in solutions was 2.0 x $10^{-6}$ M). The preparation for the solutions for to determinate the cmc is as follows depending on the solubility of the polymer 1 $cm^{-3}$ of DCM was added to the polymer and allowed to dissolve, afterward the DCM was added slowly to a stirring vial of water, then the DCM was left to evaporate. With the water soluble samples, the polymer was directly dissolved in water. DLS samples for CMC calculations were prepared by passing through a 0.45 μm filter.

## 6.3. Making the $CaCl_2$ and $K_2HPO_4$ solutions

Trizma sase (1.211 g) was made up to 1 $dm^3$ using HPLC grade water and the pH adjusted to 7.4 using NaOH and HCl. Calcium chloride hexahydrate (0.493 g) was made up to 500 $cm^3$ using 10mM Tris buffer and the pH adjusted to 7.4 using NaOH and HCl. Potassium phosphate dibasic (0.183 g) was made up to 500 $cm^3$ using 10mM Tris buffer and the pH adjusted to 7.4 using NaOH and HCl.

## 6.4. Preparing polymer samples and polymer samples with CaP for SEM

The silica wafers were washed with acetone then isopropanol to remove the protective film. The silica wafers were then placed in a 40 kHz/100 W Zepto $O_2$ plasma generator. The vacuum was produced (0.5 mbar) and $O_2$ flowed at a rate of 50 sccm. The wafers were treated for 10 minutes with a power set between 50 – 100 W. After venting the slides were washed with deionised water and ethanol then dried with $N_2$.

For the polymer only samples an aliquot of the polymer solution was directly placed on the silica wafer and left to air dry.

For the nucleation samples, 100 μL of polymer solution was mixed with 450 μL of the relevant concentrations of $CaCl_2$ and $K_2HPO_4$ then a silica wafer was submerged into the solution. The solution was incubated at 37 °C for a 10, 30, 60 and 240 minutes and 24 hrs. Once the allotted duration had ended, the silica wafer was removed from the solution, placed in deionised water, then ethanol and finally the solvent was removed with an aerosol can.

### 6.5. Preparing polymer samples for dry TEM

The preparation for the dry samples used in determining polymer morphology is as follows. CryoTEM grids (Ni/C, Quantifoil Holey Carbon, Micro Tools GmbH) with were plasma treated using a Quorumtech Glow Discharge system for 45 seconds. 4 µl of the polymer sample was placed on the grid and allowed to settle for 2 minutes. Afterwards the excess was blotted away, the 2 x 15 µL of water was picked up onto the grid and blotted away. Then 15 µL of uranyl acetate was picked up onto the grid and blotted. A final 15 µL of uranyl acetate was picked up and allowed to sit on the grid for 2 mins. Afterwards the excess was blotted away, and the grid was allowed to air dry.

### 6.6. Preparing polymer samples with CaP for dry TEM and electron diffraction

The preparation of the calcium phosphate/polymer samples is as follows. 100 µL of polymer solution was mixed with 450 µL of the relevant concentrations of $CaCl_2$ and $K_2HPO_4$ and left for 24 hrs and 6 days in a preheated water bath at 37 °C. An 15 µL aliquot of the sample was placed on a plasma treated TEM grid (Ni/C, Quantifoil Holey Carbon, Micro Tools GmbH) and allowed to sit for 2 minutes. Then the grid was then blotted and submerged twice in distilled water and once in ethanol and allowed to air dry.

### 6.7. Acid erosion experiments

Human enamel was partially tape with acid resistant tape, exposing half the enamel. The enamel was placed in a chosen polymer solution for 2 mins and rinsed with deionised water. Then the enamel was placed in a citric acid solution (1 % w/v, pH = 3.8) for 5 mins. The enamel was rinsed with deionised water and the surface was measured with a profilometer.

## 6.8. MeAl[Salen]

### 6.8.1. Synthesis of salen

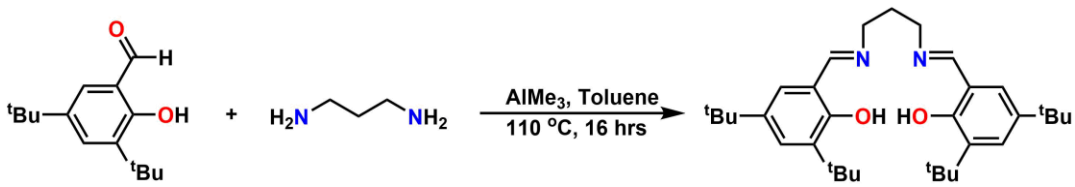


*Figure 6.1 A schematic for the synthesis of Salen.*

2,4-ditert-butylsalicylaldehyde (21.47 g, 0.1 mol) was dissolved in methanol (600 $cm^{-3}$) to which 1,3-diaminopropane (3.83 $cm^{-3}$, 0.046 mol) was added dropwise. The reaction was stirred for three hours under reflux at 70 °C prior to stirring at room temperature for 16 hours. The precipitate was filtered and dried to yield 20.3 g (87.1 %) of a yellow solid.

$^1$H NMR (500 MHz, $CDCl_3$) δ= 8.39 (d, 2H, $HOC_6H_2[C(CH_3)_3]_2C\mathbf{H_2}N(CH_2)_3N$), 7.39 (d, 2H, $HOC_6\mathbf{H_2}[C(CH_3)_3]_2CH_2N(CH_2)_3N$), 7.09 (d, 2H, $HOC_6\mathbf{H_2}[C(CH_3)_3]_2CH_2N(CH_2)_3N$), 3.71 (td, 1.2 Hz, 2H, $HOC_6H_2[C(CH_3)_3]_2CH_2N(C\mathbf{H_2})_3N$), 2.13 (m, $HOC_6H_2[C(CH_3)_3]_2CH_2N(C\mathbf{H_2})_3N$), 1.46 (s, 2H, $HOC6H_2[C(C\mathbf{H_3})_3]_2CH_2N(CH_2)_3N$), 1.31 (s, 2H, $HOC_6H_2[C(C\mathbf{H_3})_3]_2CH_2N(CH2)_3N$).

$^{13}$C NMR (126 MHz, $CDCl_3$) δ 166.48 ($HOC_6H_2[C(CH_3)_3]_2\mathbf{C}H_2N(CH_2)_3N$), 158.1 ($HO\mathbf{C_6}H_2[C(CH_3)_3]_2CH_2N(CH_2)_3N$), 140.05 ($HO\mathbf{C_6}H_2[C(CH_3)_3]_2CH_2N(CH_2)_3N$), 136.70

(HO**C**$_6$H$_2$[C(CH$_3$)$_3$]$_2$CH$_2$N(CH$_2$)$_3$N), 126.89 (HO**C**$_6$H$_2$[C(CH$_3$)$_3$]$_2$CH$_2$N(CH$_2$)$_3$N), 125.84
(HO**C**$_6$H$_2$[C(CH$_3$)$_3$]$_2$CH$_2$N(CH$_2$)$_3$N), 117.86 (HO**C**$_6$H$_2$[C(CH$_3$)$_3$]$_2$CH$_2$N(CH$_2$)$_3$N), 56.76
(HOC$_6$H$_2$[C(CH$_3$)$_3$]$_2$CH$_2$N(**C**H$_2$)$_3$N), 35.05 (HOC$_6$H$_2$[**C**(CH$_3$)$_3$]$_2$CH$_2$N(CH$_2$)$_3$N), 34.14
(HOC$_6$H$_2$[**C**(CH$_3$)$_3$]$_2$CH$_2$N(CH$_2$)$_3$N), 31.72 (HOC$_6$H$_2$[C(CH$_3$)$_3$]$_2$CH$_2$N(**C**H$_2$)$_3$N) 31.62
(HOC$_6$H$_2$[C(**C**H$_3$)$_3$]$_2$CH$_2$N(CH$_2$)$_3$N), 29.44 (HOC$_6$H$_2$[C(**C**H$_3$)$_3$]$_2$CH$_2$N(CH$_2$)$_3$N).

### 6.8.2. Synthesis of MeAl[salen]

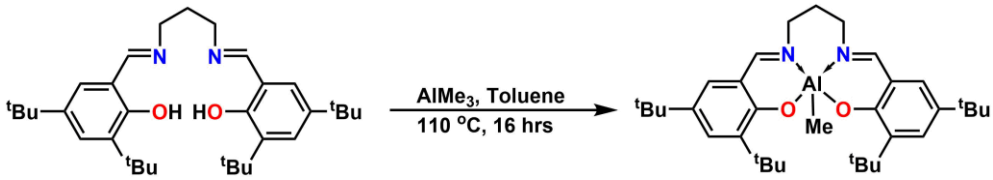


*Figure 6.2 A schematic for the synthesis of MeAl[Salen].*

Trimethyl aluminium (2M in toluene, 7.59 cm$^{-3}$, 15.2 mmol) was added dropwise to a Shlenk flask contaning Salen (7 g, 13.8 mmol) and toluene (0.5 cm$^{-3}$) and was stirred for 16 hours at 110 $^{o}$C. The reaction was concentrated under vacuum and washed three times with anhydrous hexane via a canula and canula filter. The remaining solid was dried under vacuum for four hours to yield 2.5 g (26.5 %) of a pale yellow solid.

$^{1}$H NMR (500 MHz, C$_6$D$_6$) δ= 7.73 (d, 2H, OC$_6$H$_2$[C(CH$_3$)$_3$]$_2$C**H$_2$**N(CH$_2$)$_3$NAlCH$_3$), 7.38 (s,2H, OC$_6$**H$_2$**[C(CH$_3$)$_3$]$_2$CH$_2$N(CH$_2$)$_3$NAlCH$_3$), 6.90 (d, 2H, OC$_6$**H$_2$**[C(CH$_3$)$_3$]$_2$CH$_2$N(CH$_2$)$_3$NAlCH$_3$), 3.06 (m, 2H, OC$_6$H$_2$[C(C**H$_3$**)$_3$]$_2$CH$_2$N(CH$_2$)$_3$NAlC**H$_3$**), 2.77 (m,2H, OC$_6$H$_2$[C(C**H$_3$**)$_3$]$_2$ CH$_2$N(CH$_2$)$_3$NAlCH$_3$), 1.79 (s, 18H, OC6H$_2$[C(C**H$_3$**)$_3$]$_2$ CH$_2$N(CH$_2$)$_3$NAlCH$_3$), 1.38 (s, 18H, OC$_6$H$_2$[C(C**H$_3$**)$_3$]$_2$CH$_2$N(CH$_2$)$_3$NAlCH$_3$), -0.34(OC$_6$H$_2$[C(CH$_3$)$_3$]$_2$ CH$_2$N(CH$_2$)$_3$NAlC**H$_3$**).

$^{13}$C NMR (126 MHz, CDCl$_3$) δ= 163.88 (OC$_6$H$_2$[C(CH$_3$)$_3$]$_2$**C**H$_2$N(CH$_2$)$_3$NAlCH$_3$), 140.92 (O**C**$_6$H$_2$[C(CH$_3$)$_3$]$_2$CH$_2$N(CH$_2$)$_3$NAlCH$_3$), 137.15 (O**C**$_6$H$_2$[C(CH$_3$)$_3$]$_2$CH$_2$N(CH$_2$)$_3$NAlCH$_3$), 130.04 (O**C**$_6$H$_2$[C(CH$_3$)$_3$]$_2$CH$_2$N(CH$_2$)$_3$NAlCH$_3$), 126.99 (O**C**$_6$H$_2$[C(CH$_3$)$_3$]$_2$CH$_2$N(CH$_2$)$_3$NAlCH$_3$), 118.71 (O**C**$_6$H$_2$ [C(CH$_3$)$_3$]$_2$CH$_2$N(CH$_2$)$_3$NAlCH$_3$), 54.83 (OC$_6$H$_2$[C(CH$_3$)$_3$]$_2$CH$_2$N(**C**H$_2$)$_3$NAlCH$_3$), 35.55 (OC$_6$H$_2$[C(CH$_3$)$_3$]$_2$CH$_2$N(**C**H2)$_3$NAlCH$_3$), 33.81 (OC$_6$H$_2$[C(CH$_3$)$_3$]$_2$CH$_2$N(**C**H$_2$)$_3$NAlCH$_3$), 31.64 (OC$_6$H$_2$[C(CH$_3$)$_3$]$_2$CH$_2$N(**C**H$_2$)$_3$NAlCH$_3$), 31.50 (OC$_6$H$_2$[C(**C**H$_3$)$_3$]$_2$CH$_2$N(CH$_2$)$_3$NAlCH$_3$), 29.77 (OC$_6$H$_2$[C(**C**H$_3$)$_3$]$_2$CH$_2$N(CH$_2$)$_3$NAlCH$_3$), 1.07 (OC$_6$H$_2$[C(CH$_3$)$_3$]$_2$CH$_2$N(CH$_2$)$_3$NAl**C**H$_3$).

## 6.9. Synthesis of β-HL

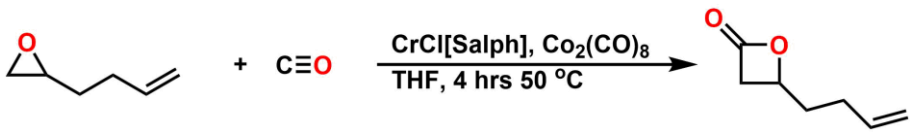


*Figure 6.3 A schematic for the carbonylation of βHL.*

In a glove box [salph]CrCl (0.105 g, 0.306 mmol) and Co$_2$(CO)$_8$, (0.286 g, 0.460 mmol) were dissolved in THF (14.40 cm$^{-3}$) and added to an oven dried ampoule. Outside the box 1,2-epoxy-5-hexene (3.00 g, 0.177 mol), was weighed in a vial, added to an ampoule and de-gassed by three freeze-pump-thaw cycles. The Cr/Co solution was transferred to the ampoule containing the epoxide via cannula transfer under an atmosphere for nitrogen. Using a second cannula transfer under nitrogen, the contents were moved to a 100 mL pressure reactor, which had been pre-heated and evacuated prior to use. The pressure reactor was purged three times with

carbon monoxide (~50 psi), then pressurised to 200 psi. The reaction was then heated to 50 °C for ~4 hr or until the carbon monoxide level ceased to decrease. The product was purified via vacuum distillation to yield a colourless oil. $^{1}$H and $^{13}$C NMR spectroscopy characterisation was consistent with literature reports.[99]

$^{1}$H NMR (600 MHz, $CDCl_3$) δ= 5.68 (ddt, J = 12, 12, 6 Hz, 1H, $O(CO)CH_2C\mathbf{H}(CH_2)_2CHCH_2$), 4.92 (m, 2 H, $O(CO)CH_2CH(CH_2)_2CHC\mathbf{H_2}$), 4.42 - 4.37 (m, 1H, $O(CO)CH_2CH(CH_2)_2C\mathbf{H}CH_2$) , 3.39 (dd, J = 18, 6 Hz, 1H, $O(CO)C\mathbf{H}_2CH(CH_2)_2CHCH_2$), 2.93 (dd, J = 18, 6 Hz, 1H, $O(CO)C\mathbf{H}_2CH(CH_2)_2CHCH_2$), 2.13 - 1.98 (m, 2H, $O(CO)CH_2CH(C\mathbf{H_2})_2CHCH_2$), 1.86 - 1.78 (m, 1H, $O(CO)CH_2CH(C\mathbf{H_2})_2CHCH_2$), 1.76 - 1.69 (m, 1 H, $O(CO)CH_2CH(CH_2)_2CHCH_2$).

$^{13}$C NMR (150 MHz, $CDCl_3$) δ= 168.17 ($O(\mathbf{C}O)CH_2CH(CH_2)_2CHCH_2$)), 136.59 (($O(CO)CH_2CH(CH_2)_2\mathbf{C}HCH_2$)), 115.66 ((($O(CO)CH_2CH(CH_2)_2CH\mathbf{C}H_2$)), 70.61 (($O(CO)\mathbf{C}H_2CH(CH_2)_2CHCH_2$)), 42.71 (($O(CO)CH_2CH(\mathbf{C}H_2)_2CHCH_2$)), 33.62 (($O(CO)CH_2CH(\mathbf{C}H_2)_2CHCH_2$)), 29.00 (($O(CO)CH_2\mathbf{C}H(CH_2)_2CHCH_2$)).

## 6.10. Ring opening polymerisation of βHL

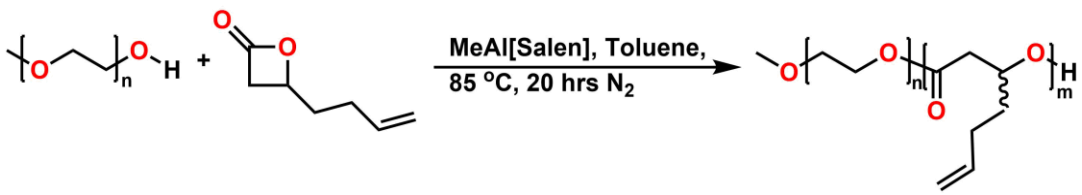


*Figure 6.4 A schematic for the ring opening polymerisation of βHL using a PEG macroinitiator.*

In the glove box PEG-OH (0.302 g, 0.604 mmol, $M_n$ = 5000), βHL (0.500 g, 39.7 mmol), MeAl[Salen] (8.70 x $10^{-2}$ g, 1.59 mmol) and toluene (4.53 g, 49.3 mmol) were added into an ampoule. The ampoule was placed in a preheated oil bath at 85 °C and stirred for 20 hrs. The $M_{n(NMR)}$ was calculated by using the methoxy of the PEG group at 3.37 ppm (which was integrated to 3H) against the methine peak of the PHEL block at 5.21 ppm.

**PH1**

$^{1}$H NMR (500 MHz, $CDCl_3$) δ= 5.76 (m, 25H, $CH_3O[(CH_2)_2O]_{142}[COCH_2CH((CH_2)_2C\mathbf{H}CH_2)O]_{25}H$), 5.21 (m, 25H, $CH_3O[(CH_2)_2O]_{142}[COCH_2C\mathbf{H}((CH_2)_2CHCH_2)O]_{25}H$), 4.98 (m, 51H, $CH_3O[(CH_2)_2O]_{142}[COCH_2CH((CH_2)_2CHC\mathbf{H_2})O]_{25}H$), 4.21 (m, 3H, $CH_3O[(C\mathbf{H_2})_2O]_{142}[COCH_2CH((CH_2)_2CHCH_2)O]_{25}H$), 3.64 (m, 566H, $CH_3O[(C\mathbf{H_2})_2O]_{142}[COCH_2CH((CH_2)_2CHCH_2)O]_{25}H$), 3.37 (s, 3H, $C\mathbf{H_3}O[(CH_2)_2O]_{142}[COCH_2CH((CH_2)_2CHCH_2)O]_{25}H$), 2.55 (m, 51H, $CH_3O[(CH_2)_2O]_{142}[COC\mathbf{H_2}CH((CH_2)_2CHCH_2)O]_{25}H$), 2.07 (m, 52H, $CH_3O[(CH_2)_2O]_{142}[COCH_2CH((C\mathbf{H_2})_2CHCH_2)O]_{25}H$), 1.78 - 1.69 (m, 72H, $CH_3O[(CH_2)_2O]_{142}[COCH_2CH((C\mathbf{H_2})_2CHCH_2)O]_{25}H$).

Conversion = 95 % $M_{n(NMR)}$ = 9300 g mol$^{-1}$ $M_{n(GPC)}$ = 29700 g mol$^{-1}$ Đ = 1.30

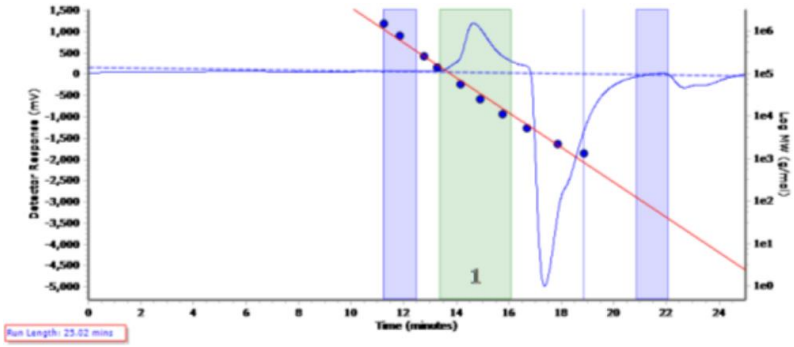


*Figure 6.5 The raw GPC trace of **PH1**. The blue rectangles are where the baseline was corrected to and the green rectangle is the area which the $M_n$ and Đ was calculated.*

**PH2**

$^1$H NMR (500 MHz, $CDCl_3$) δ 5.88 – 5.69 (m, 10H, $CH_3O[(CH_2)_2O]_{141}[COCH_2CH((CH_2)_2C\mathbf{H}CH_2)O]_9H$), 5.21 (s, 9H, $CH_3O[(CH_2)_2O]_{141}[COCH_2C\mathbf{H}((CH_2)_2CHCH_2)O]_9H$), 5.08 – 4.91 (m, 20H, $CH_3O[(CH_2)_2O]_{141}[COCH_2CH((CH_2)_2CHC\mathbf{H}_2)O]_9H$), 4.21 (t, 3H, $CH_3O[(C\mathbf{H}_2)_2O]_{141}[COCH_2CH((CH_2)_2CHCH_2)O]_9H$), 3.64 (m, 565H, $CH_3O[(C\mathbf{H}_2)_2O]_{141}[COCH_2CH((CH_2)_2CHCH_2)O]_9H$), 3.37 (s, 3H, $C\mathbf{H}_3O[(CH_2)_2O]_{141}[COCH_2CH((CH_2)_2CHCH_2)O]_9H$), 2.66 – 2.42 (m, 20H, $CH_3O[(CH_2)_2O]_{141}[COC\mathbf{H}_2CH((CH_2)_2CHCH_2)O]_9H$), 2.14 – 1.99 (m, 20H, $CH_3O[(CH_2)_2O]_{141}[COCH_2CH((C\mathbf{H}_2)_2CHCH_2)O]_9H$), 1.72 (s, 52H, $CH_3O[(CH_2)_2O]_{141}[COCH_2CH((C\mathbf{H}_2)_2CHCH_2)O]_9H$).

Conversion = 93 % $M_{n(NMR)}$ = 7300 g mol$^{-1}$ $M_{n(GPC)}$ = 22400 Đ = 1.34

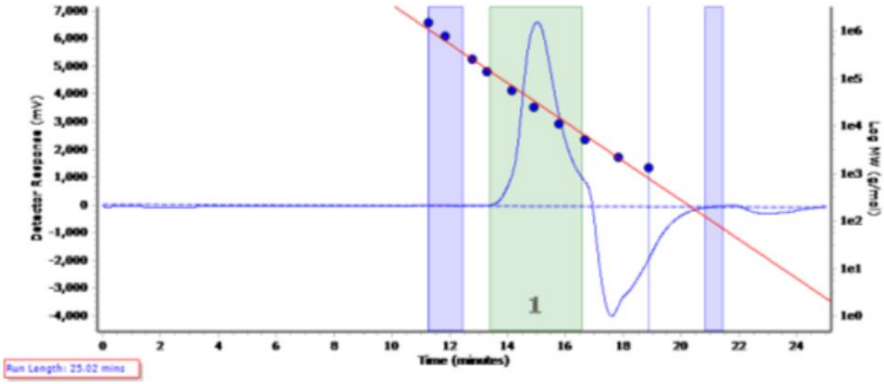


*Figure 6.6 The raw GPC trace of **PH2**. The blue rectangles are where the baseline was corrected to and the green rectangle is the area which the $M_n$ and Đ was calculated.*

**PH3**

$^1$H NMR (500 MHz, $CDCl_3$) δ 5.86 – 5.67 (m, 49H, $CH_3O[(CH_2)_2O]_{143}[COCH_2CH((CH_2)_2C\mathbf{H}CH_2)O]_{50}$ H), 5.21 (s, 50H, $CH_3O[(CH_2)_2O]_{143}[COCH_2C\mathbf{H}((CH_2)_2CHCH_2)O]_{50}$ H), 5.09 – 4.93 (m, 100H, $CH_3O[(CH_2)_2O]_{143}[COCH_2CH((CH_2)_2CHC\mathbf{H}_2)O]_{50}$ H), 4.21 (t, 3H, $CH_3O[(C\mathbf{H}_2)_2O]_{143}[COCH_2CH((CH_2)_2CHCH_2)O]_{50}$ H), 3.64 (m, 573H, $CH_3O[(C\mathbf{H}_2)_2O]_{143}[COCH_2CH((CH_2)_2CHCH_2)O]_{50}$ H), 3.37 (s, 3H, $C\mathbf{H}_3O[(CH_2)_2O]_{143}[COCH_2CH((CH_2)_2CHCH_2)O]_{50}$ H), 2.67 – 2.46 (m, 101H, $CH_3O[(CH_2)_2O]_{143}[COC\mathbf{H}_2CH((CH_2)_2CHCH_2)O]_{50}$ H), 2.13 – 1.97 (m, 104H, $CH_3O[(CH_2)_2O]_{143}[COCH_2CH((C\mathbf{H}_2)_2CHCH_2)O]_{50}$ H), 1.79 – 1.54 (m, 167H, $CH_3O[(CH_2)_2O]_{143}[COCH_2CH((C\mathbf{H}_2)_2CHCH_2)O]_{50}$ H).

Conversion = 98 % $M_{n(NMR)}$ = 12500 g mol$^{-1}$ $M_{n(GPC)}$ = 31600 Đ = 1.38

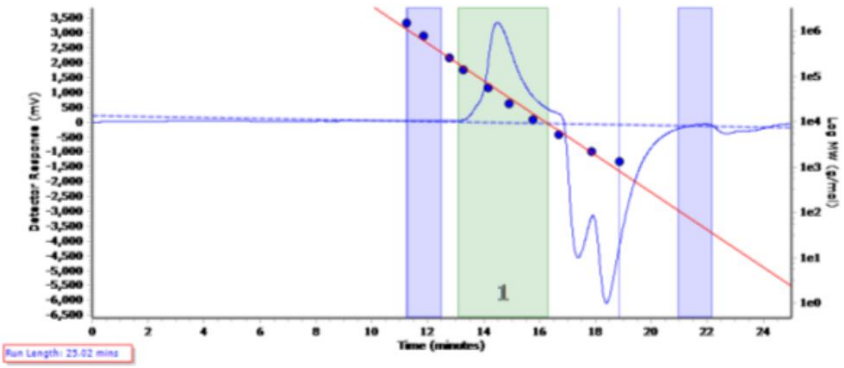


*Figure 6.7 The raw GPC trace of **PH3**. The blue rectangles are where the baseline was corrected to and the green rectangle is the area which the $M_n$ and Đ was calculated.*

**PH4**

$^1$H NMR (500 MHz $CDCl_3$) δ 5.83 – 5.68 (m, 15H, $CH_3O[(CH_2)_2O]_{47}[COCH_2CH((CH_2)_2C\mathbf{H}CH_2)O]_{15}H$), 5.20 (s, 17H, $CH_3O[(CH_2)_2O]_{47}[COCH_2C\mathbf{H}((CH_2)_2CHCH_2)O]_{15}H$), 5.06 – 4.90 (m, 31H, $CH_3O[(CH_2)_2O]_{47}[COCH_2CH((CH_2)_2CHC\mathbf{H_2})O]_{15}H$), 4.21 (t, 2H, $CH_3O[(C\mathbf{H_2})_2O]_{47}[COCH_2CH((CH_2)_2CHCH_2)O]_{15}H$), 3.63 (m, 186H, $CH_3O[(C\mathbf{H_2})_2O]_{47}[COCH_2CH((CH_2)_2CHCH_2)O]_{15}H$), 3.36 (s, 3H, $C\mathbf{H_3}O[(CH_2)_2O]_{47}[COCH_2CH((CH_2)_2CHCH_2)O]_{15}H$), 2.66 – 2.45 (m, 33H, $CH_3O[(CH_2)_2O]_{47}[COC\mathbf{H_2}CH((CH_2)_2CHCH_2)O]_{15}H$), 2.14 – 1.93 (m, 35H, $CH_3O[(CH_2)_2O]_{47}[COCH_2CH((C\mathbf{H_2})_2CHCH_2)O]_{15}H$), 1.79 – 1.57 (m, 34H, $CH_3O[(CH_2)_2O]_{47}[COCH_2CH((C\mathbf{H_2})_2CHCH_2)O]_{15}H$).

Conversion = 98 % $M_{n(NMR)}$ = 4000 g mol$^{-1}$, $M_{n(GPC)}$ = 14900 Đ = 1.21

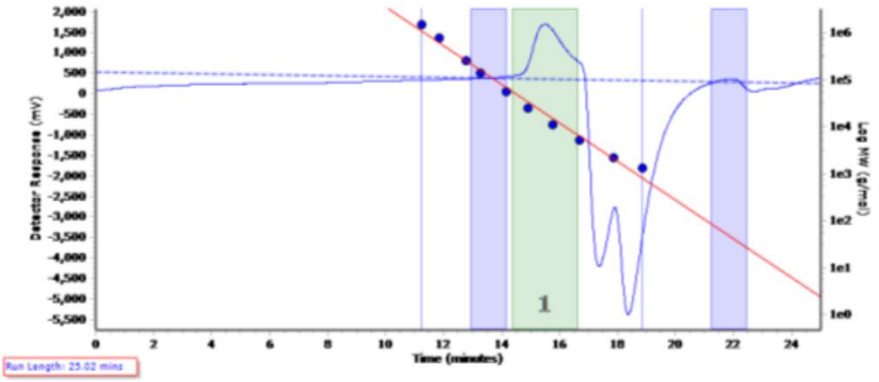


*Figure 6.8 The raw GPC trace of **PH4**. The blue rectangles are where the baseline was corrected to and the green rectangle is the area which the $M_n$ and Đ was calculated.*

**PH5**

$^1$H NMR (500 MHz, *$CDCl_3$*) δ 5.89 – 5.67 (m, 9H, $CH_3O[(CH_2)_2O]_{46}[COCH_2CH((CH_2)_2C\mathbf{H}CH_2)O]_9H$), 5.20 (s, 9H, $CH_3O[(CH_2)_2O]_{46}[COCH_2C\mathbf{H}((CH_2)_2CHCH_2)O]_9H$), 5.09 – 4.90 (m, 17H, $CH_3O[(C\mathbf{H_2})_2O]_{46}[COCH_2CH((CH_2)_2CHCH_2)O]_9H$), 4.20 (t, 2H, $CH_3O[(C\mathbf{H_2})_2O]_{46}[COCH_2CH((CH_2)_2CHCH_2)O]_9H$), 3.65 (s, 185H, $CH_3O[(C\mathbf{H_2})_2O]_{46}[COCH_2CH((CH_2)_2CHCH_2)O]_9H$), 3.37 (s, 3H, $C\mathbf{H_3}O[(CH_2)_2O]_{46}[COCH_2CH((CH_2)_2CHCH_2)O]_9H$), 2.67 – 2.43 (m, 18H, $CH_3O[(CH_2)_2O]_{46}[COC\mathbf{H_2}CH((CH_2)_2CHCH_2)O]_9H$), 2.16 – 1.96 (m, 17H, $CH_3O[(CH_2)_2O]_{46}[COCH_2CH((C\mathbf{H_2})_2CHCH_2)O]_9H$), 1.79 – 1.57 (m, 18H, $CH_3O[(CH_2)_2O]_{46}[COCH_2CH((C\mathbf{H_2})_2CHCH_2)O]_9H$).

Conversion = 97 % $M_{n(NMR)}$ = 4000 g mol$^{-1}$, $M_{n(GPC)}$ = 12500 Đ = 1.18

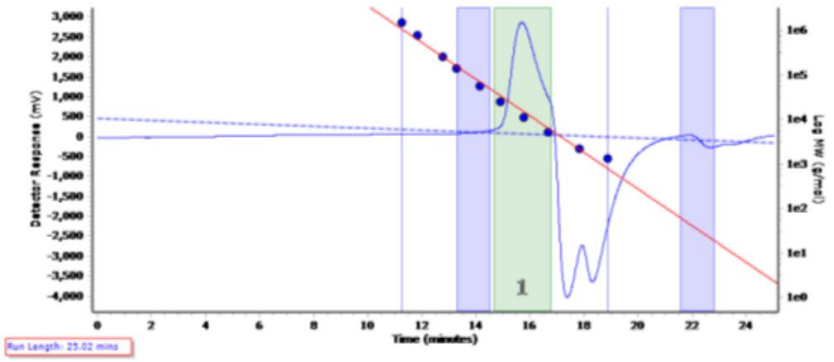


*Figure 6.9 The raw GPC trace of **PH5**. The blue rectangles are where the baseline was corrected to and the green rectangle is the area which the $M_n$ and Đ was calculated.*

**PH6**

$^1$H NMR (400 MHz, $CDCl_3$) δ= 5.75 (m, 15H, $CH_3O[(CH_2)_2O]_{147}[COCH_2CH((CH_2)_2\mathbf{C}\mathbf{H}CH_2)O]_{15}H$), 5.20 (m, 14H, $CH_3O[(CH_2)_2O]_{147}[COCH_2\mathbf{C}\mathbf{H}((CH_2)_2CHCH_2)O]_{15}H$), 4.98 (m, 31H $CH_3O[(CH_2)_2O]_{147}[COCH_2CH((CH_2)_2CH\mathbf{C}\mathbf{H_2})O]_{15}H$), 4.18 (m, 3H, $CH_3O[(\mathbf{C}\mathbf{H_2})_2O]_{147}[COCH_2CH((CH_2)_2CHCH_2)O]_{15}H$), 3.62 (m, 586H, $CH_3O[(\mathbf{C}\mathbf{H_2})_2O]_{147}[COCH_2CH((CH_2)_2CHCH_2)O]_{15}H$), 3.36 (m, 3H, $\mathbf{C}\mathbf{H_3}O[(CH_2)_2O]_{147}[COCH_2CH((CH_2)_2CHCH_2)O]_{15}H$), 2.53 (m, 28H, $CH_3O[(CH_2)_2O]_{147}[COC\mathbf{H_2}CH((CH_2)_2CHCH_2)O]_{15}H$), 2.06 (m, 29H, $CH_3O[(CH_2)_2O]_{147}[COCH_2CH((C\mathbf{H_2})_2CHCH_2)O]_{15}H$), 1.70 (m, 28H, $CH_3O[(CH_2)_2O]_{147}[COCH_2CH((C\mathbf{H_2})_2CHCH_2)O]_{15}H$).

Conversion = 96 % $M_{n(NMR)}$ = 8300 g mol$^{-1}$, $M_{n(GPC)}$ = 26800 g mol$^{-1}$ Đ = 1.26

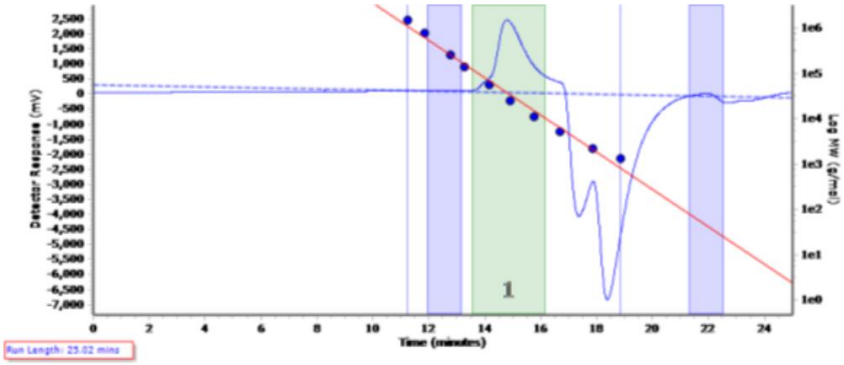


*Figure 6.10 The raw GPC trace of **PH6**. The blue rectangles are where the baseline was corrected to and the green rectangle is the area which the $M_n$ and Đ was calculated.*

**PH7**

$^1$H NMR (500 MHz, $CDCl_3$) δ 5.76 (m, 26H, $CH_3O[(CH_2)_2O]_{141}[COCH_2CH((CH_2)_2\mathbf{C}\mathbf{H}CH_2)O]_{25}H$), 5.21 (m, 25H, ($CH_3O[(CH_2)_2O]_{141}[COCH_2\mathbf{C}\mathbf{H}((CH_2)_2CHCH_2)O]_{25}H$), 5.00 (m, 53H, ($CH_3O[(CH_2)_2O]_{141}[COCH_2CH((CH_2)_2CH\mathbf{C}\mathbf{H_2})O]_{25}H$), 4.21 (m, 3H, ($CH_3O[(\mathbf{C}\mathbf{H_2})_2O]_{141}[COCH_2CH((CH_2)_2CHCH_2)O]_{25}H$), 3.64 (m, 562H, $CH_3O[(\mathbf{C}\mathbf{H_2})_2O]_{141}[COCH_2CH((CH_2)_2CHCH_2)O]_{25}H$), 3.37 (s, 3H, $\mathbf{C}\mathbf{H_3}O[(CH_2)_2O]_{141}[COCH_2CH((CH_2)_2CHCH_2)O]_{25}H$), 2.56 (m, 51H, ($CH_3O[(CH_2)_2O]_{141}[COC\mathbf{H_2}CH((CH_2)_2CHCH_2)O]_{25}H$), 2.07 (m, 50H, ($CH_3O[(CH_2)_2O]_{141}[COCH_2CH((C\mathbf{H_2})_2CHCH_2)O]_{25}H$), 1.70 (m, 49H, ($CH_3O[(CH_2)_2O]_{141}[COCH_2CH((C\mathbf{H_2})_2CHCH_2)O]_{25}H$).

Conversion = 98 % $M_{n(NMR)}$ = 9400 g mol$^{-1}$, $M_{n(GPC)}$ = 26400 g mol$^{-1}$ Đ = 1.26

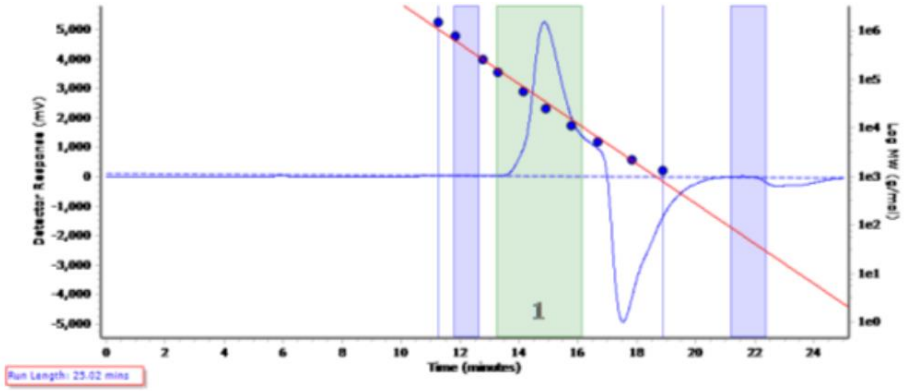


*Figure 6.11 The raw GPC trace of **PH7**. The blue rectangles are where the baseline was corrected to and the green rectangle is the area which the $M_n$ and Đ was calculated.*

## 6.11. Ring opening polymerisation of εCl

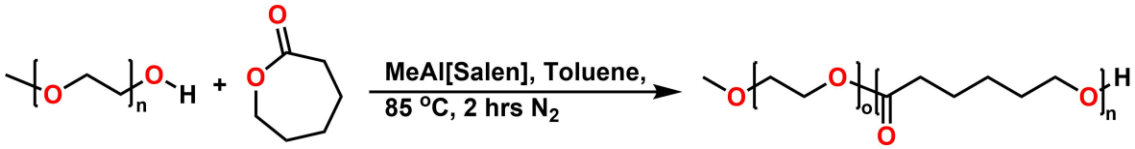


*Figure 6.12 A schematic for the ring opening polymerisation of ε-caprolactione using a PEG macroinitiator.*

In the glove box PEG-OH (0.740 g, 0.100 mmol, Mn = 5000), εCL (0.0.287 g, 2.50 mmol), MeAl[Salen] (8.10 x 10-2 g, 0.100 mmol) and toluene (1.69 g, 18.3 mmol) were added into an ampoule. The ampoule was placed in a preheated oil bath at 85 °C and stirred for 2 hrs. The polymerisation was terminated by precipitation into cold hexane (10 % MeOH). The $M_{n(NMR)}$ was calculated by using the methoxy of the PEG group at 3.37 ppm (which was integrated to 3H) against the methylene peak of the PCl block at 4.04 ppm.

**PC1**

$^1$H NMR (500 MHz, $CDCl_3$) δ 4.04 (t, *J* = 6.7 Hz, 204H, $CH_3O[(CH_2)_2O]_{242}[COC\mathbf{H_2}CH_2CH_2CH_2CH_2O]_{102}H$), 3.62 (s, 969H, $CH_3O[(C\mathbf{H_2})_2O]_{242}[COCH_2CH_2CH_2CH_2CH_2O]_{102}H$), 3.35 (s, 3H, $C\mathbf{H_3}O[(CH_2)_2O]_{242}[COCH_2CH_2CH_2CH_2CH_2O]_{102}H$), 2.28 (t, *J* = 7.5 Hz, 206H, $CH_3O[(CH_2)_2O]_{242}[COCH_2CH_2CH_2CH_2C\mathbf{H_2}O]_{102}H$), 1.68 – 1.54 (m, 418H, $CH_3O[(CH_2)_2O]_{242}[COCH_2C\mathbf{H_2}CH_2C\mathbf{H_2}CH_2O]_{102}H$), 1.41 – 1.31 (m, 214H, $CH_3O[(CH_2)_2O]_{242}[COCH_2C\mathbf{H_2}CH_2C\mathbf{H_2}CH_2O]_{102}H$), 1.31 – 1.17 (m, 289H $CH_3O[(CH_2)_2O]_{242}[COCH_2CH_2C\mathbf{H_2}CH_2CH_2O]_{102}H$).

Conversion = 98 % $M_{n(NMR)}$ = 22300 g mol$^{-1}$ $M_{n(GPC)}$ = 6308 g mol$^{-1}$ Đ = 1.40

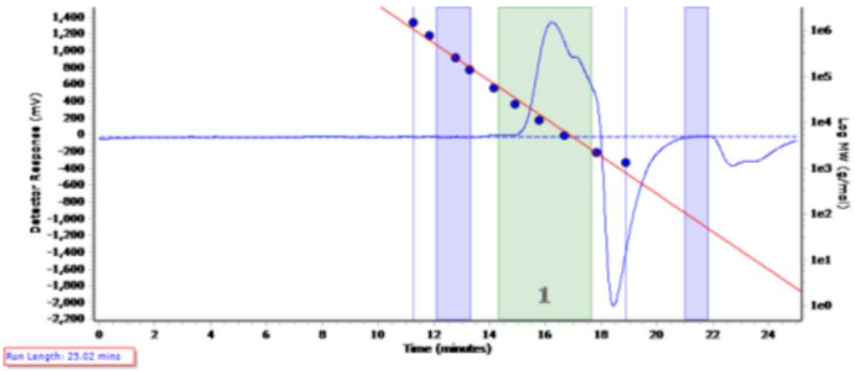


*Figure 6.13 The raw GPC of **PC1**. The blue rectangles are where the baseline was corrected to and the green rectangle is the area which the $M_n$ and Đ was calculated.*

**PC2** $^{1}$H NMR (500 MHz, $CDCl_3$) δ 4.04 (t, *J* = 6.7 Hz, 200H, $CH_3O[(CH_2)_2O]_{146}[COC\mathbf{H_2}CH_2CH_2CH_2CH_2O]_{100}H$), 3.62 (m, 584H, $CH_3O[(C\mathbf{H_2})_2O]_{146}[COCH_2CH_2CH_2CH_2CH_2O]_{100}H$), 3.36 (s, 3H, $C\mathbf{H_3}O[(CH_2)_2O]_{146}[COCH_2CH_2CH_2CH_2CH_2O]_{100}H$), 2.29 (t, *J* = 7.5 Hz, 218H, $CH_3O[(CH_2)_2O]_{146}[COCH_2CH_2CH_2CH_2C\mathbf{H_2}O]_{100}H$), 1.64 (m, 413H, $CH_3O[(CH_2)_2O]_{146}[COCH_2C\mathbf{H_2}CH_2C\mathbf{H_2}CH_2O]_{100}H$), 1.36 (m, 212H, $CH_3O[(CH_2)_2O]_{146}[COCH_2CH_2C\mathbf{H_2}CH_2CH_2O]_{100}H$).

Conversion = 97 % $M_{n(NMR)}$ = 17,800 g mol$^{-1}$ $M_{n(GPC)}$ = 30300 Đ = 1.73

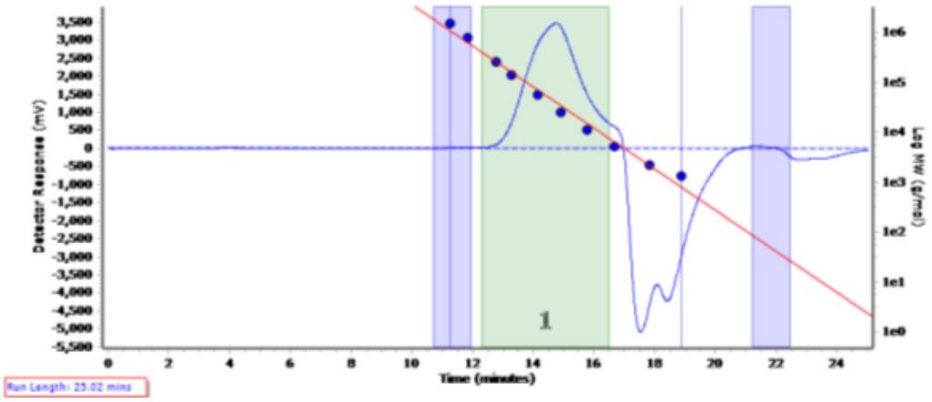


*Figure 6.14 The raw GPC of **PC2**. The blue rectangles are where the baseline was corrected to and the green rectangle is the area which the $M_n$ and Đ was calculated.*

**PC3**

$^{1}$H NMR (500 MHz, $CDCl_3$) δ 4.05 (t, *J* = 6.7 Hz, 87H, $CH_3O[(CH_2)_2O]_{133}[COC\mathbf{H_2}CH_2CH_2CH_2CH_2O]_{44}H$), 3.63 (m, 533H, $CH_3O[(C\mathbf{H_2})_2O]_{133}[COCH_2CH_2CH_2CH_2CH_2O]_{44}H$), 3.37 (s, 3H, $C\mathbf{H_3}O[(CH_2)_2O]_{133}[COCH_2CH_2CH_2CH_2CH_2O]_{44}H$), 2.30 (t, *J* = 7.5 Hz, 95H, $CH_3O[(CH_2)_2O]_{133}[COCH_2CH_2CH_2CH_2C\mathbf{H_2}O]_{44}H$), 1.87 (s, 35H, $CH_3O[(CH_2)_2O]_{133}[COCH_2CH_2CH_2CH_2CH_2O]_{44}\mathbf{H}$), 1.70 – 1.58 (m, 179H, $CH_3O[(CH_2)_2O]_{133}[COCH_2C\mathbf{H_2}CH_2C\mathbf{H_2}CH_2O]_{44}H$), 1.46 – 1.32 (m, 98H, $CH_3O[(CH_2)_2O]_{133}[COCH_2CH_2C\mathbf{H_2}CH_2CH_2O]_{44}H$).

Conversion = 96 % $M_{n(NMR)}$ = 10,900 g mol$^{-1}$ $M_{n(GPC)}$ = 33000 Đ = 1.50

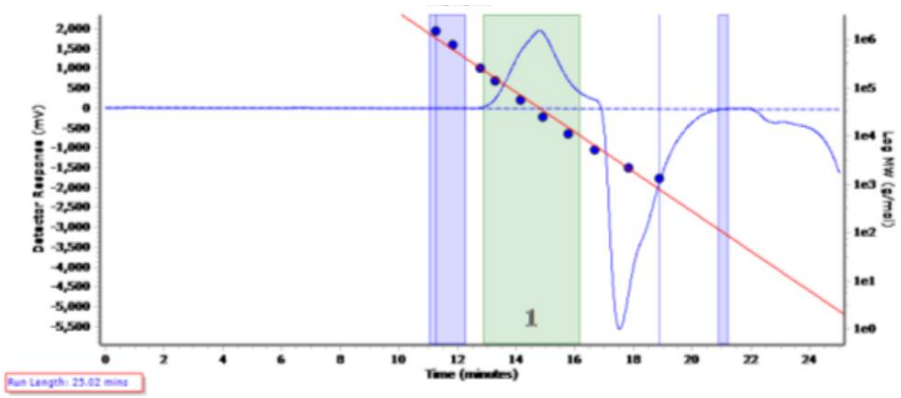


*Figure 6.15 The raw GPC of **PC3**. The blue rectangles are where the baseline was corrected to and the green rectangle is the area which the $M_n$ and Đ was calculated.*

**PC4**

$^{1}$H NMR (500 MHz, $CDCl_3$) δ 4.05 (t, *J* = 13.4 Hz, 53H, $CH_3O[(CH_2)_2O]_{52}[COC\mathbf{H_2}CH_2CH_2CH_2CH_2O]_{27}H$), 3.63 (m, 206H, $CH_3O[(C\mathbf{H_2})_2O]_{52}[COCH_2CH_2CH_2CH_2CH_2O]_{27}H$), 3.37 (s, 3H, $C\mathbf{H}_3O[(CH_2)_2O]_{52}[COCH_2CH_2CH_2CH_2CH_2O]_{27}H$), 2.30 (t, *J* = 7.5 Hz, 57H, $CH_3O[(CH_2)_2O]_{52}[COCH_2CH_2CH_2CH_2C\mathbf{H_2}O]_{27}H$), 1.74 (s, 26H, $CH_3O[(CH_2)_2O]_{52}[COCH_2CH_2CH_2CH_2CH_2O]_{27}\mathbf{H}$), 1.70 – 1.54 (m, 114H, $CH_3O[(CH_2)_2O]_{52}[COCH_2C\mathbf{H_2}CH_2C\mathbf{H_2}CH_2O]_{27}H$), 1.47 – 1.32 (m, 61H, $CH_3O[(CH_2)_2O]_{52}[COCH_2CH_2C\mathbf{H_2}CH_2CH_2O]_{27}H$).

Conversion = 94 % $M_{n(NMR)}$ = 5400 g mol$^{-1}$ $M_{n(GPC)}$ = 12900 g mol$^{-1}$ Đ = 1.63

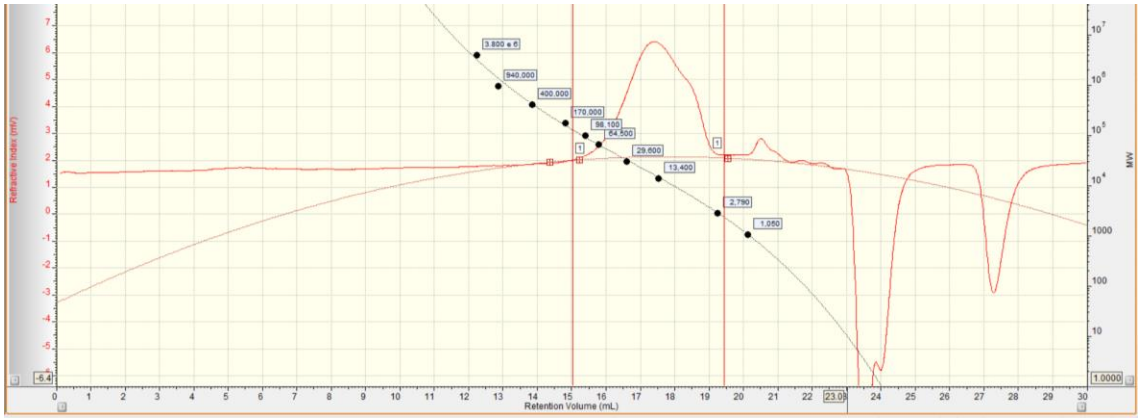


*Figure 6.16 The raw GPC of **PC4**. The area between the two re vertical lines is where the $M_n$ and Đ was calculated. The black circles are the polystyrene standards.*

## 6.12. Ring opening polymerisation of βHL using a PEG-*b*-PCL macroinitiator

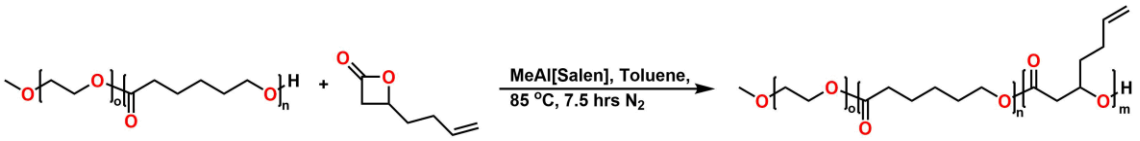


*Figure 6.17 A schematic for the ring opening polymerisation of βHL using a PEG-b-PCL macroinitiator.*

In the glove box PEG-pεCL (0.200. g, 0.0200 mmol, Mn = 5000), βHL (0.0765 g, 0.600 mmol), MeAl[Salen] (0.0133 g, 0.0200 mmol) and toluene (0.277 g, 3.00 mmol) were added into an ampoule. The ampoule was placed in a preheated oil bath at 85 °C and stirred for 7.5 hrs. The polymerisation was terminated by precipitation into cold hexane (10 % MeOH). The $M_{n(NMR)}$ was calculated by using the methoxy of the PEG group at 3.37 ppm (which was integrated to 3H) against the methylene peak of the PCl block at 4.04 ppm and the methine peak of the PHEL block at 5.13 ppm.

**PCH1** uses **PC2**

$^1$H NMR (500 MHz, $CDCl_3$) δ 5.70 (s, 29H, $CH_3O[(CH_2)_2O]_{144}[COCH_2CH_2CH_2CH_2CH_2O]_{99}[COCH_2CH((CH_2)_2\mathbf{C}\mathbf{H}CH_2)O]_{27}H$), 5.13 (s, 20H, $CH_3O[(CH_2)_2O]_{144}[COCH_2CH_2CH_2CH_2CH_2O]_{99}[COCH_2\mathbf{C}\mathbf{H}((CH_2)_2CHCH_2)O]_{30}H$), 4.90 (m, 60H, $CH_3O[(CH_2)_2O]_{144}[COCH_2CH_2CH_2CH_2CH_2O]_{99}[COCH_2CH((CH_2)_2CH\mathbf{C}\mathbf{H_2})O]_{30}H$), 3.98 (t, *J* = 6.6 Hz, 197H, $CH_3O[(CH_2)_2O]_{144}[COC\mathbf{H_2}CH_2CH_2CH_2CH_2O]_{99}[COCH_2CH((CH_2)_2CHCH_2)O]_{30}H$), 3.56 (s, 578H, $CH_3O[(C\mathbf{H_2})_2O]_{144}[COCH_2CH_2CH_2CH_2CH_2O]_{99}[COCH_2CH((CH_2)_2CHCH_2)O]_{30}H$), 3.29 (s, 3H, $C\mathbf{H_3}O[(CH_2)_2O]_{144}[COCH_2CH_2CH_2CH_2CH_2O]_{99}[COCH_2CH((CH_2)_2CHCH_2)O]_{30}H$), 2.48 (s, 81H, $CH_3O[(CH_2)_2O]_{144}[COCH_2CH_2CH_2CH_2C\mathbf{H_2}O]_{99}[COCH_2CH((CH_2)_2CHCH_2)O]_{30}H$), 2.08 (s, 197H, $CH_3O[(CH_2)_2O]_{144}[COCH_2CH_2CH_2CH_2CH_2O]_{99}[COCH_2CH((C\mathbf{H_2})_2CHCH_2)O]_{30}H$), 1.62 (s, 470H, $CH_3O[(CH_2)_2O]_{144}[COCH_2C\mathbf{H_2}CH_2C\mathbf{H_2}CH_2O]_{99}[COCH_2CH((C\mathbf{H_2})_2CHCH_2)O]_{30}H$), 1.30 (s, 208H, $CH_3O[(CH_2)_2O]_{144}[COCH_2CH_2C\mathbf{H_2}CH_2CH_2O]_{99}[COCH_2CH((CH_2)_2CHCH_2)O]_{30}H$).

Conversion = 51 % $M_{n(NMR)}$ = 21400 g mol$^{-1}$ $M_{n(GPC)}$ = bimodal 800, 33100 g mol$^{-1}$ Đ = 1.26, 1.61

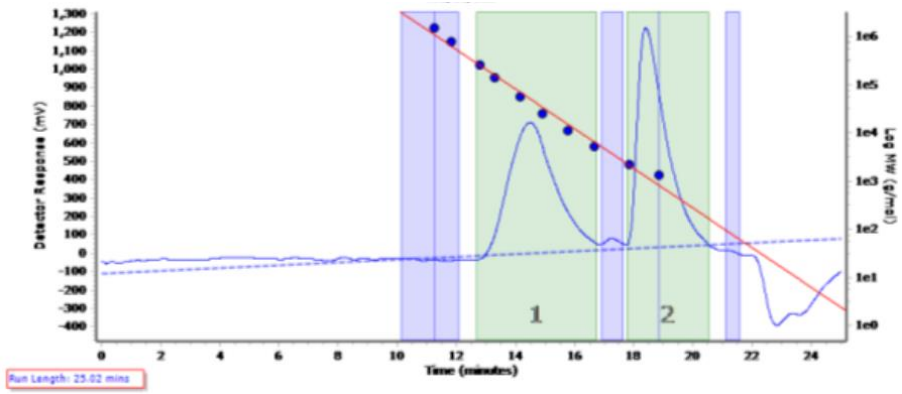


*Figure 6.18 The raw GPC of **PCH1**. The blue rectangles are where the baseline was corrected to and the green rectangles is the area which the $M_n$ and Đ was calculated.*

**PCH2** uses **PC1**

$^1$H NMR (500 MHz, $CDCl_3$) δ 5.75 (m, 50H, $CH_3O[(CH_2)_2O]_{241}[COCH_2CH_2CH_2CH_2CH_2O]_{100}[COCH_2CH((CH_2)_2C\mathbf{H}CH_2)O]_{50}H$), 5.19 (s, 52H, $CH_3O[(CH_2)_2O]_{241}[COCH_2CH_2CH_2CH_2CH_2O]_{100}[COCH_2C\mathbf{H}((CH_2)_2CHCH_2)O]_{50}H$), 4.98 (m, 101H, $CH_3O[(CH_2)_2O]_{241}[COCH_2CH_2CH_2CH_2CH_2O]_{100}[COCH_2CH((CH_2)_2CHC\mathbf{H_2})O]_{50}H$), 4.05 (t, *J* = 6.7 Hz, 202H, $CH_3O[(CH_2)_2O]_{241}[COC\mathbf{H_2}CH_2CH_2CH_2CH_2O]_{100}[COCH_2CH((CH_2)_2CHCH_2)O]_{50}H$), 3.63 (m, 971H, $CH_3O[(C\mathbf{H_2})_2O]_{241}[COCH_2CH_2CH_2CH_2CH_2O]_{100}[COCH_2CH((CH_2)_2CHCH_2)O]_{50}H$), 3.37 (s, 3H, $C\mathbf{H_3}O[(CH_2)_2O]_{241}[COCH_2CH_2CH_2CH_2CH_2O]_{100}[COCH_2CH((CH_2)_2CHCH_2)O]_{50}H$), 2.55 (m, 106H, $CH_3O[(CH_2)_2O]_{241}[COCH_2CH_2CH_2CH_2CH_2O]_{100}[COC\mathbf{H_2}CH((CH_2)_2CHCH_2)O]_{50}H$), 2.29 (t, *J* = 7.5 Hz, 203H, $CH_3O[(CH_2)_2O]_{241}[COCH_2CH_2CH_2CH_2C\mathbf{H_2}O]_{100}[COCH_2CH((CH_2)_2CHCH_2)O]_{50}H$), 2.05 (m, 101H, $CH_3O[(CH_2)_2O]_{241}[COCH_2CH_2CH_2CH_2CH_2O]_{100}[COCH_2CH((C\mathbf{H_2})_2CHCH_2)O]_{50}H$), 1.67 (m, 511H, $CH_3O[(CH_2)_2O]_{241}[COCH_2C\mathbf{H_2}CH_2C\mathbf{H_2}CH_2O]_{100}[COCH_2CH((C\mathbf{H_2})_2CHCH_2)O]_{50}H$), 1.37 (m, 204H, $CH_3O[(CH_2)_2O]_{241}[COCH_2CH_2C\mathbf{H_2}CH_2CH_2O]_{100}[COCH_2CH((CH_2)_2CHCH_2)O]_{50}H$).

Conversion = 84 % $M_{n(NMR)}$ = 28300 g mol$^{-1}$ $M_{n(GPC)}$ =190400 g mol$^{-1}$ Đ = 1.42

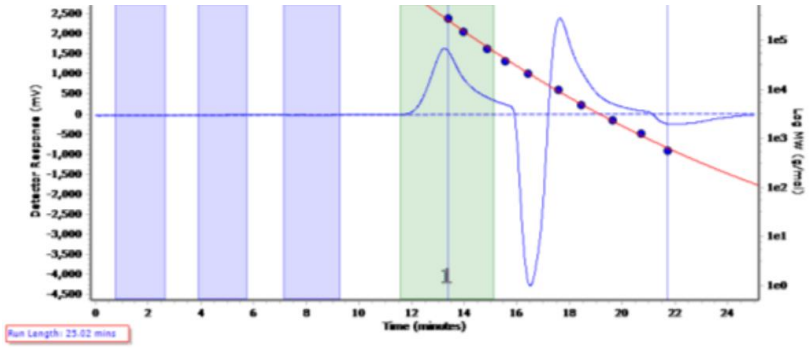


*Figure 6.19 The raw GPC of **PCH2**. The blue rectangles are where the baseline was corrected to and the green rectangle is the area which the $M_n$ and Đ was calculated.*

**PCH3** uses **PC3**

$^1$H NMR (500 MHz, $CDCl_3$) δ 5.81 – 5.64 (m, 42H, $CH_3O[(CH_2)_2O]_{140}[COCH_2CH_2CH_2CH_2CH_2O]_{43}[COCH_2CH((CH_2)_2C\mathbf{H}CH_2)O]_{48}H$), 5.16 (s, 48H, $CH_3O[(CH_2)_2O]_{140}[COCH_2CH_2CH_2CH_2CH_2O]_{43}[COCH_2C\mathbf{H}((CH_2)_2CHCH_2)O]_{48}H$), 5.02 – 4.86 (m, 86H, $CH_3O[(CH_2)_2O]_{140}[COCH_2CH_2CH_2CH_2CH_2O]_{43}[COCH_2CH((CH_2)_2CHC\mathbf{H_2})O]_{48}H$), 4.00 (t, *J* = 7.6 Hz, 87H, $CH_3O[(CH_2)_2O]_{140}[COC\mathbf{H_2}CH_2CH_2CH_2CH_2O]_{43}[COCH_2CH((CH_2)_2CHCH_2)O]_{48}H$), 3.58 (m, 559H, $CH_3O[(C\mathbf{H_2})_2O]_{140}[COCH_2CH_2CH_2CH_2CH_2O]_{43}[COCH_2CH((CH_2)_2CHCH_2)O]_{48}H$), 3.31 (s, 3H, $C\mathbf{H_3}O[(CH_2)_2O]_{140}[COCH_2CH_2CH_2CH_2CH_2O]_{43}[COCH_2CH((CH_2)_2CHCH_2)O]_{48}H$), 2.64 – 2.39 (m, 100H, $CH_3O[(CH_2)_2O]_{140}[COCH_2CH_2CH_2CH_2CH_2O]_{43}[COC\mathbf{H_2}CH((CH_2)_2CHCH_2)O]_{48}H$), 2.24 (t, 135H, $CH_3O[(CH_2)_2O]_{140}[COCH_2CH_2CH_2CH_2C\mathbf{H_2}O]_{43}[COCH_2CH((CH_2)_2CHCH_2)O]_{48}H$), 2.03 – 1.95 (m, 192H, $CH_3O[(CH_2)_2O]_{140}[COCH_2CH_2CH_2CH_2CH_2O]_{43}[COCH_2CH((C\mathbf{H_2})_2CHCH_2)O]_{48}H$), 1.71 – 1.52 (m, 274H, $CH_3O[(CH_2)_2O]_{140}[COCH_2C\mathbf{H_2}CH_2C\mathbf{H_2}CH_2O]_{43}[COCH_2CH((C\mathbf{H_2})_2CHCH_2)O]_{48}H$), 1.38 – 1.26 (m, 93H, $CH_3O[(CH_2)_2O]_{140}[COCH_2CH_2C\mathbf{H_2}CH_2CH_2O]_{43}[COCH_2CH((CH_2)_2CHCH_2)O]_{48}H$).

Conversion = N/A $M_{n(NMR)}$ = 17100 g mol$^{-1}$ $M_{n(GPC)}$ = 121400 g mol$^{-1}$ Đ = 1.40

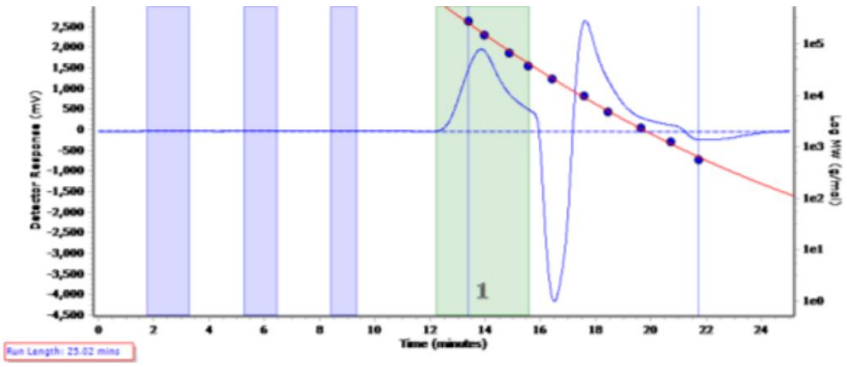


*Figure 6.20 The raw GPC of **PCH3**. The blue rectangles are where the baseline was corrected to and the green rectangle is the area which the $M_n$ and Đ was calculated.*

**PCH4** uses **PC4**

$^1$H NMR (500 MHz, $CDCl_3$) δ 5.89 – 5.70 (m, 19H, $CH_3O[(CH_2)_2O]_{49}[COCH_2CH_2CH_2CH_2CH_2O]_{23}[COCH_2CH((CH_2)_2C\mathbf{H}CH_2)O]_{20}H$), 5.21 (s, 21H, $CH_3O[(CH_2)_2O]_{49}[COCH_2CH_2CH_2CH_2CH_2O]_{23}[COCH_2C\mathbf{H}((CH_2)_2CHCH_2)O]_{20}H$), 5.09 – 4.93 (m, 38H, $CH_3O[(CH_2)_2O]_{49}[COCH_2CH_2CH_2CH_2CH_2O]_{23}[COCH_2CH((CH_2)_2CHC\mathbf{H_2})O]_{20}H$), 4.06 (t, *J* = 13.4 Hz, 45H, $CH_3O[(CH_2)_2O]_{49}[COC\mathbf{H_2}CH_2CH_2CH_2CH_2O]_{23}[COCH_2CH((CH_2)_2CHCH_2)O]_{20}H$), 3.64 (m, 197H, $CH_3O[(C\mathbf{H_2})_2O]_{49}[COCH_2CH_2CH_2CH_2CH_2O]_{23}[COCH_2CH((CH_2)_2CHCH_2)O]_{20}H$), 3.37 (s, 3H, $C\mathbf{H_3}O[(CH_2)_2O]_{49}[COCH_2CH_2CH_2CH_2CH_2O]_{23}[COCH_2CH((CH_2)_2CHCH_2)O]_{20}H$), 2.66 – 2.46 (m, 40H, $CH_3O[(CH_2)_2O]_{49}[COCH_2CH_2CH_2CH_2CH_2O]_{23}[COC\mathbf{H_2}CH((CH_2)_2CHCH_2)O]_{20}H$), 2.30 (t, *J* = 15.0 Hz, 48H, $CH_3O[(CH_2)_2O]_{49}[COCH_2CH_2CH_2CH_2C\mathbf{H_2}O]_{23}[COCH_2CH((CH_2)_2CHCH_2)O]_{20}H$), 2.15 – 1.99 (m, 38H, $CH_3O[(CH_2)_2O]_{49}[COCH_2CH_2CH_2CH_2CH_2O]_{23}[COCH_2CH((C\mathbf{H_2})_2CHCH_2)O]_{20}H$), 1.79 – 1.53 (m, 148H, $CH_3O[(CH_2)_2O]_{49}[COCH_2C\mathbf{H_2}CH_2C\mathbf{H_2}CH_2O]_{23}[COCH_2CH((C\mathbf{H_2})_2CHCH_2)O]_{20}H$), 1.44 – 1.32 (m, 48H, $CH_3O[(CH_2)_2O]_{49}[COCH_2CH_2C\mathbf{H_2}CH_2CH_2O]_{23}[COCH_2CH((CH_2)_2CHCH_2)O]_{20}H$).

Conversion = 48 % $M_{n(NMR)}$ = 7300 g mol$^{-1}$ $M_{n(GPC)}$ =80900 g mol$^{-1}$ Đ = 1.31

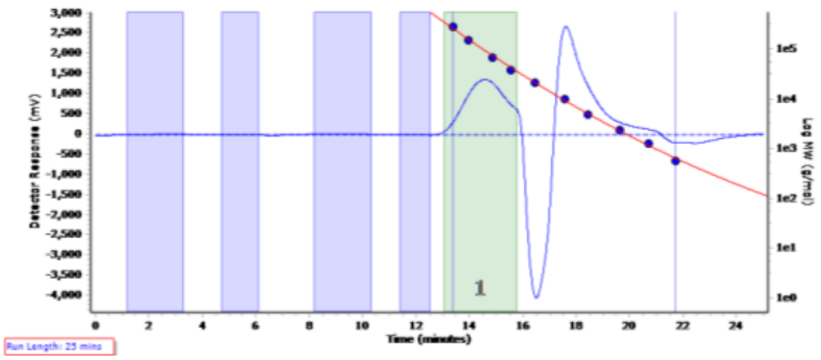


*Figure 6.21 The raw GPC of **PCH4**. The blue rectangles are where the baseline was corrected to and the green rectangle is the area which the $M_n$ and Đ was calculated.*

## 6.13. Representative thiol-ene click functionalisation

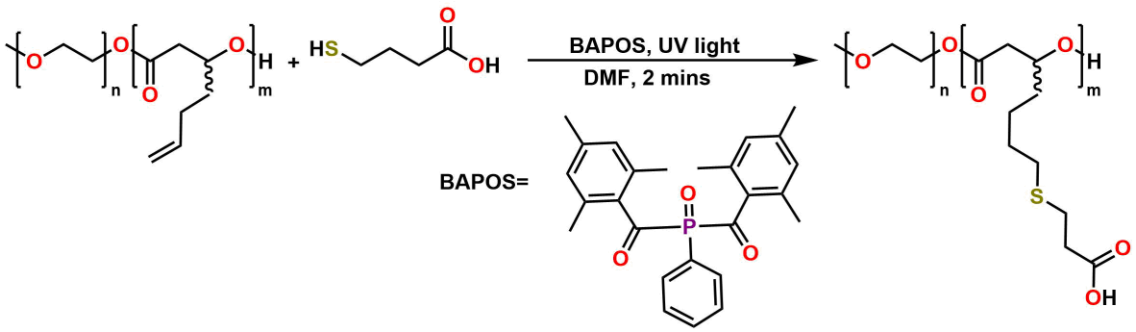


*Figure 6.22 A schematic showing the thiol-click reaction of PEG-b-PHEL.*

The polymer containing βHL (0.15 g, 0.0303 mmmol) was added to a mixture of MCPA (0.45 g, 4.24 mmol, 140 molar equivalents relative to the polymer), BAPOS (0.054 g, 0.212 mmol, 7 molar equivalents relative to the polymer) and DMF (1.50 mL, 19.4 mmol, 640 molar equivalent relative to the polymer). The mixture was split into 3 equal aliquots and irradiated with UV light for 2 minutes. The product was dialysed against water for 24 hours. The $M_{n(NMR)}$ was calculated by using the methoxy of the PEG group at 3.37 ppm (which was integrated to 3H) against the methylene peak of the PCl block at 4.04 ppm and the methine peak of the PHEL(S) block at 5.15 ppm.

**PS1 uses PH2**

$^1$H NMR (500 MHz, $CDCl_3$) δ 5.15 (s, 9H, $CH_3O[(CH_2)_2O]_{141}[COCH_2C\mathbf{H}((CH_2)_2(CH_2)_2S(CH_2)_2COOH)O]_9H$), 3.59 (m, 564H, $CH_3O[(C\mathbf{H_2})_2O]_{141}[COCH_2CH((CH_2)_2(CH_2)_2S(CH_2)_2COOH)O]_9H$), 3.33 (s, 3H, $C\mathbf{H}_3O[(CH_2)_2O]_{141}[COCH_2CH((CH_2)_2(CH_2)_2S(CH_2)_2COOH)O]_9H$), 2.63 (m, 323H, $[COC\mathbf{H_2}CH((CH_2)_2(CH_2)_2S(CH_2)_2COOH)O]_9H$)), 2.24 (m, 40H, $[COCH_2CH((CH_2)_2(CH_2)_2S(CH_2)_2COOH)O]_9H$)), 1.79 – 1.48 (m, 93H, $[COCH_2CH((CH_2)_2(CH_2)_2S(CH_2)_2COOH)O]_9H$)), 1.35 (m, 19H, $[COCH_2CH((CH_2)_2(CH_2)_2S(CH_2)_2COOH)O]_9H$)).

$M_{n(NMR)}$ = 8300 g mol$^{-1}$ $M_{n(GPC)}$ = 16500 g mol$^{-1}$ Đ = 1.52

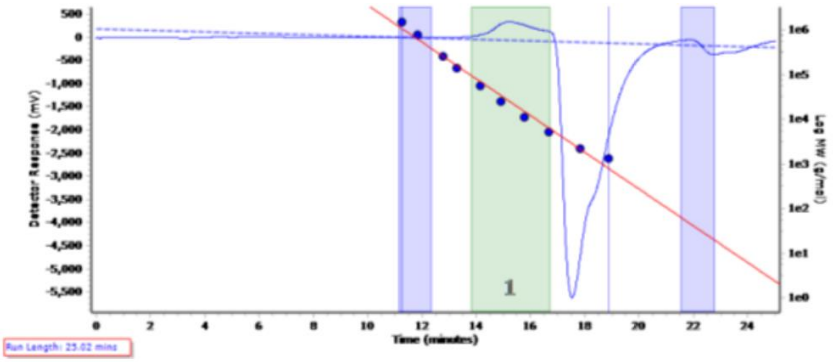


*Figure 6.23 The raw GPC of **PS2**. The blue rectangles are where the baseline was corrected to and the green rectangle is the area which the $M_n$ and Đ was calculated.*

**PCS1** uses **PCH1**

$^1$H NMR (500 MHz, $CDCl_3$) δ 5.19 (s, 28H, $CH_3O[(CH_2)_2O]_{144}[COCH_2CH_2CH_2CH_2CH_2O]_{102}[COCH_2C\mathbf{H}((CH_2)_2(CH_2)_2S(CH_2)_2COOH)O]_{28}H$), 4.06 (t, *J* = 6.7 Hz, 206H, $CH_3O[(CH_2)_2O]_{144}[COC\mathbf{H_2}CH_2CH_2CH_2CH_2O]_{102}[COCH_2CH((CH_2)_2(CH_2)_2S(CH_2)_2COOH)O]_{28}H$), 3.64

(m, 579H, $CH_3O[(C\mathbf{H_2})_2O]_{144}[COCH_2CH_2CH_2CH_2CH_2O]_{60}[COCH_2CH((CH_2)_2(CH_2)_2S(CH_2)_2COOH)O]_{28}H$), 3.38 (s, 3H, $C\mathbf{H_3}O[(CH_2)_2O]_{144}[COCH_2CH_2CH_2CH_2CH_2O]_{102}[COCH_2CH((CH_2)_2(CH_2)_2S(CH_2)_2COOH)O]_{18}H$), 2.79 (m, 65H, $CH_3O[(CH_2)_2O]_{144}[COCH_2CH_2CH_2CH_2CH_2O]_{102}[COC\mathbf{H_2}CH((CH_2)_2(CH_2)_2S(CH_2)_2COOH)O]_{28}H$), 2.60 (m, 177H, $CH_3O[(CH_2)_2O]_{144}COCH_2CH_2CH_2CH_2CH_2O]_{102}[COCH_2CH((CH_2)_2(CH_2)_2S(C\mathbf{H_2})_2COOH)O]_{28}H$), 2.31 (t, *J* = 7.4 Hz, 210H, $CH_3O[(CH_2)_2O]_{144}[COCH_2CH_2CH_2CH_2C\mathbf{H_2}O]_{102}[COCH_2CH((CH_2)_2(CH_2)_2S(CH_2)_2COOH)O]_{28}H$), 1.65 (m, 490H, $CH_3O[(CH_2)_2O]_{144}[COCH_2C\mathbf{H_2}CH_2C\mathbf{H_2}CH_2O]_{102}[COCH_2CH((CH_2)_2(C\mathbf{H_2})_2S(CH_2)_2COOH)O]_{28}H$), 1.38 (m, 241H, $CH_3O[(CH_2)_2O]_{144}[COCH_2CH_2C\mathbf{H_2}CH_2CH_2O]_{102}[COCH_2CH((C\mathbf{H_2})_2(CH_2)_2S(CH_2)_2COOH)O]_{28}H$).

$M_{n(NMR)}$ = 24500 g mol$^{-1}$ $M_{n(GPC)}$ = bimodal 150000, 20900 g mol$^{-1}$ Đ = 1.25, 1.38

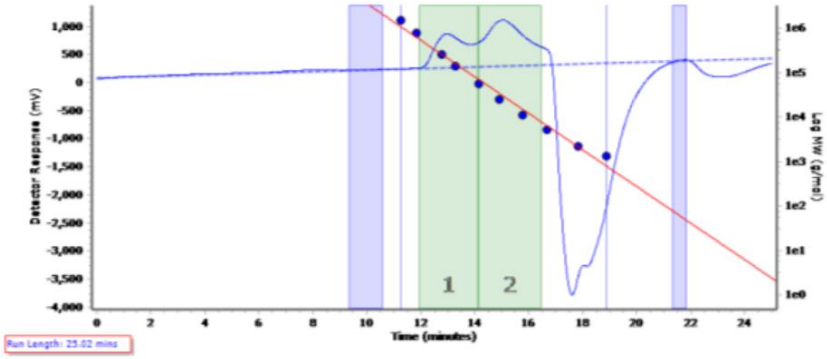


*Figure 6.24 The raw GPC of **PCS1**. The blue rectangles are where the baseline was corrected to and the green rectangle is the area which the $M_n$ and Đ was calculated.*

**PCS2** uses **PCH2**

$^1$H NMR (500 MHz ,$CDCl_3$) δ 5.19 (s, 34H, $CH_3O[(CH_2)_2O]_{239}[COCH_2CH_2CH_2CH_2CH_2O]_{104}[COCH_2C\mathbf{H}((CH_2)_2(CH_2)_2S(CH_2)_2COOH)O]_{49}H$), 4.06 (t, *J* = 6.7 Hz, 168H, $CH_3O[(CH_2)_2O]_{239}[COC\mathbf{H_2}CH_2CH_2CH_2CH_2O]_{104}[COCH_2CH((CH_2)_2(CH_2)_2S(CH_2)_2COOH)O]_{49}H$), 3.64 (s, 726H, $CH_3O[(C\mathbf{H_2})_2O]_{239}[COCH_2CH_2CH_2CH_2CH_2O]_{104}[COCH_2CH((CH_2)_2(CH_2)_2S(CH_2)_2COOH)O]_{49}H$), 3.38 (s, 3H, $C\mathbf{H_3}O[(CH_2)_2O]_{239}[COCH_2CH_2CH_2CH_2CH_2O]_{104}COCH_2CH((CH_2)_2(CH_2)_2S(CH_2)_2COOH)O]_{49}H$), 2.77 (s, 93H, $CH_3O[(CH_2)_2O]_{239}[COCH_2CH_2CH_2CH_2CH_2O]_{104}[COC\mathbf{H_2}CH((CH_2)_2(CH_2)_2S(CH_2)_2COOH)O]_{49}H$), 2.73 – 2.44 (m, 211H, $CH_3O[(CH_2)_2O]_{239}[COCH_2CH_2CH_2CH_2CH_2O]_{104}[COCH_2CH((CH_2)_2(CH_2)_2S(C\mathbf{H_2})_2COOH)O]_{49}H$), 2.30 (t, *J* = 7.5 Hz, 164H, $CH_3O[(CH_2)_2O]_{239}[COCH_2CH_2CH_2CH_2C\mathbf{H_2}O]_{104}[COCH_2CH((CH_2)_2(CH_2)_2S(CH_2)_2COOH)O]_{49}H$), 1.65 (s, 436H, $CH_3O[(CH_2)_2O]_{239}[COCH_2C\mathbf{H_2}CH_2C\mathbf{H_2}CH_2O]_{104}[COCH_2CH((CH_2)_2(C\mathbf{H_2})_2S(CH_2)_2COOH)O]_{49}H$), 1.38 (s, 222H, $CH_3O[(CH_2)_2O]_{239}[COCH_2CH_2C\mathbf{H_2}CH_2CH_2O]_{104}[COCH_2CH((C\mathbf{H_2})_2(CH_2)_2S(CH_2)_2COOH)O]_{49}H$).

$M_{n(NMR)}$ = 33700 g mol$^{-1}$ $M_{n(GPC)}$ = 1057600 g mol$^{-1}$, Đ = 1.19

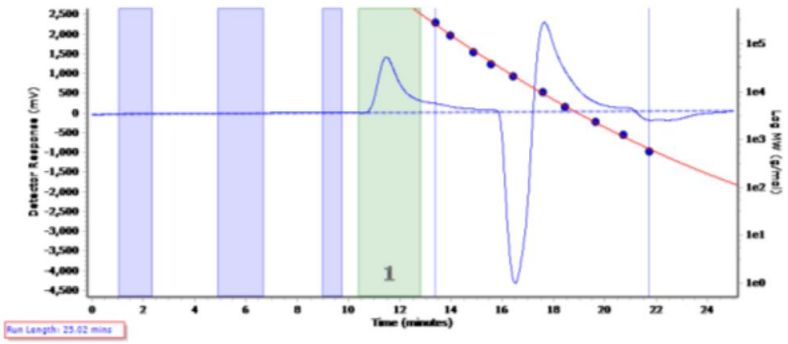


*Figure 6.25 The raw GPC of **PCS2**. The blue rectangles are where the baseline was corrected to and the green rectangle is the area which the $M_n$ and Đ was calculated.*

**$PCS_{iso}$** uses **PCH2**

$^1$H NMR (500 MHz, $CDCl_3$) δ 5.19 (s, 50H, $CH_3O[(CH_2)_2O]_{246}[COCH_2CH_2CH_2CH_2CH_2O]_{100}[COCH_2C\mathbf{H}((CH_2)_2(CH_2)_2SCH(CH_3)COOH)O]_{50}H$), 4.06 (t, *J* = 6.7 Hz, 201H, $CH_3O[(CH_2)_2O]_{246}[COC\mathbf{H_2}CH_2CH_2CH_2CH_2O]_{100}[COCH_2CH((CH_2)_2(CH_2)_2SCH(CH_3)COOH)O]_{50}H$), 3.64 (s, 984H, $CH_3O[(C\mathbf{H_2})_2O]_{246}[COCH_2CH_2CH_2CH_2CH_2O]_{100}[COCH_2CH((CH_2)_2(CH_2)_2SCH(CH_3)COOH)O]_{50}H$), 3.41 (s, 47H, $CH_3O[(CH_2)_2O]_{246}[COCH_2CH_2CH_2CH_2CH_2O]_{100}[COCH_2CH((CH_2)_2(CH_2)_2SC\mathbf{H}(CH_3)COOH)O]_{50}H$), 3.38 (s, 3H, $C\mathbf{H_3}O[(CH_2)_2O]_{246}[COCH_2CH_2CH_2CH_2CH_2O]_{100}[COCH_2CH((CH_2)_2(CH_2)_2SCH(CH_3)COOH)O]_{50}H$), 2.76 – 2.48 (m, 207H, $CH_3O[(CH_2)_2O]_{246}[COCH_2CH_2CH_2CH_2CH_2O]_{100}[COC\mathbf{H_2}CH((CH_2)_2(CH_2)_2SCH(C\mathbf{H_3})COOH)O]_{50}H$), 2.31 (t, *J* = 7.5 Hz, 207H, $CH_3O[(CH_2)_2O]_{246}[COCH_2CH_2CH_2CH_2C\mathbf{H_2}O]_{100}[COCH_2CH((CH_2)_2(CH_2)_2SCH(CH_3)COOH)O]_{50}H$), 1.64 (s, 586H, $CH_3O[(CH_2)_2O]_{246}[COCH_2C\mathbf{H_2}CH_2C\mathbf{H_2}CH_2O]_{100}[COCH_2CH((CH_2)_2(C\mathbf{H_2})_2SCH(CH_3)COOH)O]_{50}H$), 1.41 (s, 415H, $CH_3O[(CH_2)_2O]_{246}[COCH_2CH_2C\mathbf{H_2}CH_2CH_2O]_{100}[COCH_2CH((C\mathbf{H_2})_2(CH_2)_2SCH(CH_3)COOH)O]_{50}H$).

$M_{n(NMR)}$ = 33800 g mol$^{-1}$ $M_{n(GPC)}$ = 891400 g mol$^{-1}$ Đ = 1.22

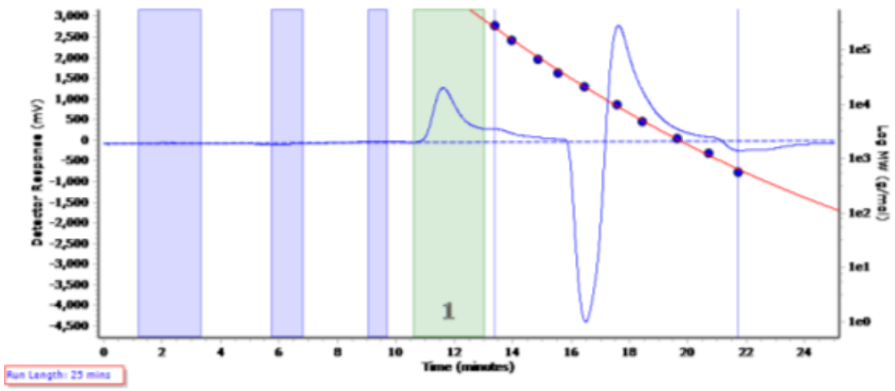


*Figure 6.26 The raw GPC of **$PCS_{ISO}$**. The blue rectangles are where the baseline was corrected to and the green rectangle is the area which the $M_n$ and Đ was calculated.*

**PCS3** uses **PCH3**

$^1$H NMR (500 MHz, $CDCl_3$) δ 5.18 (s, 42H, $CH_3O[(CH_2)_2O]_{131}[COCH_2CH_2CH_2CH_2CH_2O]_{48}[COCH_2C\mathbf{H}((CH_2)_2(CH_2)_2S(CH_2)_2COOH)O]_{42}H$), 4.05 (t, *J*

= 6.7 Hz, 92H, $CH_3O[(CH_2)_2O]_{131}[COC\mathbf{H_2}CH_2CH_2CH_2CH_2O]_{48}[COCH_2CH((CH_2)_2(CH_2)_2S(CH_2)_2COOH)O]_{42}H$), 3.63 (m, 524H, $CH_3O[(C\mathbf{H_2})_2O]_{131}[COCH_2CH_2CH_2CH_2CH_2O]_{48}[COCH_2CH((CH_2)_2(CH_2)_2S(CH_2)_2COOH)O]_{42}H$), 3.37 (s, 3H, $C\mathbf{H_3}O[(CH_2)_2O]_{131}[COCH_2CH_2CH_2CH_2CH_2O]_{48}[COCH_2CH((CH_2)_2(CH_2)_2S(CH_2)_2COOH)O]_{42}H$), 2.76 (s, 113H, $CH_3O[(CH_2)_2O]_{131}[COCH_2CH_2CH_2CH_2CH_2O]_{48}[COC\mathbf{H_2}CH((CH_2)_2(CH_2)_2S(CH_2)_2COOH)O]_{42}H$), 2.70 – 2.45 (m, 247H, $CH_3O[(CH_2)_2O]_{131}[COCH_2CH_2CH_2CH_2CH_2O]_{48}[COCH_2CH((CH_2)_2(CH_2)_2S(C\mathbf{H_2})_2COOH)O]_{42}H$), 2.30 (t, *J* = 6.9 Hz, 98H, $CH_3O[(CH_2)_2O]_{131}[COCH_2CH_2CH_2CH_2C\mathbf{H_2}O]_{48}[COCH_2CH((CH_2)_2(CH_2)_2S(CH_2)_2COOH)O]_{42}H$), 1.80 – 1.50 (m, 331H, $CH_3O[(CH_2)_2O]_{131}[COCH_2C\mathbf{H_2}CH_2C\mathbf{H_2}CH_2O]_{48}[COC\mathbf{H_2}CH((C\mathbf{H_2})_2(C\mathbf{H_2})_2S(CH_2)_2COOH)O]_{42}H$), 1.50 – 1.32 (m, 162H, $CH_3O[(CH_2)_2O]_{131}[COCH_2C\mathbf{H_2}CH_2CH_2C\mathbf{H_2}O]_{48}[COCH_2CH((C\mathbf{H_2})_2(C\mathbf{H_2})_2S(CH_2)_2COOH)O]_{42}H$), 1.32 – 1.21 (m, 41H, $CH_3O[(CH_2)_2O]_{131}[COCH_2CH_2C\mathbf{H_2}CH_2CH_2O]_{48}[COCH_2CH((CH_2)_2(CH_2)_2S(CH_2)_2COOH)O]_{42}H$).

$M_{n(NMR)}$ = 21000 g mol$^{-1}$ $M_{n(GPC)}$ = 127300 g mol$^{-1}$ Đ = 1.42

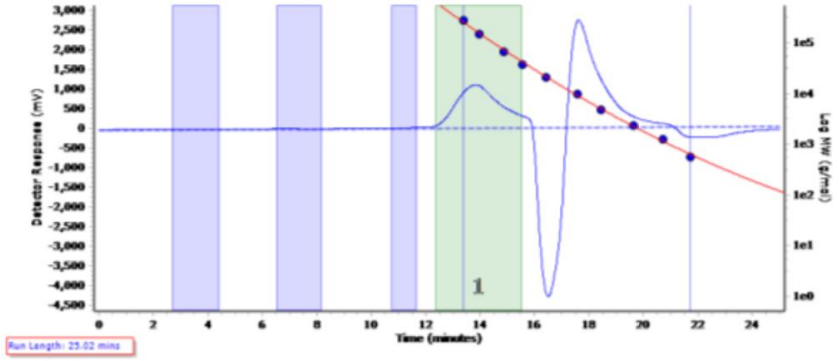


*Figure 6.27 The raw GPC of **PCS3**. The blue rectangles are where the baseline was corrected to and the green rectangle is the area which the $M_n$ and Đ was calculated.*

## 6.14. Representative hydrophosphorylation of PHEL block

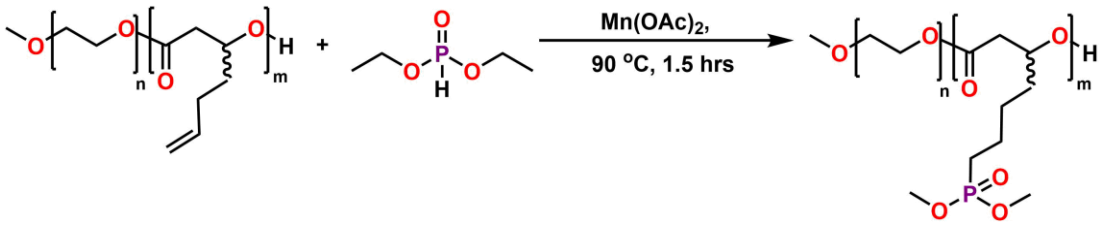


*Figure 6.28 Schematic for the hydrophosphorylation of PEG-b-PHEL.*

The polymer (0.0800 g, 0.6300 mmol), dimethyl phosphate (1.30 cm$^{-3}$, 14.2 mmol, 1200 molar equivalents relative to the polymer), and Manganese acetate (2.41 x 10$^{-3}$ g, 9.84 x 10$^{-3}$ mmol, 0.83 molar equivalents relative to the polymer) were added into a flask and stirred at 90 °C for 1.5 hours. The mixture was then dialysed for 24 hours and lyophilized. The $M_{n(NMR)}$ was calculated by using the methoxy of the PEG group at 3.37 ppm (which was integrated to 3H) against the methine peak of the PHEL(P) block at 5.17 ppm.

**PCM1** uses **PCH2**

$^{1}$H NMR (500 MHz, $CDCl_3$) δ 5.17 (s, 46H, $CH_3O[(CH_2)_2O]_{251}[COCH_2CH_2CH_2CH_2CH_2O]_{84}[COCH_2C\mathbf{H}((CH_2)_2(CH_2)_2PO(OCH_3)_2)O]_{50}H$), 4.06 (t, *J* = 6.7 Hz, 168H, $CH_3O[(CH_2)_2O]_{251}[COC\mathbf{H_2}CH_2CH_2CH_2CH_2O]_{84}[COCH_2CH((CH_2)_2(CH_2)_2PO(OCH_3)_2)O]_{50}H$), 3.73 (d, *J* = 10.7 Hz, 250H, $CH_3O[(CH_2)_2O]_{251}[COCH_2CH_2CH_2CH_2CH_2O]_{84}[COCH_2CH((CH_2)_2(CH_2)_2PO(OC\mathbf{H_3})_2)O]_{50}H$), 3.64 (s, 1007H, $CH_3O[(C\mathbf{H_2})_2O]_{251}[COCH_2CH_2CH_2CH_2CH_2O]_{84}[COCH_2CH((CH_2)_2(CH_2)_2PO(OCH_3)_2)O]_{50}H$), 3.38 (s, 3H, $C\mathbf{H_3}O[(CH_2)_2O]_{251}[COCH_2CH_2CH_2CH_2CH_2O]_{84}[COCH_2CH((CH_2)_2(CH_2)_2PO(OCH_3)_2)O]_{50}H$), 2.55 (s, 100H, $CH_3O[(CH_2)_2O]_{251}[COCH_2CH_2CH_2CH_2CH_2O]_{48}[COC\mathbf{H_2}CH((CH_2)_2(CH_2)_2PO(OCH_3)_2)O]_{50}H$), 2.30 (t, *J* = 7.5 Hz, 99H, $CH_3O[(CH_2)_2O]_{251}[COCH_2CH_2CH_2CH_2C\mathbf{H_2}O]_{84}[COCH_2CH((CH_2)_2(CH_2)_2PO(OCH_3)_2)O]_{50}H$), 1.74 - 1.64 (m, 628H, $CH_3O[(CH_2)_2O]_{251}[COC\mathbf{H_2}CH_2CH_2C\mathbf{H_2}CH_2O]_{84}[COCH_2CH((C\mathbf{H_2})_2(CH_2)_2PO(OCH_3)_2)O]_{50}H$), 1.38 (m, 258H $CH_3O[(CH_2)_2O]_{251}[COCH_2CH_2C\mathbf{H_2}CH_2CH_2O]_{84}[COCH_2CH((CH_2)_2(C\mathbf{H_2})_2PO(OCH_3)_2)O]_{50}H$).

$^{31}$P NMR (202 MHz, $CDCl_3$) δ 34.48 ($CH_3O[(CH_2)_2O]_{251}[COCH_2CH_2CH_2CH_2CH_2O]_{84}[COCH_2CH((CH_2)_2(CH_2)_2\mathbf{P}O(OCH_3)_2)O]_{50}H$)

$M_{n(NMR)}$ = 32400 g mol$^{-1}$ $M_{n(GPC)}$ = 54700 g mol$^{-1}$ Đ = 1.40

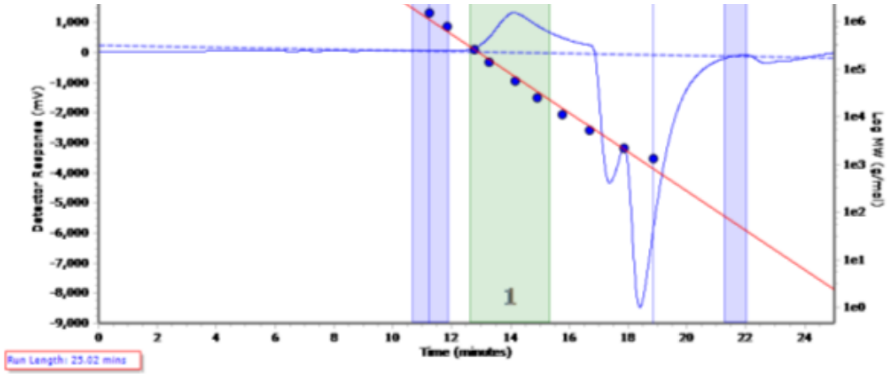


*Figure 6.29 The raw GPC of **PCM1**. The blue rectangles are where the baseline was corrected to and the green rectangle is the area which the $M_n$ and Đ was calculated.*

**PM1** uses **PH6**

$^{1}$H NMR (500 MHz, $CDCl_3$) δ 5.17 (s, 14H, $CH_3O[(CH_2)_2O]_{147}[COCH_2C\mathbf{H}((CH_2)_2(CH_2)_2PO(OCH_3)_2)O]_{14}H$), 3.73 (d, *J* = 10.5 Hz, 82H, $CH_3O[(CH_2)_2O]_{147}[COCH_2CH((CH_2)_2(CH_2)_2PO(OC\mathbf{H_3})_2)O]_{14}H$), 3.70 – 3.46 (m, 564H, $CH_3O[(C\mathbf{H_2})_2O]_{147}[COCH_2CH((CH_2)_2(CH_2)_2PO(OCH_3)_2)O]_{14}H$), 3.38 (s, 3H, $C\mathbf{H_3}O[(CH_2)_2O]_{147}[COCH_2CH((CH_2)_2(CH_2)_2PO(OCH_3)_2)O]_{14}H$), 2.56 (s, 28H, $CH_3O[(CH_2)_2O]_{147}[COC\mathbf{H_2}CH((CH_2)_2(CH_2)_2PO(OCH_3)_2)O]_{14}H$), 1.86 – 1.48 (m, 118H, $CH_3O[(CH_2)_2O]_{147}[COCH_2CH((C\mathbf{H_2})_2(C\mathbf{H_2})_2PO(OCH_3)_2)O]_{14}H$), 1.48 – 1.21 (m, 28H $CH_3O[(CH_2)_2O]_{147}[COCH_2CH((C\mathbf{H_2})_2(C\mathbf{H_2})_2PO(OCH_3)_2)O]_{14}H$).

$^{31}$P NMR (202 MHz, $CDCl_3$) δ 34.40 ($CH_3O[(CH_2)_2O]_{147}$ $[COCH_2CH((CH_2)_2(CH_2)_2\mathbf{P}O(OCH_3)_2)O]_{14}H$).

$M_{n(NMR)}$ = 9800 g mol$^{-1}$ $M_{n(GPC)}$ = 23100 g mol$^{-1}$ Đ = 1.46

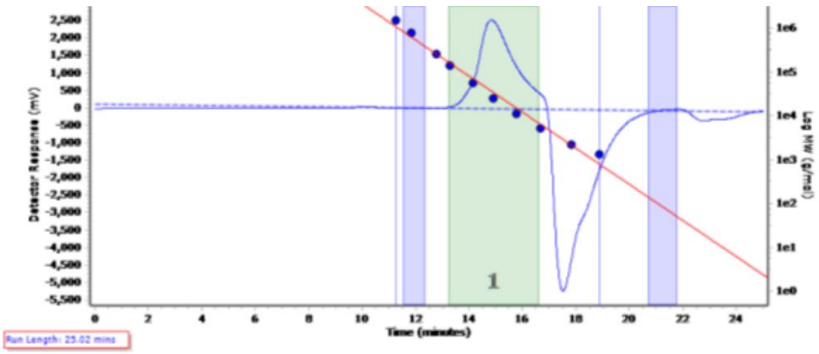

*Figure 6.30 The raw GPC of **PM1**. The blue rectangles are where the baseline was corrected to and the green rectangle is the area which the $M_n$ and Đ was calculated.*

**PM2** uses **PH7**

$^1$H NMR (500 MHz, $CDCl_3$) δ 5.16 (s, 22H, $CH_3O[(CH_2)_2O]_{148}$ $[COCH_2C\mathbf{H}((CH_2)_2(CH_2)_2PO(OCH_3)_2)O]_{22}H$), 3.74 (s, 105H, $CH_3O[(CH_2)_2O]_{148}$ $[COCH_2CH((CH_2)_2(CH_2)_2PO(OC\mathbf{H_3})_2)O]_{22}H$), 3.64 (s, 594H, $CH_3O[(C\mathbf{H_2})_2O]_{148}$ $[COCH_2CH((CH_2)_2(CH_2)_2PO(OCH_3)_2)O]_{22}H$), 3.37 (s, 3H, $C\mathbf{H_3}O[(CH_2)_2O]_{148}$ $[COCH_2CH((CH_2)_2(CH_2)_2PO(OCH_3)_2)O]_{22}H$), 2.75 – 2.02 (m, 89H, $CH_3O[(CH_2)_2O]_{148}$ $[COC\mathbf{H_2}CH((CH_2)_2(CH_2)_2PO(OCH_3)_2)O]_{22}H$), 1.96 – 1.10 (m, 208H, $CH_3O[(CH_2)_2O]_{148}$ $[COCH_2CH((C\mathbf{H_2})_2(C\mathbf{H_2})_2PO(OCH_3)_2)O]_{22}H$).

$^{31}$P NMR (202 MHz, $CDCl_3$) δ 34.48 ($CH_3O[(CH_2)_2O]_{148}$ $[COCH_2CH((CH_2)_2(CH_2)_2\mathbf{P}O(OCH_3)_2)O]_{22}H$).

$M_{n(NMR)}$ = 12000 g mol$^{-1}$ $M_{n(GPC)}$ = 26400 g mol$^{-1}$ Đ = 1.68

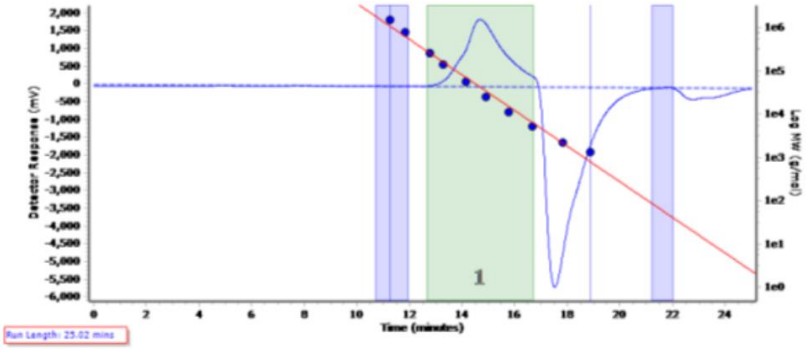

*Figure 6. 31 The raw GPC of **PM2**. The blue rectangles are where the baseline was corrected to and the green rectangle is the area which the $M_n$ and Đ was calculated.*

## 6.15. RAFT polymerisations

### 6.15.1. Representative RAFT polymerisation of MAPC1

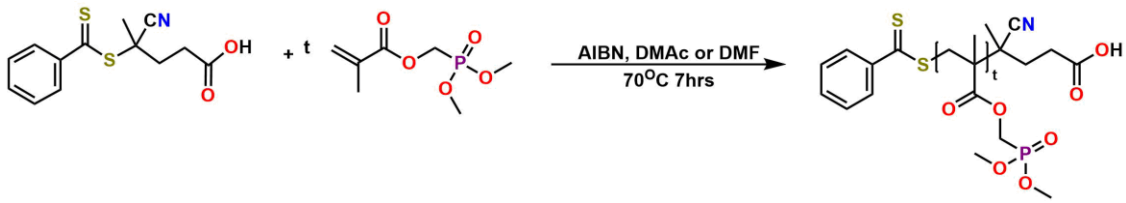


*Figure 6.32 A schematic of the RAFT polymerisation of MAPC1.*

MAPC1 was first passed through a basic alumina column to remove the inhibitor. MAPC1 (0.500 g, 2.40 mmol), CPAD (0.0140 g, 0.0501 mmol), AIBN (2.88 x 10$^{-3}$ g, 0.0175 mmol) and DMF (1.75 cm$^{-3}$, 22.6 mmol) were added into an ampoule and sealed. The mixture was degassed via three freeze-pump-thaw-degas cycle then left to stir at 70 °C for 7 hours. The polymerisation was

stopped when cooled the mixture was cooled down and opened to air. The crude mixture was then dialyzed against water for 24 hrs and lyophilized. The $M_{n(NMR)}$ was calculated by integrating the phenyl hydrogens of CPAD (equal to 5H) between 7.87 – 7.83 ppm against the methylene peak of PMAPC1 at 3.84 ppm.

**D1** uses DMF

$^1$H NMR (500 MHz, $CDCl_3$) δ 7.87 (m, 2H, $C_6\mathbf{H_5}CS_2[CCH_3(COOCH_2PO(OCH_3)_2)CH_2]_{63}C(CH_3CN)(CH_2)_2COOH)$), 7.54 (m, 1H, $C_6\mathbf{H_5}CS_2[CCH_3(COOCH_2PO(OCH_3)_2)CH_2]_{63}C(CH_3CN)(CH_2)_2COOH)$), 7.38 (m, 2H, $C_6\mathbf{H_5}CS_2[CCH_3(COOCH_2PO(OCH_3)_2)CH_2]_{63}C(CH_3CN)(CH_2)_2COOH)$), 4.25 (m, 126H, $C_6H_5CS_2[CCH_3(COOC\mathbf{H_2}PO(OCH_3)_2)CH_2]_{63}C(CH_3CN)(CH_2)_2COOH)$), 3.84 (d, *J* = 10.6 Hz, 395H, $C_6H_5CS_2[CCH_3(COOCH_2PO(OC\mathbf{H_3})_2)CH_2]_{63}C(CH_3CN)(CH_2)_2COOH)$), 1.91 (m, 118H, $C_6H_5CS_2[CCH_3(COOCH_2PO(OCH_3)_2)C\mathbf{H_2}]_{63}C(CH_3CN)(CH_2)_2COOH)$), 1.62 (m, 395H, $C_6H_5CS_2[CCH_3(COOCH_2PO(OCH_3)_2)CH_2]_{63}C(C\mathbf{H_3}CN)(CH_2)_2COOH)$), 1.27 (m, 51H, $C_6H_5CS_2[CCH_3(COOCH_2PO(OCH_3)_2)CH_2]_{63}C(CH_3CN)(C\mathbf{H_2})_2COOH)$), 1.09 (m, 89H $C_6H_5CS_2[CCH_3(COOCH_2PO(OCH_3)_2)CH_2]_{63}C(CH_3CN)(C\mathbf{H_2})_2COOH)$), 0.86 (m, 156H, $C_6H_5CS_2[CC\mathbf{H_3}(COOCH_2PO(OCH_3)_2)CH_2]_{63}C(CH_3CN)(CH_2)_2COOH)$).

$^{31}$P NMR (202 MHz, $CDCl_3$) δ 21.44 (d, $C_6H_5CS_2[CCH_3(COOCH_2\mathbf{P}O(OCH_3)_2)CH_2]_{53}C(CH_3CN)(CH_2)_2COOH)$).

Conversion = 89 % $M_{n(NMR)}$ = 13400 g mol$^{-1}$ $M_{n(GPC)}$ = N/A g mol$^{-1}$ Đ = 1.69

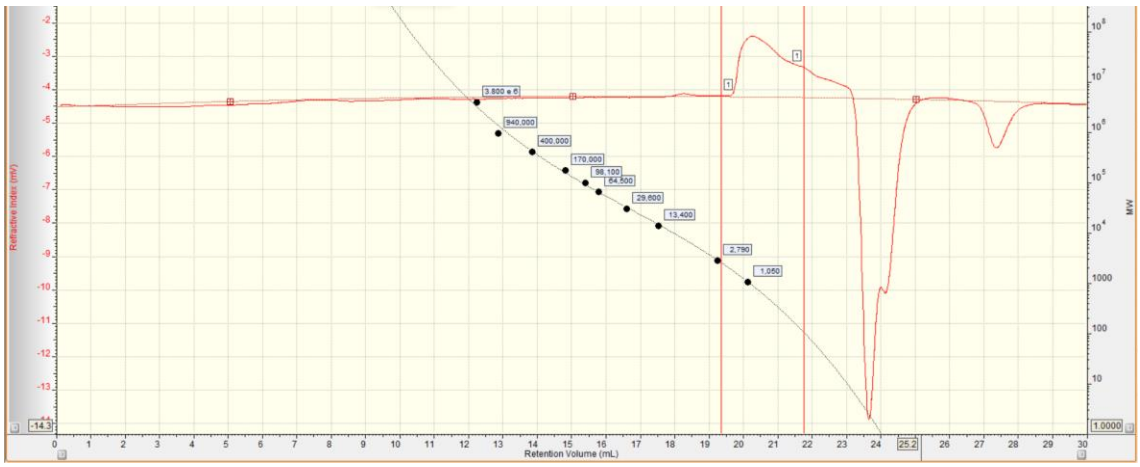


*Figure 6.33 The raw GPC of **D1**. The area between the two re vertical lines is where the $M_n$ and Đ was calculated. The black circles are the polystyrene standards.*

**D2** uses DMAc

$^1$H NMR (500 MHz, $CDCL_3$) δ 4.25 (s, 18H, $C_6H_5CS_2[CCH_3(COOC\mathbf{H_2}PO(OCH_3)_2)CH_2]_9C(CH_3CN)(CH_2)_2COOH)$), 3.84 (d, *J* = 10.8 Hz, 57H, $C_6H_5CS_2[CCH_3(COOCH_2PO(OC\mathbf{H_3})_2)CH_2]_9C(CH_3CN)(CH_2)_2COOH)$), 2.07 – 1.78 (m, 16H, $C_6H_5CS_2[CCH_3(COOCH_2PO(OCH_3)_2)C\mathbf{H_2}]_9C(CH_3CN)(CH_2)_2COOH)$), 1.78 – 1.37 (m, 18H), 1.34 – 0.79 (m, 29H, $C_6H_5CS_2[CC\mathbf{H_3}(COOCH_2PO(OCH_3)_2)CH_2]_9C(CH_3CN)(CH_2)_2COOH)$).

Conversion = 80 % $M_{n(NMR)}$ = 1900 g mol$^{-1}$ $M_{n(GPC)}$ = 276000 g mol$^{-1}$ Đ =2.01

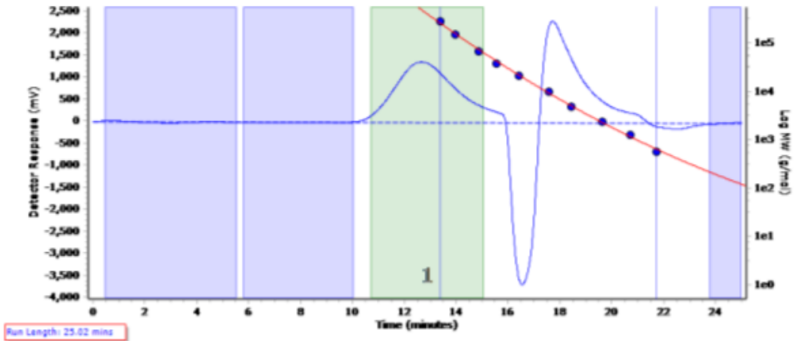


*Figure 6.34 The raw GPC of **D2**. The blue rectangles are where the baseline was corrected to and the green rectangle is the area which the $M_n$ and Đ was calculated.*

**D3** uses DMAc

$^1$H NMR (500 MHz, $CDCl_3$) δ 7.87 (m, 2H, $C_6\mathbf{H_5}CS_2[CCH_3(COOCH_2PO(OCH_3)_2)CH_2]_{40}C(CH_3CN)(CH_2)_2COOH)$), 7.53 (m, 1H, $C_6\mathbf{H_5}CS_2[CCH_3(COOCH_2PO(OCH_3)_2)CH_2]_{40}C(CH_3CN)(CH_2)_2COOH)$), 7.38 (m, 2H, $C_6\mathbf{H_5}CS_2[CCH_3(COOCH_2PO(OCH_3)_2)CH_2]_{40}C(CH_3CN)(CH_2)_2COOH)$), 4.24 (m, 80H, $C_6H_5CS_2[CCH_3(COOC\mathbf{H_2}PO(OCH_3)_2)CH_2]_{40}C(CH_3CN)(CH_2)_2COOH)$), 3.83 (d, *J* = 9.5 Hz, 250H, $C_6H_5CS_2[CCH_3(COOCH_2PO(OC\mathbf{H_3})_2)CH_2]_{40}C(CH_3CN)(CH_2)_2COOH)$), 2.60 (m, 4H, $C_6H_5CS_2[CCH_3(COOCH_2PO(OCH_3)_2)CH_2]_{40}C(CH_3CN)(C\mathbf{H_2})_2COOH)$), 1.93 – 1.40 (m, 83H, $C_6H_5CS_2[CCH_3(COOCH_2PO(OCH_3)_2)C\mathbf{H_2}]_{40}C(CH_3CN)(CH_2)_2COOH)$), 1.28 – 1.01 (m, 130H, $C_6H_5CS_2[CC\mathbf{H_3}(COOCH_2PO(OCH_3)_2)CH_2]_{40}C(CH_3CN)(CH_2)_2COOH)$).

$^{31}$P NMR (202 MHz, $CDCl_3$) δ 21.37 (d, $C_6H_5CS_2[CCH_3(COOCH_2\mathbf{P}O(OCH_3)_2)CH_2]_{53}C(CH_3CN)(CH_2)_2COOH)$).

Conversion = 84 % $M_{n(NMR)}$ = 8300 g mol$^{-1}$ $M_{n(GPC)}$ = 111200 g mol$^{-1}$ Đ =1.29

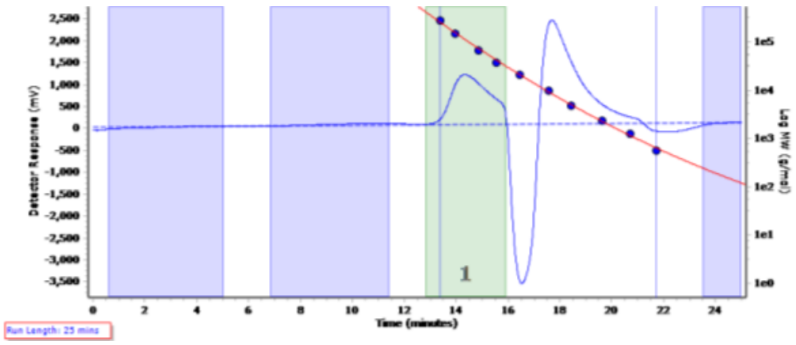


*Figure 6.35 The raw GPC of **D3**. The blue rectangles are where the baseline was corrected to and the green rectangle is the area which the $M_n$ and Đ was calculated.*

**D4** uses DMSO

$^1$H NMR (500 MHz, $CDCl_3$) δ 7.98 – 7.36 (m, 5H, $C_6\mathbf{H_5}CS_2[CCH_3(COOCH_2PO(OCH_3)_2)CH_2]_{35}C(CH_3CN)(CH_2)_2COOH)$), 4.27 (s, 70H, $C_6H_5CS_2[CCH_3(COOC\mathbf{H_2}PO(OCH_3)_2)CH_2]_{35}C(CH_3CN)(CH_2)_2COOH)$), 3.86 (d, *J* = 7.2 Hz, 228H, $C_6H_5CS_2[CCH_3(COOCH_2PO(OC\mathbf{H_3})_2)CH_2]_{35}C(CH_3CN)(CH_2)_2COOH)$), 260 – 2.40 (m, 5H, $C_6H_5CS_2[CCH_3(COOCH_2PO(OCH_3)_2)CH_2]_{35}C(CH_3CN)(CH_2)_2COOH)$), 2.10 – 1.52 (m, 103H, $C_6H_5CS_2[CCH_3(COOCH_2PO(OCH_3)_2)C\mathbf{H_2}]_{35}C(C\mathbf{H_3}CN)(CH_2)_2COOH)$), 1.45 – 1.23 (m, 26H, $C_6H_5CS_2[CC\mathbf{H_3}(COOCH_2PO(OCH_3)_2)CH_2]_{35}C(CH_3CN)(CH_2)_2COOH)$), 1.18 – 0.76 (m, 102H, $C_6H_5CS_2[CC\mathbf{H_3}(COOCH_2PO(OCH_3)_2)CH_2]_{35}C(CH_3CN)(CH_2)_2COOH)$).

$^{31}$P NMR (202 MHz, $CDCl_3$) δ 21.41 (d, $C_6H_5CS_2[CCH_3(COOCH_2\mathbf{P}O(OCH_3)_2)CH_2]_{35}C(CH_3CN)(CH_2)_2COOH)$).

Conversion = 94 % $M_{n(NMR)}$ = 7300 g $mol^{-1}$ $M_{n(GPC)}$ = 113200 g $mol^{-1}$ Đ =1.29

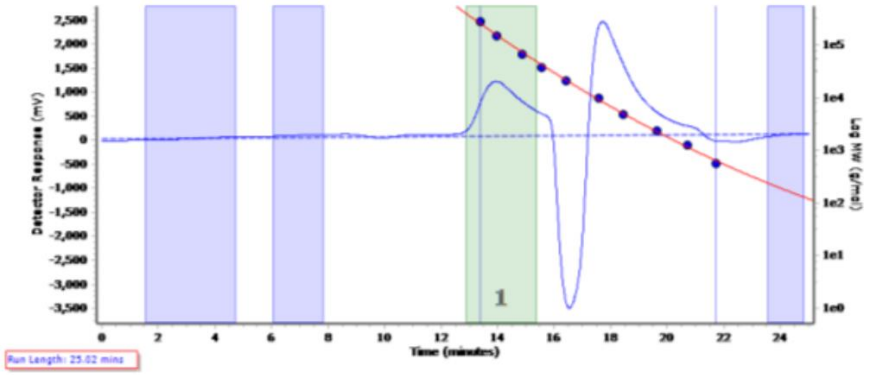

*Figure 6.36 The raw GPC of **D4**. The blue rectangles are where the baseline was corrected to and the green rectangle is the area which the $M_n$ and Đ was calculated.*

**D5 uses DMAc**

$^1$H NMR (500 MHz, $CDCl_3$) δ 8.02 – 7.34 (m, 5H, $C_6\mathbf{H_5}CS_2[CCH_3(COOCH_2PO(OCH_3)_2)CH_2]_{53}C(CH_3CN)(CH_2)_2COOH$), 4.34 – 4.18 (m, 106H $C_6H_5CS_2[CCH_3(COOC\mathbf{H_2}PO(OCH_3)_2)CH_2]_{53}C(CH_3CN)(CH_2)_2COOH$), 3.83 (d, 337H, $C_6H_5CS_2[CCH_3(COOCH_2PO(OC\mathbf{H_3})_2)CH_2]_{53}(CH_3CN)(CH_2)_2COOH$), 2.12 – 1.74 (m, 110H $C_6H_5CS_2[CCH_3(COOCH_2PO(OCH_3)_2)C\mathbf{H_2}]_{53}C(CH_3CN)(CH_2)_2COOH$), 1.74 – 1.42 (m, 88H, $C_6H_5CS_2[CCH_3(COOC\mathbf{H_2}PO(OCH_3)_2)CH_2]_{53}C(CH_3CN)(CH_2)_2COOH$)) 1.18 – 0.82 (m, 165H, $C_6H_5CS_2[CC\mathbf{H_3}(COOCH_2PO(OCH_3)_2)CH_2]_{53}C(CH_3CN)(CH_2)_2COOH$.

$^{31}$P NMR (202 MHz, $CDCl_3$) δ 21.37 ($C_6H_5CS_2[CCH_3(COOCH_2\mathbf{P}O(OCH_3)_2)CH_2]_{44}C(CH_3CN)(CH_2)_2COOH$

Conversion = 88 % $M_{n(NMR)}$ = 11300 g $mol^{-1}$ $M_{n(GPC)}$ = 111200 g $mol^{-1}$ Đ =1.37

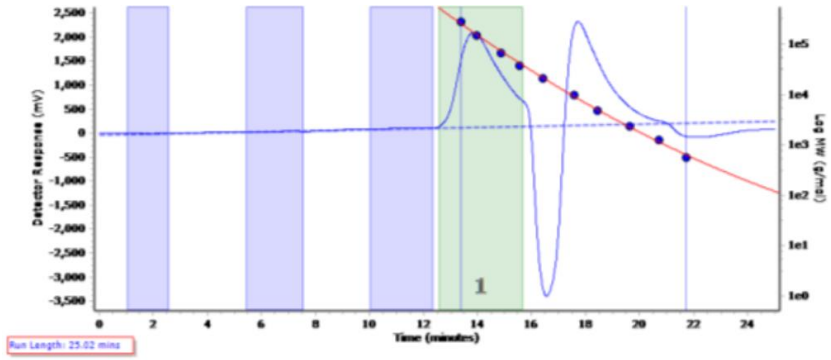

*Figure 6.37 The raw GPC of **D5**. The blue rectangles are where the baseline was corrected to and the green rectangle is the area which the $M_n$ and Đ was calculated.*

## 6.15.2. Representative RAFT polymerisation of MMA

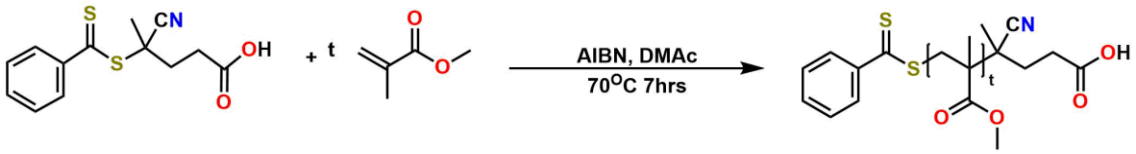


*Figure 6.38 A schematic showing the RAFT polymerisation of MMA.*

MMA was first passed through a basic alumina column to remove the inhibitor. MMA (1.00 g, 9.99 mmol), CPAD (0.0523 g, 0.187 mmol), AIBN (0.021 g, 0.0175 mmol) and dioxane (6.38 $cm^-$

$^{3}$, 74.9 mmol) were added into an ampoule and sealed. The mixture was degassed via three freeze-pump-thaw-degas cycle then left to stir at 70 °C for 7 hours. The polymerisation was stopped when cooled the mixture was cooled down and opened to air. The crude mixture was then dialyzed against water for 24 hrs and lyophilized. The crude mixture was then dialyzed against water for 24 hrs and lyophilized. The $M_{n(NMR)}$ was calculated by integrating the phenyl hydrogens of CPAD (equal to 5H) between 7.87 – 7.83 ppm against the methyl peak of PMMA at 3.60 ppm.

**N1**

$^{1}$H NMR (500 MHz, Chloroform-*d*) δ 7.94 – 7.31 (m, 5H, $C_6\mathbf{H_5}CS_2[CCCH_3(COOCH_3)CH_2]_{23}C(CH_3CN)(CH_2)_2COOH$), 3.59 (s, 74H, $C_6H_5CS_2[CCCH_3(COOC\mathbf{H_3})CH_2]_{23}C(CH_3CN)(CH_2)_2COOH$), 2.54 (s, 3H, $C_6H_5CS_2[CCCH_3(COOCH_3)CH_2]_{24}C(CH_3CN)(CH_2)_2COOH$), 2.11 – 1.69 (m, 50H, $C_6H_5CS_2[CCCH_3(COOCH_3)C\mathbf{H_2}]_{23}C(CH_3CN)(CH_2)_2COOH$), 1.49 – 1.16 (m, 17H, $C_6H_5CS_2[CCCH_3(COOCH_3)CH_2]_{23}C(C\mathbf{H_3}CN)(C\mathbf{H_2})_2COOH$), 1.12 – 0.75 (m, 65H, $C_6H_5CS_2[CCC\mathbf{H_3}(COOCH_3)CH_2]_{23}C(CH_3CN)(CH_2)_2COOH$).

Conversion = 54 % $M_{n(NMR)}$ = 2300 g mol$^{-1}$ $M_{n(GPC)}$ = 43260 g mol$^{-1}$ Đ =1.10

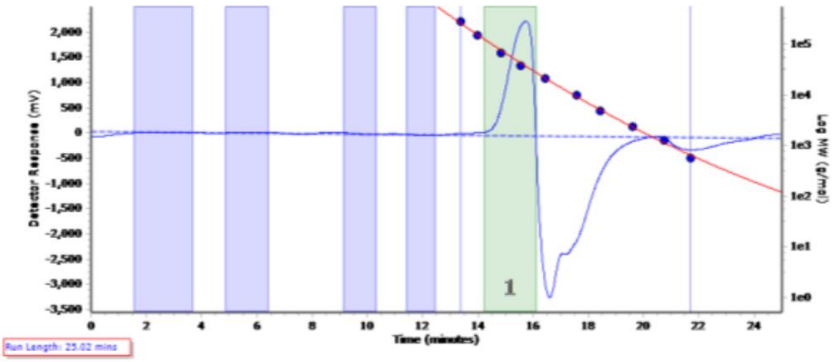


*Figure 6.39 The raw GPC of **N1**. The blue rectangles are where the baseline was corrected to and the green rectangle is the area which the $M_n$ and Đ was calculated.*

**N2**

$^{1}$H NMR (500 MHz, $CDCl_3$) δ 7.93 – 7.33 (m, 5H, $C_6\mathbf{H_5}CS_2[CCCH_3(COOCH_3)CH_2]_{24}C(CH_3CN)(CH_2)_2COOH$), 3.60 (s, 72H, $C_6H_5CS_2[CCCH_3(COOC\mathbf{H_3})CH_2]_{24}C(CH_3CN)(CH_2)_2COOH$), 2.62 – 2.21 (m, 10H, $C_6H_5CS_2[CCCH_3(COOCH_3)CH_2]_{24}C(CH_3CN)(CH_2)_2COOH$), 2.03 – 1.73 (m, 43H, $C_6H_5CS_2[CCCH_3(COOCH_3)C\mathbf{H_2}]_{24}C(CH_3CN)(CH_2)_2COOH$), 1.51 – 1.16 (m, 18H, $C_6H_5CS_2[CCCH_3(COOCH_3)CH_2]_{24}C(C\mathbf{H_3}CN)(C\mathbf{H_2})_2COOH$), 1.14 – 0.73 (m, 64H, $C_6H_5CS_2[CCC\mathbf{H_3}(COOCH_3)CH_2]_{24}C(CH_3CN)(CH_2)_2COOH$).

Conversion = 51 % $M_{n(NMR)}$ = 2400 g mol$^{-1}$ $M_{n(GPC)}$ = 10300 g mol$^{-1}$ Đ =1.25

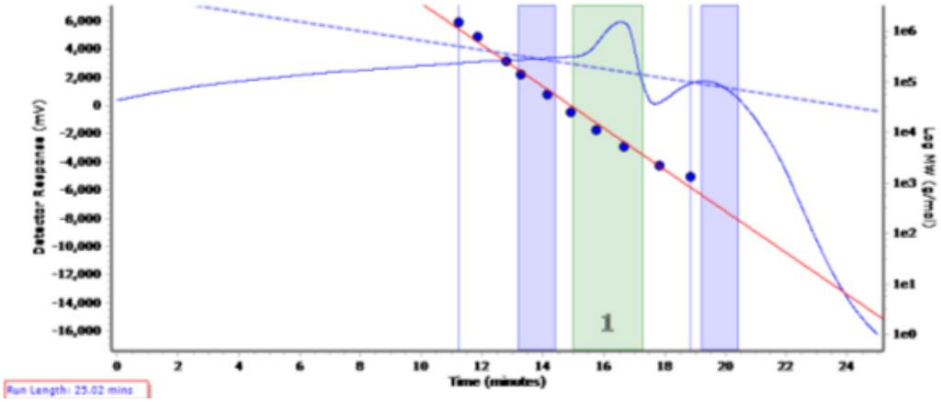


*Figure 6.40 The raw GPC of **N2**. The blue rectangles are where the baseline was corrected to and the green rectangle is the area which the $M_n$ and Đ was calculated.*

**N3**

$^1$H NMR (500 MHz, $CDCl_3$) δ 7.41 – 7.32 (m, 2H, $C_6\mathbf{H_5}CS_2[CCCH_3(COOCH_3)CH_2]_{71}C(CH_3CN)(CH_2)_2COOH$), 3.59 (s, 213H, $C_6H_5CS_2[CCCH_3(COOC\mathbf{H_3})CH_2]_{71}C(CH_3CN)(CH_2)_2COOH$), 2.10 – 1.71 (m, 138H, $C_6H_5CS_2[CCCH_3(COOCH_3)C\mathbf{H_2}]_{71}C(CH_3CN)(CH_2)_2COOH$), 1.71 – 1.36 (m, 39H, $C_6H_5CS_2[CCCH_3(COOCH_3)C\mathbf{H_2}]_{71}C(CH_3CN)(CH_2)_2COOH$), 1.36 – 1.15 (m, 111H, $C_6H_5CS_2[CCCH_3(COOCH_3)C\mathbf{H_2}]_{71}C(CH_3CN)(CH_2)_2COOH$), 1.01 (s, 72H, $C_6H_5CS_2[CCCH_3(COOC\mathbf{H_3})CH_2]_{71}C(CH_3CN)(CH_2)_2COOH$), 0.96 – 0.77 (m, 199H, $C_6H_5CS_2[CCC\mathbf{H_3}(COOCH_3)CH_2]_{71}C(CH_3CN)(CH_2)_2COOH$).

Conversion – 96 % $M_{n(NMR)}$ = 7100 g mol$^{-1}$ $M_{n(GPC)}$ = 14200 g mol$^{-1}$ Đ = 1.25

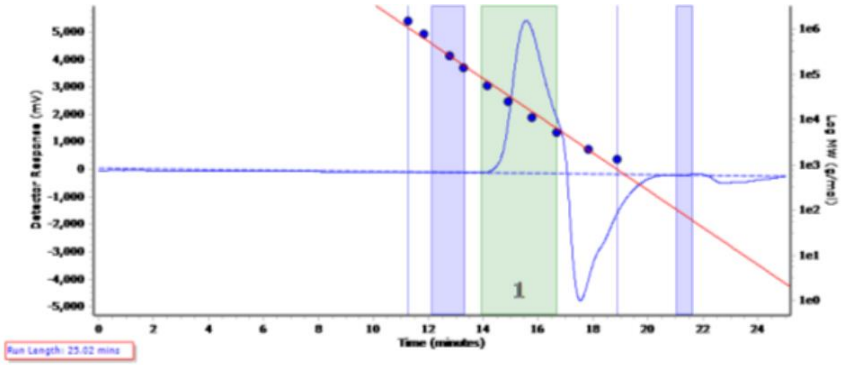


*Figure 6.41 The raw GPC of **N3**. The blue rectangles are where the baseline was corrected to and the green rectangle is the area which the $M_n$ and Đ was calculated.*

**N4**

$^1$H NMR (500 MHz, $CDCl_3$) δ 7.94 – 7.32 (m, 5H, $C_6\mathbf{H_5}CS_2[CCCH_3(COOCH_3)CH_2]_{36}C(CH_3CN)(CH_2)_2COOH$), 3.60 (s, 107H, $C_6H_5CS_2[CCCH_3(COOC\mathbf{H_3})CH_2]_{36}C(CH_3CN)(CH_2)_2COOH$), 2.11 – 1.75 (m, 70H, $C_6H_5CS_2[CCCH_3(COOCH_3)C\mathbf{H_2}]_{36}C(CH_3CN)(CH_2)_2COOH$), 1.68 – 1.35 (m, 45H, $C_6H_5CS_2[CCC\mathbf{H_3}(COOCH_3)CH_2]_{36}C(CH_3CN)(CH_2)_2COOH$), 1.35 – 1.18 (m, 86H, $C_6H_5CS_2[CCC\mathbf{H_3}(COOC\mathbf{H_3})CH_2]_{36}C(C\mathbf{H_3}CN)(C\mathbf{H_2})_2COOH$), 1.13 – 0.77 (m, 159H, $C_6H_5CS_2[CCCH_3(COOC\mathbf{H_3})CH_2]_{36}C(CH_3CN)(CH_2)_2COOH$).

Conversion = 77 % $M_{n(NMR)}$ = 3600 g mol$^{-1}$ $M_{n(GPC)}$ = 9700 g mol$^{-1}$ Đ = 1.18

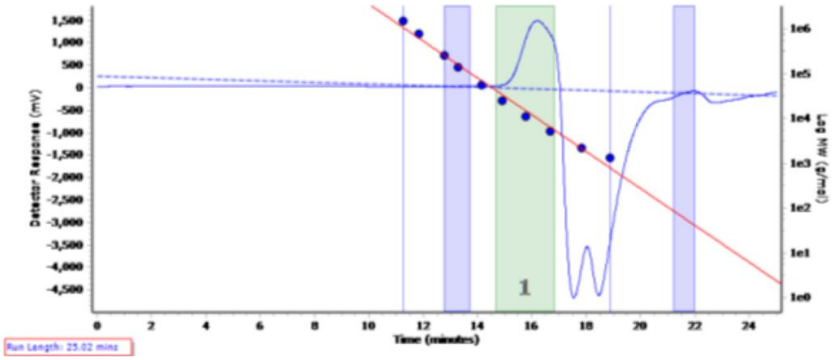


*Figure 6.42 The raw GPC of **N4**. The blue rectangles are where the baseline was corrected to and the green rectangle is the area which the $M_n$ and Đ was calculated.*

### 6.15.3. Representative RAFT polymerisation of TBuMA

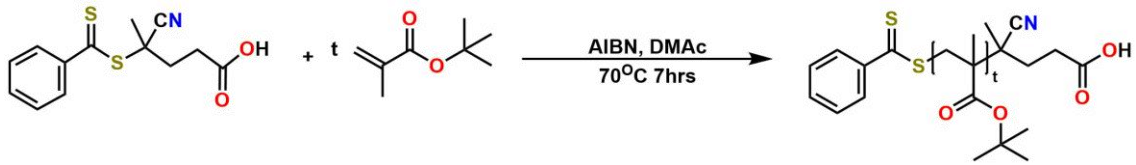


*Figure 6.43 A Schematic of the RAFT polymerisation of TBuMA.*

TBuMA was first passed through a basic alumina column to remove the inhibitor. MMA (1.00 g, 7.03 mmol), CPAD (0.0164 g, 0.0586 mmol), AIBN (0.00331 g, 0.0195 mmol) and DMAc (2.35 $cm^3$, 25.2 mmol) were added into an ampoule and sealed. The mixture was degassed via three freeze-pump-thaw-degas cycle then left to stir at 70 °C for 7 hours. The polymerisation was stopped when cooled the mixture was cooled down and opened to air. The crude mixture was then dialyzed against water for 24 hrs and lyophilized. The $M_{n(NMR)}$ was calculated by integrating the phenyl hydrogens of CPAD (equal to 5H) between 7.87 – 7.83 ppm against the *tert*-butyl peak of PTBuMA between 1.58 – 1.31 ppm.

**T1**

$^1$H NMR (500 MHz, $CDCl_3$) δ 7.87 – 7.30 (m, 5H, $C_6\mathbf{H_5}CS_2[CCCH_3(COOC(CH_3)_3)CH_2]_{148}C(CH_3CN)(CH_2)_2COOH$), 2.20 – 1.58 (m, 288H, $C_6H_5CS_2[CCCH_3(COOC(CH_3)_3)C\mathbf{H_2}]_{148}C(CH_3CN)(CH_2)_2COOH$), 1.58 – 1.31 (m, 1333H, $C_6H_5CS_2[CCCH_3(COOC(C\mathbf{H_3})_3)CH_2]_{148}C(CH_3CN)(CH_2)_2COOH$), 1.20 – 0.89 (m, 407H, $C_6H_5CS_2[CCC\mathbf{H_3}(COOC(CH_3)_3)CH_2]_{148}C(CH_3CN)(CH_2)_2COOH$).

Conversion = 82 % $M_{n(NMR)}$ = 21000 g $mol^{-1}$ $M_{n(GPC)}$ = 14000 g $mol^{-1}$ Đ = 1.24

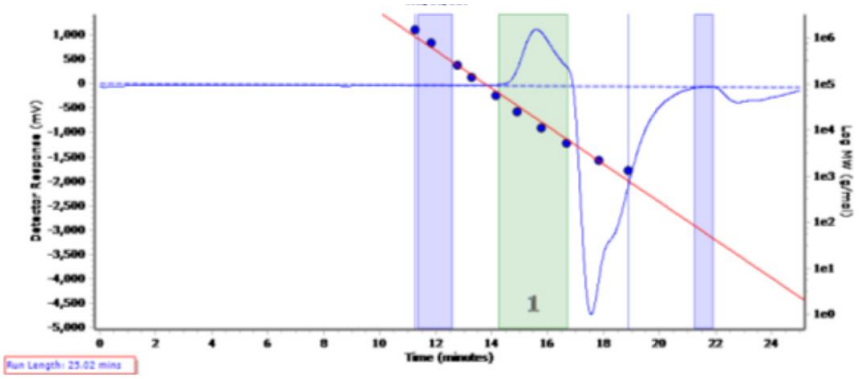


*Figure 6.44 The raw GPC of **T1**. The blue rectangles are where the baseline was corrected to and the green rectangle is the area which the $M_n$ and Đ was calculated.*

### 6.15.4. Representative RAFT polymerisation of MAPC1 using a pMMA macroRAFT agent

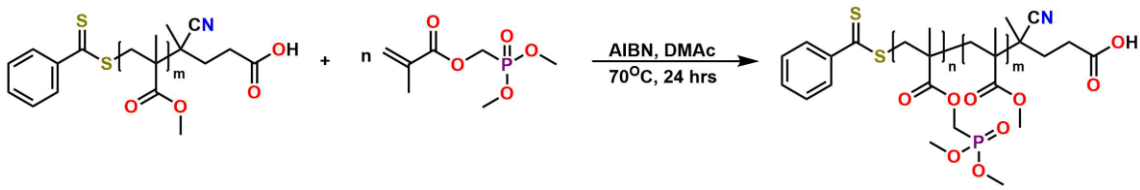


*Figure 6.45 A Schematic of the RAFT polymerisation of MAPC1 using a PMMA macroRAFT agent.*

MAPC1 was first passed through a basic alumina column to remove the inhibitor. MAPC1 (0.194 g, 0.930 mmol), PMMA (0.0500 g, 0.0310 mmol), AIBN (0.00102 g, 0.00620 mmol) and DMAc (1.22 $cm^{-3}$, 13.2 mmol) were added into an ampoule and sealed. The mixture was degassed via three freeze-pump-thaw-degas cycle then left to stir at 70 °C for 24 hours. The polymerisation was stopped when cooled the mixture was cooled down and opened to air. The crude mixture was then dialyzed against water for 24 hrs and lyophilized. The $M_{n(NMR)}$ was calculated by integrating the methyl of PMMA (equal to hydrogens determine in section 6.15.2) between 3.60 ppm against the methylene peak of PMAPC1 at 3.83 ppm.

**ND1** uses **N1**

$^1$H NMR (500 MHz, $CDCl_3$) δ 4.27 (m, 100H, $C_6H_5CS_2$ [$CCH_3(COOC\mathbf{H_2}PO(OCH_3)_2$ $CH_2]_{50}[CCCH_3(COOCH_3)CH_2]_{23}C(CH_3CN)(CH_2)_2COOH$), 3.83 (m, 310H, $C_6H_5CS_2CCH_3(COOCH_2PO(OC\mathbf{H_3})_2CH_2]_{50}[CCCH_3(COOCH_3)CH_2]_{23}C(CH_3CN)(CH_2)_2COOH$), 3.60 (s, 69H, $C_6H_5CS_2$ [$CCH_3(COOCH_2PO(OCH_3)_2$ $CH_2]_{50}[CCCH_3(COOC\mathbf{H_3})CH_2]_{23}C(CH_3CN)(CH_2)_2COOH$), 2.20 - 1.75 (m, 388H, $C_6H_5CS_2$ [$CC\mathbf{H_3}(COOCH_2PO(OCH_3)_2CH_2]_{50}[CCC\mathbf{H_3}(COOCH_3)CH_2]_{23}C(CH_3CN)(CH_2)_2COOH$)) 1.55 - 1.21 (m, 40H), 1.09 - 0.84 (m, 223H, $C_6H_5CS_2$ [$CCH_3(COOCH_2PO(OCH_3)_2C\mathbf{H_2}]_{50}[CCCH_3(COOCH_3)C\mathbf{H_2}]_{23}C(CH_3CN)(CH_2)_2COOH$).

$^{31}$P NMR (202 MHz, $CDCl_3$) δ 21.37 (s, $C_6H_5CS_2[CCH_3(COOCH_2\mathbf{P}O(OCH_3)_2CH_2]_{50}[CCCH_3(COOCH_3)CH_2]_{23}C(CH_3CN)(CH_2)_2COOH$)

Conversion = 96 % $M_{n(NMR)}$ = 12700 g $mol^{-1}$ $M_{n(GPC)}$ = 102100 g $mol^{-1}$ Đ = 1.45

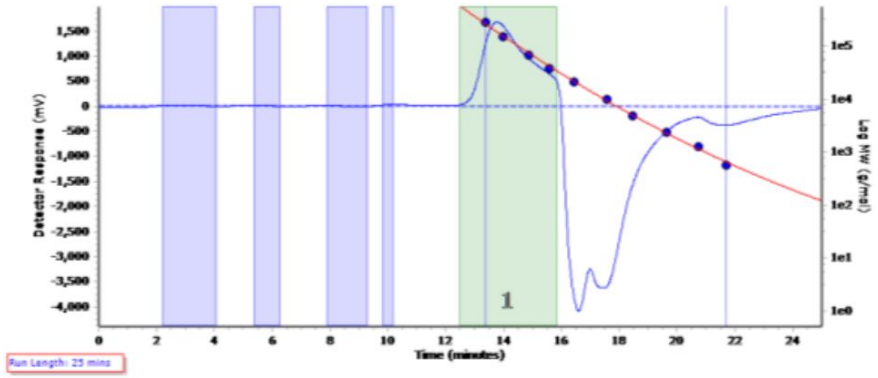


*Figure 6.46 The raw GPC of **ND1**. The blue rectangles are where the baseline was corrected to and the green rectangle is the area which the $M_n$ and Đ was calculated.*

**ND2** uses **N2**

$^{1}$H NMR (500 MHz, $CDCl_3$) δ 4.27 (m, 150H, $C_6H_5CS_2$ [$CCH_3(COOCH_2PO(OCH_3)_2CH_2]_{75}$[$CCCH_3(COOCH_3)CH_2]_{23}C(CH_3CN)(CH_2)_2COOH$), 3.85 (d, J = 10Hz, 473H, $C_6H_5CS_2$ [$CCH_3(COOCH_2PO(OC\mathbf{H_3})_2CH_2]_{75}$[$CCCH_3(COOCH_3)CH_2]_{23}C(CH_3CN)(CH_2)_2COOH$), 3.60 (s, 69H, $C_6H_5CS_2$[$CCH_3(COOCH_2PO(OCH_3)_2CH_2]_{75}$[$CCCH_3(COOC\mathbf{H_3})CH_2]_{23}C(CH_3CN)(CH_2)_2COOH$), 1.99 - 1.82 (m, 186H, $C_6H_5CS_2$ [$CC\mathbf{H_3}(COOCH_2PO(OCH_3)_2CH_2]_{75}$[$CCC\mathbf{H_3}(COOCH_3)CH_2]_{23}C(CH_3CN)(CH_2)_2COOH$)), 1.51 - 1.25 (m, 88H), 1.09 - 0.83 (m, 306H, $C_6H_5CS_2$[$CCH_3(COOCH_2PO(OCH_3)_2C\mathbf{H_2}]_{75}$[$CCCH_3(COOCH_3)C\mathbf{H_2}]_{23}C(CH_3CN)(CH_2)_2COOH$).

$^{31}$P NMR (202 MHz, $CDCl_3$) δ 21.36 (d, $C_6H_5CS_2$[$CCH_3(COOCH_2\mathbf{P}O(OCH_3)_2CH_2]_{75}$[$CCCH_3(COOCH_3)CH_2]_{23}C(CH_3CN)(CH_2)_2COOH$)

Conversion = 90 % $M_{n(NMR)}$ = 17900 g $mol^{-1}$ $M_{n(GPC)}$ = 53500 g $mol^{-1}$ Đ = 1.61

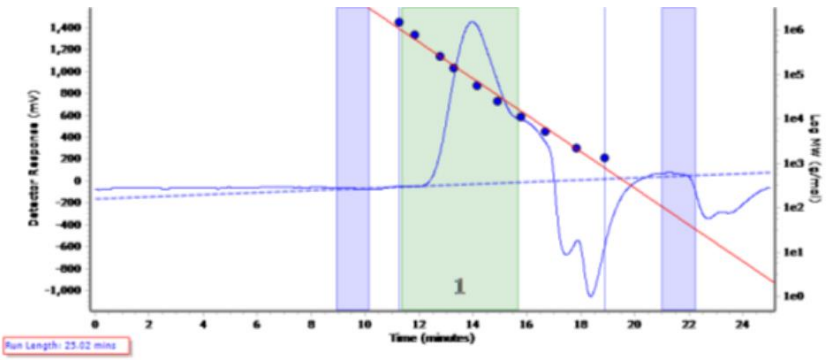


*Figure 6.47 The raw GPC of **ND2**. The blue rectangles are where the baseline was corrected to and the green rectangle is the area which the $M_n$ and Đ was calculated.*

### 6.15.5. Representative RAFT polymerisation of DMAE using a PMMA macroRAFT agent

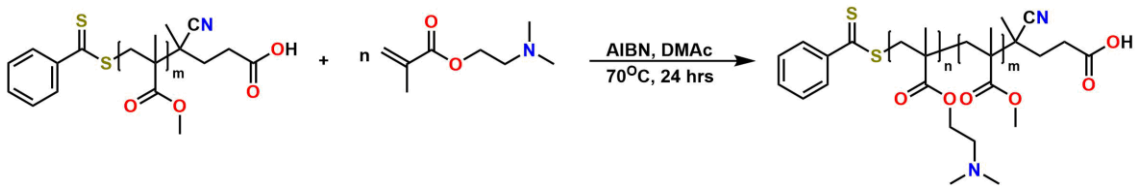


*Figure 6.48 A Schematic of the RAFT polymerisation of DMAE using a PMMA macroRAFT agent.*

DMAE was first passed through a basic alumina column to remove the inhibitor. DMAE (0.15 g, 0.954 mmol), PMMA (0.126 g, 0.0286 mmol), AIBN (0.00313 g, 0.00191 mmol) and DMAc (1.06 $cm^{-3}$, 11.5 mmol) were added into an ampoule and sealed. The mixture was degassed via three freeze-pump-thaw-degas cycle then left to stir at 70 °C for 7 hours. The polymerisation was stopped when cooled the mixture was cooled down and opened to air. The crude mixture was then dialyzed against water for 24 hrs and lyophilized. The $M_{n(NMR)}$ was calculated by integrating the methyl of PMMA (equal to hydrogens determine in section 6.15.2) at 3.60 ppm against the methylene peak of PDMAE at 4.06 ppm.

**NDA1** uses **N3**

1H NMR (500 MHz, $CDCl_3$) δ 4.06 (s, 201H, $C_6H_5CS_2[CCCH_3(COO(C\mathbf{H_2})_2N(CH_3)_2)CH_2]_{99}[CCCH_3(COOCH_3)CH_2]_{71}C(CH_3CN)(CH_2)_2COOH$), 3.59 (s, 213H, $C_6H_5CS_2[CCCH_3(COO(CH_2)_2N(CH_3)_2)CH_2]_{99}[CCCH_3(COOC\mathbf{H_3})CH_2]_{71}C(CH_3CN)(CH_2)_2COOH$), 2.56 (s, 201H, $C_6H_5CS_2[CCCH_3(COO(C\mathbf{H_2})_2N(CH_3)_2)CH_2]_{99}[CCCH_3(COOCH_3)CH_2]_{71}C(CH_3CN)(CH_2)_2COOH$), 2.28 (s, 204H, $C_6H_5CS_2[CCCH_3(COO(CH_2)_2N(C\mathbf{H_3})_2)CH_2]_{99}[CCCH_3(COOCH_3)CH_2]_{71}C(CH_3CN)(CH_2)_2COOH$), 2.07 – 1.74 (m, 423H, $C_6H_5CS_2[CCCH_3(COO(CH_2)_2N(CH_3)_2)C\mathbf{H_2}]_{99}[CCCH_3(COOCH_3)C\mathbf{H_2}]_{71}C(CH_3CN)(CH_2)_2COOH$), 1.49 – 1.18 (m, 186H, $C_6H_5CS_2[CCCH_3(COO(CH_2)_2N(CH_3)_2)C\mathbf{H_2}]_{99}[CCCH_3(COOCH_3)C\mathbf{H_2}]_{71}C(CH_3CN)(CH_2)_2COOH$), 1.11 – 0.96 (m, 180H, $C_6H_5CS_2[CCC\mathbf{H_3}(COO(CH_2)_2N(CH_3)_2)CH_2]_{99}[CCC\mathbf{H_3}(COOCH_3)CH_2]_{71}C(CH_3CN)(CH_2)_2COOH$), 0.95 – 0.77 (m, 396H, $C_6H_5CS_2[CCC\mathbf{H_3}(COO(CH_2)_2N(CH_3)_2)CH_2]_{99}[CCC\mathbf{H_3}(COOCH_3)CH_2]_{71}C(CH_3CN)(CH_2)_2COOH$).

Conversion = 70 % $M_{n(NMR)}$ = 15000 g $mol^{-1}$ $M_{n(GPC)}$ = 21100 g $mol^{-1}$ Đ = 1.52

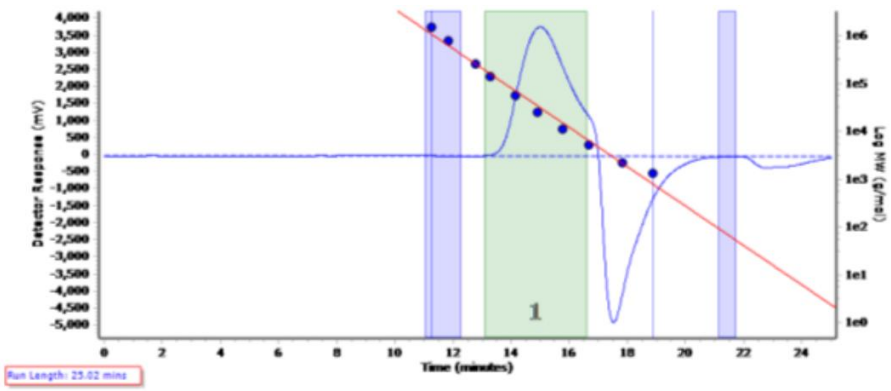


*Figure 6.49 The raw GPC of **NDA1**. The blue rectangles are where the baseline was corrected to and the green rectangle is the area which the $M_n$ and Đ was calculated.*

### 6.15.6. Representative RAFT polymerisation of HEMA using a PMMA macroRAFT agent

HEMA was first passed through a basic alumina column to remove the inhibitor. HEMA (0.15 g,

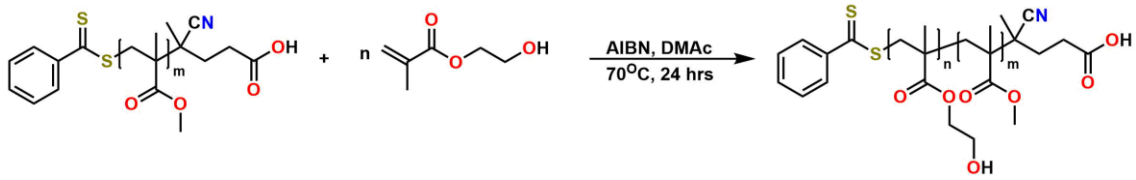


*Figure 6.50 A schematic showing the RAFT polymerisation of HEMA using a PMMA macroRAFT agent.*

1.15 mmol), PMMA (0.127 g, 0.0288 mmol), AIBN (0.00316 g, 0.00192 mmol) and DMAc (1.07 $cm^{-3}$, 11.5 mmol) were added into an ampoule and sealed. The mixture was degassed via three freeze-pump-thaw-degas cycle then left to stir at 70 °C for 7 hours. The polymerisation was stopped when cooled the mixture was cooled down and opened to air. The crude mixture was then dialyzed against water for 24 hrs and lyophilized. The $M_{n(NMR)}$ was calculated by integrating the methyl of PMMA (equal to hydrogens determine in section 6.15.2) at 3.60 ppm against the methylene peak of PHEMA at 4.09 ppm.

**NDE1** uses **N3**

1H NMR (500 MHz, MeOD) δ 4.09 (s, 232H $C_6H_5CS_2[CCCH_3(COO(C\mathbf{H_2})_2OH)CH_2]_{116}[CCCH_3(COOCH_3)CH_2]_{71}C(CH_3CN)(CH_2)_2COOH$), 3.82 (s, 244H, $C_6H_5CS_2[CCCH_3(COO(C\mathbf{H_2})_2OH)CH_2]_{116}[CCCH_3(COOCH_3)CH_2]_{71}C(CH_3CN)(CH_2)_2COOH$), 3.70, (s, 213H, , $C_6H_5CS_2[CCCH_3(COO(CH_2)_2OH)CH_2]_{116}[CCCH_3(COOC\mathbf{H_3})CH_2]_{71}C(CH_3CN)(CH_2)_2COOH$), 2.25 – 1.80 (m, 309H $C_6H_5CS_2[CCCH_3(COO(CH_2)_2OH)C\mathbf{H_2}]_{116}[CCCH_3(COOCH_3)C\mathbf{H_2}]_{71}C(CH_3CN)(CH_2)_2COOH$), 1.74 – 1.62 (m, 29H, $C_6H_5CS_2[CCC\mathbf{H_3}(COO(CH_2)_2OH)CH_2]_{116}[CCC\mathbf{H_3}(COOCH_3)CH_2]_{71}C(CH_3CN)(CH_2)_2COOH$), 1.40 – 1.28 (m, 38H, $C_6H_5CS_2[CCC\mathbf{H_3}(COO(CH_2)_2OH)CH_2]_{116}[CCC\mathbf{H_3}(COOCH_3)CH_2]_{71}C(CH_3CN)(CH_2)_2COOH$), 1.23 – 0.82 (m, 487H, $C_6H_5CS_2[CCC\mathbf{H_3}(COO(CH_2)_2OH)CH_2]_{116}[CCC\mathbf{H_3}(COOCH_3)CH_2]_{71}C(CH_3CN)(CH_2)_2COOH$).

Conversion = 56 % $M_{n(NMR)}$ = 22200 g $mol^{-1}$ $M_{n(GPC)}$ = 36400 g $mol^{-1}$ Đ = 1.70

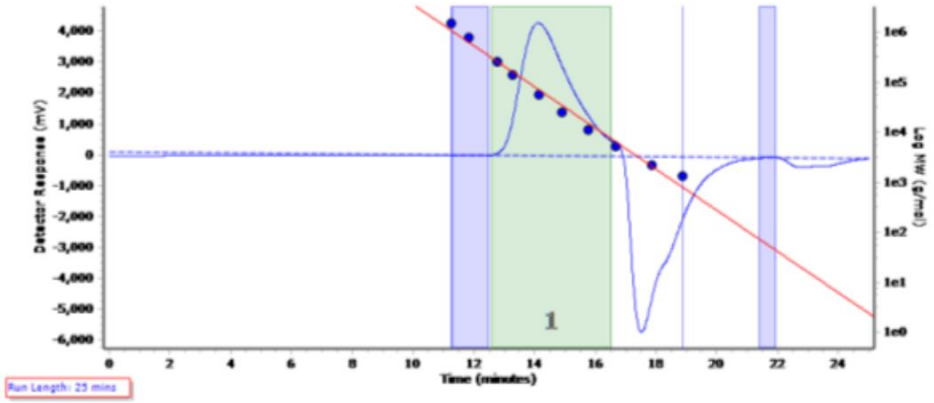


*Figure 6.51 The raw GPC of **NDE1**. The blue rectangles are where the baseline was corrected to and the green rectangle is the area which the $M_n$ and Đ was calculated.*

### 6.15.7. Representative RAFT polymerisation of TBuMA using a PMMA macroRAFT agent

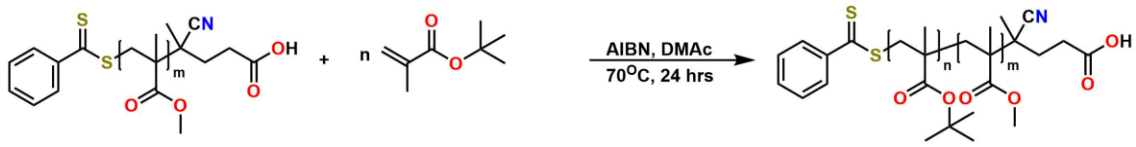


*Figure 6.52 A schematic of a RAFT polymerisation of TBuMA using a PMMA macroRAFT.*

HEMA was first passed through a basic alumina column to remove the inhibitor. HEMA (0.15 g, 1.06 mmol), PMMA (0.127 g, 0.0288 mmol), AIBN (0.00316 g, 0.00192 mmol) and DMAc (1.07 $cm^{-3}$, 11.5 mmol) were added into an ampoule and sealed. The mixture was degassed via three freeze-pump-thaw-degas cycle then left to stir at 70 °C for 3 hours. The polymerisation was stopped when cooled the mixture was cooled down and opened to air. The crude mixture was then dialyzed against water for 24 hrs and lyophilized. The $M_{n(NMR)}$ was calculated by integrating the methyl of PMMA (equal to hydrogens determine in section 6.15.2) at 3.60 ppm against the *tert*-butyl group of PTBuMA between 1.49 – 1.33 ppm.

**NDT1** uses **N3**

$^1$H NMR (500 MHz, $CDCl_3$) δ 3.60 (s, 213H, $C_6H_5CS_2[CCCH_3(COO(CH_3)_3CH_2]_{43}[CCCH_3(COOC\mathbf{H_3})CH_2]_{71}$ $C(CH_3CN)(CH_2)_2COOH$), 1.99 – 1.76 (m, 177H, $C_6H_5CS_2[CCCH_3(COO(CH_3)_3C\mathbf{H_2}]_{43}[CCCH_3(COOCH_3)C\mathbf{H_2}]_{71}C(CH_3CN)(CH_2)_2COOH$), 1.49 – 1.33 (m, 389H, $C_6H_5CS_2[CCCH_3(COO(C\mathbf{H_3})_3CH_2]_{43}[CCCH_3(COOCH_3)CH_2]_{71}C(CH_3CN)(CH_2)_2COOH$), 1.32 – 1.14 (m, 54H, $C_6H_5CS_2[CCCH_3(COO(CH_3)_3C\mathbf{H_2}]_{43}[CCCH_3(COOCH_3)C\mathbf{H_2}]_{71}C(C\mathbf{H_3}CN)(C\mathbf{H_2})_2COOH$), 1.14 – 0.78 (m, 336H, $C_6H_5CS_2[CCC\mathbf{H_3}(COO(CH_3)_3CH_2]_{43}[CCC\mathbf{H_3}(COOCH_3)CH_2]_{71}C(CH_3CN)(CH_2)_2COOH$).

Conversion: 64 % $M_{n(NMR)}$ = 13200 g $mol^{-1}$ $M_{n(GPC)}$ = 18000 g $mol^{-1}$ Đ = 1.37

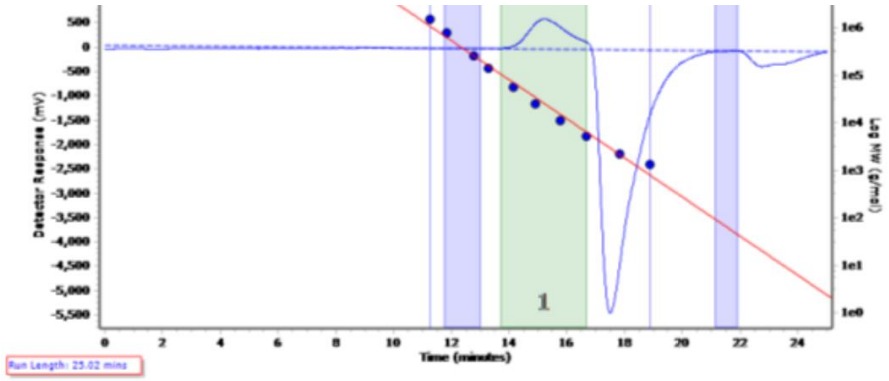


*Figure 6.53 The raw GPC trace of **NDT1**. The blue rectangles are where the baseline was corrected to and the green rectangle is the area which the $M_n$ and Đ was calculated.*

**NDT2** uses **N4**

$^1$H NMR (500 MHz, $CDCl_3$) δ 3.60 (s, 108H, $C_6H_5CS_2[CCCH_3(COO(CH_3)_3CH_2]_{29}[CCCH_3(COOC\mathbf{H_3})CH_2]_{36}C(CH_3CN)(CH_2)_2COOH$), 2.07 – 1.69 (m, 129H, $C_6H_5CS_2[CCCH_3(COO(CH_3)_3C\mathbf{H_2}]_{29}[CCCH_3(COOCH_3)C\mathbf{H_2}]_{36}C(CH_3CN)(CH_2)_2COOH$), 1.54 – 1.30 (m, 257H, $C_6H_5CS_2[CCCH_3(COO(C\mathbf{H_3})_3CH_2]_{29}[CCCH_3(COOCH_3)CH_2]_{36}C(CH_3CN)(CH_2)_2COOH$), 1.20 – 0.74 (m, 186H, $C_6H_5CS_2[CCC\mathbf{H_3}(COO(CH_3)_3CH_2]_{29}[CCC\mathbf{H_3}(COOCH_3)CH_2]_{36}C(CH_3CN)(CH_2)_2COOH$).

Conversion = 75 % $M_{n(NMR)}$ = 7700 g $mol^{-1}$ $M_{n(GPC)}$ = 13100 g $mol^{-1}$ Đ = 1.27

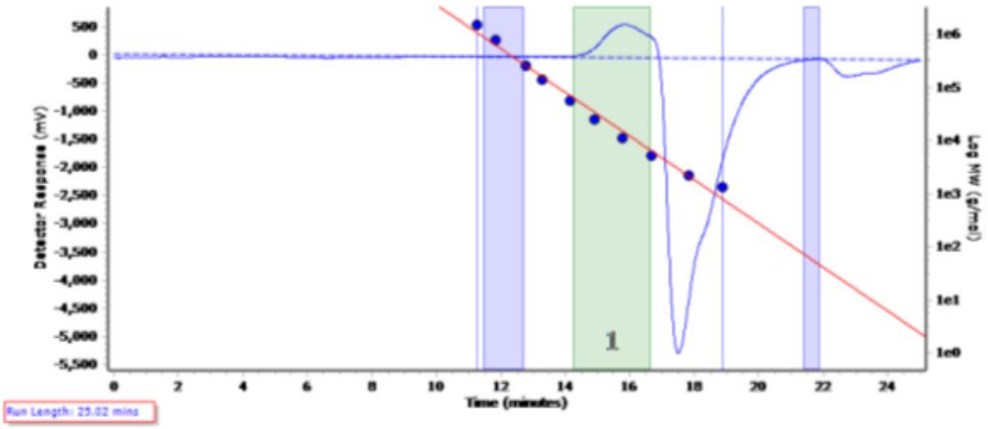


*Figure 6. 54 The raw GPC trace of **NDT2**. The blue rectangles are where the baseline was corrected to and the green rectangle is the area which the $M_n$ and Đ was calculated.*

### 6.15.8. Representative RAFT polymerisation of MMA using a PEG-*b*-PMAPC1 macroRAFT agent

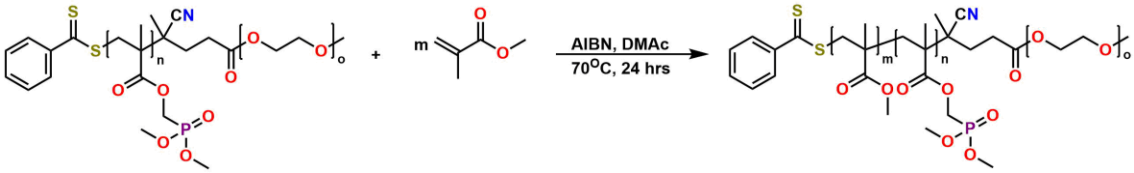


*Figure 6.55 A schematic showing the RAFT polymerisation of MMA using a PMAPC1 macroRAFT agent.*

MMA was first passed through a basic alumina column to remove the inhibitor. MMA (0.194 g, 0.930 mmol), PMAPC1 (0.0500 g, 0.0310 mmol), AIBN (0.00102 g, 0.00620 mmol) and DMAc (1.22 $cm^{-3}$, 13.2 mmol) were added into an ampoule and sealed. The mixture was degassed via three freeze-pump-thaw-degas cycle then left to stir at 70 °C for 24 hours. The polymerisation was stopped when cooled the mixture was cooled down and opened to air. The crude mixture was then dialyzed against water for 24 hrs and lyophilized. The $M_{n(NMR)}$ was calculated by integrating the methoxy of PEG (equal to 3H) at 3.38 ppm against the methyl peak of PMMA at 3.60 ppm and the methylene peak of PMAPC1 at 3.83 ppm.

**PDN1** uses **PD3**

$^1$H NMR (500 MHz, $CDCl_3$) δ 4.26 (s, 11H, $C_6H_5CS_2[CCCH_3(COOCH_3)CH_2]_{22}[CCH_3(COOC\mathbf{H_2}PO(OCH_3)_2CH_2]_7C(CH_3CN)(CH_2)_2COO[(CH_2)_2O]_{49}CH_3$), 3.83 (d, 40H, $C_6H_5CS_2[CCCH_3(COOCH_3)CH_2]_{22}[CCH_3(COOCH_2PO(OC\mathbf{H_3})_2CH_2]_7C(CH_3CN)(CH_2)_2COO[(CH_2)_2O]_{49}CH_3$), 3.73 – 3.60 (m 263H, $C_6H_5CS_2[CCCH_3(COOC\mathbf{H_3})CH_2]_{22}[CCH_3(COOCH_2PO(OCH_3)_2CH_2]_7C(CH_3CN)(CH_2)_2COO[(C\mathbf{H_2})_2O]_{49}CH_3$), 3.38 (s, 3H, $C_6H_5CS_2[CCCH_3(COOCH_3)CH_2]_{22}[CCH_3(COOCH_2PO(OCH_3)_2CH_2]_7C(CH_3CN)(CH_2)_2COO[(CH_2)_2O]_{49}C\mathbf{H_3}$), 2.10 – 1.76 (m, 66H, $C_6H_5CS_2[CCCH_3(COOCH_3)C\mathbf{H_2}]_{22}[CCH_3(COOCH_2PO(OCH_3)_2C\mathbf{H_2}]_7C(CH_3CN)(CH_2)_2COO[(CH_2)_2O]_{49}CH_3$), 1.76 – 1.49 (m, 36H, $C_6H_5CS_2[CCCH_3(COOCH_3)CH_2]_{22}[CCH_3(COOCH_2PO(OCH_3)_2CH_2]_7C(CH_3CN)(CH_2)_2COO[(CH_2)_2O]_{49}CH_3$), 1.49 – 1.18 (m, 19H), 1.17 – 0.72 (m, 104H, $C_6H_5CS_2[CCC\mathbf{H_3}(COOCH_3)CH_2]_{22}[CC\mathbf{H_3}(COOCH_2PO(OCH_3)_2CH_2]_7C(CH_3CN)(CH_2)_2COO[(CH_2)_2O]_{49}CH_3$).

$^{31}$P NMR (202 MHz, $CDCl_3$) δ 21.37 (d, $C_6H_5CS_2[CCC\mathbf{H_3}(COOCH_3)CH_2]_{22}[CC\mathbf{H_3}(COOCH_2\mathbf{P}O(OCH_3)_2CH_2]_6C(CH_3CN)(CH_2)_2COO[(CH_2)_2O]_{46}CH_3$ ).

Conversion = 69 % $M_{n(NMR)}$ = 5800 g mol$^{-1}$ $M_{n(GPC)}$ = 83900 g mol$^{-1}$ Đ = 1.59

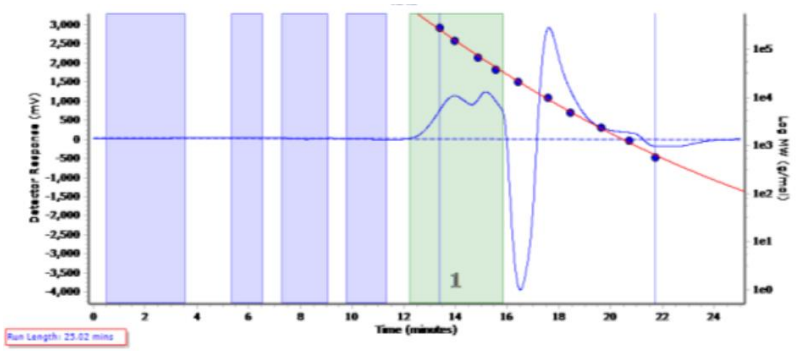


*Figure 6.56 The raw GPC trace of **PDN1**. The blue rectangles are where the baseline was corrected to and the green rectangle is the area which the $M_n$ and Đ was calculated.*

**PDN2** uses **PD1**

$^{1}$H NMR (500 MHz$CDCl_3$) δ 4.25 (m, 22H, $C_6H_5CS_2[CCCH_3(COOCH_3)CH_2]_{15}[CCH_3(COOC\mathbf{H_2}PO(OCH_3)_2CH_2]_{12}C(CH_3CN)(CH_2)_2COO[(CH_2)_2O]_{146}CH_3$), 3.83 (d, *J* = 10.1 Hz, 70H, $C_6H_5CS_2[CCCH_3(COOCH_3)CH_2]_{15}[CCH_3(COOCH_2PO(OC\mathbf{H_3})_2CH_2]_{12}C(CH_3CN)(CH_2)_2COO[(CH_2)_2O]_{146}CH_3$), 3.73 – 3.46 (m, 631H, $C_6H_5CS_2[CCCH_3(COOC\mathbf{H_3})CH_2]_{15}[CCH_3(COOCH_2PO(OCH_3)_2CH_2]_{12}C(CH_3CN)(CH_2)_2COO[(C\mathbf{H_2})_2O]_{146}CH_3$), 3.37 (s, 3H, $C_6H_5CS_2[CCCH_3(COOCH_3)CH_2]_{15}[CCH_3(COOCH_2PO(OCH_3)_2CH_2]_{12}C(CH_3CN)(CH_2)_2COO[(CH_2)_2O]_{146}C\mathbf{H_3}$), 2.01 – 1.75 (m, 38H, $C_6H_5CS_2[CCCH_3(COOCH_3)CH_2]_{15}[CCH_3(COOCH_2PO(OCH_3)_2CH_2]_{12}C(CH_3CN)(CH_2)_2COO[(CH_2)_2O]_{146}CH_3$), 1.61 – 1.15 (m, 66H, $C_6H_5CS_2[CCCH_3(COOCH_3)C\mathbf{H_2}]_{15}[CCH_3(COOCH_2PO(OCH_3)_2C\mathbf{H_2}]_{12}C(CH_3CN)(CH_2)_2COO[(CH_2)_2O]_{146}CH_3$), 1.13 – 0.76 (m, 116H, $C_6H_5CS_2[CCC\mathbf{H_3}(COOCH_3)CH_2]_{15}[CC\mathbf{H_3}(COOCH_2PO(OCH_3)_2CH_2]_{12}C(CH_3CN)(CH_2)_2COO[(CH_2)_2O]_{146}CH_3$).

$^{31}$P NMR (202 MHz, $CDCl_3$) δ 21.39 (d, $C_6H_5CS_2[CCCH_3(COOCH_3)CH_2]_{15}[CCH_3(COOCH_2\mathbf{P}O(OCH_3)_2CH_2]_{12}C(CH_3CN)(CH_2)_2COO[(CH_2)_2O]_{146}CH_3$),

Conversion = 34 % $M_{n(NMR)}$ = 10400 g mol$^{-1}$ $M_{n(GPC)}$ = 98700 g mol$^{-1}$ Đ = 1.37

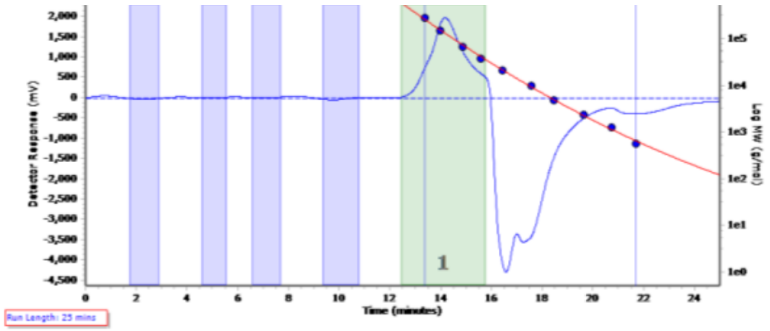


*Figure 6.57 The raw GPC trace of **PDN2**. The blue rectangles are where the baseline was corrected to and the green rectangle is the area which the $M_n$ and Đ was calculated.*

**PDN3** uses **PD2**

$^1$H NMR (500 MHz, $CDCl_3$) δ, 3.70 – 3.50 (m, 655H, $C_6H_5CS_2[CCCH_3(COOC\mathbf{H_3})CH_2]_{50}[CCH_3(COOCH_2PO(OCH_3)_2CH_2]_{23}C(CH_3CN)(CH_2)_2COO[(C\mathbf{H_2})_2O]_{126}CH_3$),3.37 (s, 3H, $C_6H_5CS_2[CCCH_3(COOCH_3)CH_2]_{50}[CCH_3(COOCH_2PO(OCH_3)_2CH_2]_{23}C(CH_3CN)(CH_2)_2COO[(CH_2)_2O]_{126}C\mathbf{H_3}$), 2.00 – 1.42 (m, 87H, $C_6H_5CS_2[CCCH_3(COOCH_3)C\mathbf{H_2}]_{50}[CCH_3(COOCH_2PO(OCH_3)_2C\mathbf{H_2}]_{22}C(CH_3CN)(CH_2)_2COO[(CH_2)_2O]_{126}CH_3$), 1.42 – 0.74 (m, 220H, $C_6H_5CS_2[CCC\mathbf{H_3}(COOCH_3)CH_2]_{50}[CC\mathbf{H_3}(COOCH_2PO(OCH_3)_2CH_2]_{23}C(CH_3CN)(CH_2)_2COO[(CH_2)_2O]_{126}CH_3$).

Conversion = 61 % $M_{n(NMR)}$ = 15300 g mol$^{-1}$ $M_{n(GPC)}$ = 86000 g mol$^{-1}$ Đ = 1.29

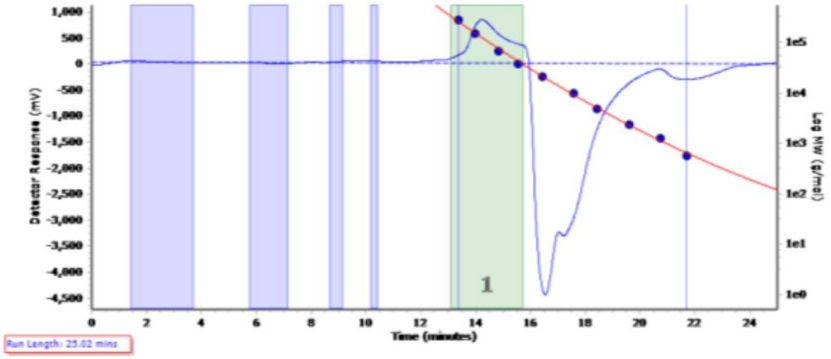


*Figure 6.58 The raw GPC trace of **PDN3**. The blue rectangles are where the baseline was corrected to and the green rectangle is the area which the $M_n$ and Đ was calculated.*

### 6.15.9. Representative RAFT polymerisation of MMA using a PTBuMA-PEG macroRAFT

MMA was first passed through a basic alumina column to remove the inhibitor. MMA (0.0.35 g,

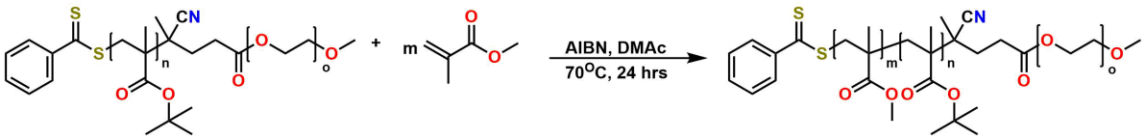


*Figure 6.59 A schematic showing the RAFT polymerisation of MMA using a PTBuMA-PEG macroRAFT agent.*

0.930 mmol), **PT1** (0.120 g, 0.0233 mmol), AIBN (0.0013 g, 0.0078 mmol) and DMAc (0.93 cm$^{-3}$, 10.0 mmol) were added into an ampoule and sealed. The mixture was degassed via three freeze-pump-thaw-degas cycle then left to stir at 70 °C for 24 hours. The polymerisation was stopped when cooled the mixture was cooled down and opened to air. The crude mixture was then dialyzed against water for 24 hrs and lyophilized. The $M_{n(NMR)}$ was calculated by integrating the methoxy of PEG (equal to 3H) at 3.38 ppm against the *tert*-butyl peak of PTBuMA between 1.51 – 1.35 ppm and the methylene peak of PMAPC1 at 3.83 ppm.

**PTN1** uses **PT1**

$^1$H NMR (500 MHz, $CDCl_3$) δ 3.73 – 3.46 (m, 235H, $C_6H_5CS_2[CCCH_3(COOC\mathbf{H_3})CH_2]_{16}[CCH_3(OC(CH_3)_3)CH_2]_{21}C(CH_3CN)(CH_2)_2COO[(C\mathbf{H_2})_2O]_{47}CH_3$), 3.38 (s, 3H, $C_6H_5CS_2[CCCH_3(COOCH_3)CH_2]_{16}[CCH_3(OC(CH_3)_3)CH_2]_{21}C(CH_3CN)(CH_2)_2COO[(CH_2)_2O]_{47}C\mathbf{H_3}$), 2.15 – 1.74 (m, 117H, $C_6H_5CS_2[CCCH_3(COOCH_3)C\mathbf{H_2}]_{16}[CCH_3(OC(CH_3)_3)C\mathbf{H_2}]_{21}C(CH_3CN)(CH_2)_2COO[(CH_2)_2O]_{47}CH_3$), 1.51 – 1.35 (m, 436H,

$C_6H_5CS_2[CCC\mathbf{H_3}(COOCH_3)CH_2]_{16}[CC\mathbf{H_3}(OC(C\mathbf{H_3})_3)CH_2]_{21}C(CH_3CN)(CH_2)_2COO[(CH_2)_2O]_{47}CH_3)$, 1.19 – 0.80 (m, 180H, $C_6H_5CS_2[CCC\mathbf{H_3}(COOCH_3)CH_2]_{16}[CC\mathbf{H_3}(OC(CH_3)_3)CH_2]_{21}C(CH_3CN)(CH_2)_2COO[(CH_2)_2O]_{47}CH_3)$.

Conversion = 61 % $M_{n(NMR)}$ = 6700 g mol$^{-1}$ $M_{n(GPC)}$ = 17500 g mol$^{-1}$ Đ = 1.48

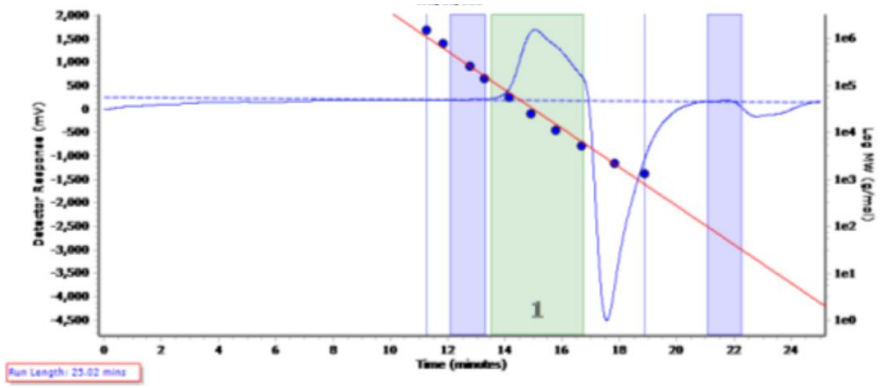


*Figure 6.60 The raw GPC of **PTN1**. The blue rectangles are where the baseline was corrected to and the green rectangle is the area which the $M_n$ and Đ was calculated.*

## 6.16. Representative PEGlaytions of RAFT polymers

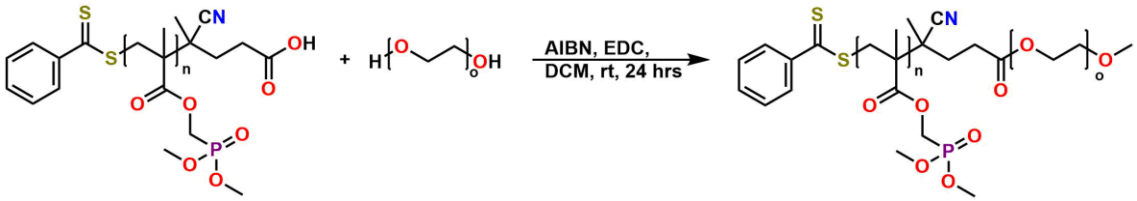


*Figure 6.61 A schematic showing the PEGylation of PMAPC1.*

The polymer (0.100 g, 0.0138 mmol), PEG (0.100, 0.00553 mmol, $M_n$ = 114) 4 molar equivalents in respect to the polymer), DMAP (4.03 x 10$^{-3}$ g, 0.00346 mmol, 2.5 molar equivalents in respect to the polymer), EDC (0.0859 g, 0.553 mmol, 10 molar equivalents in respect to the polymer) and DCM (0.176 cm$^{-3}$, 2.77 mmol) were added into a vial. The mixture was stirred at room temperature for 24 hrs. Then the mixture was dialysed against water for 24 hrs then lyophilized. The $M_{n(NMR)}$ was calculated by integrating the methoxy of PEG (equal to 3H) at 3.38 ppm against the characteristic peaks of the other monomers mentioned in the previous experimental sections.

**PND1** uses **ND1**

$^1$H NMR (500 MHz, $CDCl_3$) δ 4.25 (m, 19H, $C_6H_5CS_2[CCH_3(COOC\mathbf{H_2}PO(OCH_3)_2CH_2]_{10}[CCCH_3(COOCH_3)CH_2]_{19}C(CH_3CN)(CH_2)_2COO[(CH_2)_2O]_{140}CH_3)$, 3.83 (d, J = 12 Hz , 55H, $C_6H_5CS_2[CCH_3(COOCH_2PO(OC\mathbf{H_3})_2CH_2]_{10}[CCCH_3(COOCH_3)CH_2]_{19}C(CH_3CN)(CH_2)_2COO[(CH_2)_2O]_{140}CH_3)$, 3.64 (m, 560H, $C_6H_5CS_2[CCH_3(COOCH_2PO(OCH_3)_2CH_2]_{10}[CCCH_3(COOCH_3)CH_2]_{19}C(CH_3CN)(CH_2)_2COO[(C\mathbf{H_2})_2O]_{114}CH_3)$, 3.60 (s, 56H, $C_6H_5CS_2[CCH_3(COOCH_2PO(OCH_3)_2CH_2]_{10}[CCCH_3(COOC\mathbf{H_3})CH_2]_{19}C(CH_3CN)(CH_2)_2COO[(CH_2)_2O]_{140}CH_3)$, 3.38 (s, 3H, (m, 19H, $C_6H_5CS_2[CCH_3(COOCH_2PO(OCH_3)_2CH_2]_{10}[CCCH_3(COOCH_3)CH_2]_{19}C(CH_3CN)(CH_2)_2COO[(CH_2)_2O]_{114}C\mathbf{H_3})$, 2.04 - 1.78 (m, 116H, $C_6H_5CS_2[CC\mathbf{H_3}(COOCH_2PO(OCH_3)_2CH_2]_{10}[CCC\mathbf{H_3}(COOCH_3)CH_2]_{19}C(C\mathbf{H_3}CN)(C\mathbf{H_2})_2COO[(CH_2)_2O]_{140}C$

$H_3$), 1.09 - 0.85 (m, 41H, $C_6H_5CS_2$[$CCH_3(COOCH_2PO(OCH_3)_2C\mathbf{H_2}]_{10}[CCCH_3(COOCH_3)C\mathbf{H_2}]_{19}C(CH_3CN)(CH_2)_2COO[(CH_2)_2O]_{140}CH_3$).

$^{31}$P NMR (202 MHz, $CDCl_3$) δ 21.33 (d, $C_6H_5CS_2$[$CCH_3(COOCH_2\mathbf{P}O(OCH_3)_2CH_2]_{10}[CCCH_3(COOCH_3)CH_2]_{19}C(CH_3CN)(CH_2)_2COO[(CH_2)_2O]_{140}CH_3$)

$M_{n(NMR)}$ = 10100 g mol$^{-1}$ $M_{n(GPC)}$ = 20600 g mol$^{-1}$ Đ = 1.50

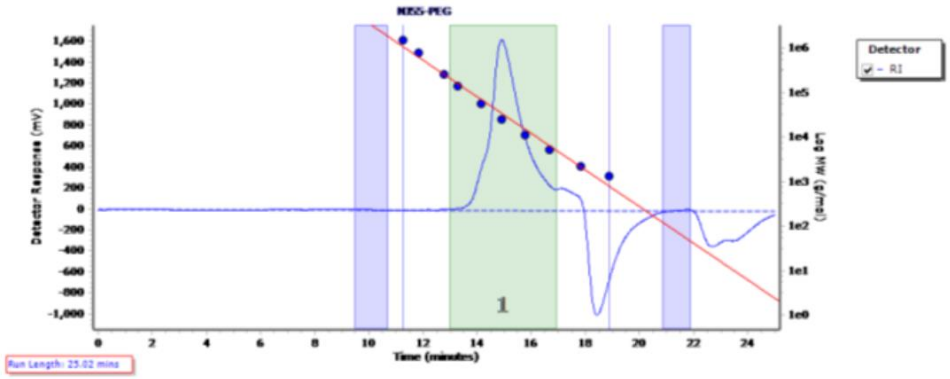


*Figure 6.62 The raw GPC of **PND1**. The blue rectangles are where the baseline was corrected to and the green rectangle is the area which the $M_n$ and Đ was calculated.*

**PND2** uses **ND2**

$^1$H NMR (500 MHz, $CDCl_3$) δ 4.27 (s, 6H, $C_6H_5CS_2[CCH_3(COOCH_2\mathbf{P}O(OCH_3)_2CH_2]_3[CCCH_3(COOCH_3)CH_2]_{11}C(CH_3CN)(CH_2)_2COO[(CH_2)_2O]_{122}CH_3$), 3.85 (s, 16H, $C_6H_5CS_2[CCH_3(COOCH_2PO(OC\mathbf{H_3})_2CH_2]_3[CCCH_3(COOCH_3)CH_2]_{11}C(CH_3CN)(CH_2)_2COO[(CH_2)_2O]_{122}CH_3$), 3.64 (s, 487H, $C_6H_5CS_2[CCH_3(COOCH_2PO(OCH_3)_2CH_2]_3[CCCH_3(COOCH_3)CH_2]_{11}C(CH_3CN)(CH_2)_2COO[(C\mathbf{H_2})_2O]_{122}CH_3$), 3.60 (s, 34H, $C_6H_5CS_2[CCH_3(COOCH_2PO(OCH_3)_2CH_2]_3[CCCH_3(COOC\mathbf{H_3})CH_2]_{11}C(CH_3CN)(CH_2)_2COO[(CH_2)_2O]_{122}CH_3$), 3.38 (s, 3H, $C_6H_5CS_2[CCH_3(COOCH_2PO(OCH_3)_2CH_2]_3[CCCH_3(COOC\mathbf{H_3})CH_2]_{11}C(CH_3CN)(CH_2)_2COO[(CH_2)_2O]_{122}CH_3$), 2.06 – 1.76 (m, 15H, $C_6H_5CS_2[CCH_3(COOCH_2PO(OCH_3)_2C\mathbf{H_2}]_3[CCCH_3(COOCH_3)C\mathbf{H_2}]_{11}C(CH_3CN)(CH_2)_2COO[(CH_2)_2O]_{122}CH_3$), 1.31 – 0.76 (m, 30H, $C_6H_5CS_2[CC\mathbf{H_3}(COOCH_2PO(OCH_3)_2CH_2]_3[CCC\mathbf{H_3}(COOCH_3)CH_2]_{11}C(CH_3CN)(CH_2)_2COO[(CH_2)_2O]_{122}CH_3$).

$^{31}$P NMR (202 MHz, $CDCl_3$) δ 21.19 (d, $C_6H_5CS_2[CCH_3(COOCH_2\mathbf{P}O(OCH_3)_2CH_2]_3[CCCH_3(COOCH_3)CH_2]_{11}C(CH_3CN)(CH_2)_2COO[(CH_2)_2O]_{122}CH_3$).

$M_{n(NMR)}$ = 7100 g mol$^{-1}$ $M_{n(GPC)}$ = 21500 g mol$^{-1}$ Đ = 1.57

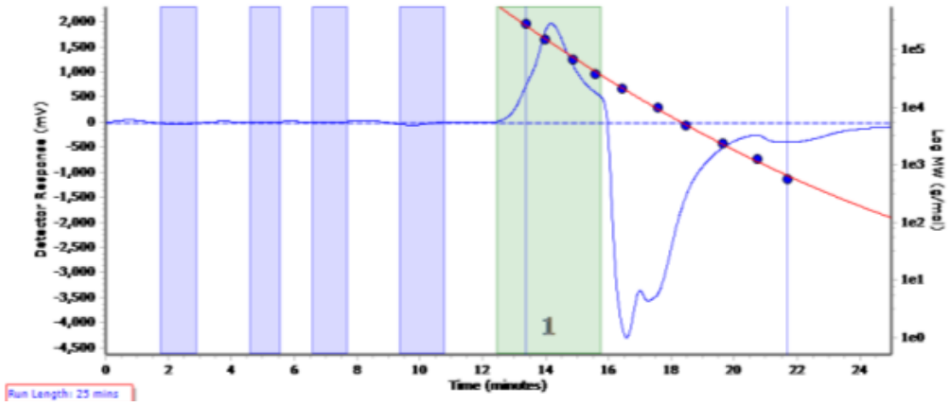


*Figure 6.63 The raw GPC of **PND2**. The blue rectangles are where the baseline was corrected to and the green rectangle is the area which the $M_n$ and Đ was calculated.*

**PD1** uses **D3**

$^1$H NMR (500 MHz, $CDCl_3$) δ 4.25 (m, 24H, $C_6H_5CS_2[CCH_3(COOC\mathbf{H_2}PO(OCH_3)_2CH_2]_{12}C(CH_3CN)(CH_2)_2COO[(CH_2)_2O]_{146}CH_3$), 3.83 (d, *J* = 10.6 Hz, 73H, $C_6H_5CS_2[CCH_3(COOCH_2PO(OC\mathbf{H_3})_2CH_2]_{12}C(CH_3CN)(CH_2)_2COO[(CH_2)_2O]_{146}CH_3$), 3.64 (m, 584H, $C_6H_5CS_2[CCH_3(COOCH_2PO(OCH_3)_2CH_2]_{12}C(CH_3CN)(CH_2)_2COO[(C\mathbf{H_2})_2O]_{146}CH_3$), 3.37 (s, 3H, $C_6H_5CS_2[CCH_3(COOCH_2PO(OCH_3)_2CH_2]_{12}C(CH_3CN)(CH_2)_2COO[(CH_2)_2O]_{146}C\mathbf{H_3}$), 2.07 – 1.84 (m, 31H, $C_6H_5CS_2[CCH_3(COOCH_2PO(OCH_3)_2C\mathbf{H_2}]_{12}C(CH_3CN)(CH_2)_2COO[(CH_2)_2O]_{146}CH_3$), 1.65 (s, 81H), 1.39 – 0.80 (m, 68H, $C_6H_5CS_2[CC\mathbf{H_3}(COOCH_2PO(OCH_3)_2CH_2]_{12}C(CH_3CN)(CH_2)_2COO[(CH_2)_2O]_{146}CH_3$).

$^{31}$P NMR (202 MHz, $CDCl_3$) δ 21.31 (d, $C_6H_5CS_2[CCH_3(COOCH_2\mathbf{P}O(OCH_3)_2CH_2]_{12}C(CH_3CN)(CH_2)_2COO[(CH_2)_2O]_{146}CH_3$)

$M_{n(NMR)}$ = 8900 g mol$^{-1}$ $M_{n(GPC)}$ = 93200 g mol$^{-1}$ Đ = 1.36

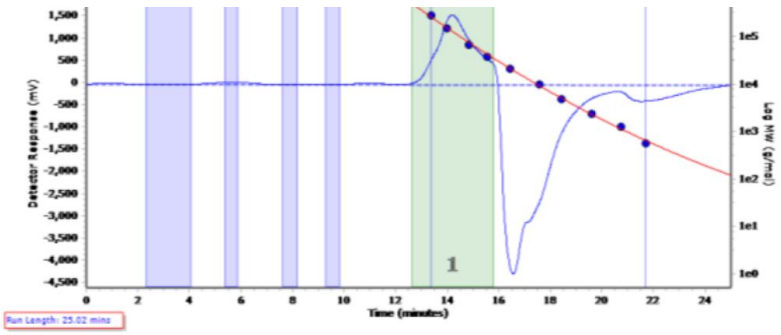


*Figure 6.64 The raw GPC of **PD1**. The blue rectangles are where the baseline was corrected to and the green rectangle is the area which the $M_n$ and Đ was calculated.*

**PD2** uses **D4**

$^1$H NMR (500 MHz, $D_2O$) δ 4.15 (s, 5H, $C_6H_5CS_2[CCH_3(COOCH_2PO(OCH_3)_2)CH_2]_{40}C(CH_3CN)(CH_2)_2CO[O(C\mathbf{H_2})_2]_{126}OCH_3$), 3.75 (m, 507H, $C_6H_5CS_2[CCH_3(COOCH_2PO(OCH_3)_2)CH_2]_{40}C(CH_3CN)(CH_2)_2CO[O(C\mathbf{H_2})_2]_{126}OCH_3$), 3.43 (s, 3H, $C_6H_5CS_2[CCH_3(COOCH_2PO(OCH_3)_2)CH_2]_{40}C(CH_3CN)(CH_2)_2CO[O(CH_2)_2]_{126}OC\mathbf{H_3}$), 3.31 – 3.12 (m, 32H, $C_6H_5CS_2[CCH_3(COOCH_2PO(OCH_3)_2)CH_2]_{40}C(CH_3CN)(CH_2)_2CO[O(CH_2)_2]_{126}OCH_3$), 3.06 – 2.89 (m, 22H, $C_6H_5CS_2[CCH_3(COOCH_2PO(OCH_3)_2)CH_2]_{40}C(CH_3CN)(CH_2)_2CO[O(CH_2)_2]_{126}OCH_3$), 2.41 – 1.89 (m, 16H, $C_6H_5CS_2[CCH_3(COOCH_2PO(OCH_3)_2)CH_2]_{40}C(CH_3CN)(CH_2)_2CO[O(CH_2)_2]_{126}OCH_3$), 1.52

– 1.16 (m, 8H, $C_6H_5CS_2[CCH_3(COOCH_2PO(OCH_3)_2)CH_2]_{40}C(CH_3CN)(CH_2)_2CO[O(CH_2)_2]_{126}OCH_3$), 1.04 – 0.85 (m, 5H, $C_6H_5CS_2[CCH_3(COOCH_2PO(OCH_3)_2)CH_2]_{40}C(CH_3CN)(CH_2)_2CO[O(CH_2)_2]_{126}OCH_3$).

$^{31}P$ NMR (202 MHz, $D_2O$) δ 15.08 ($C_6H_5CS_2[CCH_3(COOCH_2\mathbf{P}O(OCH_3)_2)CH_2]_{40}C(CH_3CN)(CH_2)_2CO[O(CH_2)_2]_{126}OCH$).

$M_{n(NMR)}$ = 14000 g mol$^{-1}$ $M_{n(\ aqGPC)}$ = 97400 g mol$^{-1}$ Đ = 1.21

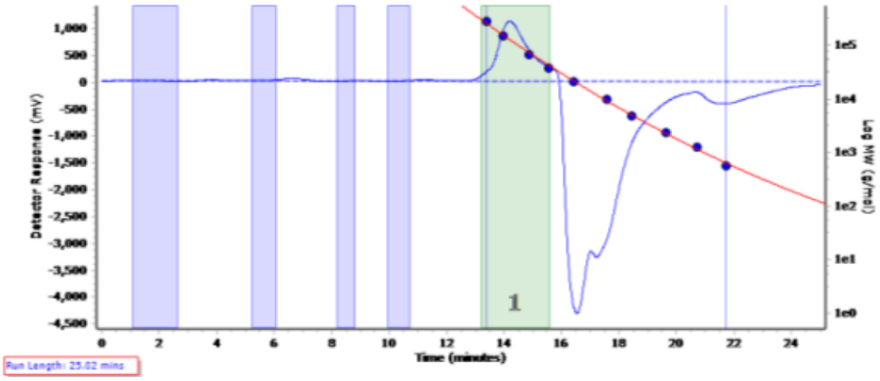


*Figure 6. 65 The raw GPC trace of **PD2**. The blue rectangles are where the baseline was corrected to and the green rectangle is the area which the $M_n$ and Đ was calculated.*

**PD3** uses **D1**

$^1H$ NMR (500 MHz, $CDCl_3$) δ 4.25 (m, 14H, $C_6H_5CS_2[CCH_3(COOC\mathbf{H_2}PO(OCH_3)_2CH_2]_7C(CH_3CN)(CH_2)_2COO[(CH_2)_2O]_{49}CH_3$), 3.84 (d, *J* = 9.3 Hz, 46H, $C_6H_5CS_2[CCH_3(COOCH_2PO(OC\mathbf{H_3})_2CH_2]_7C(CH_3CN)(CH_2)_2COO[(CH_2)_2O]_{49}CH_3$), 3.64 (m, 196H, $C_6H_5CS_2[CCH_3(COOCH_2PO(OCH_3)_2CH_2]_7C(CH_3CN)(CH_2)_2COO[(C\mathbf{H_2})_2O]_{49}CH_3$), 3.38 (s, 3H, $C_6H_5CS_2[CCH_3(COOCH_2PO(OCH_3)_2CH_2]_7C(CH_3CN)(CH_2)_2COO[(CH_2)_2O]_{49}C\mathbf{H_3}$), 2.05 – 1.83 (m, 15H, $C_6H_5CS_2[CCH_3(COOC\mathbf{H_2}PO(OCH_3)_2CH_2]_7C(CH_3CN)(CH_2)_2COO[(CH_2)_2O]_{49}CH_3$), 1.41 – 1.16 (m, 15H, $C_6H_5CS_2[CCH_3(COOCH_2PO(OCH_3)_2CH_2]_7C(CH_3CN)(CH_2)_2COO[(CH_2)_2O]_{49}CH_3$), 1.16 – 0.77 (m, 34H, $C_6H_5CS_2[CC\mathbf{H_3}(COOCH_2PO(OCH_3)_2CH_2]_7C(CH_3CN)(CH_2)_2COO[(CH_2)_2O]_{49}CH_3$).

$^{31}P$ NMR (202 MHz, $CDCl_3$) δ 21.38 (d, $C_6H_5CS_2[CCH_3(COOCH_2\mathbf{P}O(OCH_3)_2CH_2]_7C(CH_3CN)(CH_2)_2COO[(CH_2)_2O]_{49}CH_3$).

$M_{n(NMR)}$ = 3600 g mol$^{-1}$ $M_{n(GPC)}$ = 67200 g mol$^{-1}$ Đ = 1.37

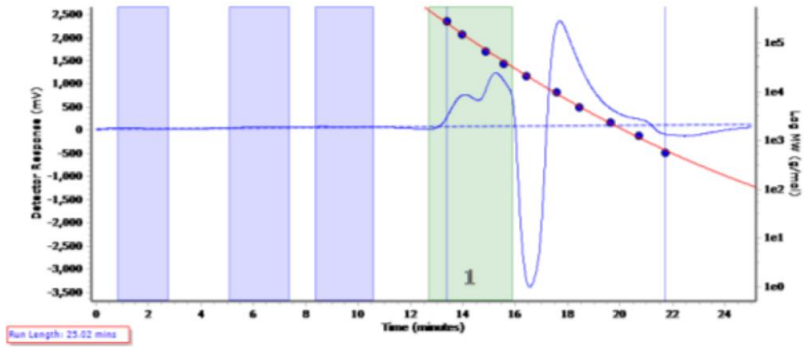


*Figure 6.66 The raw GPC trace of **PD3**. The blue rectangles are where the baseline was corrected to and the green rectangle is the area which the $M_n$ and Đ was calculated.*

**PD4** uses **D5**

$^1H$ NMR (500 MHz, $CDCl_3$) δ 4.25 (s, 12H $C_6H_5CS_2[CCH_3(COOCH_3\mathbf{CH_2}PO(OCH_3)_2CH_2]_6C(CH_3CN)(CH_2)_2COO[(CH_2)_2O]_{47}CH_3$), 3.83 (d, *J* = 10.6 Hz, 38H, $C_6H_5CS_2[CCH_3(COOCH_3\mathbf{C}H_2PO(OC\mathbf{H_3})_2CH_2]_6C(CH_3CN)(CH_2)_2COO[(CH_2)_2O]_{47}CH_3$), 3.65 (s,

188H, $C_6H_5CS_2[CCH_3(COOCH_3CH_2PO(OCH_3)_2CH_2]_6C(CH_3CN)(CH_2)_2COO[(C\mathbf{H_2})_2O]_{47}CH_3$), 3.38 (s, 3H, $C_6H_5CS_2[CCH_3(COOCH_3\mathbf{CH_2}PO(OCH_3)_2CH_2]_6C(CH_3CN)(CH_2)_2COO[(CH_2)_2O]_{47}C\mathbf{H_3}$), 2.09 – 1.72 (m, 25H, $C_6H_5CS_2[CCH_3(COOCH_3(CH_2PO(OCH_3)_2)C\mathbf{H_2}]_6C(CH_3CN)(CH_2)_2COO[(CH_2)_2O]_{47}CH_3$), 1.57 – 0.76 (m, 37H, $C_6H_5CS_2[CCH_3(COOC\mathbf{H_3}CH_2PO(OCH_3)_2CH_2]_6C(CH_3CN)(CH_2)_2COO[(CH_2)_2O]_{47}CH_3$).

$^{31}P$ NMR (202 MHz, $CDCl_3$) δ 21.41 (d, $C_6H_5CS_2[CCH_3(COOCH_3CH_2\mathbf{P}O(OCH_3)_2CH_2]_6C(CH_3CN)(CH_2)_2COO[(CH_2)_2O]_{47}CH_3$).

$M_{n(NMR)}$ = 3300 g mol$^{-1}$ $M_{n(GPC)}$ = 61700 g mol$^{-1}$ Đ = 1.31

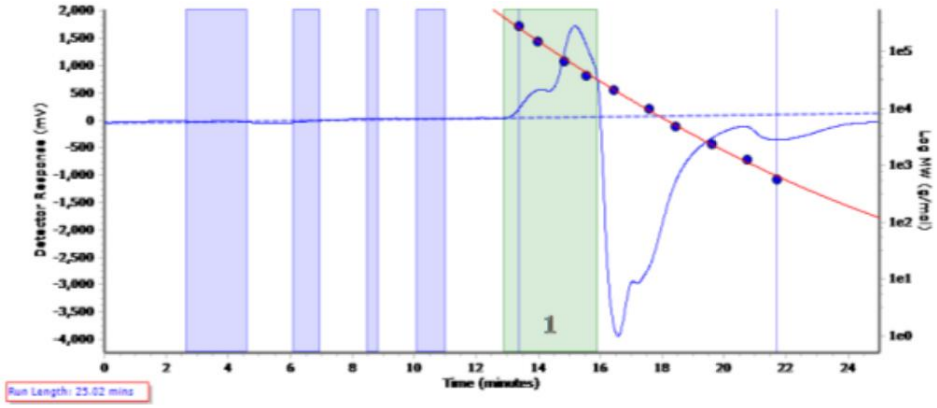


*Figure 6.67 The raw GPC trace of **PD4**. The blue rectangles are where the baseline was corrected to and the green rectangle is the area which the $M_n$ and Đ was calculated.*

**PNA1** uses **NA1**

$^1H$ NMR (500 MHz, $CD_3CO_2D$) δ 4.74 – 4.28 (m, 26H, $C_6H_5CS_2[CCCH_3(COO(C\mathbf{H_2})_2N(CH_3)_2)CH_2]_7[CCCH_3(COOCH_3)CH_2]_{12}C(CH_3CN)(CH_2)_2CO[O(CH_2)_2]_{47}OCH_3$), 3.68 (m, 186H, $C_6H_5CS_2[CCCH_3(COO(CH_2)_2N(CH_3)_2)CH_2]_7[CCCH_3(COOCH_3)CH_2]_{12}C(CH_3CN)(CH_2)_2CO[O(C\mathbf{H_2})_2]_{47}OCH_3$), 3.65 (s, 35H, $C_6H_5CS_2[CCCH_3(COO(CH_2)_2N(CH_3)_2)CH_2]_7[CCCH_3(COOC\mathbf{H_3})CH_2]_{12}C(CH_3CN)(CH_2)_2CO[O(CH_2)_2]_{47}OCH_3$), 3.39 (s, 7H, $C_6H_5CS_2[CCCH_3(COO(CH_2)_2N(CH_3)_2)CH_2]_7[CCCH_3(COOCH_3)CH_2]_{12}C(CH_3CN)(CH_2)_2CO[O(CH_2)_2]_{47}OC\mathbf{H_3}$), 3.13 – 3.00 (m, 45H, $C_6H_5CS_2[CCCH_3(COO(CH_2)_2N(C\mathbf{H_3})_2)CH_2]_{13}[CCCH_3(COOCH_3)CH_2]_{12}C(CH_3CN)(CH_2)_2CO[O(CH_2)_2]_{47}OCH_3$), 1.56 – 0.83 (m, 81H, $C_6H_5CS_2[CCC\mathbf{H_3}(COO(CH_2)_2N(CH_3)_2)CH_2]_{13}[CCC\mathbf{H_3}(COOCH_3)CH_2]_{12}C(CH_3CN)(CH_2)_2CO[O(CH_2)_2]_{47}OCH_3$).

$M_{n(NMR)}$ = 4400 g mol$^{-1}$ $M_{n(GPC)}$ = 14800 g mol$^{-1}$ Đ = 1.43

**PNE1** uses **NE1**

$^1H$ NMR (500 MHz, MeOD) δ 4.09 (s, 24H, $C_6H_5CS_2[CCCH_3(COO(C\mathbf{H_2})_2OH)CH_2]_{12}[CCCH_3(COOCH_3)CH_2]_{12}C(CH_3CN)(CH_2)_2CO[O(CH_2)_2]_{50}OCH_3$), 3.82 (s, 24H, $C_6H_5CS_2[CCCH_3(COO(C\mathbf{H_2})_2OH)CH_2]_{12}[CCCH_3(COOCH_3)CH_2]_{12}C(CH_3CN)(CH_2)_2CO[O(CH_2)_2]_{50}OCH_3$), 3.67 (m, 202H, $C_6H_5CS_2[CCCH_3(COO(CH_2)_2OH)CH_2]_{12}[CCCH_3(COOCH_3)CH_2]_{12}C(CH_3CN)(CH_2)_2CO[O(C\mathbf{H_2})_2]_{50}OCH_3$), 3.40 (s, 3H, $C_6H_5CS_2[CCCH_3(COO(CH_2)_2OH)CH_2]_{12}[CCCH_3(COOCH_3)CH_2]_{12}C(CH_3CN)(CH_2)_2CO[O(CH_2)_2]_{50}OC\mathbf{H_3}$), 2.88 – 2.42 (m, 16H, $C_6H_5CS_2[CCCH_3(COO(CH_2)_2OH)C\mathbf{H_2}]_{12}[CCCH_3(COOCH_3)C\mathbf{H_2}]_7C(CH_3CN)(CH_2)_2CO[O(CH_2)_2]_{43}OCH_3$), 2.26 – 1.86 (m, 42H, $C_6H_5CS_2[CCCH_3(COO(CH_2)_2OH)C\mathbf{H_2}]_{12}[CCCH_3(COOCH_3)C\mathbf{H_2}]_7C(CH_3CN)(CH_2)_2CO[O(CH_2)_2]_{43}OCH_3$),

1.73 – 1.48 (m, 4H, $C_6H_5CS_2[CCC\mathbf{H_3}(COO(CH_2)_2OH)CH_2]_{12}[CCC\mathbf{H_3}(COOCH_3)CH_2]_{12}C(CH_3CN)(CH_2)_2CO[O(CH_2)_2]_{50}OCH_3$), 1.40 – 0.86 (m, 72H, $C_6H_5CS_2[CCC\mathbf{H_3}(COO(CH_2)_2OH)CH_2]_{12}[CCC\mathbf{H_3}(COOCH_3)CH_2]_{12}C(CH_3CN)(CH_2)_2CO[O(CH_2)_2]_{50}OCH_3$).

$M_{n(NMR)}$ = 5000 g mol$^{-1}$ $M_{n(GPC)}$ = bimodal 10600, 80000 g mol$^{-1}$ Đ = 1.11, 1.78

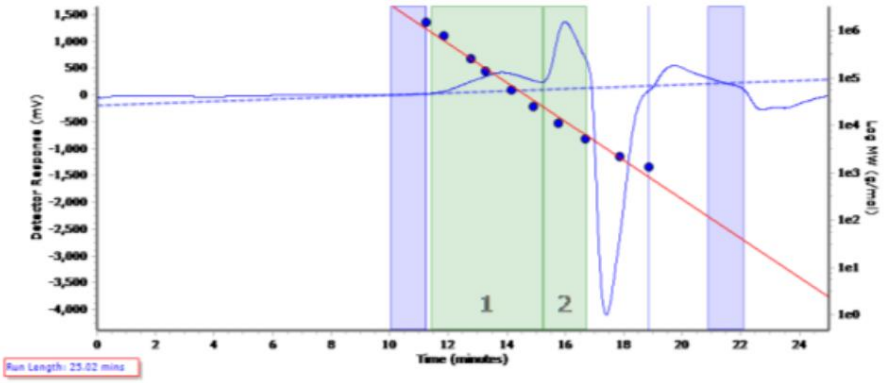


*Figure 6.68 The raw GPC of **PNE1**. The blue rectangles are where the baseline was corrected to and the green rectangles are the areas which the $M_n$ and Đ were calculated.*

**PNT1** uses **NT2**

$^1$H NMR (500 MHz, $CDCl_3$) δ 3.64 (s, 202H, $C_6H_5CS_2[CCCH_3(COO(CH_3)_3CH_2]_{10}[CCCH_3(COOCH_3)CH_2]_{12}C(CH_3CN)(CH_2)_2COO[(C\mathbf{H_2})_2O]_{50}CH_3$), 3.59 (s, 36H, $C_6H_5CS_2[CCCH_3(COO(CH_3)_3CH_2]_{10}[CCCH_3(COO\mathbf{CH_3})CH_2]_{12}C(CH_3CN)(CH_2)_2COO[(CH_2)_2O]_{50}CH_3$), 3.37 (s, 3H, $C_6H_5CS_2[CCCH_3(COO(CH_3)_3CH_2]_{10}[CCCH_3(COOCH_3)CH_2]_{12}C(CH_3CN)(CH_2)_2COO[(CH_2)_2O]_{50}C\mathbf{H_3}$), 2.13 – 1.63 (m, 60H, $C_6H_5CS_2[CCCH_3(COO(CH_3)_3C\mathbf{H_2}]_{10}[CCCH_3(COOCH_3)C\mathbf{H_2}]_{12}C(C\mathbf{H_3}CN)(C\mathbf{H_2})_2COO[(CH_2)_2O]_{50}CH_3$), 1.44 (s, 86H, $C_6H_5CS_2[CCCH_3(COO(C\mathbf{H_3})_3CH_2]_{10}[CCCH_3(COOCH_3)CH_2]_2C(CH_3CN)(CH_2)_2COO[(CH_2)_2O]_{50}CH_3$), 1.30 – 0.77 (m, 68H, $C_6H_5CS_2[CCC\mathbf{H_3}(COO(CH_3)_3CH_2]_{10}[CCC\mathbf{H_3}(COOCH_3)CH_2]_{12}C(CH_3CN)(CH_2)_2COO[(CH_2)_2O]_{50}CH_3$).

$M_{n(NMR)}$ = 4800 g mol$^{-1}$ $M_{n(GPC)}$ = 12300 g mol$^{-1}$ Đ = 1.22

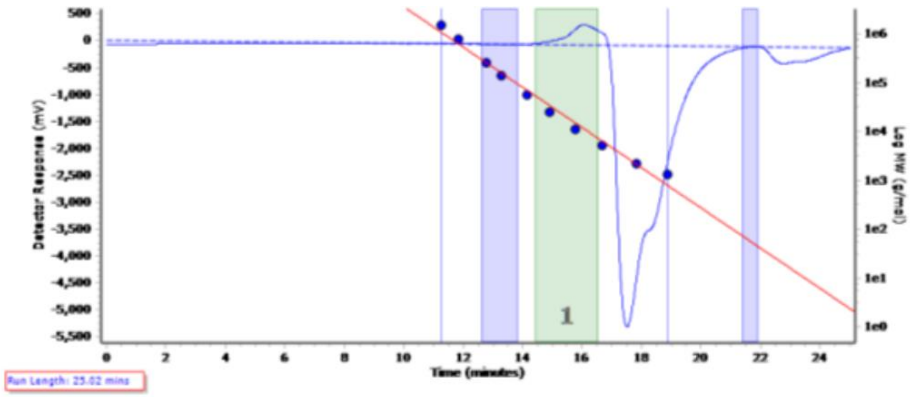


*Figure 6.69 The raw GPC of **PNT1**. The blue rectangles are where the baseline was corrected to and the green rectangle is the area which the $M_n$ and Đ was calculated.*

**PNT2** uses **NT1**

$^1$H NMR (500 MHz, $CDCl_3$) δ 3.62 (s, 191H, $C_6H_5CS_2[CCCH_3(COO(CH_3)_3CH_2]_6[CCCH_3(COOCH_3)CH_2]_{12}C(CH_3CN)(CH_2)_2COO[(CH_2)_2O]_{48}CH_3$), 3.58

(s, 36H, $C_6H_5CS_2[CCCH_3(COO(CH_3)_3CH_2]_6[CCCH_3(COO\mathbf{CH_3})CH_2]_{12}C(CH_3CN)(CH_2)_2COO[(CH_2)_2O]_{48}CH_3)$, 3.36 (s, 3H, $C_6H_5CS_2[CCCH_3(COO(CH_3)_3CH_2]_6[CCCH_3(COOCH_3)CH_2]_{12}C(CH_3CN)(CH_2)_2COO[(CH_2)_2O]_{48}C\mathbf{H_3})$, 2.12 – 1.72 (m, 34H, $C_6H_5CS_2[CCCH_3(COO(CH_3)_3CH_2]_6[CCCH_3(COOCH_3)CH_2]_{12}C(CH_3CN)(CH_2)_2COO[(CH_2)_2O]_{48}CH_3)$, 1.42 (s, 54H, $C_6H_5CS_2[CCCH_3(COO(CH_3)_3CH_2]_6[CCCH_3(COOCH_3)CH_2]_{12}C(CH_3CN)(CH_2)_2COO[(CH_2)_2O]_{48}C\mathbf{H_3})$, 1.15 – 0.76 (m, 48H, $C_6H_5CS_2[CCCH_3(COO(CH_3)_3CH_2]_6[CCCH_3(COOCH_3)CH_2]_{12}C(CH_3CN)(CH_2)_2COO[(CH_2)_2O]_{48}C\mathbf{H_3})$. $M_{n(NMR)}$ = 4200 g mol$^{-1}$ $M_{n(GPC)}$ = 15400 g mol$^{-1}$ Đ = 1.49

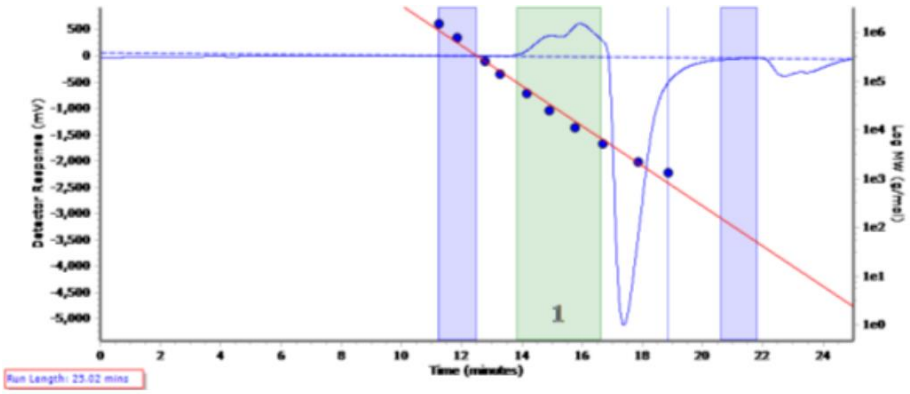


*Figure 6.70 The raw GPC of **PNT2**. The blue rectangles are where the baseline was corrected to and the green rectangle is the area which the $M_n$ and Đ was calculated.*

**PT1** uses **T1**

$^1$H NMR (500 MHz, $CDCl_3$) δ 3.63 (m, 186H, $C_6H_5CS_2[CCCH_3(COOC(CH_3)_3)CH_2]_{21}C(CH_3CN)(CH_2)_2CO[O((C\mathbf{H_2})_2)]_{47}OCH_3)$, 3.37 (s, 3H. $C_6H_5CS_2[CCCH_3(COOC(CH_3)_3)CH_2]_{21}C(CH_3CN)(CH_2)_2CO[O((C\mathbf{H_2})_2)]_{47}OC\mathbf{H_3})$, 2.18 – 1.71 (m, 43H, $C_6H_5CS_2[CCCH_3(COOC(CH_3)_3)C\mathbf{H_2}]_{21}C(CH_3CN)(CH_2)_2CO[O((C\mathbf{H_2})_2)]_{47}OCH_3)$, 1.57 – 1.22 (m, 186H, $C_6H_5CS_2[CCCH_3(COOC(C\mathbf{H_3})_3)CH_2]_{21}C(CH_3CN)(CH_2)_2CO[O((C\mathbf{H_2})_2)]_{47}OCH_3)$, 1.18 – 0.93 (m, 53H, $C_6H_5CS_2[CCC\mathbf{H_3}(COOC(CH_3)_3)CH_2]_{21}C(CH_3CN)(CH_2)_2CO[O((C\mathbf{H_2})_2)]_{47}OCH_3)$.

$M_{n(NMR)}$ = 5100 g mol$^{-1}$ $M_{n(GPC)}$ = 3100 g mol$^{-1}$ Đ = 1.05

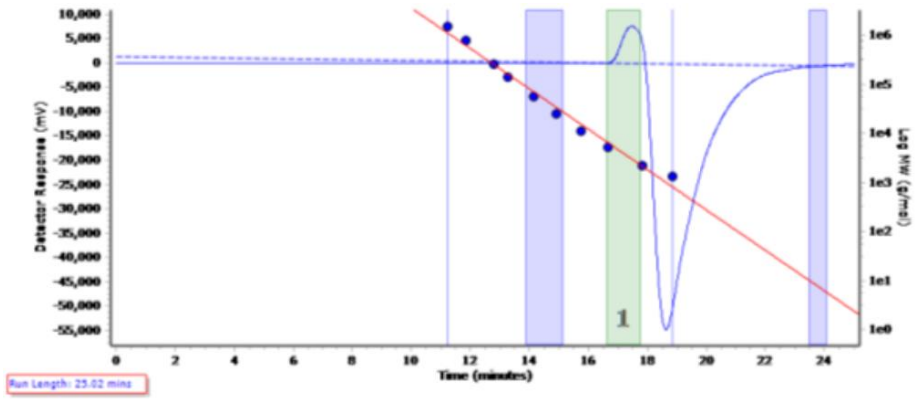


*Figure 6.71 The raw GPC of **PT1**. The blue rectangles are where the baseline was corrected to and the green rectangle is the area which the $M_n$ and Đ was calculated.*

## 6.17. Representative deprotection of the phosphorous containing polymer

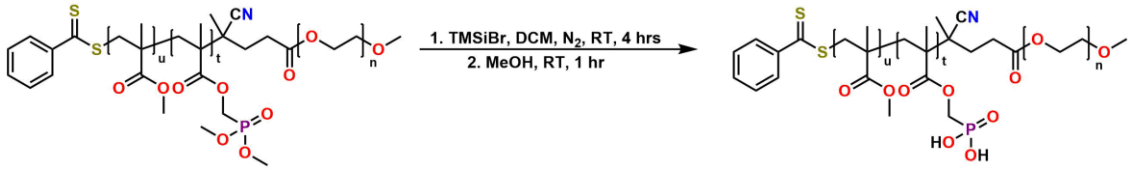


*Figure 6.72 A schematic shows the deprotection of polyphosphonates using trimethylsiyl bromide.*

TMSBr (0.147 g, 0.962 mmol, 2 molar equivalences in respect to number of MAPC1 units) was added to a solution of polymer (0.100 g, 0.0272 mmol) in anhydrous dichloromethane (1.33 $cm^3$, 15.6 mmol) and stirred for 4 hours at room temperature. After 4 hours, the mixture was concentrated under reduced pressure and methanol (3.96 $cm^3$, 12.3 mmol) was added and the mixture was stirred for 1 hour at room temperature. The mixture was dialyzed for 24 hours against water and then lyophilized. The $M_{n(NMR)}$ was calculated subtracting $M_n$ of the two methyl groups of the phosphonate from the $M_{n(NMR)}$ of the deprotected polymer precursor.

**PNF1** uses **PND1**

$^1$H NMR (500 MHz, MeOD) δ 4.20 (s, 9H, $[CCH_3(COOCH_2PO(O\mathbf{H})_2CH_2]_{10}[CCCH_3(COOCH_3)CH_2]_{19}C(CH_3CN)(CH_2)_2COO[(CH_2)_2O]_{140}CH_3$), 3.68 (m, 560H, $[CCH_3(COOC\mathbf{H_2}PO(OH)_2CH_2]_{10}[CCCH_3(COOCH_3)CH_2]_{19}C(CH_3CN)(CH_2)_2COO[(C\mathbf{H_2})_2O]_{140}CH_3$), 3.40 (s, 3H, $[CCH_3(COOCH_2PO(OH)_2CH_2]_{10}[CCCH_3(COOCH_3)CH_2]_{19}C(CH_3CN)(CH_2)_2COO[(CH_2)_2O]_{140}C\mathbf{H_3}$), 2.39 – 1.75 (m, 20H, $[CCH_3(COOCH_2PO(OH)_2C\mathbf{H_2}]_{10}[CCCH_3(COOCH_3)CH_2]_{19}C(CH_3CN)(CH_2)_2COO[(CH_2)_2O]_{140}CH_3$), 1.46 – 0.72 (m, 39H, $[CC\mathbf{H_3}(COOCH_2PO(OH)_2CH_2]_{10}[CCCH_3(COOCH_3)CH_2]_{19}C(CH_3CN)(CH_2)_2COO[(CH_2)_2O]_{140}CH_3$).

$M_{n(NMR)}$ = 9800 g $mol^{-1}$

**PNF2** uses **PND2**

$^1$H NMR (500 MHz, $D_2O$) δ 4.21 (bs, 14H, $[CCH_3(COOCH_2PO(O\mathbf{H})_2CH_2]_3[CCCH_3(COOCH_3)CH_2]_{11}C(CH_3CN)(CH_2)_2COO[(CH_2)_2O]_{140}CH_3$), 3.76 (m, 576H, $[CCH_3(COOCH_2PO(OH)_2CH_2]_3[CCCH_3(COOCH_3)CH_2]_{11}C(CH_3CN)(CH_2)_2COO[(C\mathbf{H_2})_2O]_{140}CH_3$), 3.43 (s, 3H, $[CCH_3(COOCH_2PO(OH)_2CH_2]_3[CCCH_3(COOCH_3)CH_2]_{11}C(CH_3CN)(CH_2)_2COO[(CH_2)_2O]_{140}C\mathbf{H_3}$), 3.32 – 3.12 (m, 6H, $[CCH_3(COOCH_2PO(OH)_2C\mathbf{H_2}]_3[CCCH_3(COOCH_3)C\mathbf{H_2}]_{11}C(CH_3CN)(CH_2)_2COO[(CH_2)_2O]_{140}CH_3$), 2.48 – 1.72 (m, 21H, $[CCH_3(COOCH_2PO(OH)_2CH_2]_3[CCCH_3(COOCH_3)CH_2]_{11}C(CH_3CN)(CH_2)_2COO[(CH_2)_2O]_{140}CH_3$), 1.45 – 0.75 (m, 40H, $[CC\mathbf{H_3}(COOCH_2PO(OH)_2CH_2]_3[CCC\mathbf{H_3}(COOCH_3)CH_2]_{11}C(CH_3CN)(CH_2)_2COO[(CH_2)_2O]_{140}CH_3$).

$^{31}$P NMR (202 MHz, $D_2O$) δ 5.27 ($[CCH_3(COOCH_2\mathbf{P}O(OH)_2CH_2]_3[CCCH_3(COOCH_3)CH_2]_{11}C(CH_3CN)(CH_2)_2COO[(CH_2)_2O]_{140}CH_3$.

$M_{n(NMR)}$ = 7800 g $mol^{-1}$

**PFN1** uses **PDN1**

$^{1}$H NMR (500 MHz, $D_2O$) δ 4.32 (s, 38H, $C_6H_5CS_2[CCCH_3(COOCH_3)CH_2]_{22}[CCH_3(COOCH_2PO(O\mathbf{H})_2CH_2]_7C(CH_3CN)(CH_2)_2COO[(CH_2)_2O]_{49}CH_3$), 3.76 (m, 208H, $C_6H_5CS_2[CCCH_3(COOCH_3)CH_2]_{22}[CCH_3(COOCH_2PO(OH)_2CH_2]_7C(CH_3CN)(CH_2)_2COO[(C\mathbf{H_2})_2O]_{49}CH_3$), 3.44 (s, 3H, $C_6H_5CS_2[CCCH_3(COOCH_3)CH_2]_{22}[CCH_3(COOCH_2PO(OH)_2CH_2]_7C(CH_3CN)(CH_2)_2COO[(CH_2)_2O]_{49}C\mathbf{H_3}$), 2.47 – 1.65 (m, 51H, $C_6H_5CS_2[CCCH_3(COOCH_3)C\mathbf{H_2}]_{22}[CCH_3(COOCH_2PO(OH)_2C\mathbf{H_2}]_7C(CH_3CN)(CH_2)_2COO[(CH_2)_2O]_{49}CH_3$), 1.65 – 0.69 (m, 65H, $C_6H_5CS_2[CCC\mathbf{H_3}(COOCH_3)CH_2]_{22}[CC\mathbf{H_3}(COOCH_2PO(OH)_2CH_2]_7C(CH_3CN)(CH_2)_2COO[(CH_2)_2O]_{49}CH_3$ ).

$M_{n(NMR)}$ = 5600 g mol$^{-1}$

**PFN2** uses **PDN2**

$^{1}$H NMR (500 MHz, $D_2O$) δ 4.15 (s, 15H, $C_6H_5CS_2[CCCH_3(COOCH_3)CH_2]_{15}[CCH_3(COOCH_2PO(O\mathbf{H})_2CH_2]_{12}C(CH_3CN)(CH_2)_2COO[(CH_2)_2O]_{146}CH_3$), 3.75 (m, 588H, $C_6H_5CS_2[CCCH_3(COOCH_3)CH_2]_{15}[CCH_3(COOCH_2PO(OH)_2CH_2]_{12}C(CH_3CN)(CH_2)_2COO[(C\mathbf{H_2})_2O]_{146}CH_3$), 3.43 (s, 3H, $C_6H_5CS_2[CCCH_3(COOCH_3)CH_2]_{15}[CCH_3(COOCH_2PO(OH)_2CH_2]_{12}C(CH_3CN)(CH_2)_2COO[(CH_2)_2O]_{146}C\mathbf{H_3}$), 3.21 (m, 37H, $C_6H_5CS_2[CCCH_3(COOCH_3)CH_2]_{15}[CCH_3(COOCH_2PO(OH)_2CH_2]_{12}C(CH_3CN)(CH_2)_2COO[(CH_2)_2O]_{146}CH_3$), 2.93 (s, 29H, $C_6H_5CS_2[CCCH_3(COOCH_3)CH_2]_{15}[CCH_3(COOCH_2PO(OH)_2CH_2]_{12}C(CH_3CN)(CH_2)_2COO[(CH_2)_2O]_{146}CH_3$), 2.10 (s, 31H, $C_6H_5CS_2[CCCH_3(COOCH_3)C\mathbf{H_2}]_{15}[CCH_3(COOCH_2PO(OH)_2C\mathbf{H_2}]_{12}C(CH_3CN)(CH_2)_2COO[(CH_2)_2O]_{146}CH_3$), 1.01 (s, 58H, $C_6H_5CS_2[CCC\mathbf{H_3}(COOCH_3)CH_2]_{15}[CC\mathbf{H_3}(COOCH_2PO(OH)_2CH_2]_{12}C(CH_3CN)(CH_2)_2COO[(CH_2)_2O]_{146}CH_3$)

$M_{n(NMR)}$ = 10300 g mol$^{-1}$

**PF1** uses **PD4**

$^{1}$H NMR (500 MHz, $D_2O$) δ 4.26 (s, 527H, $C_6H_5CS_2[CCH_3(COOCH_3CH_2PO(OH)_2CH_2]_5C(CH_3CN)(CH_2)_2COO[(C\mathbf{H_2})_2O]_{38}CH_3$), 2.35 – 1.61 (m, 639H, $C_6H_5CS_2[CCH_3(COOCH_3CH_2PO(OH)_2C\mathbf{H_2}]_5C(CH_3CN)(CH_2)_2COO[(CH_2)_2O]_{38}CH_3$), 1.38 – 0.65 (m, 1017H, $C_6H_5CS_2[CCH_3(COOC\mathbf{H_3}CH_2PO(OH)_2CH_2]_5C(CH_3CN)(CH_2)_2COO[(CH_2)_2O]_{38}CH_3$).

$^{31}$P NMR (202 MHz, $D_2O$) δ 16.46 ($C_6H_5CS_2[CCH_3(COOCH_3CH_2\mathbf{P}O(OH)_2CH_2]_5C(CH_3CN)(CH_2)_2COO[(CH_2)_2O]_{38}CH_3$.

$M_{n(NMR)}$ = 3100 g mol$^{-1}$

## 6.18. Representitive deprotection of pTBuMA polymers

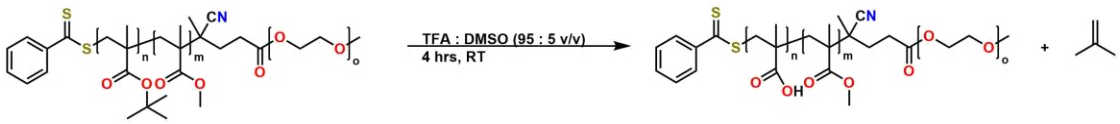


*Figure 6.73 Schematic showing a representive deprotection of PTBuMA-b-PMMA-b-PEG.*

The polymer (0.100 g) was dissolved in DMSO (0.250 $cm^3$, 3.52 mmol) and then TFA (4.75 $cm^3$, 0.0621 mol) so that the final concentration of polymer was 20 mg $cm^{-3}$ in 5 / 95 (v/v) DMSO / TFA. The mixture was stirred for 3 hrs at room temperature before the TFA was removed at reduced pressure with dioxane (3 x 2 $cm^3$). Deionised water (4 $cm^3$) was added to the polymer and slowing basified with 10 M NaOH. Then the mixture was washed with EtOAc (3 x 4 $cm^3$) and the aqueous solution was collected and dialysed against water for 24 hrs before being lyophilised. The $M_{n(NMR)}$ was calculated subtracting $M_n$ of the *tert*-butyl group of the PTBuMA from the $M_{n(NMR)}$ of the deprotected polymer precursor.

**PNQ1** uses **PNT2**

$^1H$ NMR (500 MHz, $D_2O$) δ 3.76 (m, 188H, $C_6H_5CS_2[CCCH_3(COOH)CH_2]_6[CCCH_3(COOCH_3)CH_2]_{12}C(CH_3CN)(CH_2)_2COO[(C\mathbf{H_2})_2O]_{48}CH_3$), 3.43 (s, 3H, $C_6H_5CS_2[CCCH_3(COOH)CH_2]_6[CCCH_3(COOCH_3)CH_2]_{12}C(CH_3CN)(CH_2)_2COO[(CH_2)_2O]_{48}C\mathbf{H_3}$), 1.38 – 0.85 (m, 9H, $C_6H_5CS_2[CCC\mathbf{H_3}(COOH)CH_2]_6[CCCH_3(COOC\mathbf{H_3})CH_2]_{12}C(CH_3CN)(CH_2)_2COO[(CH_2)_2O]_{48}CH_3$).

$M_{n(NMR)}$ = 3800 g $mol^{-1}$

**PNQ2** uses **PNT1**

$^1H$ NMR (500 MHz, $D_2O$) δ 3.74 (m, 197H, $C_6H_5CS_2[CCCH_3(COO(OH)CH_2]_{10}[CCCH_3(COOCH_3)CH_2]_{12}C(CH_3CN)(CH_2)_2COO[(C\mathbf{H_2})_2O]_{50}CH_3$), 3.42 (s, 3H. $C_6H_5CS_2[CCCH_3(COO(OH)CH_2]_{10}[CCCH_3(COOCH_3)CH_2]_{12}C(CH_3CN)(CH_2)_2COO[(CH_2)_2O]_{50}C\mathbf{H_3}$), 2.15 – 1.59 (m, 46H, $C_6H_5CS_2[CCCH_3(COO(OH)C\mathbf{H_2}]_{10}[CCCH_3(COOCH_3)C\mathbf{H_2}]_{12}C(CH_3CN)(CH_2)_2COO[(CH_2)_2O]_{50}CH_3$), 1.42 – 0.75 (m, 44H, $C_6H_5CS_2[CCC\mathbf{H_3}(COO(OH)CH_2]_{10}[CCC\mathbf{H_3}(COOCH_3)CH_2]_{12}C(CH_3CN)(CH_2)_2COO[(CH_2)_2O]_{50}CH_3$)

$M_{n(NMR)}$ = 4300 g $mol^{-1}$

**PQN1** uses **PTN1**

$V_{max}$ / $cm^{-1}$ 3340 (OH, bs), (1674, C=O), (1539, C=O), 1435($CH_3$), (1184, C-O), (1130, C-O)

$C_6H_5CS_2[CCC\mathbf{H_3}(COOCH_3)CH_2]_{16}[CCH_3(COOH)CH_2]_{21}C(CH_3CN)(CH_2)_2COO[(CH_2)_2O]_{47}CH_3$)

$M_n$= 4300 g $mol^{-1}$

# Bibliography


1 Y. Yin, S. Yun, J. Fang and H. Chen, *Chem. Commun.*, 2009, 5892.

2 Y. Wang, K. Lin, C. Wu, X. Liu and J. Chang, *J. Mater. Chem. B*, 2014, **3**, 65–71.

3 E. Beniash, J. P. Simmer and H. C. Margolis, *J. Struct. Biol.*, 2005, **149**, 182–190.

4 Q. Ruan and J. Moradian-Oldak, *J. Mater. Chem. B*, 2015, **3**, 3112–3129.

5 S. H. João-Souza, A. Lussi, T. Baumann, T. Scaramucci, A. C. C. Aranha and T. S. Carvalho, *Sci. Rep.*, 2017, **7**, 1–8.

6 K. R. Jain and N. C. Chauhan, *Dental Image Analysis for Disease Diagnosis*, Springer International Publishing, Cham, 2019.

7 S. Busch, U. Schwarz and R. Kniep, *Chem. Mater.*, 2001, 13, 3260–3271.

8 J. P. Simmer and A. G. Fincham, *Crit. Rev. Oral Biol. Med.*, 1995, **6**, 84–108.

9 C. Combes, S. Cazalbou and C. Rey, *Minerals*, 2016, **6**, 1–25.

10 S. V. Dorozhkin, *J. Colloid Interface Sci.*, 1997, **191**, 489–497.

11 X. Li, J. Wang, A. Joiner and J. Chang, *J. Dent.*, 2014, **42**, S12–S20.

12 E. A. A. Neel, A. Aljabo, A. Strange, S. Ibrahim, M. Coathup, A. M. Young, L. Bozec and V. Mudera, *Int. J. Nanomedicine*, 2016, **11**, 4743–4763.

13 J. D. Featherstone and A. Lussi, *Monogr. oral Sci.*, 2006, **20**, 66–76.

14 J. Menanteau, D. Mitre and G. Daculsi, *Calcif. Tissue Int.*, 1984, **36**, 677–681.

15 K. Yamagishi, K. Onuma, T. Suzuki, F. Okada, J. Tagami, M. Otsuki and P. Senawangse, *Nature*, 2005, **433**, 819.

16 S. Habelitz, S. J. Marshall, G. W. Marshall and M. Balooch, *Arch. Oral Biol.*, 2001, **46**, 173–183.

17 J. J. De Yoreo, P. U. P. A. Gilbert, N. A. J. M. Sommerdijk, R. L. Penn, S. Whitelam, D. Joester, H. Zhang, J. D. Rimer, A. Navrotsky, J. F. Banfield, A. F. Wallace, F. M. Michel, F. C. Meldrum, H. Colfen and P. M. Dove, *Science (80-. ).*, 2015, **349**, aaa6760–aaa6760.

18 P. R. Ten Wolde and D. Frenkel, *Phys. Chem. Chem. Phys.*, 1999, **1**, 2191–2196.

19 W. J. E. M. Habraken, J. Tao, L. J. Brylka, H. Friedrich, L. Bertinetti, A. S. Schenk, A. Verch, V. Dmitrovic, P. H. H. Bomans, P. M. Frederik, J. Laven, P. van der Schoot, B. Aichmayer, G. de With, J. J. DeYoreo and N. A. J. M. Sommerdijk, *Nat. Commun.*, 2013, **4**, 1507.

20 C. Robinson, P. Fuchs, D. Deutsch and J. A. Weatherell, *Caries Res.*, 1978, **12**, 1–11.

21 C. E. Smith, *Crit. Rev. Oral Biol. Med.*, 1998, **9**, 128–161.

22 J. Moradian-Oldak, *Front. Biosci.*, 2012, **17**, 1996.

23 X. Zhang, B. E. Ramirez, X. Liao and T. G. H. Diekwisch, *PLoS One*, 2011, **6**, e24952.

24 J. Moradian-Oldak, I. Jimenez, D. Maltby and A. G. Fincham, *Biopolymers*, 2001, **58**, 606–616.

25 Z. Sun, D. Fan, Y. Fan, C. Du and J. Moradian-Oldak, *J. Dent. Res.*, 2008, **87**, 1133–1137.

26 D. L. Masica, J. J. Gray and W. J. Shaw, *J. Phys. Chem. C*, 2011, **115**, 13775–13785.

27 J. Lu, Y. S. Xu and W. J. Shaw, *Biochemistry*, 2013, **52**, 2196–2205.

28 A. George and A. Veis, *Chem. Rev.*, 2008, **108**, 4670–4693.

29 N. Philip, *Caries Res.*, 2019, **53**, 284–295.

30 T. Vos, A. A. Abajobir, K. H. Abate, C. Abbafati, K. M. Abbas, F. Abd-Allah, R. S. Abdulkader, A. M. Abdulle, T. A. Abebo, S. F. Abera, V. Aboyans, L. J. Abu-Raddad, I. N. Ackerman, A. A. Adamu, O. Adetokunboh, M. Afarideh, A. Afshin, S. K. Agarwal, R. Aggarwal, A. Agrawal, S. Agrawal, H. Ahmadieh, M. B. Ahmed, M. T. E. Aichour, A. N. Aichour, I. Aichour, S. Aiyar, R. O. Akinyemi, N. Akseer, F. H. Al Lami, F. Alahdab, Z. Al-Aly, K. Alam, N. Alam, T. Alam, D. Alasfoor, K. A. Alene, R. Ali, R. Alizadeh-Navaei, A. Alkerwi, F. Alla, P. Allebeck, C. Allen, F. Al-Maskari, R. Al-Raddadi, U. Alsharif, S. Alsowaidi, K. A. Altirkawi, A. T. Amare, E. Amini, W. Ammar, Y. A. Amoako, H. H. Andersen, C. A. T. Antonio, P. Anwari, J. Ärnlöv, A. Artaman, K. K. Aryal, H. Asayesh, S. W. Asgedom, R. Assadi, T. M. Atey, N. T. Atnafu, S. R. Atre, L. Avila-Burgos, E. F. G. A. Avokphako, A. Awasthi, U. Bacha, A. Badawi, K. Balakrishnan, A. Banerjee, M. S. Bannick, A. Barac, R. M. Barber, S. L. Barker-Collo, T. Bärnighausen, S. Barquera, L. Barregard, L. H. Barrero, S. Basu, B. Battista, K. E. Battle, B. T. Baune, S. Bazargan-Hejazi, J. Beardsley, N. Bedi, E. Beghi, Y. Béjot, B. B. Bekele, M. L. Bell, D. A. Bennett, I. M. Bensenor, J. Benson, A. Berhane, D. F. Berhe, E. Bernabé, B. D. Betsu, M. Beuran, A. S. Beyene, N. Bhala, A. Bhansali, S. Bhatt, Z. A. Bhutta, S. Biadgilign, B. K. Bicer, K. Bienhoff, B. Bikbov, C. Birungi, S. Biryukov, D. Bisanzio, H. M. Bizuayehu, D. J. Boneya, S. Boufous, R. R. A. Bourne, A. Brazinova, T. S. Brugha, R. Buchbinder, L. N. B. Bulto, B. R. Bumgarner, Z. A. Butt, L. Cahuana-Hurtado, E. Cameron, M. Car, H. Carabin, J. R. Carapetis, R. Cárdenas, D. O. Carpenter, J. J. Carrero, A. Carter, F. Carvalho, D. C. Casey, V. Caso, C. A. Castañeda-Orjuela, C. D. Castle, F. Catalá-López, H.-Y. Chang, J.-C. Chang, F. J. Charlson, H. Chen, M. Chibalabala, C. E. Chibueze, V. H. Chisumpa, A. A. Chitheer, D. J. Christopher, L. G. Ciobanu, M. Cirillo, D. Colombara, C. Cooper, P. A. Cortesi, M. H. Criqui, J. A. Crump, A. F. Dadi, K. Dalal, L. Dandona, R. Dandona, J. das Neves, D. V Davitoiu, B. de Courten, D. De De Leo, B. K. Defo, L. Degenhardt, S. Deiparine, R. P. Dellavalle, K. Deribe, D. C. Des Jarlais, S. Dey, S. D. Dharmaratne, P. K. Dhillon, D. Dicker, E. L. Ding, S. Djalalinia, H. P. Do, E. R. Dorsey, K. P. B. dos Santos, D. Douwes-Schultz, K. E. Doyle, T. R. Driscoll, M. Dubey, B. B. Duncan, Z. Z. El-Khatib, J. Ellerstrand, A. Enayati, A. Y. Endries, S. P. Ermakov, H. E. Erskine, B. Eshrati, S. Eskandarieh, A. Esteghamati, K. Estep, F. B. B. Fanuel, C. S. E. S. Farinha, A. Faro, F. Farzadfar, M. S. Fazeli, V. L. Feigin, S.-M. Fereshtehnejad, J. C. Fernandes, A. J. Ferrari, T. R. Feyissa, I. Filip, F. Fischer, C. Fitzmaurice, A. D. Flaxman, L. S. Flor, N. Foigt, K. J. Foreman, R. C. Franklin, N. Fullman, T. Fürst, J. M. Furtado, N. D. Futran, E. Gakidou, M. Ganji, A. L. Garcia-Basteiro, T. Gebre, T. T. Gebrehiwot, A. Geleto, B. L. Gemechu, H. A. Gesesew, P. W. Gething, A. Ghajar, K. B. Gibney, P. S. Gill, R. F. Gillum, I. A. M. Ginawi, A. Z. Giref, M. D. Gishu, G. Giussani, W. W. Godwin, A. L. Gold, E. M. Goldberg, P. N. Gona, A. Goodridge, S. V. Gopalani, A. Goto, A. C. Goulart, M. Griswold, H. C. Gugnani, R. Gupta, R. Gupta, T. Gupta, V. Gupta, N. Hafezi-Nejad, G. B. Hailu, A. D. Hailu, R. R. Hamadeh, S. Hamidi, A. J. Handal, G. J. Hankey, S. W. Hanson, Y. Hao, H. L. Harb, H. A. Hareri, J. M. Haro, J. Harvey, M. S. Hassanvand, R. Havmoeller, C. Hawley, S. I. Hay, R. J. Hay, N. J. Henry, I. B. Heredia-Pi, J. M. Hernandez, P. Heydarpour, H. W. Hoek, H. J. Hoffman, N. Horita, H. D. Hosgood, S. Hostiuc, P. J. Hotez, D. G. Hoy, A. S. Htet, G. Hu, H. Huang, C. Huynh, K. M. Iburg, E. U. Igumbor, C. Ikeda, C. M. S. Irvine, K. H. Jacobsen, N. Jahanmehr, M. B. Jakovljevic, S. K. Jassal, M. Javanbakht, S. P. Jayaraman, P. Jeemon, P. N. Jensen, V. Jha, G. Jiang, D. John, S. C. Johnson, C. O. Johnson, J. B. Jonas, M. Jürisson, Z. Kabir, R. Kadel, A. Kahsay, R. Kamal, H. Kan, N. E. Karam, A. Karch, C. K. Karema, A. Kasaeian, G. M. Kassa, N. A. Kassaw, N. J. Kassebaum, A. Kastor, S. V. Katikireddi, A. Kaul, N. Kawakami, P. N. Keiyoro, A. P. Kengne, A. Keren, Y. S. Khader, I. A. Khalil, E. A. Khan, Y.-H. Khang, A. Khosravi, J. Khubchandani, A. A. Kiadaliri, C. Kieling, Y. J. Kim, D. Kim, P. Kim, R. W.

Kimokoti, Y. Kinfu, A. Kisa, K. A. Kissimova-Skarbek, M. Kivimaki, A. K. Knudsen, Y. Kokubo, D. Kolte, J. A. Kopec, S. Kosen, P. A. Koul, A. Koyanagi, M. Kravchenko, S. Krishnaswami, K. J. Krohn, G. A. Kumar, P. Kumar, S. Kumar, H. H. Kyu, D. K. Lal, R. Lalloo, N. Lambert, Q. Lan, A. Larsson, P. M. Lavados, J. L. Leasher, P. H. Lee, J.-T. Lee, J. Leigh, C. T. Leshargie, J. Leung, R. Leung, M. Levi, Y. Li, Y. Li, D. Li Kappe, X. Liang, M. L. Liben, S. S. Lim, S. Linn, P. Y. Liu, A. Liu, S. Liu, Y. Liu, R. Lodha, G. Logroscino, S. J. London, K. J. Looker, A. D. Lopez, S. Lorkowski, P. A. Lotufo, N. Low, R. Lozano, T. C. D. Lucas, E. R. K. Macarayan, H. Magdy Abd El Razek, M. Magdy Abd El Razek, M. Mahdavi, M. Majdan, R. Majdzadeh, A. Majeed, R. Malekzadeh, R. Malhotra, D. C. Malta, A. A. Mamun, H. Manguerra, T. Manhertz, A. Mantilla, L. G. Mantovani, C. C. Mapoma, L. B. Marczak, J. Martinez-Raga, F. R. Martins-Melo, I. Martopullo, W. März, M. R. Mathur, M. Mazidi, C. McAlinden, M. McGaughey, J. J. McGrath, M. McKee, C. McNellan, S. Mehata, M. M. Mehndiratta, T. C. Mekonnen, P. Memiah, Z. A. Memish, W. Mendoza, M. A. Mengistie, D. T. Mengistu, G. A. Mensah, T. J. Meretoja, A. Meretoja, H. B. Mezgebe, R. Micha, A. Millear, T. R. Miller, E. J. Mills, M. Mirarefin, E. M. Mirrakhimov, A. Misganaw, S. R. Mishra, P. B. Mitchell, K. A. Mohammad, A. Mohammadi, K. E. Mohammed, S. Mohammed, S. K. Mohanty, A. H. Mokdad, S. K. Mollenkopf, L. Monasta, M. Montico, M. Moradi-Lakeh, P. Moraga, R. Mori, C. Morozoff, S. D. Morrison, M. Moses, C. Mountjoy-Venning, K. B. Mruts, U. O. Mueller, K. Muller, M. E. Murdoch, G. V. S. Murthy, K. I. Musa, J. B. Nachega, G. Nagel, M. Naghavi, A. Naheed, K. S. Naidoo, L. Naldi, V. Nangia, G. Natarajan, D. E. Negasa, R. I. Negoi, I. Negoi, C. R. Newton, J. W. Ngunjiri, T. H. Nguyen, Q. Le Nguyen, C. T. Nguyen, G. Nguyen, M. Nguyen, E. Nichols, D. N. A. Ningrum, S. Nolte, V. M. Nong, B. Norrving, J. J. N. Noubiap, M. J. O'Donnell, F. A. Ogbo, I.-H. Oh, A. Okoro, O. Oladimeji, T. O. Olagunju, A. T. Olagunju, H. E. Olsen, B. O. Olusanya, J. O. Olusanya, K. Ong, J. N. Opio, E. Oren, A. Ortiz, A. Osgood-Zimmerman, M. Osman, M. O. Owolabi, M. PA, R. E. Pacella, A. Pana, B. K. Panda, C. Papachristou, E.-K. Park, C. D. Parry, M. Parsaeian, S. B. Patten, G. C. Patton, K. Paulson, N. Pearce, D. M. Pereira, N. Perico, K. Pesudovs, C. B. Peterson, M. Petzold, M. R. Phillips, D. M. Pigott, J. D. Pillay, C. Pinho, D. Plass, M. A. Pletcher, S. Popova, R. G. Poulton, F. Pourmalek, D. Prabhakaran, N. M. Prasad, N. Prasad, C. Purcell, M. Qorbani, R. Quansah, B. P. A. Quintanilla, R. H. S. Rabiee, A. Radfar, A. Rafay, K. Rahimi, A. Rahimi-Movaghar, V. Rahimi-Movaghar, M. H. U. Rahman, M. Rahman, R. K. Rai, S. Rajsic, U. Ram, C. L. Ranabhat, Z. Rankin, P. C. Rao, P. V. Rao, S. Rawaf, S. E. Ray, R. C. Reiner, N. Reinig, M. B. Reitsma, G. Remuzzi, A. M. N. Renzaho, S. Resnikoff, S. Rezaei, A. L. Ribeiro, L. Ronfani, G. Roshandel, G. A. Roth, A. Roy, E. Rubagotti, G. M. Ruhago, S. Saadat, N. Sadat, M. Safdarian, S. Safi, S. Safiri, R. Sagar, R. Sahathevan, J. Salama, H. O. B. Saleem, J. A. Salomon, S. S. Salvi, A. M. Samy, J. R. Sanabria, D. Santomauro, I. S. Santos, J. V. Santos, M. M. Santric Milicevic, B. Sartorius, M. Satpathy, M. Sawhney, S. Saxena, M. I. Schmidt, I. J. C. Schneider, B. Schöttker, D. C. Schwebel, F. Schwendicke, S. Seedat, S. G. Sepanlou, E. E. Servan-Mori, T. Setegn, K. A. Shackelford, A. Shaheen, M. A. Shaikh, M. Shamsipour, S. M. Shariful Islam, J. Sharma, R. Sharma, J. She, P. Shi, C. Shields, G. T. Shifa, M. Shigematsu, Y. Shinohara, R. Shiri, R. Shirkoohi, S. Shirude, K. Shishani, M. G. Shrime, A. M. Sibai, I. D. Sigfusdottir, D. A. S. Silva, J. P. Silva, D. G. A. Silveira, J. A. Singh, N. P. Singh, D. N. Sinha, E. Skiadaresi, V. Skirbekk, E. L. Slepak, A. Sligar, D. L. Smith, M. Smith, B. H. A. Sobaih, E. Sobngwi, R. J. D. Sorensen, T. C. M. Sousa, L. A. Sposato, C. T. Sreeramareddy, V. Srinivasan, J. D. Stanaway, V. Stathopoulou, N. Steel, M. B. Stein, D. J. Stein, T. J. Steiner, C. Steiner, S. Steinke, M. A. Stokes, L. J. Stovner, B. Strub, M. Subart, M. B. Sufiyan, B. F. Sunguya, P. J. Sur, S. Swaminathan, B. L. Sykes, D. O. Sylte, R. Tabarés-Seisdedos, G. R. Taffere, J. S. Takala, N. Tandon, M. Tavakkoli, N. Taveira, H. R. Taylor, A. Tehrani-Banihashemi, T. Tekelab, A. S. Terkawi, D. J. Tesfaye, B. Tesssema, O. Thamsuwan, K. E. Thomas, A. G. Thrift, T. Y. Tiruye, R. Tobe-Gai, M. C. Tollanes, M. Tonelli, R. Topor-Madry, M. Tortajada, M. Touvier, B. X. Tran, S. Tripathi, C. Troeger, T. Truelsen, D. Tsoi, K. B. Tuem, E. M. Tuzcu,

S. Tyrovolas, K. N. Ukwaja, E. A. Undurraga, C. J. Uneke, R. Updike, O. A. Uthman, B. S. C. Uzochukwu, J. F. M. van Boven, S. Varughese, T. Vasankari, S. Venkatesh, N. Venketasubramanian, R. Vidavalur, F. S. Violante, S. K. Vladimirov, V. V. Vlassov, S. E. Vollset, F. Wadilo, T. Wakayo, Y.-P. Wang, M. Weaver, S. Weichenthal, E. Weiderpass, R. G. Weintraub, A. Werdecker, R. Westerman, H. A. Whiteford, T. Wijeratne, C. S. Wiysonge, C. D. A. Wolfe, R. Woodbrook, A. D. Woolf, A. Workicho, D. Xavier, G. Xu, S. Yadgir, M. Yaghoubi, B. Yakob, L. L. Yan, Y. Yano, P. Ye, H. H. Yimam, P. Yip, N. Yonemoto, S.-J. Yoon, M. Yotebieng, M. Z. Younis, Z. Zaidi, M. E. S. Zaki, E. A. Zegeye, Z. M. Zenebe, X. Zhang, M. Zhou, B. Zipkin, S. Zodpey, L. J. Zuhlke and C. J. L. Murray, *Lancet*, 2017, **390**, 1211–1259.

31 T. Jaeggi and A. Lussi, 2014, pp. 55–73.

32 S. J. C. Bezerra, S. H. João-Souza, I. V. Aoki, A. B. Borges, A. T. Hara and T. Scaramucci, *Caries Res.*, 2019, **000**, 305–313.

33 D. M. da S. Ávila, R. F. Zanatta, T. Scaramucci, I. V. Aoki, C. R. G. Torres and A. B. Borges, *J. Dent.*, 2017, **56**, 45–52.

34 Y. Lei, T. Wang, J. W. Mitchell, L. Zaidel, J. Qiu and L. Kilpatrick-Liverman, *RSC Adv.*, 2014, **4**, 49053–49060.

35 S. Suzuki, M. R. Whittaker, L. Grøndahl, M. J. Monteiro and E. Wentrup-Byrne, *Biomacromolecules*, 2006, **7**, 3178–3187.

36 J. Kirkham, A. Firth, D. Vernals, N. Boden, C. Robinson, R. C. Shore, S. J. Brookes and A. Aggeli, *J. Dent. Res.*, 2007, **86**, 426–430.

37 B. G. Hossein, A. Sadr, J. Espigares, I. Hariri, S. Nakashima, H. Hamba, F. Shafiei, F. Moztarzadeh and J. Tagami, *Biomed. Mater.*, 2015, **10**, 035007.

38 K. Mukherjee, Q. Ruan, D. Liberman, S. N. White and J. Moradian-Oldak, *J. Mater. Res.*, 2016, **31**, 556–563.

39 C. Shao, B. Jin, Z. Mu, H. Lu, Y. Zhao, Z. Wu, L. Yan, Z. Zhang, Y. Zhou, H. Pan, Z. Liu and R. Tang, *Sci. Adv.*, 2019, **5**, 1–10.

40 Y. W. Wang, H. K. Christenson and F. C. Meldrum, *Chem. Mater.*, 2014, **26**, 5830–5838.

41 S. B. Darling, *Prog. Polym. Sci.*, 2007, **32**, 1152–1204.

42 I. C. Stancu, R. Filmon, C. Cincu, B. Marculescu, C. Zaharia, Y. Tourmen, M. F. Baslé and D. Chappard, *Biomaterials*, 2004, **25**, 205–213.

43 J. P. MacDonald, M. P. Parker, B. W. Greenland, D. Hermida-Merino, I. W. Hamley and M. P. Shaver, *Polym. Chem.*, 2015, **6**, 1445–1453.

44 R. Tamate, K. Takahashi, T. Ueki, A. M. Akimoto and R. Yoshida, *Biomacromolecules*, 2017, **18**, 281–287.

45 G. Gaucher, M. H. Dufresne, V. P. Sant, N. Kang, D. Maysinger and J. C. Leroux, *J. Control. Release*, 2005, **109**, 169–188.

46 F. S. Bates and G. H. Fredrickson, *Annu. Rev. Phys. Chem.*, 1990, **41**, 525–557.

47 P. Chen, M. Qiu, C. Deng, F. Meng, J. Zhang, R. Cheng and Z. Zhong, *Biomacromolecules*, 2015, **16**, 1322–1330.

48 M. Karayianni and S. Pispas, *Fluorescence Studies of Polymer Containing Systems*, 2016, vol. 16.

49 T. Pietsch, N. Gindy, B. Mahltig and A. Fahmi, *J. Polym. Sci. Part B Polym. Phys.*, 2010, **48**, 1642–1650.

50 S. C. Owen, D. P. Y. Chan and M. S. Shoichet, *Nano Today*, 2012, **7**, 53–65.

51 H. Ding, S. Park, M. Zhong, X. Pan, J. Pietrasik, C. J. Bettinger and K. Matyjaszewski, *Macromolecules*, 2016, **49**, 6752–6760.

52 L. Sun, Y. Zhou, X. Zhou, Q. Fu, S. Zhao, X. Tu, X. Zhang, L. Ma, M. Liu and H. Wei, *Polym. Chem.*, 2017, **8**, 500–504.

53 S. Vircheva, R. Bryaskova, S. Miloshev and N. Dishovsky, *J. Chem. Technol. Metall.*, 2015, **50**, 135–140.

54 C. Agatemor and M. P. Shaver, *Biomacromolecules*, 2013, **14**, 699–708.

55 C. Gao, J. Wu, H. Zhou, Y. Qu, B. Li and W. Zhang, *Macromolecules*, 2016, **49**, 4490–4500.

56 J. Huang, R.-Y. Wang, J.-T. Xu and Z.-Q. Fan, *Polymer (Guildf).*, 2016, **99**, 332–339.

57 D. P. Rodrigues, J. R. C. Costa, N. Rocha, J. R. Góis, A. C. Serra and J. F. J. Coelho, *Colloids Surfaces B Biointerfaces*, 2016, **145**, 447–453.

58 A. Hanisch, P. Yang, A. N. Kulak, L. A. Fielding, F. C. Meldrum and S. P. Armes, *Macromolecules*, 2016, **49**, 192–204.

59 E. R. Jones, M. Semsarilar, A. Blanazs and S. P. Armes, *Macromolecules*, 2012, **45**, 5091–5098.

60 A. Hanisch, P. Yang, A. N. Kulak, L. A. Fielding, F. C. Meldrum and S. P. Armes, *Macromolecules*, 2016, **49**, 192–204.

61 Y. Lei, T. Wang, J. W. Mitchell, J. Qiu and L. Kilpatrick-Liverman, *J. Dent. Res.*, 2014, **93**, 1264–1269.

62 R. E. Dey, X. Zhong, P. J. Youle, Q. G. Wang, I. Wimpenny, S. Downes, J. A. Hoyland, D. C. Watts, J. E. Gough and P. M. Budd, *Macromolecules*, 2016, **49**, 2656–2662.

63 N. M. Hidzir, D. J. T. Hill, D. Martin and L. Grøndahl, *Bioact. Mater.*, 2017, **2**, 27–34.

64 J. Li, J. J. Yang, J. Li, L. Chen, K. Liang, W. Wu, X. Chen and J. Li, *Biomaterials*, 2013, **34**, 6738–6747.

65 M. Vert, S. M. Li, G. Spenlehauer and P. Guerin, *J. Mater. Sci. Mater. Med.*, 1992, **3**, 432–446.

66 A. D. Padsalgikar, in *Plastics in Medical Devices for Cardiovascular Applications*, Elsevier Inc., 2017, pp. 1–29.

67 T. J. Matray, R. J. Twieg and J. L. Hedrick, 1996, pp. 266–275.

68 P. Nesvadba, *Encycl. Radicals Chem. Biol. Mater.*, 2012, 1–36.

69 O. Nuyken and S. Pask, *Polymers (Basel).*, 2013, **5**, 361–403.

70 F. Sanda, T. Fueki and T. Endo, *Macromolecules*, 1999, **32**, 4220–4224.

71 J. Matsuo, K. Aoki, F. Sanda and T. Endo, *Macromolecules*, 1998, **31**, 4432–4438.

72 H. Janeczek, J. Kasperczyk, M. Bero, B. Czapla and P. Dobrzyn, *Macromol. Chem. Phys.*, 1999, **916**, 911–916.

73 A. P. Dove, *Chem. Commun.*, 2008, 6446.

74 J. W. Kramer, E. B. Lobkovsky and G. W. Coates, *Org. Lett.*, 2006, **8**, 3709–3712.

75 A. Löfgren, A. C. Albertsson, P. H. Dubois, R. Jérôme and P. H. Teyssié, *Macromolecules*, 1994, **27**, 5556–5562.

76 A.-C. Albertsson and I. K. Varma, *Biomacromolecules*, 2003, **4**, 1466–1486.

77 J. Penczek, Stanislaw Szymanski, Ryzard Duda, Andrzej, Baran, *Macromol. Symp.*, 2003, **201**, 261–269.

78 D. A. Macdonald and M. F. A. Goosen, *J. Polym. Chem.*, 1994, **32**, 2965–2970.

79 Y. Masutani, Kazunari Kimiura, in *Poly(lactic acid) Science and Technology: Processing, Properties, Additives and Applications*, Royal Society of Chemistry, 2014, pp. 1–36.

80 T. Naolou, A. Lendlein and A. T. Neffe, *Front. Chem.*, 2019, **7**, 1–12.

81 A. Duda, *Macromolecules*, 1996, **29**, 1399–1406.

82 C. Jacobs, P. Dubois, R. Jerome and P. Teyssie, *Macromolecules*, 1991, **24**, 3027–3034.

83 O. T. du Boullay, N. Saffon, J.-P. Diehl, B. Martin-Vaca and D. Bourissou, *Biomacromolecules*, 2010, **11**, 1921–1929.

84 N. Spassky, M. Wisniewski, C. Pluta and A. Le, *Macromol. Chem. Phys.*, 1996, **2637**, 2627–2637.

85 A. L. E. Borgne, V. Vincens, M. Jouglard, N. Spassky, L. D. C. Macromol and U. Pierre, *Macromol Chem., Macromol. Symp*, 1993, **46**, 37–46.

86 Z. Zhong, P. J. Dijkstra and J. Feijen, *Angew. Chem. Int. Ed*, 2002, **8**, 4510–4513.

87 P. A. Cameron, D. Jhurry, V. C. Gibson, A. J. P. White, D. J. Williams and S. Williams, *Macromol. Rapid Commun.*, 1999, **618**, 616–618.

88 P. Hormnirun, E. L. Marshall, V. C. Gibson, R. I. Pugh and A. J. P. White, *Proc. Natl. Acad. Sci.*, 2006, **103**, 15343–15348.

89 N. Nomura, R. Ishii, M. Akakura and K. Aoi, *J. Am. Chem. Soc.*, 2002, 5938–5939.

90 V. Vincens, A. Le Borgne and N. Spassky, *makromol. Chem. Macromol. Symp*, 1991, **291**, 285–291.

91 E. D. Cross, L. E. N. Allan, A. Decken and M. P. Shaver, *Polym. Chem.*, 2013, **51**, 1137–1146.

92 A. Poli, P. Di Donato, G. R. Abbamondi and B. Nicolaus, *Archaea*, 2011, **2011**, 1–13.

93 K. Lin, C. Lan and Y. Sun, *Polym. Degrad. Stab.*, 2016, **134**, 30–40.

94 J. T. Lee, P. J. Thomas and H. Alper, *J. Org. Chem.*, 2001, **66**, 5424–5426.

95 G. B. Payne, *J. Org. Chem.*, 1962, 3819–3822.

96 J. A. R. Schmidt, V. Mahadevan, Y. D. Y. L. Getzler and G. W. Coates, *Org. Lett.*, 2004, **6**, 373–376.

97 J. A. R. Schmidt, E. B. Lobkovsky and G. W. Coates, *J. Am. Chem. Soc.*, 2005, **127**, 11426–11435.

98 J. P. MacDonald, M. P. Parker, B. W. Greenland, D. Hermida-Merino, I. W. Hamley and

M. P. Shaver, *Polym. Chem.*, 2015, **6**, 1445–1453.

99 C. Guillaume, N. Ajellal, J.-F. Carpentier and S. M. Guillaume, *J. Polym. Sci. Part A Polym. Chem.*, 2011, **49**, 907–917.

100 F. Sinclair, L. Chen, B. W. Greenland and M. P. Shaver, *Macromolecules*, 2016, **49**, 6826–6834.

101 B. M. Raycraft, J. P. MacDonald, J. T. McIntosh, M. P. Shaver and E. R. Gillies, *Polym. Chem.*, 2017, **8**, 557–567.

102 O. Coulembier, P. Degée, S. Cammas-Marion, P. Guérin and P. Dubois, *Macromolecules*, 2002, **35**, 9896–9903.

103 R. Savic, *Science (80-. ).*, 2003, **300**, 615–618.

104 V. T. Lipik, L. K. Widjaja, S. S. Liow, M. J. M. Abadie and S. S. Venkatraman, *Polym. Degrad. Stab.*, 2010, **95**, 2596–2602.

105 B. M. Raycraft, J. P. MacDonald, J. T. McIntosh, M. P. Shaver and E. R. Gillies, *Polym. Chem.*, 2017, **8**, 557–567.

106 X. Ma, Q. Xu, H. Li, C. Su, L. Yu, X. Zhang, H. Cao and L. B. Han, *Green Chem.*, 2018, **20**, 3408–3413.

107 A. R. Stiles, W. E. Vaughan and F. F. Rust, *J. Am. Chem. Soc.*, 1958, **80**, 714–716.

108 C. J. Lomoschitz, B. Feichtenschlager, N. Moszner, M. Puchberger, K. Müller, M. Abele and G. Kickelbick, *Langmuir*, 2011, **27**, 3534–3540.

109 S. Deprèle and J. L. Montchamp, *J. Org. Chem.*, 2001, **66**, 6745–6755.

110 O. Tayama, A. Nakano, T. Iwahama, S. Sakaguchi and Y. Ishii, *J. Org. Chem.*, 2004, **69**, 5494–5496.

111 B. Canniccioni, S. Monge, G. David and J. J. Robin, *Polym. Chem.*, 2013, **4**, 3676–3685.

112 E. Betthausen, M. Drechsler, M. Förtsch, F. H. Schacher and A. H. E. Müller, *Soft Matter*, 2011, **7**, 8880–8891.

113 M. Fantin, A. A. Isse, A. Gennaro and K. Matyjaszewski, *Macromolecules*, 2015, **48**, 6862–6875.

114 M. Fantin, A. A. Isse, A. Venzo, A. Gennaro and K. Matyjaszewski, *J. Am. Chem. Soc.*, 2016, **138**, 7216–7219.

115 D. J. Keddie, *Chem. Soc. Rev.*, 2013, **43**, 496–505.

116 B. Y. K. Chong, T. P. T. Le, G. Moad, E. Rizzardo and S. H. Thang, *Macromolecules*, 1999, **32**, 2071–2074.

117 C. Barner-kowollik, M. Buback, B. Charleux, M. L. Coote, M. Drache, T. Fukuda, A. Goto, B. Klumperman, A. B. Lowe, J. B. Mcleary, G. Moad, M. J. Monteiro, R. D. Sanderson, M. P. Tonge, P. Vana and P. Marie, *J. Polym. Sci. Part A Polym. Chem.*, 2006, **44**, 5809–5831.

118 C. Barner-kowollik and G. T. Russell, 2009, **34**, 1211–1259.

119 G. David, Z. El Asri, S. Rich, P. Castignolles, Y. Guillaneuf, P. Lacroix-Desmazes and B. Boutevin, *Macromol. Chem. Phys.*, 2009, **210**, 631–639.

120 L. He, E. S. Read, S. P. Armes, D. J. Adams, T. Uni, B. Hill, S. Sheffield and V. Unile,

*Macromolecules*, 2007, 4429–4438.

121 T. Yildirim, A. C. Rinkenauer, C. Weber, A. Traeger, S. Schubert and U. S. Schubert, *J. Polym. Sci. Part A Polym. Chem.*, 2015, 2711–2721.

122 J. M. Pelet and D. Putnam, *Macromol. Chem. Phys.*, 2012, **213**, 2536–2540.

123 J. Loiseau, N. Doërr, J. M. Suau, J. B. Egraz, M. F. Llauro, C. Ladavière and J. Claverie, *Macromolecules*, 2003, **36**, 3066–3077.

124 J. Ji, L. Jia, L. Yan and P. R. Bangal, *J. Macromol. Sci. Part A*, 2010, **47**, 445–451.

125 M. R. Hill, R. N. Carmean and B. S. Sumerlin, *Macromolecules*, 2015, **48**, 5459–5469.

126 J. Dziczkowski and M. D. Soucek, *J. Coat. Technol. Res*, 2010, **7**, 587–602.

127 K. Yao and C. Tang, *Macromolecules*, 2013, **46**, 1689–1712.

128 M. Arshad, R. A. Pradhan and A. Ullah, *Mater. Sci. Eng. C*, 2017, **76**, 217–223.

129 S. S. Jena, S. G. Roy, V. Azmeera and P. De, *React. Funct. Polym.*, 2016, **99**, 26–34.

130 H. Vahabi, L. Ferry, C. Longuet, B. Otazaghine, C. Negrell-Guirao, G. David and J. M. Lopez-Cuesta, *Mater. Chem. Phys.*, 2012, **136**, 762–770.

131 V. Torrisi, A. Graillot, L. Vitorazi, Q. Crouzet, G. Marletta, C. Loubat and J. F. Berret, *Biomacromolecules*, 2014, **15**, 3171–3179.

132 T. Huang, H. Liu, P. Liu, P. Liu, L. Li and J. Shen, *J. Mater. Chem. B*, 2017, **5**, 5380–5389.

133 R. Ménard, C. Negrell-Guirao, L. Ferry, R. Sonnier and G. David, *Eur. Polym. J.*, 2014, **57**, 109–120.

134 G. David, C. Negrell, A. Manseri and B. Boutevin, *J. Appl. Polym. Sci.*, 2009, **114**, 2213–2220.

135 K. Mukumoto, M. Zhong and K. Matyjaszewski, *Eur. Polym. J.*, 2014, **56**, 11–16.

136 B. Canniccioni, S. Monge, G. David and J.-J. Robin, *Am Chem Soc Div Polym Chem*, 2011, **52**, 645–646.

137 M. J. Roberts, M. D. Bentley and J. M. Harris, *Adv. Drug Deliv. Rev.*, 2012, **64**, 116–127.

138 F. M. Veronese and A. Mero, *Biodrugs*, 2008, **22**, 315–329.

139 G. Riess and C. Labbe, *Macromol. Rapid Commun.*, 2004, **25**, 401–435.

140 A. M. Dos Santos, J. Pohn, M. Lansalot and F. D'Agosto, *Macromol. Rapid Commun.*, 2007, **28**, 1325–1332.

141 H. Minami, K. Shimomura, T. Suzuki, K. Sakashita and T. Noda, *Macromolecules*, 2014, **47**, 130–136.

142 H. Walderhaug and O. Söderman, *Curr. Opin. Colloid Interface Sci.*, 2009, **14**, 171–177.

143 A. L. Boskey, *Crit. Rev. Oral Biol. Med.*, 1991, **2**, 369–387.

144 A. Linde, A. Lussi and M. A. Crenshaw, *Calcif. Tissue Int.*, 1989, **44**, 286–295.

145 M. Iijima and J. Moradian-Oldak, *Calcif. Tissue Int.*, 2004, **74**, 522–531.

146 D.-J. Wu, Z.-X. Liu, C.-Z. Gao, X.-C. Shen, X.-M. Wang and H. Liang, *Surf. Coatings Technol.*, 2013, **228**, S24–S27.

147 G. K. Toworfe, R. J. Composto, I. M. Shapiro and P. Ducheyne, *Biomaterials*, 2006, **27**, 631–642.

148 T. Hoshino, K. Sato, Y. Oaki, A. Sugawara-Narutaki, K. Shimizu, N. Ozaki and H. Imai, *RSC Adv.*, 2016, **6**, 1301–1306.

149 A. Steinhaus, R. Chakroun, M. Mullner, T. L. Nghiem, M. Hildebrandt and A. H. Groschel, *ACS Nano*, 2019, **13**, 6269–6278.

150 G. Quintieri, M. Saccone, M. Spengler, M. Giese and A. H. Gröschel, *Nanomaterials*, 2018, **8**, 1–13.

151 C. A. Fustin, V. Abetz and J. F. Gohy, *Eur. Phys. J. E*, 2005, **16**, 291–302.

152 Y. Bakkour, V. Darcos, S. Li and J. Coudane, *Polym. Chem.*, 2012, **3**, 2006–2010.

153 S. C. Owen, D. P. Y. Chan and M. S. Shoichet, *Nano Today*, 2012, **7**, 53–65.

154 K. Naka and Y. Chujo, *Chem. Mater.*, 2001, **13**, 3245–3259.

155 D. B. Robinson, J. L. Rognlien, C. A. Bauer and B. A. Simmons, *J. Mater. Chem.*, 2007, **17**, 2113–2119.

156 C. A. Figg, R. N. Carmean, K. C. Bentz, S. Mukherjee, D. A. Savin and B. S. Sumerlin, *Macromolecules*, 2017, **50**, 935–943.

157 B. Marzec, J. M. Walker, M. Panagopoulou, Y. Jhons, D. Clare, A. Wheeler, M. P. Shaver and F. Nudelman, *J. Struct. Biol.*, 2019, 0–1.

158 T. Attin and F. J. Wegehaupt, in *Erosive Tooth Wear: From Diagnosis to Therapy*, 2014, vol. 20, pp. 123–142.

159 E. Heurich, M. Beyer, K. D. Jandt, J. Reichert, V. Herold, M. Schnabelrauch and B. W. Sigusch, *Dent. Mater.*, 2010, **26**, 326–336.

160 H. Otsuka, Y. Nagasaki and K. Kataoka, *Curr. Opin. Colloid Interface Sci.*, 2001, **6**, 3–10.

161 A. Beletsi, L. Leontiadis, P. Klepetsanis, D. S. Ithakissios and K. Avgoustakis, *Int. J. Pharm.*, 1999, **182**, 187–197.

162 X. F. Xu, C. Y. Pan, W. J. Zhang and C. Y. Hong, *Macromolecules*, 2019, **52**, 1965–1975.

## Appendix Line profile graphs

### a. Line profile graphs of the enamel control discs

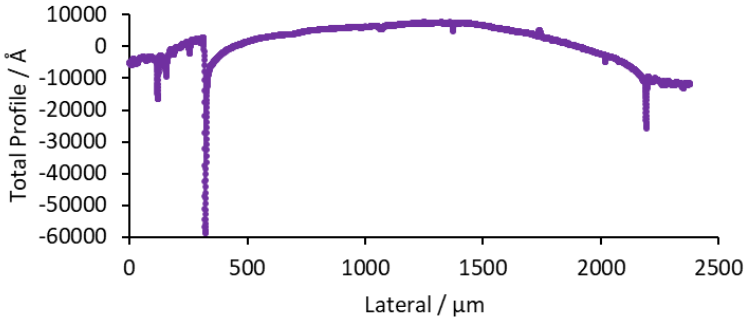


*Figure A-2 The line profile graph of enamel control sample 1.*

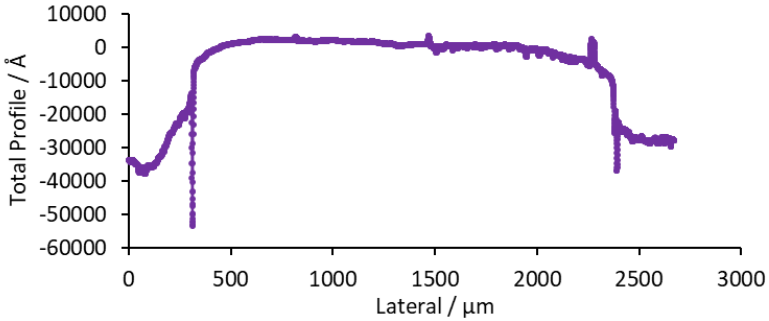


*Figure A-1 The line profile graph of enamel control sample 2a.*

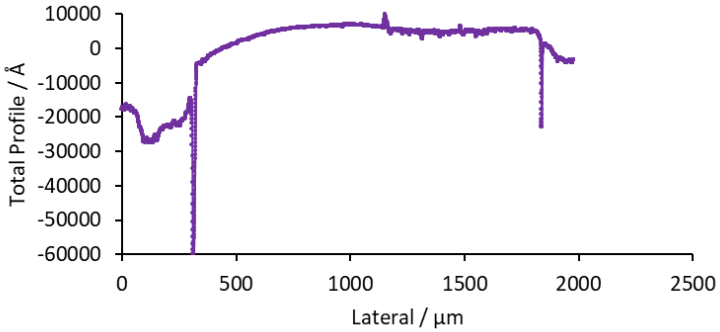


*Figure A-3 A line profile graph of enamel control sample 2b.*

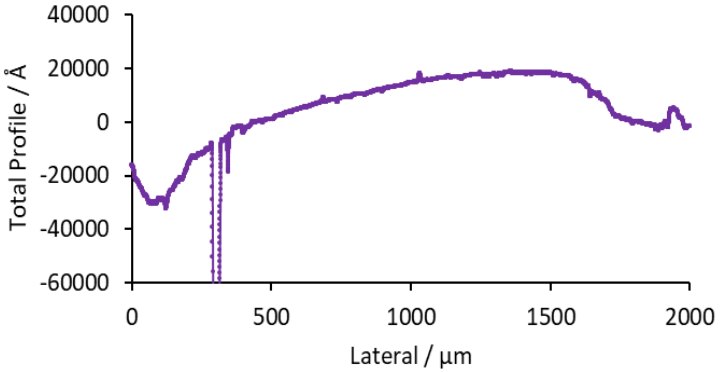


*Figure A-4 A line profile graph of enamel control sample 2c.*

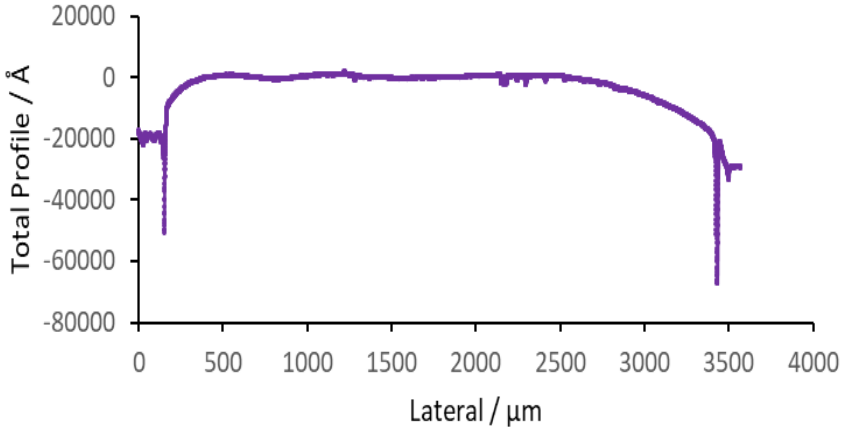


*Figure A-6 A line profile graph of enamel control sample 3a.*

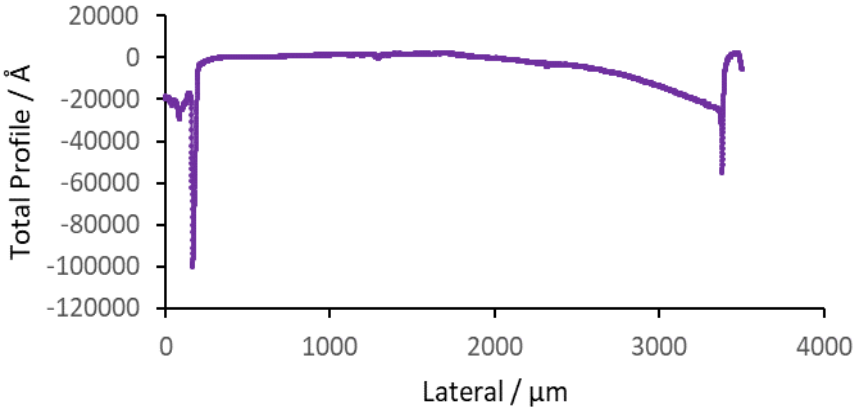


*Figure A-5 A line profile graph of enamel control sample 3b.*

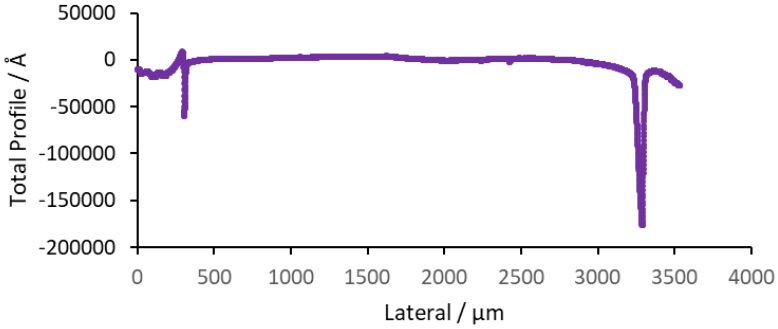


*Figure A-8 A line profile graph of enamel control sample 3c.*

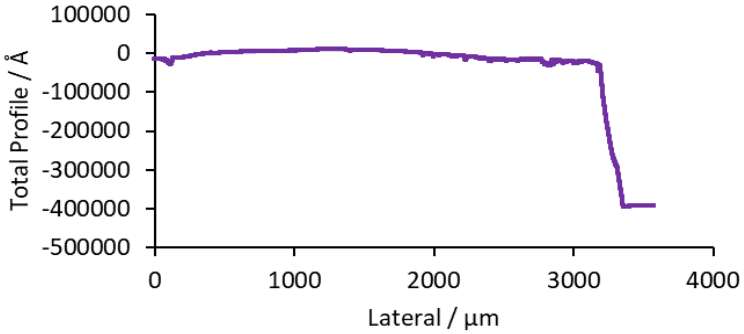


*Figure A-7 A line profile graph of enamel control sample 4.*

## b. Line profile graphs of the PFN1 covered enamel disc samples

### i. 0.02 mg $cm^{-3}$ of PFN1

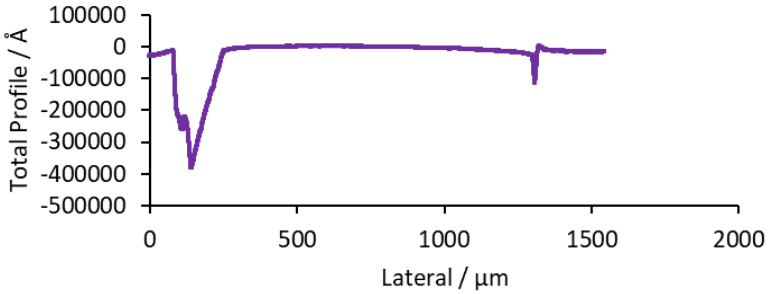


*Figure A-10 A line profile graph of enamel with 0.02 mg $cm^{-3}$ of **PFN1** sample 1*

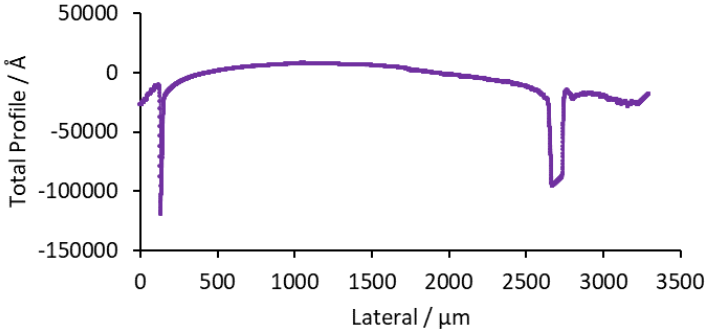


*Figure A-9 A line profile graph of enamel with 0.02 mg $cm^{-3}$ of **PFN1** sample 1*

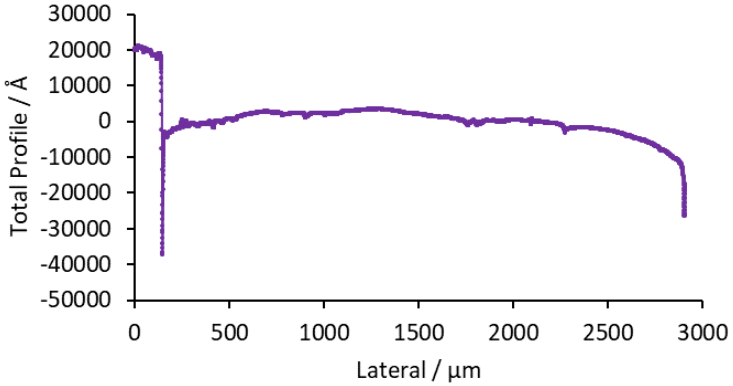


*Figure A-11 A line profile graph of enamel with 0.02 mg $cm^{-3}$ of **PFN1** sample 2*

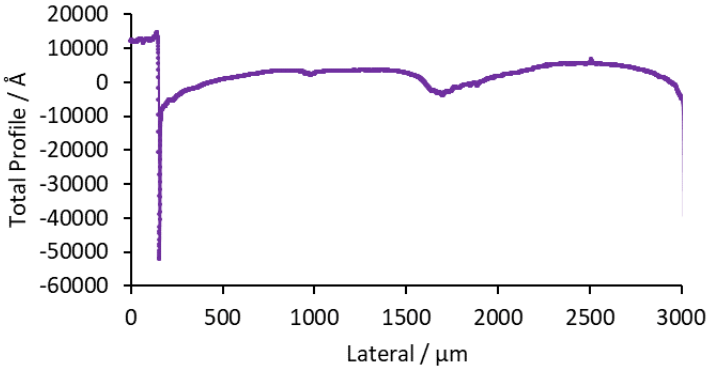


*Figure A-12 A line profile graph of enamel with 0.02 mg $cm^{-3}$ of **PFN1** sample*

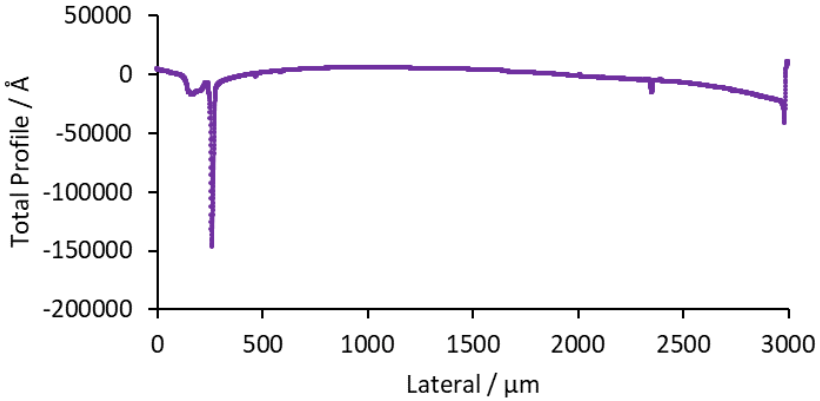


*Figure A-14 A line profile graph of enamel with 0.02 mg cm$^{-3}$ of **PFN1** sample 3a.*

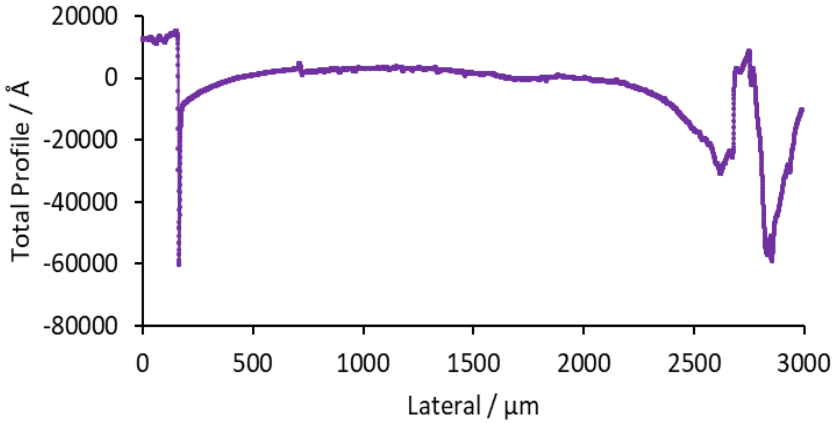


*Figure A-13 A line profile graph of enamel with 0.02 mg cm$^{-3}$ of **PFN1** sample 3b.*

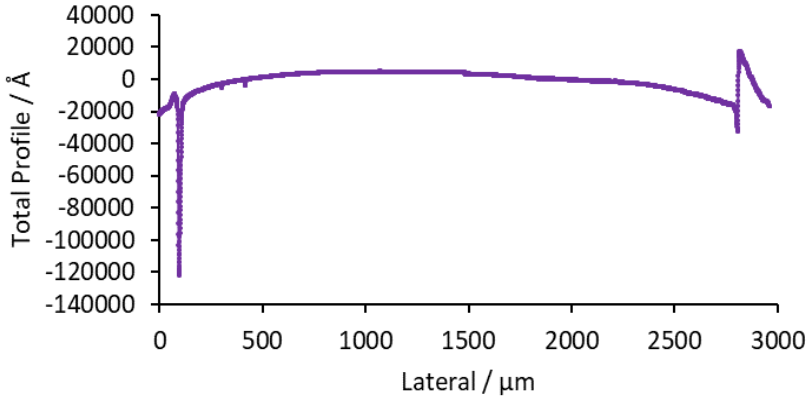


*Figure A-16 A line profile graph of enamel with 0.02 mg cm$^{-3}$ of **PFN1** sample 3c.*

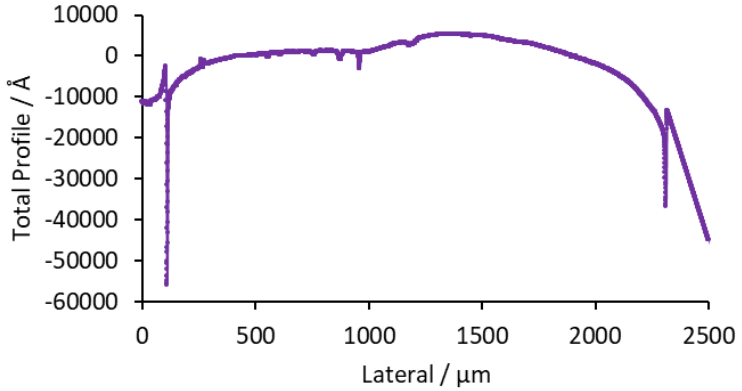


*Figure A-15 A line profile graph of enamel with 0.02 mg cm$^{-3}$ of **PFN1** sample 4a.*

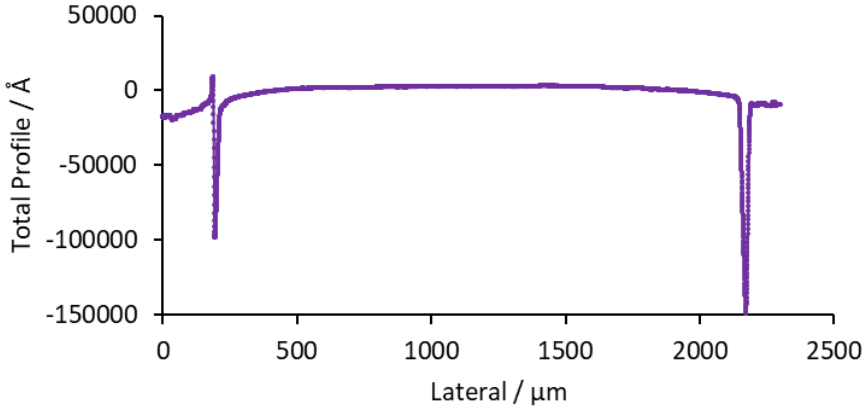


*Figure A-18 A line profile graph of enamel with 0.02 mg cm$^{-3}$ of **PFN1** sample 4b.*

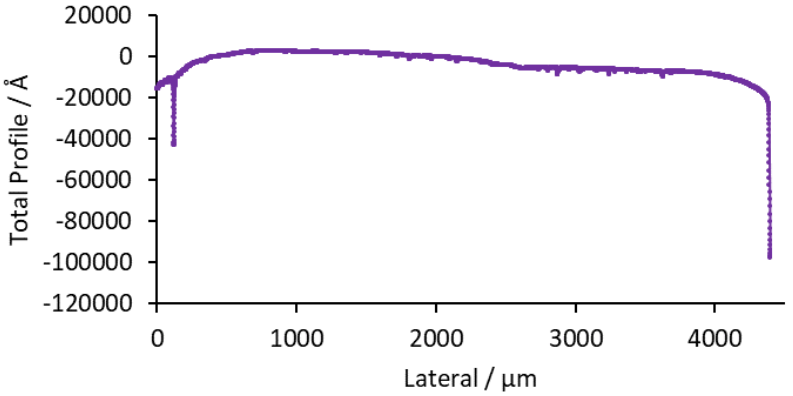


*Figure A-17 A line profile graph of enamel with 0.02 mg cm$^{-3}$ of **PFN1** sample 5.*

### ii. 0.1 mg cm$^{-3}$ of PFN1

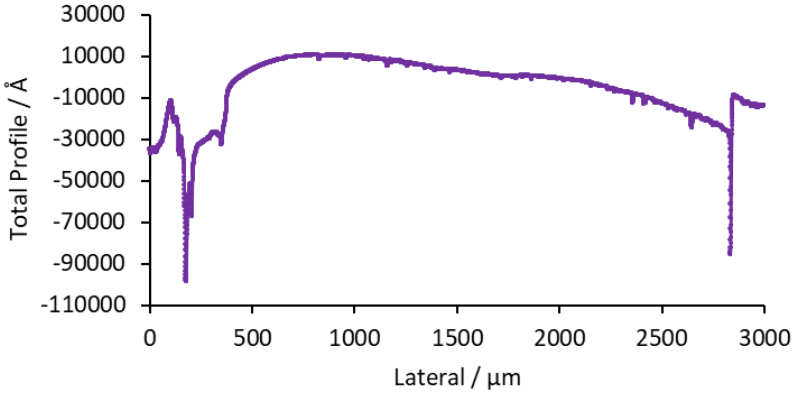


*Figure A-20 A line profile graph of enamel with 0.1 mg cm$^{-3}$ of **PFN1** sample 1.*

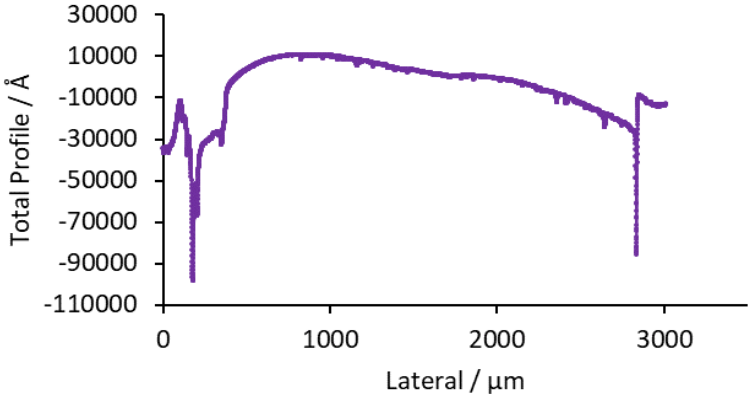


*Figure A-19 A line profile graph of enamel with 0.1 mg cm$^{-3}$ of **PFN1** sample 1.*

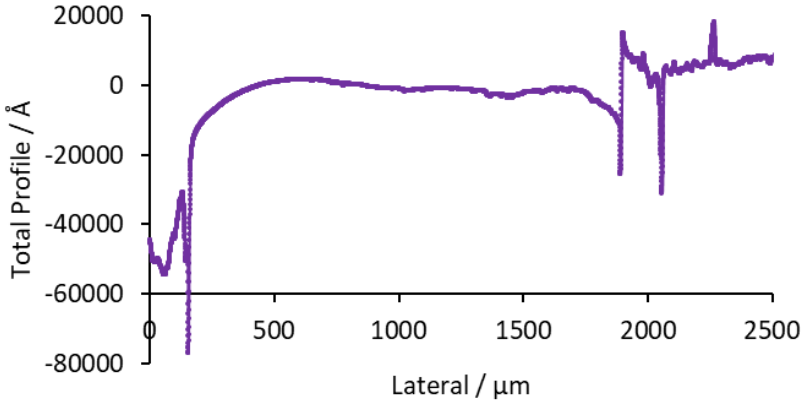


*Figure A-22 The line profile graph of enamel with 0.1 mg cm$^{-3}$ of **PFN1** sample 2*

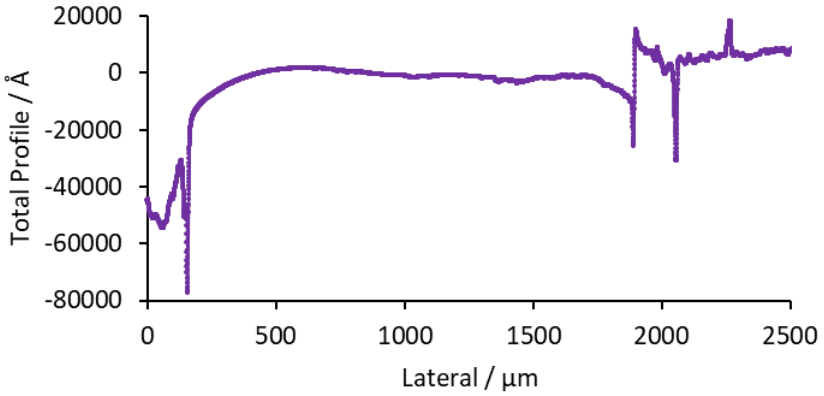


*Figure A-21 A line profile graph of enamel with 0.1 mg cm$^{-3}$ of **PFN1** sample 3*

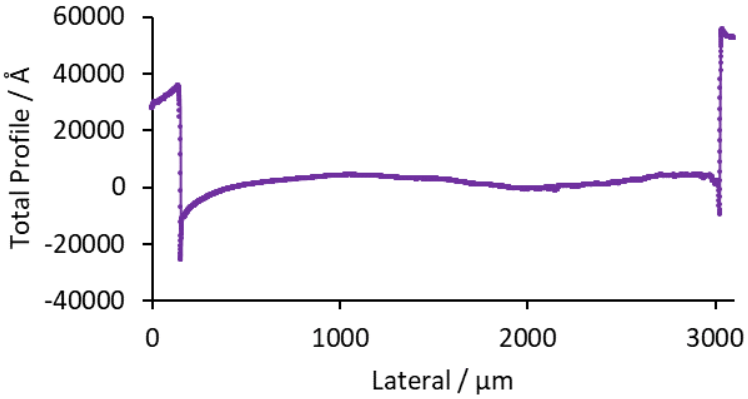


*Figure A-23 A line profile graph of enamel with 0.1 mg cm$^{-3}$ of **PFN1** sample 3*

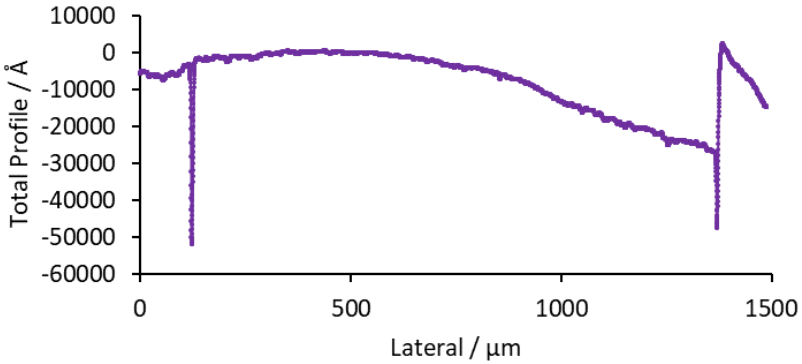


*Figure A-24 The line profile graph of enamel with 0.1 mg cm$^{-3}$ of **PFN1** sample 4*

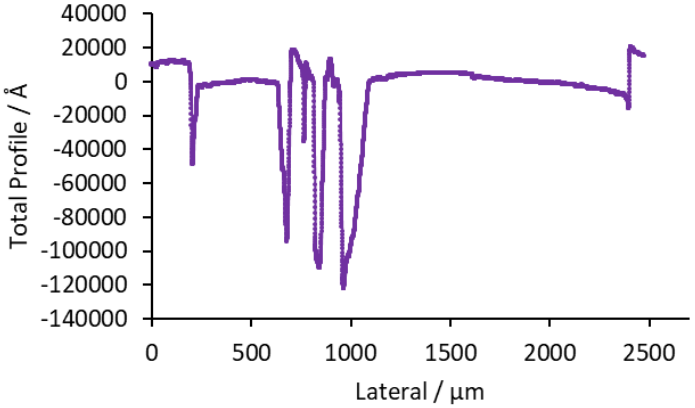


*Figure A-26 A line profile graph of enamel with 0.1 mg cm$^{-3}$ of **PFN1** sample 5*

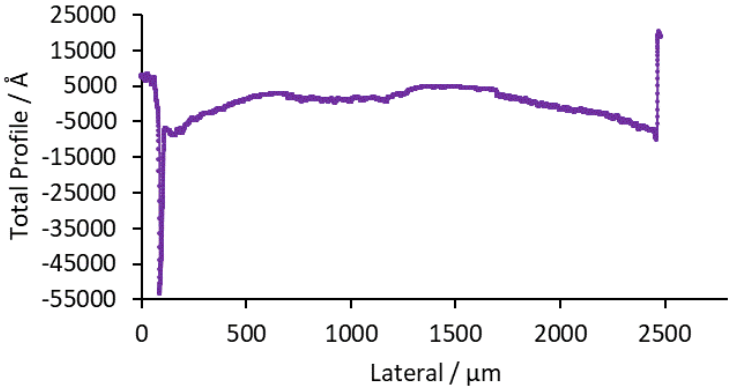


*Figure A-25 A line profile graph of enamel with 0.1 mg cm$^{-3}$ of **PFN1** sample 5*

### iii. 1 mg cm$^{-3}$ of PFN1

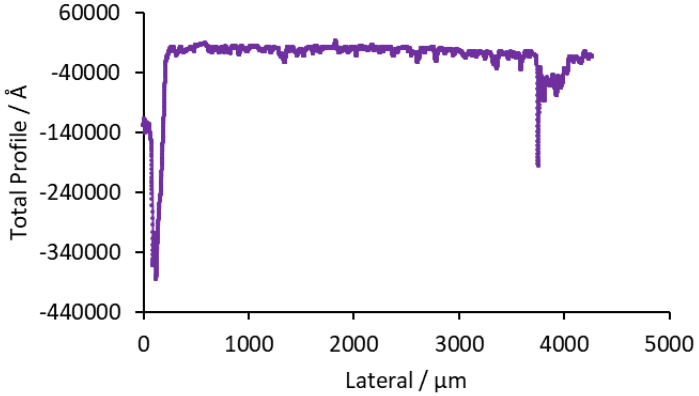


*Figure A-28 A line profile graph of enamel with 1 mg cm$^{-3}$ of **PFN1** sample 1*

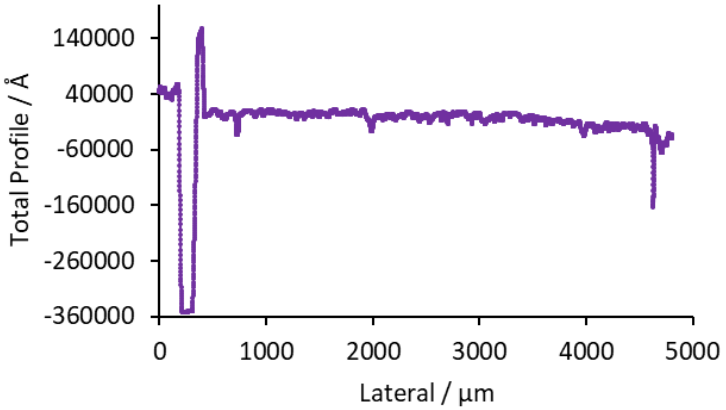


*Figure A-27 A line profile graph of enamel with 1 mg cm$^{-3}$ of **PFN1** sample 1*

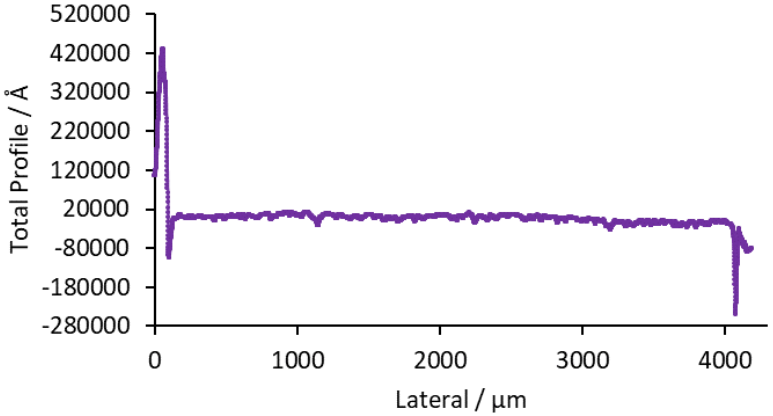


*Figure A-30 A line profile graph of enamel with 1 mg cm$^{-3}$ of **PFN1** sample 1.*

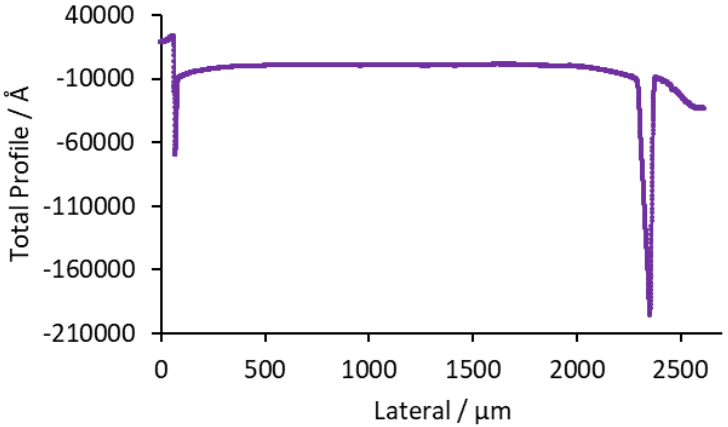


*Figure A-29 The line profile graph of enamel with 1 mg cm$^{-3}$ of **PFN1** sample 2.*

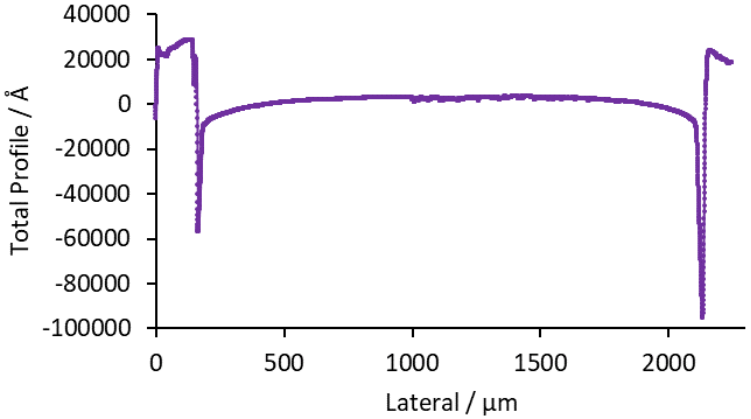


*Figure A-31 A line profile graph of enamel with 1 mg cm$^{-3}$ of **PFN1** sample 3a.*

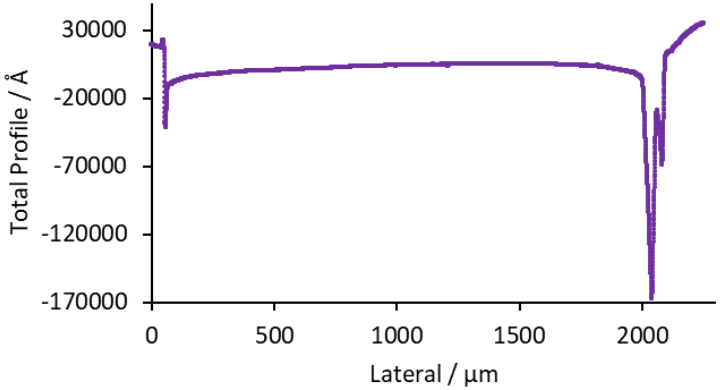


*Figure A-32 A line profile graph of enamel with 1 mg cm$^{-3}$ of **PFN1** sample 3b.*

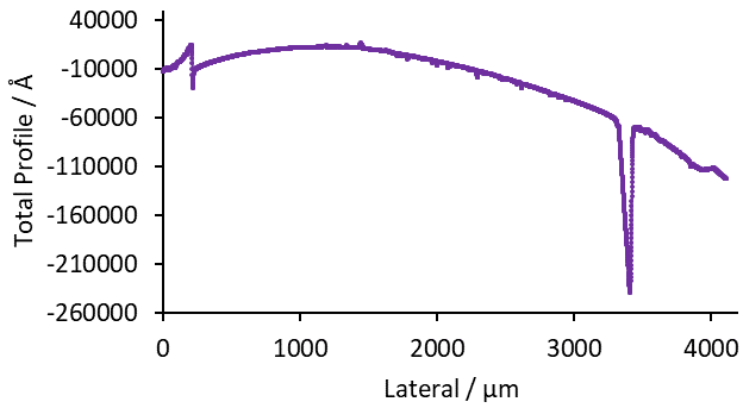


*Figure A-34 A line profile graph of enamel with 1 mg cm$^{-3}$ of **PFN1** sample 4a.*

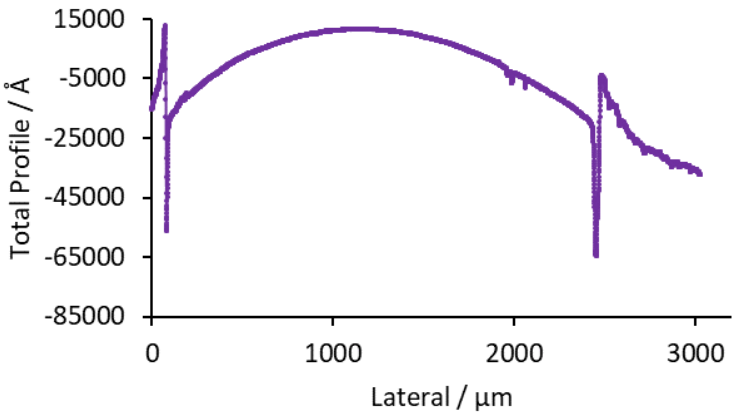


*Figure A-33 A line profile graph of enamel with 1 mg cm$^{-3}$ of **PFN1** sample 4b.*

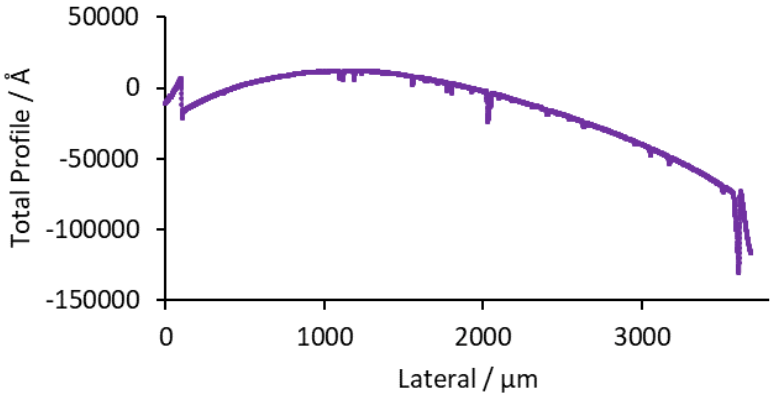


*Figure A-35 A line profile graph of enamel with 1 mg cm$^{-3}$ of **PFN1** sample 4c.*

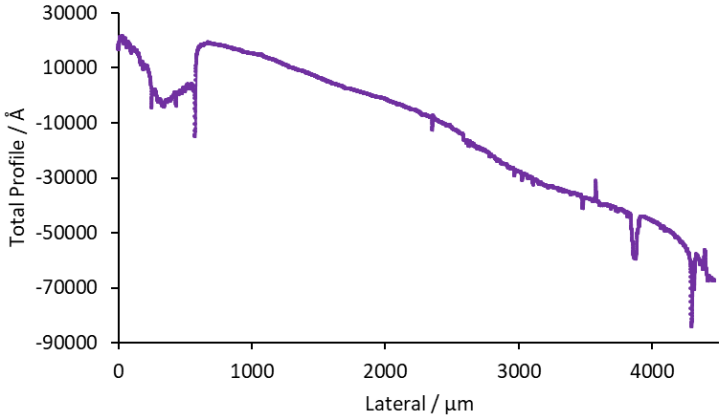


*Figure A-36 A line profile graph of enamel with 1 mg cm$^{-3}$ of **PFN1** sample 5*

## c. Line profile graphs of the PF1 covered enamel disc samples

### i. 0.02 mg $cm^{-3}$ of PF1

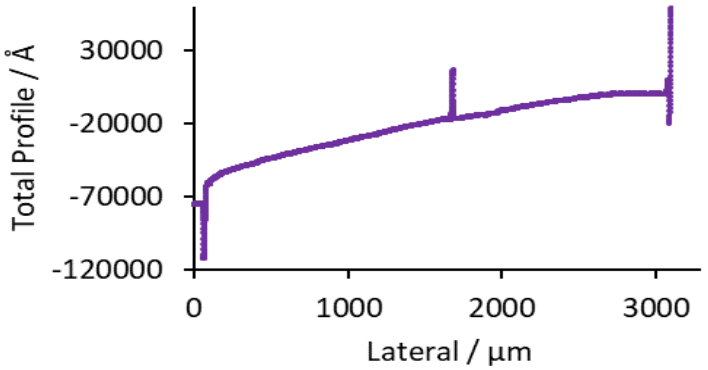


*Figure A-37 A line profile graph of enamel with 0.02 mg $cm^{-3}$ of **PF1** sample 1a.*

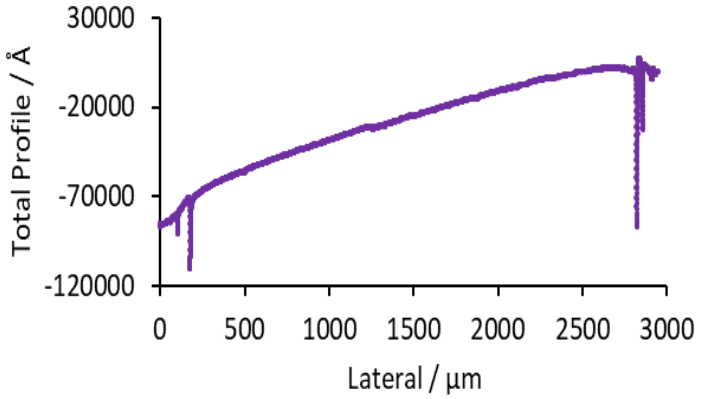


*Figure A-38 A line profile graph of enamel with 0.02 mg $cm^{-3}$ of **PF1** sample 1b.*

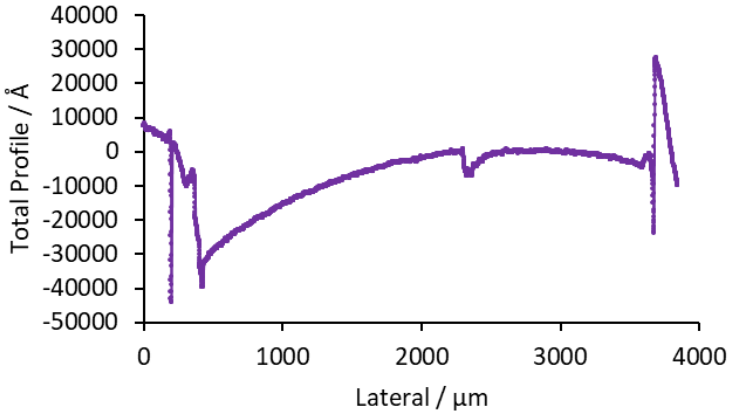


*Figure A-39 A line profile graph of enamel with 0.02 mg $cm^{-3}$ of **PF1** sample 2a.*

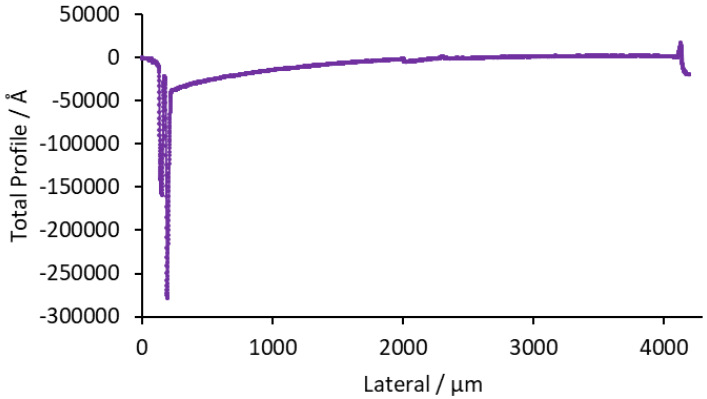


*Figure A-40 A line profile graph of enamel with 0.02 mg $cm^{-3}$ of **PF1** sample 2b*

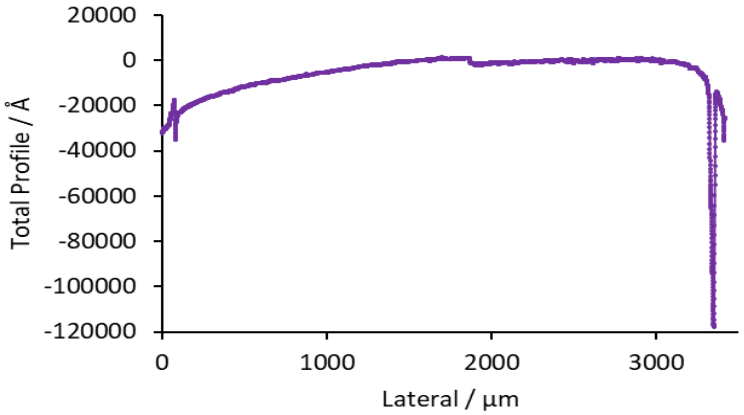


*Figure A-41 A line profile graph of enamel with 0.02 mg cm$^{-3}$ of **PF1** sample 3a.*

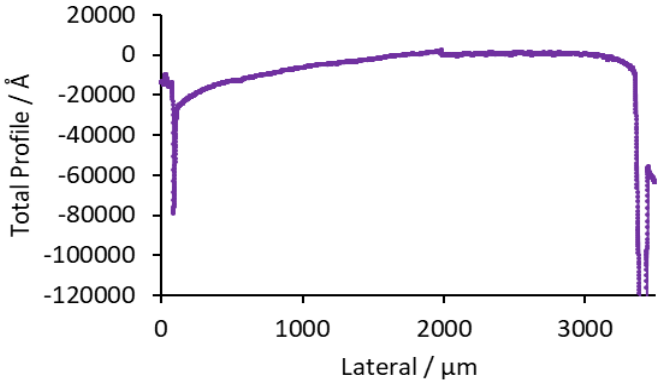


*Figure A-42 A line profile graph of enamel with 0.02 mg cm$^{-3}$ of **PF1** sample 3b.*

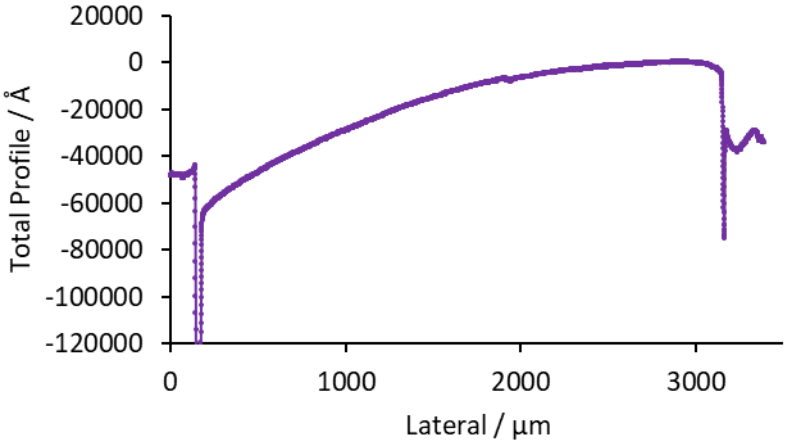


*Figure A-43 A line profile graph of enamel with 0.02 mg cm$^{-3}$ of **PF1** sample 4a.*

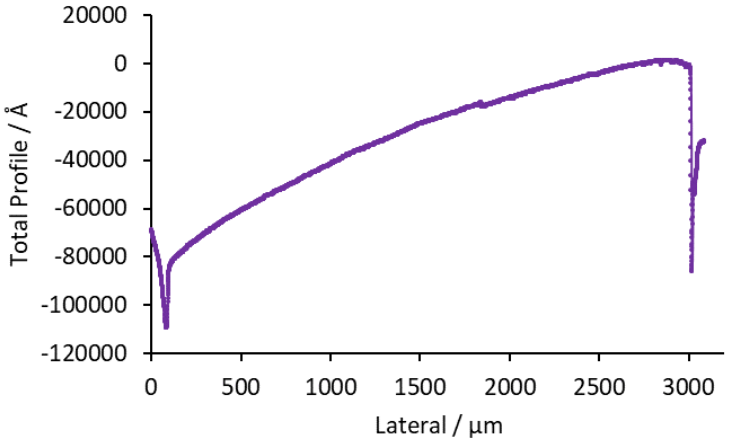


*Figure A-44 A line profile graph of enamel with 0.02 mg cm$^{-3}$ of **PF1** sample 4a.*

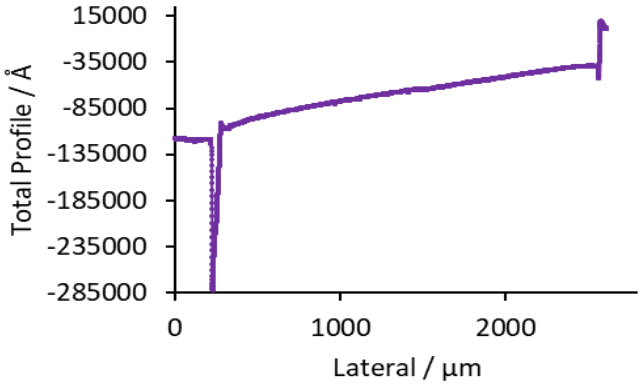


*Figure A-45 The line profile graph of enamel with 0.02 mg cm$^{-3}$ of **PF1** sample 5.*

### ii. 0.1 mg cm$^{-3}$ of PF1

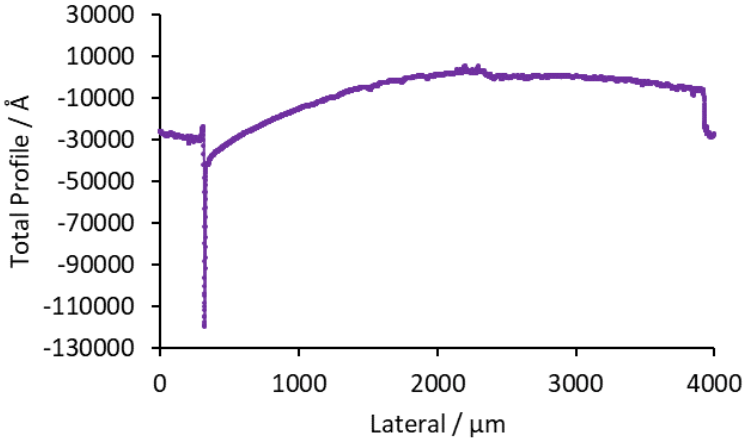


*Figure A-47 A line profile graph of enamel with 0.1 mg cm$^{-3}$ of **PF1** sample 1a.*

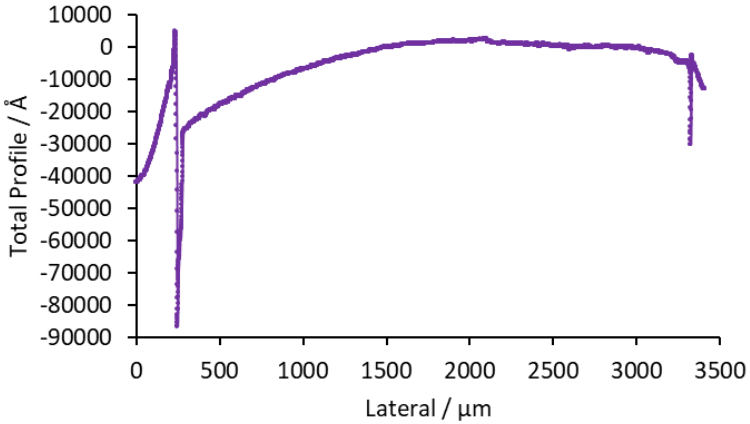


*Figure A-46 A line profile graph of enamel with 0.1 mg cm$^{-3}$ of **PF1** sample 1b.*

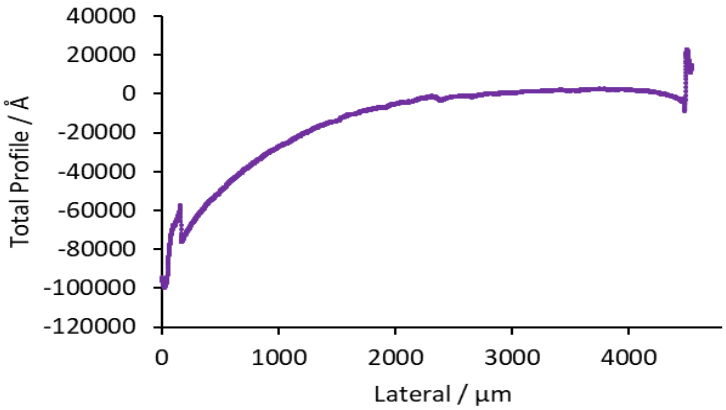


*Figure A-48 The line profile graph of enamel with 0.1 mg cm$^{-3}$ of **PF1** sample 2.*

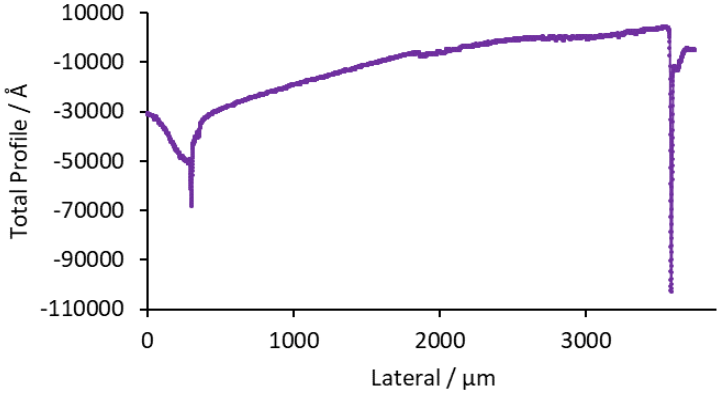


*Figure A-49 A line profile graph of enamel with 0.1 mg cm$^{-3}$ of **PF1** sample 3a.*

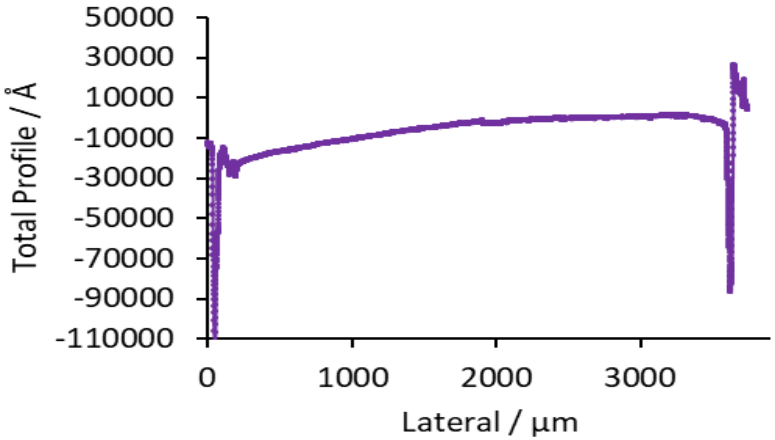


*Figure A-50 A line profile graph of enamel with 0.1 mg cm$^{-3}$ of **PF1** sample 3b.*

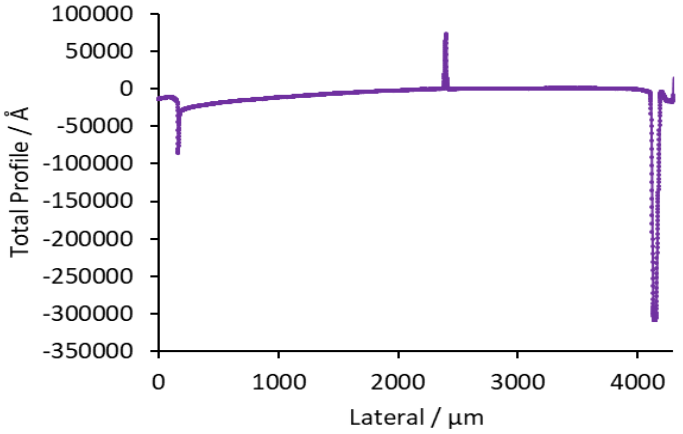


*Figure A-51 The line profile graph of enamel with 0.1 mg cm$^{-3}$ of **PF1** sample 4.*

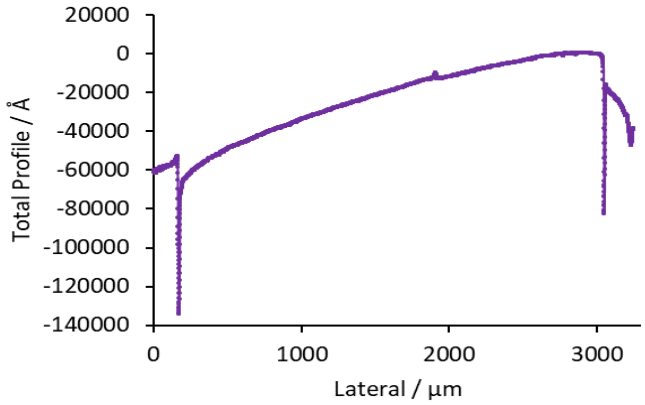


*Figure A-52 The line profile graph of enamel with 0.1 mg cm$^{-3}$ of **PF1** sample 5.*

### iii. 1 mg cm$^{-3}$ of PF1

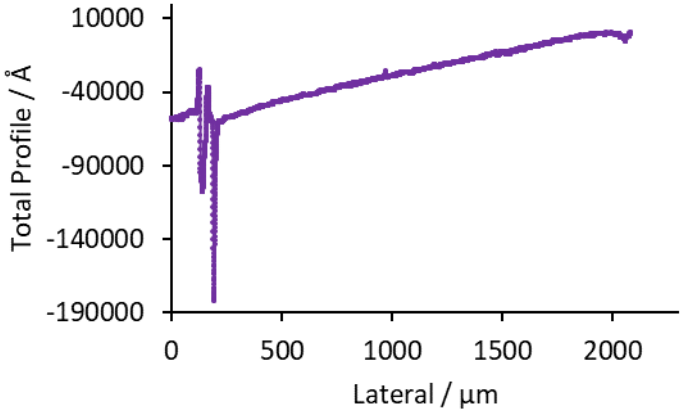


*Figure A-54 The line profile graph of enamel with 1 mg cm$^{-3}$ of **PF1** sample 1.*

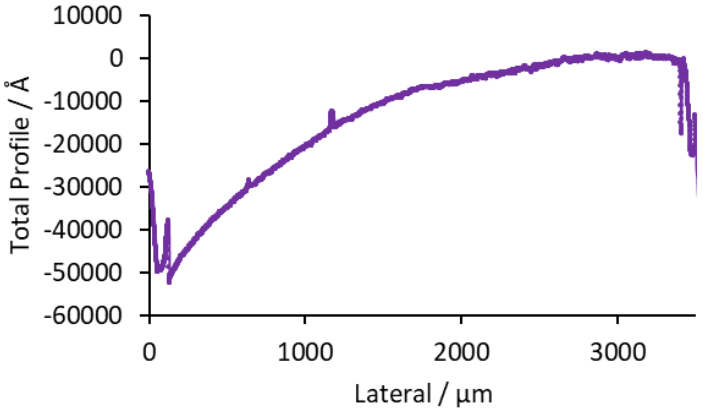


*Figure A-53 A line profile graph of enamel with 1 mg cm$^{-3}$ of **PF1** sample 2a.*

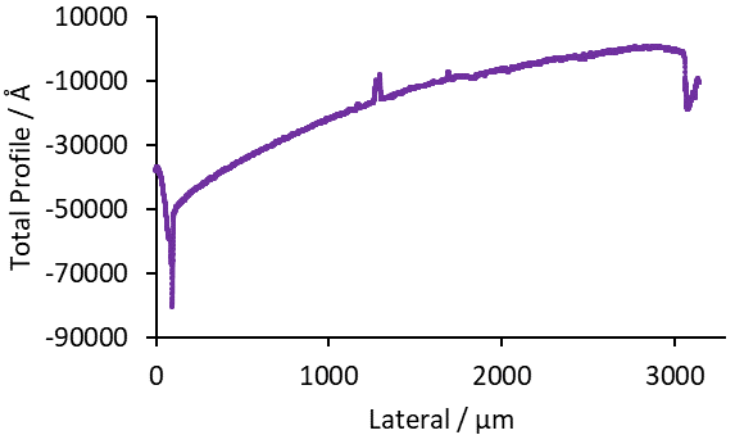


*Figure A-55 A line profile graph of enamel with 1 mg cm$^{-3}$ of **PF1** sample 2b.*

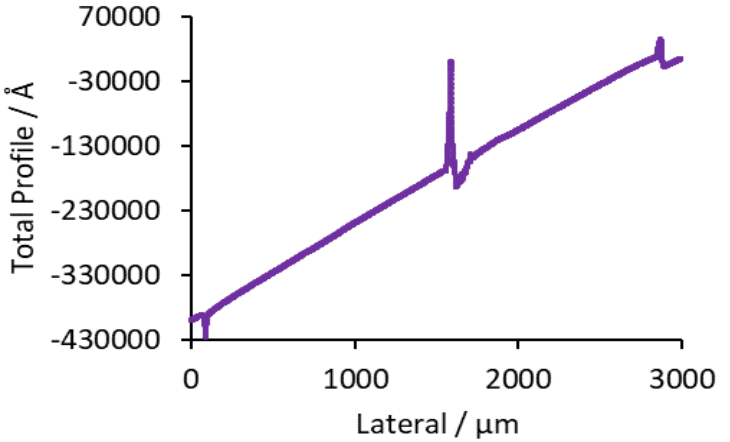


*Figure A-56 A line profile graph of enamel with 1 mg cm$^{-3}$ of **PF1** sample 3a.*

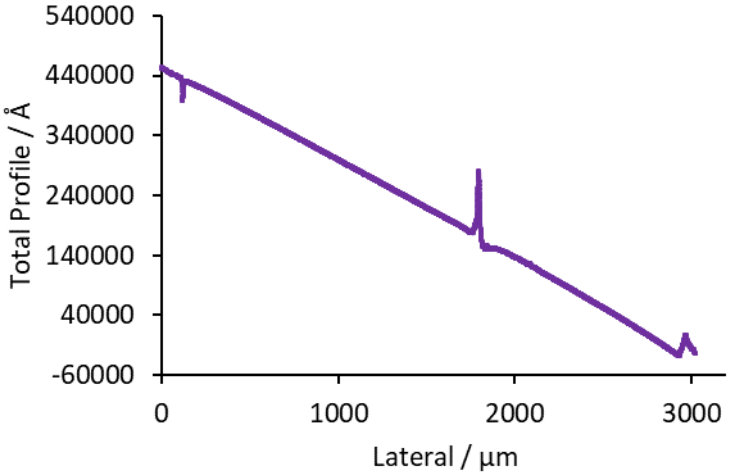


*Figure A-58 A line profile graph of enamel with 1 mg cm$^{-3}$ of **PF1** sample 3b.*

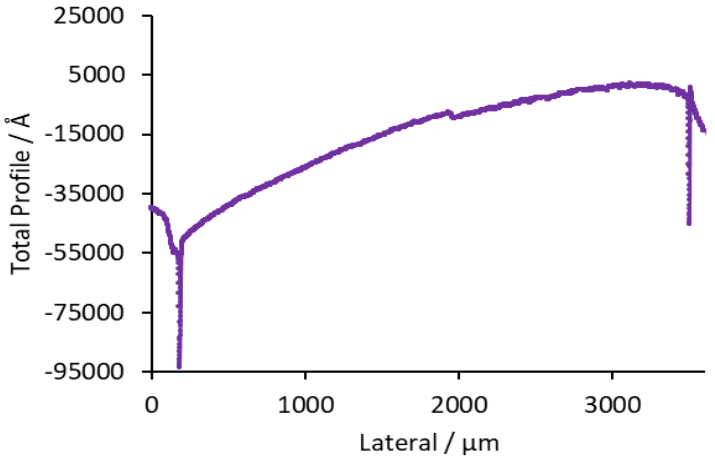


*Figure A-57 A line profile graph of enamel with 1 mg cm$^{-3}$ of **PF1** sample 4a.*

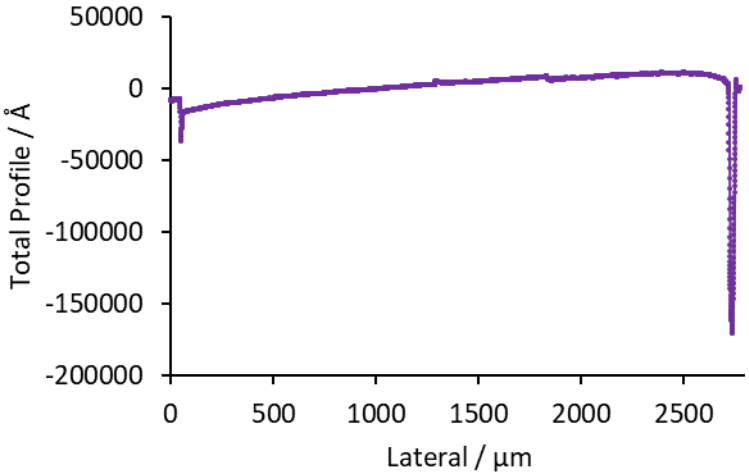


*Figure A-59 A line profile graph of enamel with 1 mg cm$^{-3}$ of **PF1** sample 4b.*

## d. Line profile graphs of the PNE1 covered enamel disc samples

### i. 0.02 mg $cm^{-3}$ of PNE1

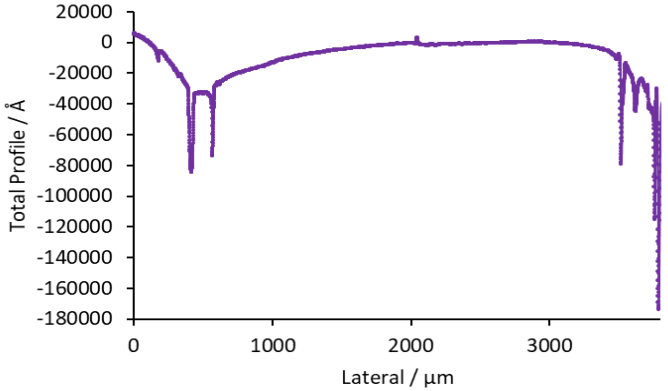


*Figure A-61 A line profile graph of enamel with 0.02 mg $cm^{-3}$ of **PNE1** sample 1a.*

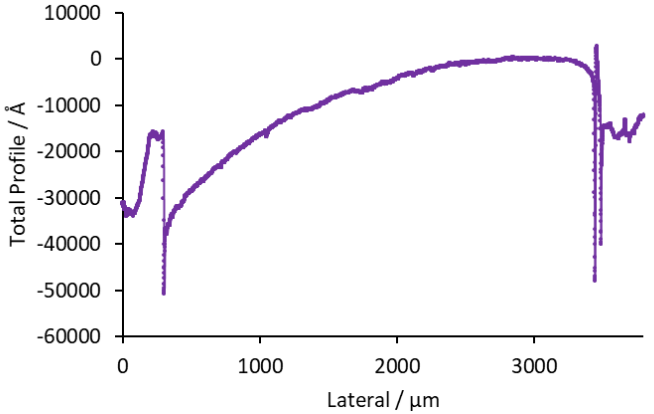


*Figure A-60 A line profile graph of enamel with 0.02 mg $cm^{-3}$ of **PNE1** sample 1b.*

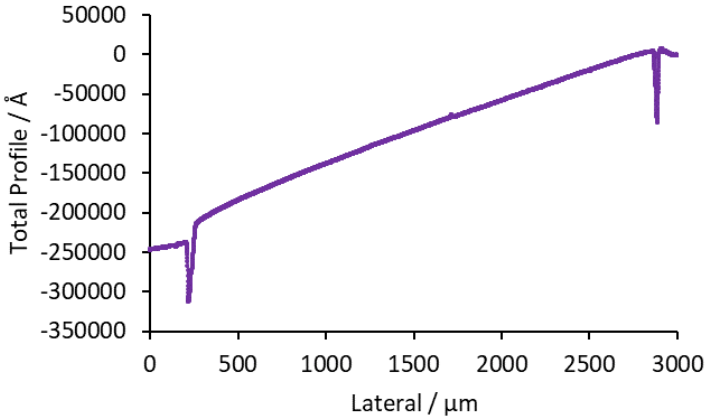


*Figure A-63 The line profile graph of enamel with 0.02 mg $cm^{-3}$ of **PNE1** sample 2.*

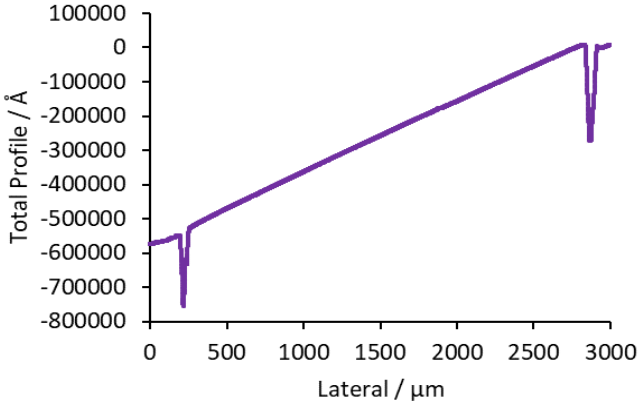


*Figure A-62 A line profile graph of enamel with 0.02 mg $cm^{-3}$ of **PNE1** sample 3a.*

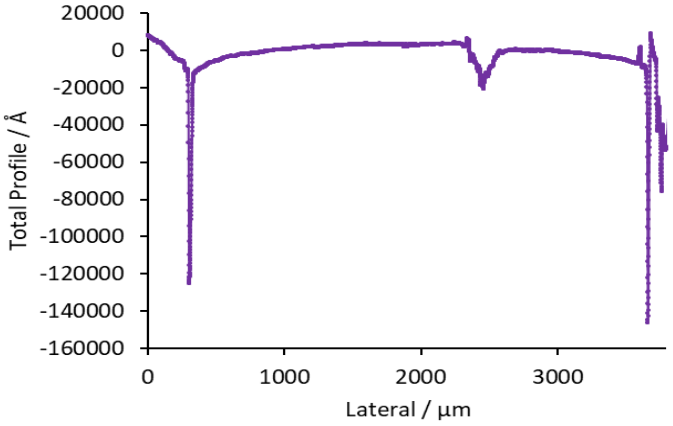


*Figure A-65 A line profile graph of enamel with 0.02 mg cm$^{-3}$ of **PNE1** sample 3b.*

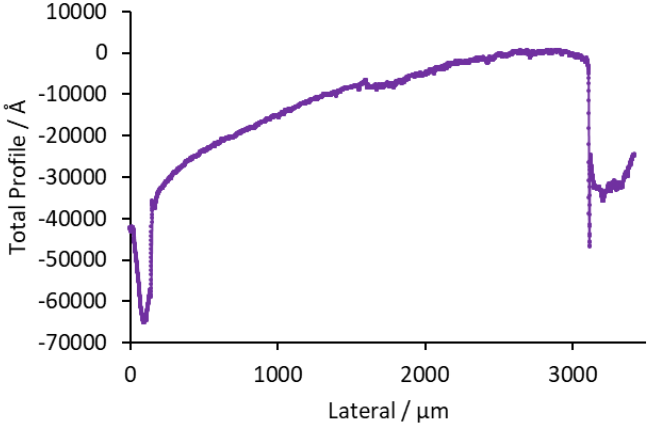


*Figure A-64 A line profile graph of enamel with 0.02 mg cm$^{-3}$ of **PNE1** sample 4a.*

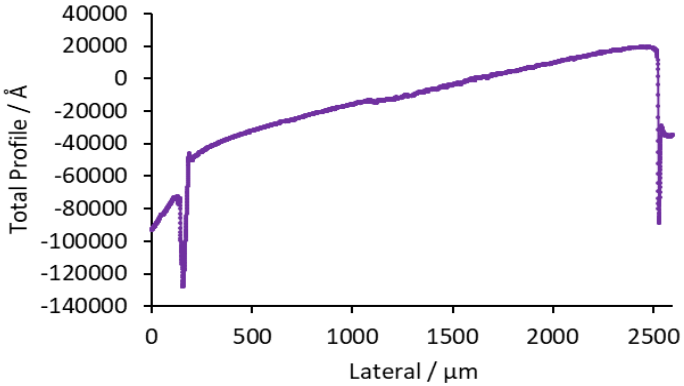


*Figure A-67 A line profile graph of enamel with 0.02 mg cm$^{-3}$ of **PNE1** sample 4b.*

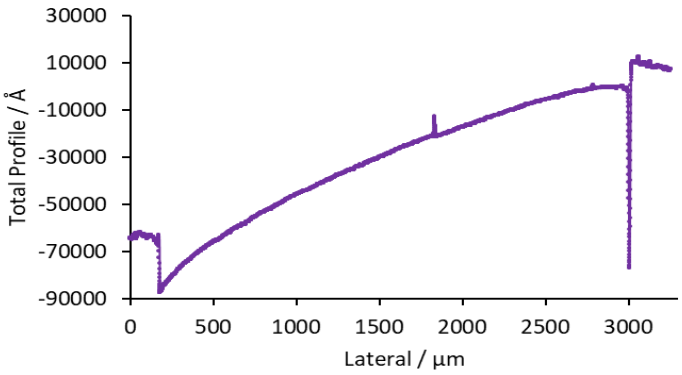


*Figure A-66 A line profile graph of enamel with 0.02 mg cm$^{-3}$ of **PNE1** sample 5a.*

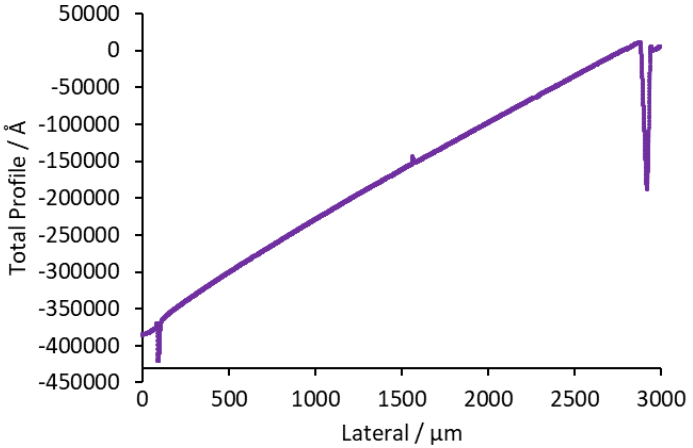


*Figure A-68 A line profile graph of enamel with 0.02 mg cm$^{-3}$ of **PNE1** sample 5b.*

### ii. 0.1 mg cm$^{-3}$ of PNE1

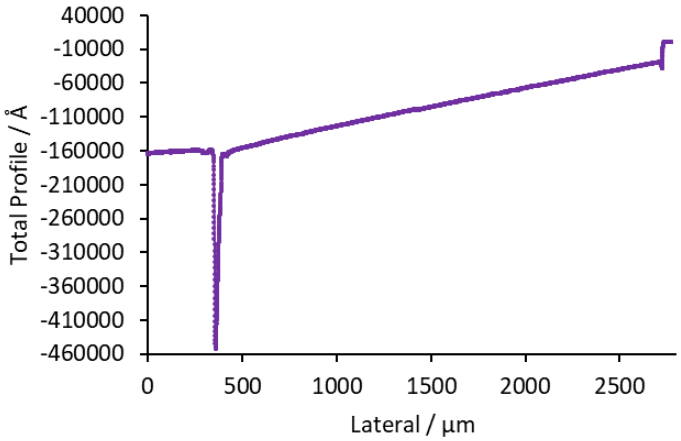


*Figure A-70 A line profile graph of enamel with 0.1 mg cm$^{-3}$ of **PNE1** sample 1a.*

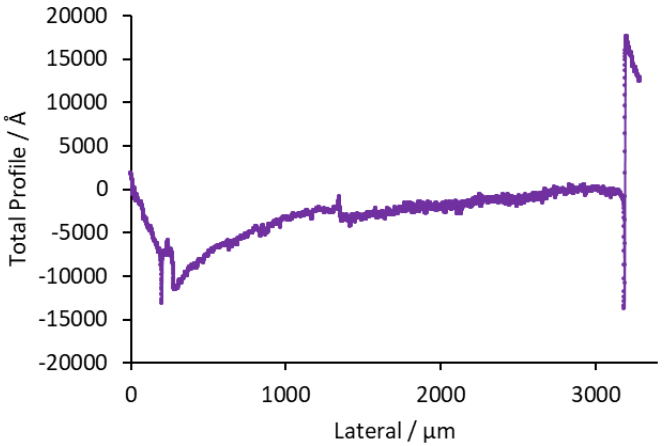


*Figure A-69 A line profile graph of enamel with 0.1 mg cm$^{-3}$ of **PNE1** sample 1b.*

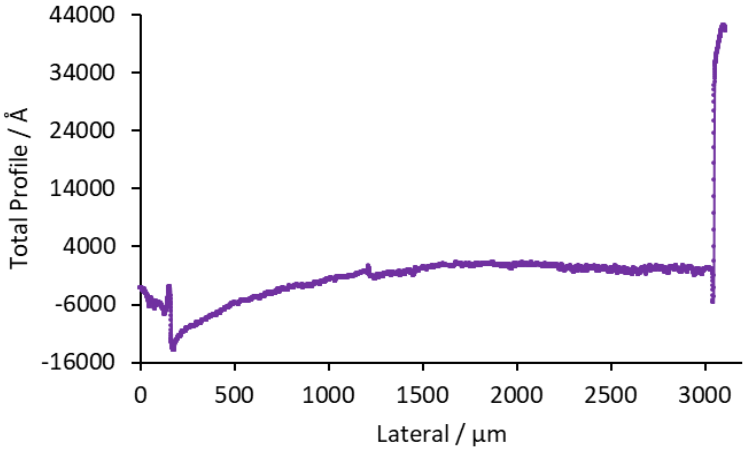


*Figure A-71 A line profile graph of enamel with 0.1 mg cm$^{-3}$ of **PNE1** sample 1c.*

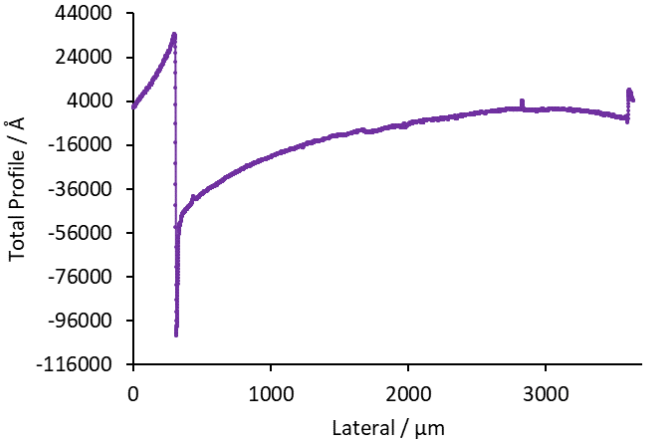


*Figure A-72 A line profile graph of enamel with 0.1 mg cm$^{-3}$ of **PNE1** sample 2a.*

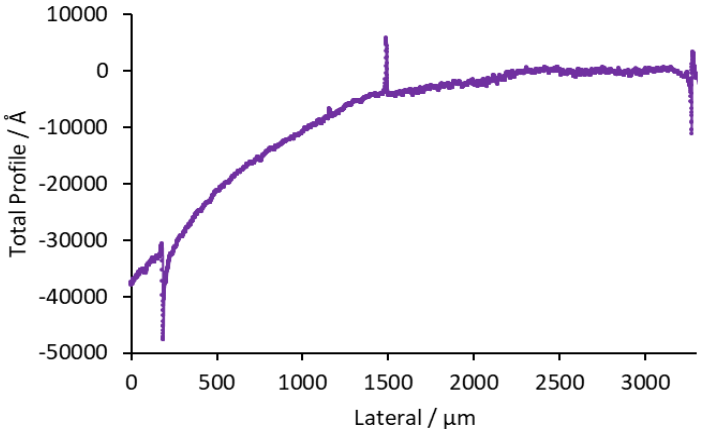


*Figure A-73 A line profile graph of enamel with 0.1 mg cm$^{-3}$ of **PNE1** sample 2a.*

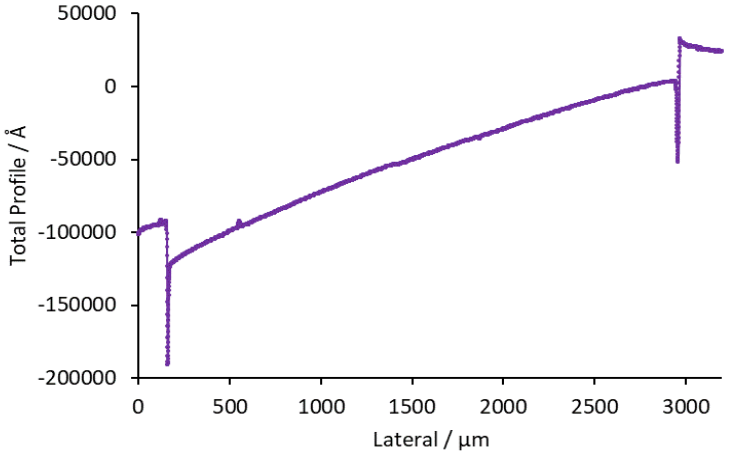


*Figure A-74 A line profile graph of enamel with 0.1 mg cm$^{-3}$ of **PNE1** sample 3a.*

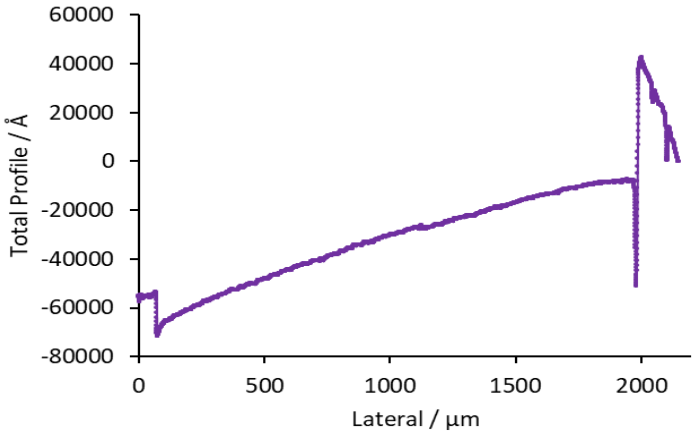


*Figure A-76 A line profile graph of enamel with 0.1 mg cm$^{-3}$ of **PNE1** sample 3b.*

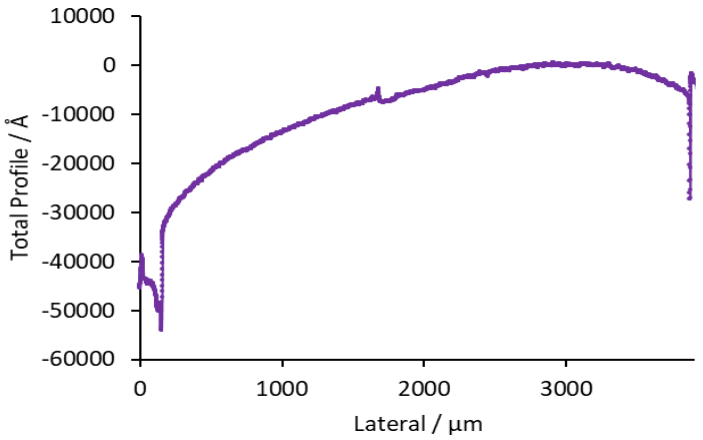


*Figure A-75 A line profile graph of enamel with 0.1 mg cm$^{-3}$ of **PNE1** sample 4a.*

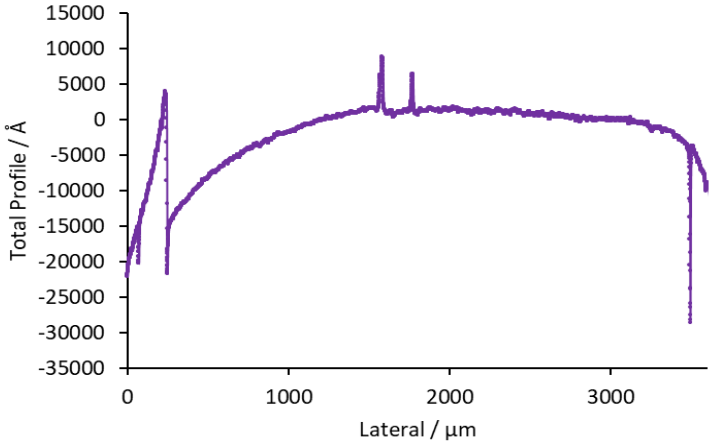


*Figure A- 77 A line profile graph of enamel with 0.1 mg cm$^{-3}$ of **PNE1** sample 4b.*